Engineering Library
620.5
458.
B99

U. S. DEPARTMENT OF COMMERCE

BUREAU OF STANDARDS JOURNAL OF RESEARCH

Vol. 7 OCTOBER, 1931 No. 4

CONTENTS

RP. No.	TITLE AND AUTHOR	Page
361.	Relation between the twist and certain properties of rayon yarns. Homer A. Hamm and Richard S. Cleveland	617
362.	The hydrolysis of chestnut and quebracho tanned leathers by sulphuric acid. E. L. Wallace	621
363.	Correlation of certain soil characteristics with pipe-line corrosion. I. A. Denison	631
364.	Further description and analysis of the first spectrum of krypton. Wm. F. Meggers, T. L. deBruin, and C. J. Humphreys	643
365.	A correlated color temperature for illuminants. Raymond Davis	659
366.	Quartz plate mountings and temperature control for piezo oscillators. Vincent E. Heaton and E. G. Lapham	683
367.	An improved audio-frequency generator. E. G. Lapham	691
368.	The porosity of electroplated chromium coatings. W. Blum, W. P. Barrows, and A. Brenner	697
369.	The use of saturated ammonium chloride in the elimination of contact potentials. C. N. Murray and S. F. Acree	713
370.	A balanced thermocouple and filter method of ultra-violet radiometry with practical applications. W. W. Coblentz, R. Stair, and J. M. Hogue	723
371.	Radiation from probe surfaces bombarded by electrons. F. L. Mohler and C. Boeckner	751

BUREAU OF STANDARDS JOURNAL OF RESEARCH

CONTENTS OF RECENT NUMBERS

April, 1931 (Vol. 6, No. 4)

RP296. The structure of the arc spectrum of zirconium. C. C. Kiess and Harriet K. Kiess. Price 15 cents.
RP297. Radiation from metals bombarded by low-speed electrons. F. L. Mohler and C. Boeckner.
RP298. Pipe-line currents and soil resistivity as indicators of local corrosive soil areas. E. R. Shepard.
RP299. Two new crystalline difructose anhydrides from hydrolyzed inulin. Richard F. Jackson and Emma McDonald. Price 5 cents.
RP300. Measurement of fiber diameters by the diffraction method. H. J. McNicholas and H. J. Curtis. Price 10 cents.
RP301. Wind pressure on a model of a mill building. Hugh L. Dryden and George C. Hill. Price 10 cents.
RP302. Stabilization of boric acid buffers by aeration. Edna H. Fawcett and S. F. Acree. Price 5 cents.

May, 1931 (Vol. 6, No. 5)

RP303. Note on contraction coefficients of jets of gas. Edgar Buckingham. Price 5 cents.
RP304. The effect of small variations in pitch upon the inductance of a solenoid. Chester Snow. Price 5 cents.
RP305. Heat content values for aqueous solutions of the chloride, nitrates, and hydroxides of hydrogen, lithium, sodium, and potassium at 18° C. Frederick D. Rossini. Price 5 cents.
RP306. Accurate measurement of small electric charges by a null method. Lauriston S. Taylor. Price 10 cents.
RP307. Light sensitivity of rosin paper-sizing materials. Arthur E. Kimberly and J. F. G. Hicks. Price 5 cents.
RP308. Dimensional changes in the manufacture of electrotypes. N. Bekkedahl and W. Blum. Price 10 cents.
RP309. The heat of ionization of water. Frederick D. Rossini. Price 5 cents.
RP310. Factors affecting the strength of masonry hollow units. Douglas E. Parsons. Price 5 cents.
RP311. Determination of the benzene and the normal hexane content of a mid-continent petroleum. Johannes H. Bruun and Mildred M. Hicks-Bruun. Price 5 cents.
RP312. Calorimetric determinations of thermal properties of methyl alcohol, ethyl alcohol, and benzene. E. F. Fiock, D. C. Ginnings, and W. B. Holton. Price 5 cents.
RP313. Characteristics of airplane antennas for radio range-beacon reception. H. Diamond and G. L. Davies. Price 5 cents.

June, 1931 (Vol. 6, No. 6)

RP314. A method for determining the change in transference number of a salt with change in concentration. A modification of the moving boundary method. Edgar Reynolds Smith. Price 5 cents.
RP315. Carpet wear testing machine. H. F. Schiefer and A. S. Best.
RP316. The lateral chromatic aberration of apochromatic microscope systems. I. C. Gardner and F. A. Case. Price 5 cents.
RP317. Phase equilibria in the system Cr_2O_3-Al_2O_3. E. N. Bunting.
RP318. Measurement of extreme ultra-violet solar radiation by a filter method. W. W. Coblentz and R. Stair.
RP319. The influence of chemical composition and heat treatment of steel forgings on machinability with shallow lathe cuts. T. G. Digges.
RP320. The index of refraction of some soda-lime-silica glasses as a function of the composition. Conrad A. Faick and A. N. Finn.
RP321. Volume changes in brick masonry materials. L. A. Palmer. Price 10 cents.
RP322. The arc spectrum of rhenium. William F. Meggers.
RP323. Purification and analysis of alkali cyanides. M. R. Thompson.
RP324. A multiple manometer and piston gages for precision measurements. C. H. Meyers and R. S. Jessup.
RP325. The Waidner-Burgess standard of light. H. T. Wensel, Wm. F. Roeser, L. E. Barbrow, and F. R. Caldwell. Price 5 cents.
RP326. The freezing point of platinum. Wm. F. Roeser, F. R. Caldwell, and H. T. Wensel. Price 5 cents.
RP327. Special refractories for use at high temperature. Wm. H. Swanger and Frank R. Caldwell.
RP328. The oxidation of sugars. I. The electrolytic oxidation of aldose sugars in the presence of a bromide and calcium carbonate. Horace S. Isabell and Harriet L. Frush.

Research papers are available as separates for purchase from the Superintendent of Documents
United States Government Printing Office, Washington, D. C.

U. S. DEPARTMENT OF COMMERCE
R. P. LAMONT, Secretary
BUREAU OF STANDARDS
GEORGE K. BURGESS, Director

BUREAU OF STANDARDS JOURNAL OF RESEARCH

October, 1931
Vol. 7, No. 4

UNITED STATES
GOVERNMENT PRINTING OFFICE
WASHINGTON : 1931

For sale by the Superintendent of Documents, Washington, D. C. - - Price $2.75 Per Year on Subscription

For a partial list of previous research papers appearing in BUREAU OF STANDARDS JOURNAL OF RESEARCH, see pages 2 and 3 of the cover

DEPOSITED BY THE
UNITED STATES OF AMERICA

RELATION BETWEEN THE TWIST AND CERTAIN PROPERTIES OF RAYON YARNS [1]

By Homer A. Hamm and Richard S. Cleveland

ABSTRACT

The results of a systematic experimental study of the relation between twist and certain physical properties of rayon yarns are given. In general the breaking strength determined by the multiple-strand method is not materially affected by an increase in twist up to about 20 turns per inch, but it decreases rapidly with an increase in twist beyond 20 turns. The proportional limit decreases with an increase in the amount of twist. The stretch at break decreases somewhat with increase in twist. The denier increases with increase in twist. The contraction resulting from twisting rayon yarn is greater for lower tensions and for higher deniers.

CONTENTS

	Page
I. Introduction	617
II. Procedure	617
III. Results	618
1. Breaking strength	618
2. Proportional limit	618
3. Stretch at break	619
4. Denier	619
5. Contraction	620

I. INTRODUCTION

The amount of twist inserted in rayon yarns depends upon the intended use. It varies from the usual few turns per inch to from 30 to 100 turns per inch in some crêpe yarns. The relation between the twist and the strength, proportional limit,[2] stretch at break, denier,[3] and contraction of the yarn is of obvious importance. The results of a systematic experimental study of this relationship are given in this paper.

II. PROCEDURE

The yarns selected for this work are described in Table 1. They were all well-known American brands and were obtained early in 1930. All had a nominal twist of but a few turns per inch.

Samples having about 12 different twists were prepared from each of these yarns using a regular commercial twisting frame equipped with travelers that would give the smallest practical tension without allowing excessive ballooning. The twists ranged from about 5 to 100 turns per inch.

[1] Since this paper was written, H. J. Ball has published a paper on "Effect of Twist Upon the Properties of Rayon Yarn" in the bulletin of the Lowell Textile Institute, Series 34, No. 4; May, 1931.

[2] The proportional limit of a yarn is taken to be the stress (or load) at which the extension (or stretch) ceases to be proportional to the stress.

[3] The denier is the unit of size of the yarns. It is the weight in grams of 9,000 m.

TABLE 1.—*Description of yarns*

Sample No.	Type	Twist, turns per inch	Number of filaments	Denier
1	Cellulose acetate	2.0	40	145
2	Cuprammonium	5.2	112	149
3	Viscose	3.3	150	150
4	Delustered viscose	2.4	24	148
5	do	2.8	36	159
6	do	3.9	60	155

The samples were thoroughly conditioned in an atmosphere of 65 per cent relative humidity and a temperature of 70° F., and were tested under these conditions.

The twist in 10-inch lengths of the yarn was determined and the results were expressed in turns per inch. The average of 10 determinations was taken to be the twist in the yarn.

The denier of the yarn was calculated from the average weight of two 80-yard skeins reeled from each bobbin.

The breaking strength, proportional limit, and stretch were determined using a pendulum type of tester with stress-strain recording attachment. The multiple strand method [4] was used and 150 ends were broken in each test. The speed of the lower jaw was 1 inch per minute, and the initial distance between the jaws was 4 inches. The breaking strength, proportional limit, and stretch were taken to be the average obtained from two stress-strain graphs for each yarn.

Additional tests were made to determine the effect of the load applied during twisting on the contraction of the yarn. A dead load was applied to the end of a 10-inch length. The yarn was then twisted and the contraction observed for increments in twist of five turns per inch. The loads used were 15 and 43 g. Viscose yarns ranging from 63 to 300 denier were studied.

III. RESULTS

1. BREAKING STRENGTH

The relation between breaking strength and amount of twist is shown graphically in Figure 1 (*a*), and in (*b*) is shown the percentage decrease in breaking strength with increase in twist. The solid curve in (*b*) represents the average values for all of the yarns and the broken curves minimum and maximum values. It will be seen that the breaking strength is not materially changed with an increase in twist up to about 20 turns per inch, but that it decreases rapidly with increase in twist beyond 20 turns. With a twist of 60 turns per inch the decrease in strength ranges from 40 to 70 per cent for the yarns studied.

2. PROPORTIONAL LIMIT

Figure 1 (*a*) shows the proportional limit and (*d*) the percentage decrease in proportional limit with increase in twist. The propor-

[4] Schoffstall, C. W., and Hamm, H. A. A Multiple Strand Test for Yarns. B. S. Jour. Research, vol. 2, pp. 871-885; 1929.

tional limit decreases with increasing twist about 1 per cent per turn. At 60 turns per inch the decrease in proportional limit varies from about 50 to 80 per cent.

3. STRETCH AT BREAK

The relation between the stretch at break and the twist is shown in Figure 1 (*g*). There is a general tendency for the stretch at break to decrease as the twist is increased though the amount of stretch and the change in stretch varies with the yarn studied.

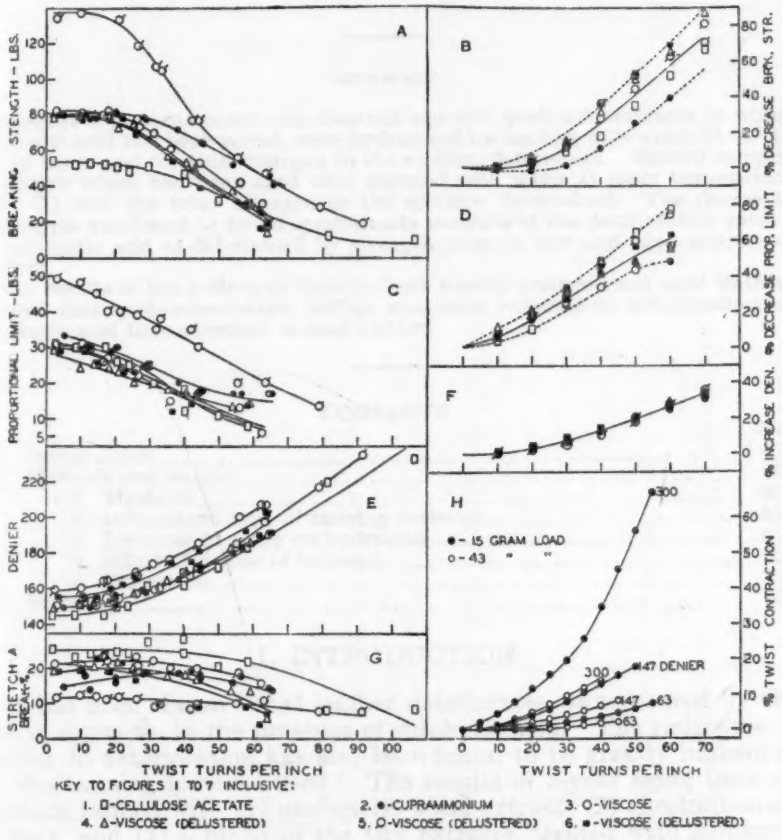

FIGURE 1.—*The effect of twist on rayon properties*

4. DENIER

The denier of the yarns at different twists and the percentage increase in denier with increase in twist are shown in Figure 1, (*e*) and (*f*), respectively. Twisting increased the denier of all of the yarns at about the same rate. This increase in denier should not be lost sight of in considering the relation between amount of twist and strength.

5. CONTRACTION

The percentage contraction resulting from twisting viscose rayon yarns under dead loads of 15 and 43g is shown in Figure 1 (*h*). The contraction is greater with the smaller load and with the higher denier yarn.

WASHINGTON, July 16, 1931.

RP 362

THE HYDROLYSIS OF CHESTNUT AND QUEBRACHO TANNED LEATHERS BY SULPHURIC ACID

By E. L. Wallace

ABSTRACT

Samples of leather tanned with chestnut and with quebracho extracts, to which sulphuric acid had been added, were hydrolyzed by heating with water at 60° C. for 18 hours and the total nitrogen in the solution determined. Similar samples of leather which had been aged were digested with water at room temperature (25° C.) and the total nitrogen in the solution determined. The degree of hydrolysis was found to be an approximate measure of the deterioration caused by sulphuric acid as determined by strength tests on new and aged samples of leather.

The results of the hydrolysis tests on both freshly prepared and aged leathers showed that quebracho-tanned leather was more resistant to deterioration by sulphuric acid than chestnut tanned leather.

CONTENTS

	Page
I. Introduction	621
II. Methods and results	623
1. Methods	623
2. Influence of type of tanning material	623
3. Influence of aging on hydrolysis	625
4. Effect of degree of tannage	626
5. Discussion	627
III. Summary	629

I. INTRODUCTION

It has been shown [1] that leather deteriorates, as measured by the loss in strength, in the presence of sulphuric acid. The resistance of leather to deterioration has also been found to be greatly influenced by the tanning material used.[1] The results of 2-year aging tests on leathers tanned with (1) quebracho-wood extract, (2) chestnut-wood extract, and (3) a blend of the two extracts, treated with sulphuric acid, are shown in Figure 1. It was considered that a chemical study of what occurred during the disintegration of these leathers might yield information which would assist in explaining their behavior in the presence of sulphuric acid and in establishing a method for evaluation of leather.

The chief constituent of animal skin is collagen, a complex protein containing approximately 18 per cent of nitrogen. Collagen can be hydrolyzed by warm water and dilute acid solutions into decomposition products consisting of less complex proteins and amino acids.

[1] Bowker, R. C., The Deterioration of Chestnut and Quebracho Tanned Leathers by Sulphuric Acid. J. Am. Lea. Chem. Assoc. 26. pp. 444-461; 1931.

Leather, a combination of animal skin and tanning materials, is more resistant to hydrolysis than collagen, is nonputrescible, and, when wet, will dry and retain its flexibility.

Vegetable-tanned leather can be hydrolyzed in boiling water. This method was used by W. Fahrion [2] and others for studying the hide-tanning combination. It was considered that any hydrolysis, resulting from the presence of sulphuric acid, might be measured in terms of soluble nitrogen at a temperature lower than that at which the hide substance would disintegrate.

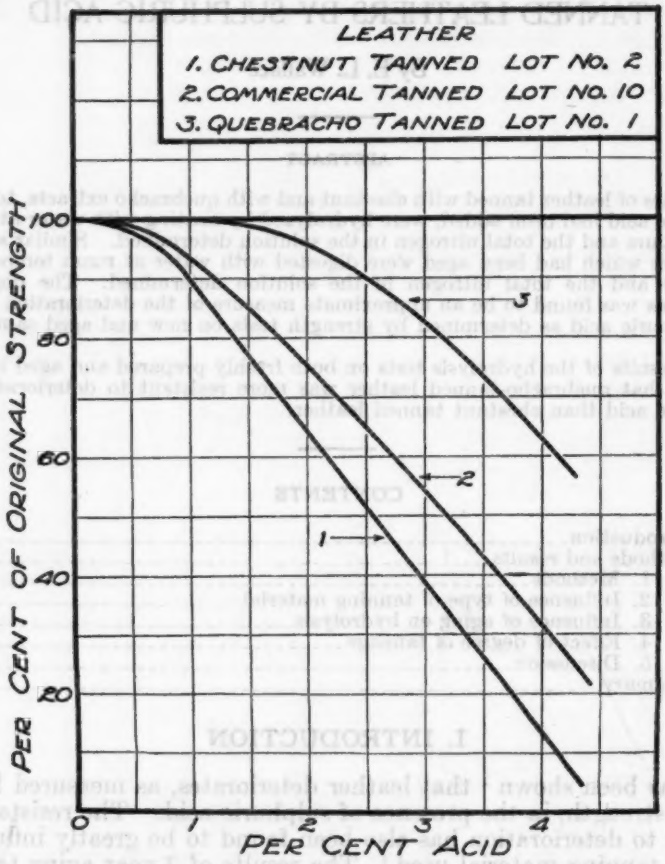

FIGURE 1.—*Results of 24 months' aging tests on chestnut leather (lot 2), quebracho leather (lot 1), and commercial leather (lot 10), treated with sulphuric acid*

Degree of tannage 62, 48, and 71, respectively.

Accordingly, a study of the hydrolysis of vegetable-tanned leather by sulphuric acid has been made on both tanned hide powder and on tanned hide aged for different periods.

[2] Collegium No. 338-339, pp. 495-50; 1908.

II. METHODS AND RESULTS

1. METHODS

Preliminary experiments showed that the treatment of leather at the boiling temperature was too drastic. The hide-tanning compound disintegrated and made it impossible to determine satisfactorily the hydrolysis resulting from the presence of sulphuric acid. Experiments at temperatures of 50°, 60°, and 70° C. were made, and it was found that leather well tanned with any of the commonly used vegetable materials would show no hydrolysis of its hide substance when digested with water for 18 hours at 50° or 60° C., whereas some leathers partially decomposed at 70° C. The temperature of 60° C. was chosen because the difference in amounts of soluble nitrogen, resulting from a small change in concentration of acid, was greater at this temperature than at 50° C., and more accurate results could be obtained. The period of 18 hours for the duration of the hydrolysis tests was selected arbitrarily after a study had been made of the effect of time and acid concentration on the rate of hydrolysis of a sample of hide powder tanned with a 50–50 blend of chestnut and quebracho extracts. Samples of this leather, each containing 5 g of hide substance, were treated with 200 ml of sulphuric acid solution. These series of tests were made to study the influence of the acid concentration on hydrolysis, using 0.03 *N*, 0.04 *N*, and 0.05 *N* acid solutions. Samples containing 5 g hide substance were digested with 200 ml of the acid solution at 60° C., and a sample from each series was tested every 2 hours, up to 22 hours, for dissolved nitrogen. The results of these tests are shown in Figure 2. The rate of hydrolysis was found to be practically constant after 10 hours and it appears that any time between 10 and 22 hours might be chosen for comparative work. Eighteen hours was selected because of convenience in handling the laboratory work and because the differences in hydrolysis, as influenced by acid concentration, may possibly be measured with less error.

In the case of aged samples of leather which contained sulphuric acid, it was found that soluble nitrogen compounds could be extracted with water at room temperature (25° C.) although none could be extracted at this temperature from leather containing no acid or from leather tested immediately after sulphuric acid was added.

The general method involved a digestion of the leather, for 18 hours, in water if acid was already present in the leather, or in an acid solution if the leather contained no acid. The temperature used was 60° C. except for one series of tests on aged leathers which were digested at room temperature (25° C.).

The hydrolyzed protein in solution was determined as nitrogen by the Kjeldahl method after first cooling the solution to room temperature and filtering it through a dry filter.

2. INFLUENCE OF TYPE OF TANNING MATERIAL

Samples of hide powder were tanned separately with chestnut, quebracho, and a 50-50 blend of chestnut and quebracho extracts. They were then washed for 24 hours in running distilled water, dried at room temperature and analyzed to determine the degree of tannage. Samples having a degree of tannage of approximately 60 were hydro-

lyzed with solutions of sulphuric acid at 60° C. for 18 hours and the soluble nitrogen determined in the extracts. The results are shown in Figure 3.

Similar tests were made also on chestnut, quebracho, and commercial leathers which had degrees of tannage of 62, 48, and 71, respectively. These leathers were treated so as to contain varying amounts of sulphuric acid and had been aged for 18 months. The

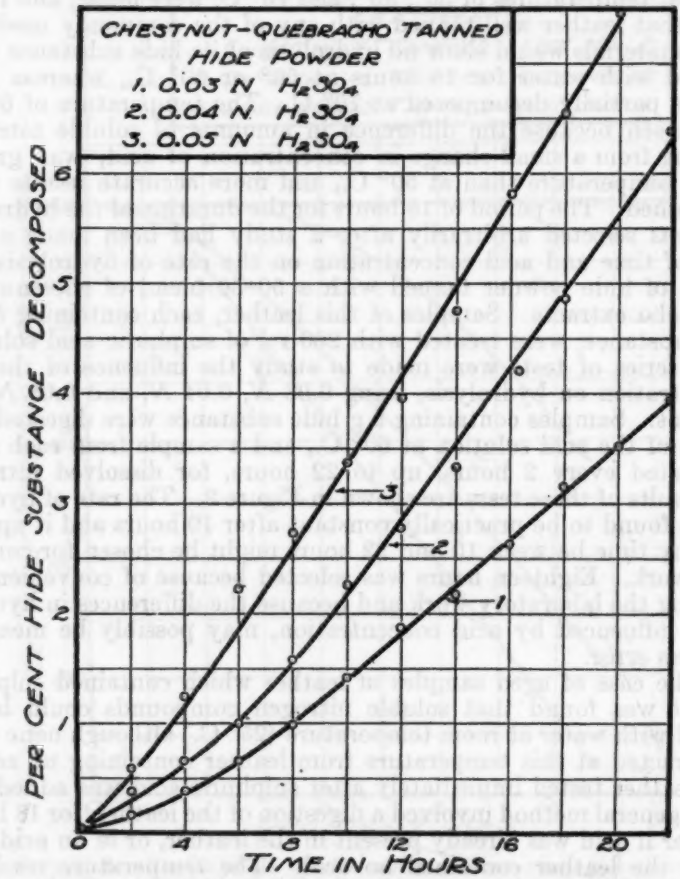

FIGURE 2.—*The influence of time and acid concentration on the hydrolysis of hide powder tanned with a 50-50 blend of chestnut and quebracho extracts*

Degree of tannage 54.

commercial leather was tanned with a blend made up chiefly of chestnut and quebracho extracts. Samples of these leathers were hydrolyzed with 200 ml of distilled water at 60° C. The results are shown in Figure 4.

These experiments, on both tanned hide powder and aged leather, showed that the kind of tanning material used greatly influenced the hydrolysis of hide substance by sulphuric acid.

3. INFLUENCE OF AGING ON HYDROLYSIS

Samples of quebracho and chestnut tanned leathers containing 5 g actual hide substance were extracted with 200 ml distilled water at room temperature (25° C.) by shaking for 18 hours, immediately after they had been treated with sulphuric acid and dried. The solution was filtered and soluble nitrogen determined. Other samples from the same blocks of leather were given a similar extrac-

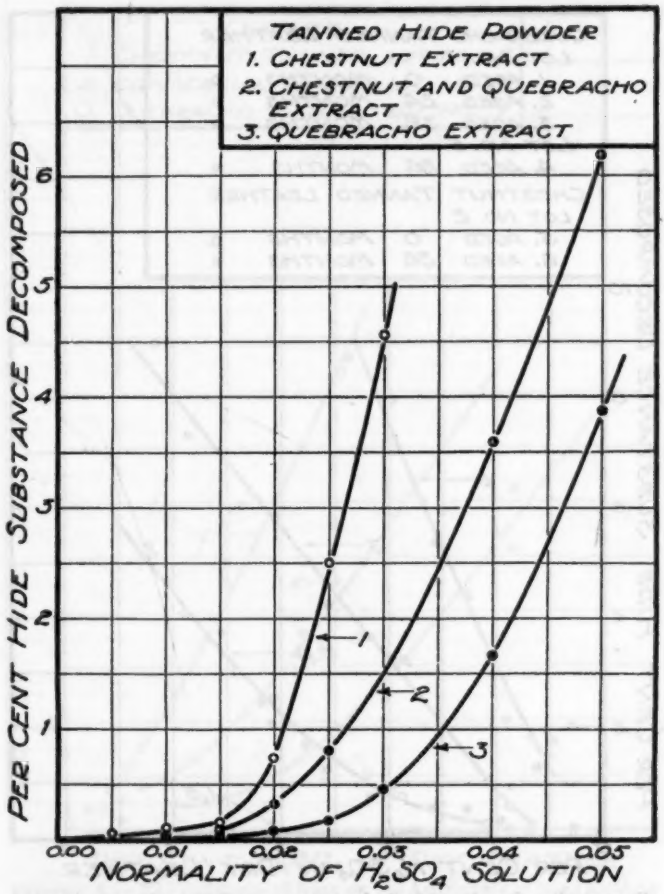

FIGURE 3.—*The hydrolysis of tanned hide powder, degree of tannage 60, as influenced by acid concentration and the type of tanning material used*

tion after aging for periods of 24 and 36 months. The results (fig. 5) show the relation between acid content, aging, and water soluble nitrogen compounds.

No hydrolysis occurred in the samples tested immediately after treatment with acid, but as aging progressed hydrolysis increased as illustrated by the results on the quebracho leather (curves 1, 2, and 3, fig. 5) and on the chestnut leather (curves 5 and 6).

4. EFFECT OF DEGREE OF TANNAGE

Samples of hide powder were tanned with different amounts of chestnut extract, quebracho extract, and a 50-50 blend of chestnut and quebracho extracts. The tanned hide powder was washed with distilled water until the wash water was free from tannin, as determined by the gelatine salt test, dried at room temperature, and analyzed to determine the degree of tannage. Samples containing 5 g of

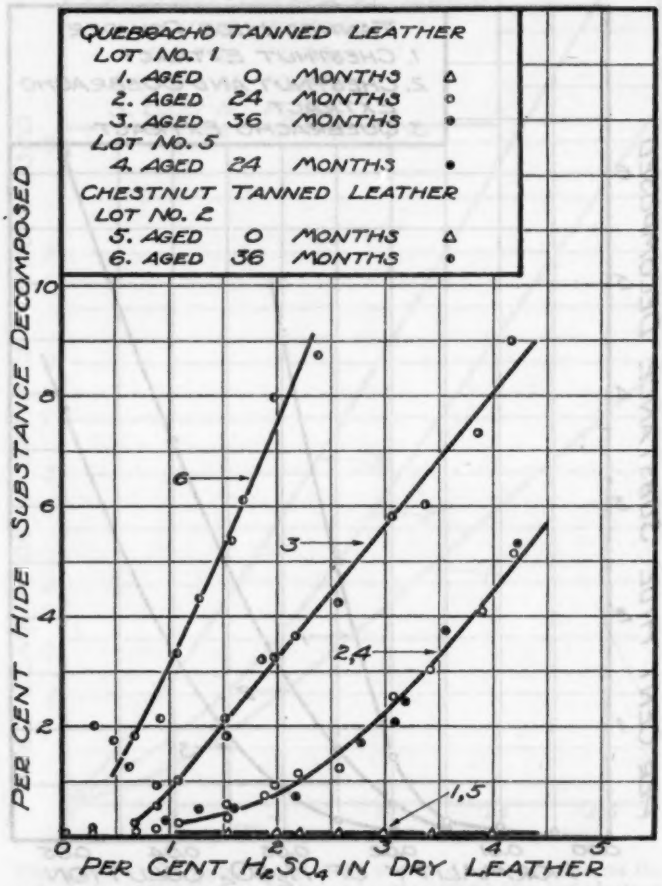

FIGURE 4.—*Results of hydrolysis tests on chestnut leather (lot 2), quebracho leather (lot 1), and commercial leather (lot 10), aged for 18 months*

Degree of tannage 62, 48, and 71, respectively.

hide substance were then hydrolyzed with 200 ml of 0.005 *N* sulphuric acid solution at 60° C. for 18 hours and the amount of soluble nitrogen per 5 g of hide substance determined. The results (fig. 6) show that there was less hydrolysis with the same quantity of acid as the degree of tannage was increased, and that more hide substance was hydrolyzed, at the same degree of tannage, for the samples tanned with chestnut extract than for those tanned with quebracho extract.

5. DISCUSSION

This investigation indicates that the disintegration of vegetable-tanned leather by sulphuric acid is accompanied by the formation of decomposition products which can be extracted from the leather, under certain arbitrary conditions, as soluble nitrogen compounds. This method of measurement showed that, for any given leather, the hydrolysis was greater as the time of aging and acid concentrations

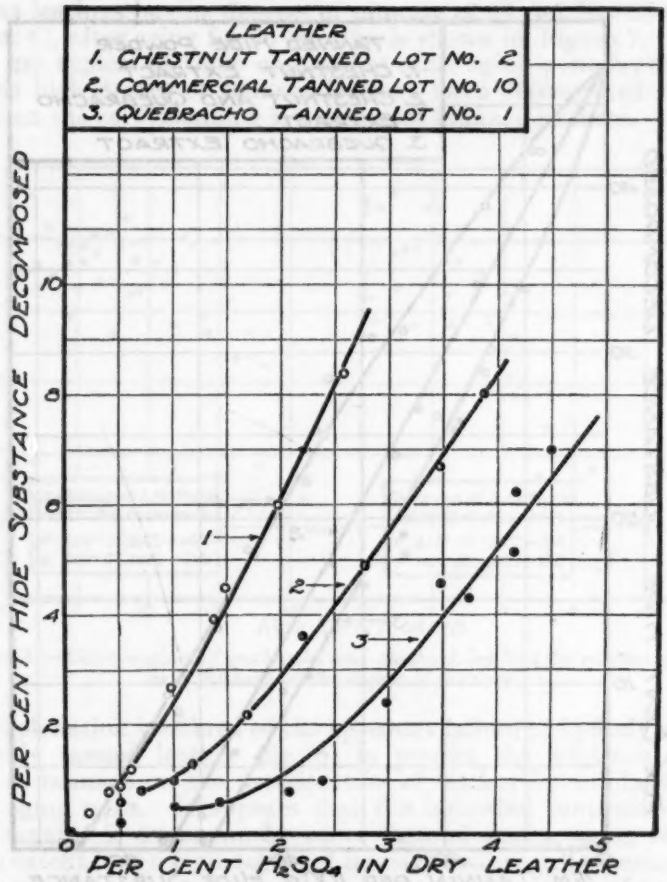

FIGURE 5.—*The influence of time on the hydrolysis of aged leathers containing sulphuric acid*

Lot 1, lot 2, and lot 5, having a degree of tannage of 48, 62, and 78, respectively.

present were increased. Similar results were secured whether leather containing acid was hydrolyzed with water or whether leather containing no added acid was hydrolyzed with acid solutions, as shown by the results in Figures 3 and 4.

The leather tanned with quebracho extract resisted hydrolysis better than the leather tanned with chestnut extract. It is significant that the hydrolysis results obtained on such leathers (fig. 4) closely parallel the deterioration of these leathers in actual aging tests as

measured by the drop in tensile strength. (Fig. 1.) There appears to be, for each leather, a limiting acid content below which deterioration proceeds at a low rate and above which it proceeds at a much greater rate as measured by both the hydrolysis and the loss of strength on aging.

This correlation of physical and chemical results indicates that the resistance to deterioration by sulphuric acid, of any vegetable-tanned leather, may be predicted by laboratory hydrolysis tests.

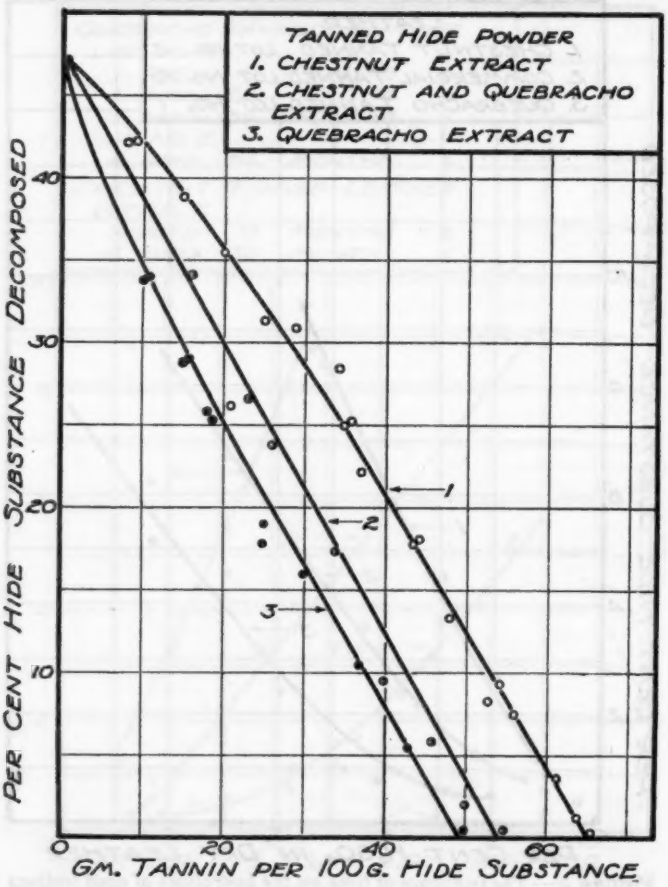

FIGURE 6.—*The influence of degree of tannage on the hydrolysis of tanned hide powder when heated with 0.005 N H_2SO_4 at 60° C. for 18 hours*

The method also suggests a possibility of being useful in determining the damage which may have already occurred in a sample of leather of unknown characteristics.

The studies of the influence of the degree of tannage on the hydrolysis of tanned hide powder definitely show (fig. 6) that hydrolysis, resulting from the action of a sulphuric acid solution on samples of leather for 18 hours at 60° C., decreased as the combined tannin increased.

From these results, in view of the parallelism between the hydrolysis tests (figs. 3 and 4) and the deterioration tests during aging (fig. 1) it might be expected that a high degree of tannage leather would show less deterioration and hydrolysis after aging than a low degree of tannage leather. However, this is not the case. Two quebracho leathers having degrees of tannage of 48 (lot No. 1) and 78 (lot No. 5) exhibited the same degree of hydrolysis after being aged for 24 months. (Curves 2 and 4, fig. 5.) The deterioration of these leathers as measured by the change in tensile strength and also of two chestnut leathers having degrees of tannage of 64 (lot No. 2) and 52 (lot No. 4), after aging for 24 months, is shown in Figure 7. These results are typical of those obtained at other aging periods and show that the high degree of tannage leathers have deteriorated slightly more than the corresponding low degree of tannage leathers.

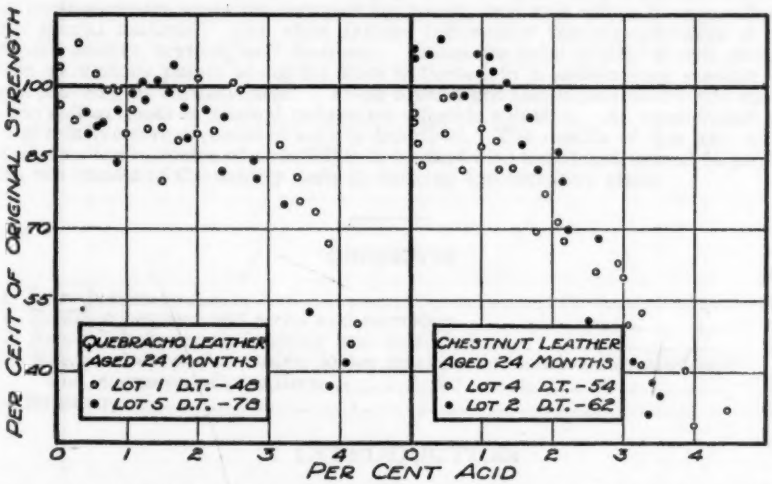

FIGURE 7.—*Deterioration of quebracho and chestnut leathers by sulphuric acid as influenced by the degree of tannage*

No explanation is offered of the apparent failure of hydrolysis tests on freshly tanned leather (fig. 6) to predict the influence of the degree of tannage on the deterioration of leather by sulphuric acid during aging tests. It appears that the indicated protective effect of the tannins is overcome by other factors, during aging tests to such an extent that a high degree of tannage leather will deteriorate at least as rapidly as a similar leather having a lower degree of tannage. Further studies of the mechanism of hydrolysis and the nature of the resulting decomposition products are in progress.

III. SUMMARY

The results for the hydrolysis of leathers examined by the methods used may be summarized as follows:

1. The disintegration of leather by sulphuric acid results in hydrolysis of the hide substance.

2. The hydrolyzed hide substance can be extracted from the leather as soluble nitrogen compounds.

3. Leather tanned with quebracho extract is more resistant to hydrolysis by sulphuric acid than leather tanned with chestnut extract.

4. The rate of hydrolysis of freshly tanned leather decreases as the degree of tannage increases.

WASHINGTON, June 26, 1931.

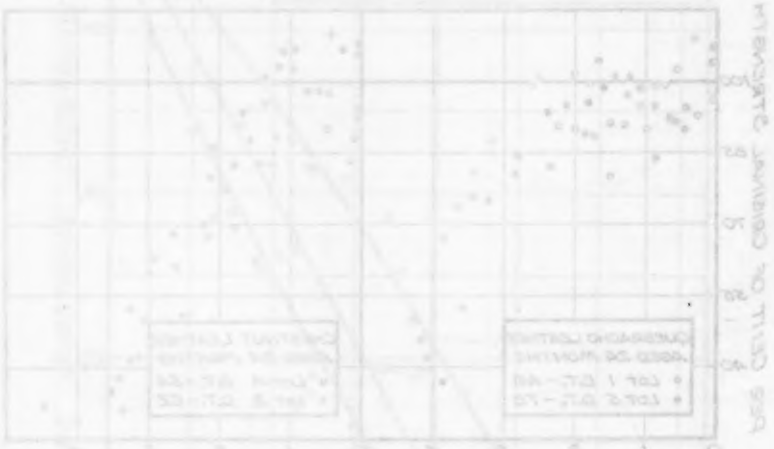

R P 363

CORRELATION OF CERTAIN SOIL CHARACTERISTICS WITH PIPE-LINE CORROSION

By I. A. Denison

ABSTRACT

Corrosion which has been experienced on a group of pipe lines in Ohio is attributed to the corrosiveness of certain soils occurring along the lines. Areas occupied by different soils correspond in a general way to corrosive and noncorrosive areas, as shown by a record of pipe replacements over a period of years. The most corrosive areas are occupied by heavy, acid soils which have developed from glacial material. The chief factors influencing the corrosiveness of the soils are acidity, texture, and drainage. Values for total acidity of soil samples taken at various points along the lines indicated in a satisfactory manner the areas differing in corrosiveness. These areas were also indicated by pH values of the soil extracts in normal potassium chloride solution. An accelerated test of the relative corrosiveness of soils is described. The results of this test, which is based on the corrosion of a steel disk in contact with moist soil, agreed in general with the results of the acidity tests in defining the corrosive areas.

CONTENTS

		Page
I.	Introduction	631
II.	Relation between soil series and corrosion	632
III.	Relation between soil acidity and corrosion	634
IV.	Relation between corrosion losses from an accelerated corrosion test and corrosion of pipe lines	637
V.	Summary	642

I. INTRODUCTION

The experience of pipe-line operators has shown that pipe lines may be severely corroded in localities where corrosion can not be ascribed to stray electric current, corrosive liquors, or to other well-recognized causes of corrosion. In such areas it would seem that the causes of corrosion must be sought in the inherent characteristics of the soils in which the pipe lines are laid. The importance of studying the relations between soil characteristics and corrosion has been emphasized by the results obtained with buried specimens of pipe in the original soil-corrosion investigation of the National Bureau of Standards. Supplementing this investigation the bureau has on several occasions undertaken the study of corrosion experienced in the operation of pipe lines. This method tends to complicate the study of soil corrosion, for the reason that pipe-line currents in certain areas may possibly accelerate or reduce the corrosion which would occur if the pipe were unconnected. It has a certain advantage, however, in that the long periods during which certain lines have been in operation have tended to minimize the effect of variations in such factors as climate and quality of pipe materials, and also the influence of temporary local conditions which might obscure the inherent corrosiveness of the soil.

A study of soil corrosion was made during 1929–30 on a group of pipe lines to determine whether corrosion is confined to certain soils occurring along the lines or whether it is induced more by local conditions than by kind of soil. A second object of the study was to define, if possible, those characteristics of the soils which seemed to influence corrosion, with the view of applying the results obtained to the development of methods for determining soil corrosiveness. This study was made possible by the fact that the company operating the lines has kept a detailed record of all leaks and pipe replacements since the lines were installed, which was, in the case of the oldest line, more than 40 years ago. Quantitative expressions for the corrosion which has occurred at various points on the lines were, therefore, available for comparison with soil conditions and with the results of laboratory studies.

The field work in this investigation was carried out on a 32-mile section of a group of pipe lines in Ohio. The lines run parallel at an average distance of 1 foot apart, and from 18 to 24 inches below the surface. Corrosion has not been general over the lines, but has occurred chiefly in restricted areas. In certain sections several thousand feet of pipe have been replaced two and three times; in other sections, however, no replacements have been made in over 40 years. The individual lines also show great variation in the extent to which they have been replaced, one line in particular having required but few replacements in certain areas where the other lines have been rather severely corroded.

The soils occurring in the area studied were derived from both glacial and lacustrine (lake-laid) material. The chief glacial soils are those of the Brookston and Nappanee series. These soils are closely associated, the latter often occupying the slopes in regions where the level areas are occupied by the Brookston soils. Owing to their somewhat exposed position the Nappanee soils have been more highly weathered than the Brookston soils, as shown by their lighter color and their heavy acid subsoil. Soils of both series are poorly drained. The lacustrine soils are, in general, much coarser in texture than the glacial soils and are usually fairly well drained. Since little corrosion has been experienced in these soils, it was considered sufficient for this study to consider the lake-laid soils as a single group. Several series, however, were recognized, namely, the Plainfield, Newton, Fox, Berrien, Lucas, Toledo, and Fulton series. Intermediate between the glacial and lacustrine soils are those of the Wauseon series, which are sandy loam soils overlying heavy glacial material at a depth usually between 20 and 30 inches.

II. RELATION BETWEEN SOIL SERIES AND CORROSION

The procedure followed in carrying out the study was first to identify the various soil series occurring along the lines and to fix their boundaries by stake number.[1] The relation obtaining between corrosion and soil series was then studied by plotting the average percentages of pipe replaced in 1,000-foot intervals along the lines, indicating on the diagram the boundaries of the soil series present. At a number of locations samples of virgin soil were taken at pipe

[1] The writer wishes to acknowledge his indebtedness to Dr. G. W. Conrey, of the Ohio agricultural experiment station, for assistance in identifying the soils.

depth for study in the laboratory of those factors which appeared to influence corrosion.

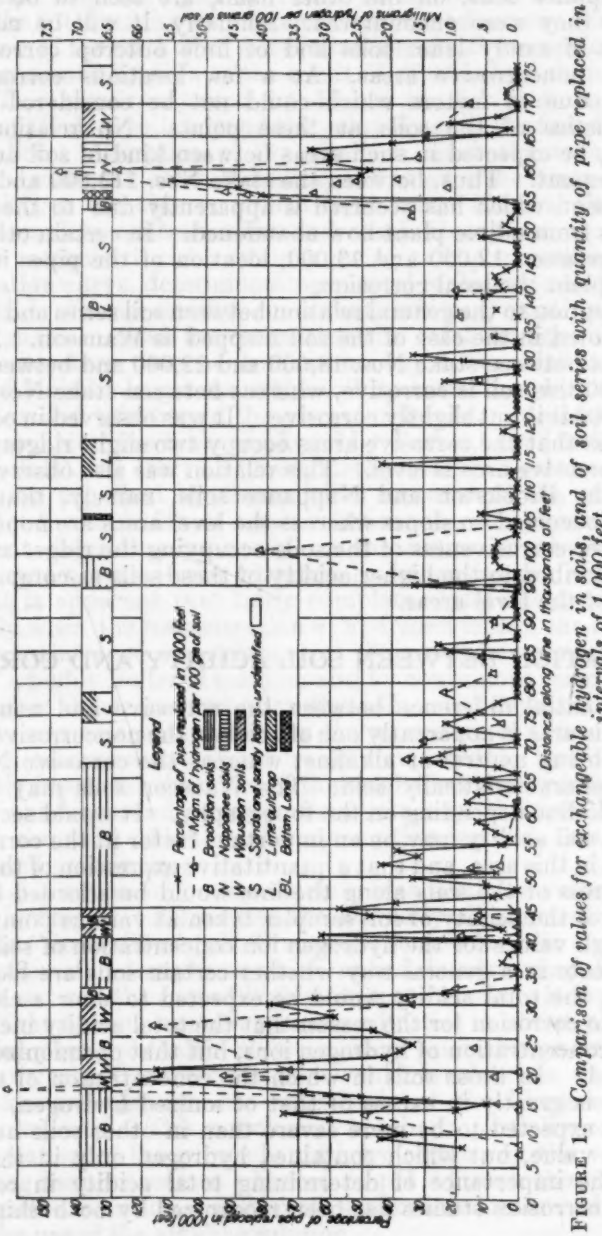
Legend
Percentage of pipe replaced in 1000 feet
Mgm of hydrogen per 100 gm of soil
B Brookston soils
N Napanee soils
W Wauseon soils
S Sands and sandy loams-undivided
L Lime outcrop
BL Bottom Land
Distance along line in thousands of feet
Percentage of pipe replaced in 1000 feet
Milligrams of hydrogen per 100 grams of soil

FIGURE 1.—*Comparison of values for exchangeable hydrogen in soils, and of soil series with quantity of pipe replaced in intervals of 1,000 feet*

Comparison of the areas differing in corrosiveness with the areas occupied by the various soils indicates a general relation between soil series and corrosion. This relation is brought out in Figure 1. The total acidity values also shown in this diagram will be referred

to in a later connection. It can be seen from the figure that the Brookston soils wherever they occur are relatively noncorrosive. The Nappanee soils, on the other hand, are seen to be corrosive wherever they were encountered. Similarly, it will be noted that the areas of sandy loam soils and of lime outcrop correspond to relatively noncorrosive areas. At a few locations corrosion was evidently due to factors which could not be considered inherent characteristics of the soils at these points. No relation would, therefore, be expected in such areas between kind of soil and extent of replacement. Thus, between the stake Nos. 113,000 and 114,000, the corrosion which has occurred is apparently due to the presence of cinders from a lime plant now abandoned. In certain other areas, such as between 12,000 and 13,000, location of the pipes in ditches would explain the local corrosion.

An exception to the general relation between soil series and corrosion is to be noted in the case of the soil mapped as Wauseon. It will be noted that between stake Nos. 18,000 and 22,000 and between 26,000 and 31,000 this soil is corrosive, whereas between stake Nos. 165,000 and 170,000 it is but slightly corrosive. It was observed in comparing these areas that the corrosive areas occupy two slight ridges; whereas the noncorrosive area is level. This relation was also observed in the case of the Brookston and Nappanee soils, namely, that marked corrosion occurred on slopes whereas the level areas are noncorrosive. The greater corrosiveness of the soils occupying the ridges and slopes is to be ascribed to the higher acidity of these soils as compared with the soils of the level areas.

III. RELATION BETWEEN SOIL ACIDITY AND CORROSION

The essential difference between the corrosive and noncorrosive soils in this area is apparently one of acidity, the noncorrosive Brookston soils being neutral or alkaline; whereas the corrosive Nappanee soils are characteristically acid. The Wauseon soils may be either acid or alkaline depending on the topography. It would seem, therefore, that soil acidity may be an important factor in the corrosion experienced in this area, and that a quantitative expression of the relative corrosiveness of the soils along the line would be afforded by determination of the acidity of soil samples taken at various points.

Although values for the hydrogen ion concentration of soil extracts may indicate in a general way whether certain soils are likely to be corrosive, the total acidity would be expected to show a closer relationship to corrosion for the reason that the total acidity includes not only the concentration of hydrogen ions, but that of unionized hydrogen as well. In those soils in which the concentration of unionized hydrogen is greatly in excess of that of ionized hydrogen, corrosion would be expected to be more severe than in other soils having the same pH value, but which contained hydrogen only in the ionized form. The importance of determining total acidity in connection with soil corrosion studies has been recognized by both Shipley[2] and Holler.[3]

[2] Shipley, J. W., McHaffie, I. R., and Clare, N. D., Corrosion of Iron in Absence of Oxygen, Jr. Ind. Eng. Chem., vol. 17, pp. 381-385; 1925.

[3] Holler, H. D., Corrosiveness of soils with respect to iron and steel, J. Ind. Eng. Chem. vol. 21, pp. 750-764; 1929.

A method which has been used to determine the total acidity of soils is the electrometric titration of suspensions of soil in water. This method was employed by Holler in his studies of the relation between the total acidity of soils and their corrosiveness. One of the chief defects of the method of direct titration of soil suspensions is that alkali is consumed by soils as the result of effects other than neutralization. This was recognized by Holler in the work mentioned. Addition of alkali to soils beyond the point of neutralization appears to result in direct absorption of the alkali, in much the same manner that animal charcoal, activated silica, and other absorbents devoid of acidic hydrogen are able to absorb basic ions. Since the transition between complete neutralization and alkali absorption by soils can seldom be recognized with certainty owing to the smoothness of the usual titration curve, determinations of total replaceable hydrogen by this method are necessarily somewhat arbitrary and inaccurate.

An alternate method for estimating the total acidity of soils by which effects other than neutralization may be avoided consists in removal of ionic hydrogen from the soil by extraction with a neutral salt solution and titration of the extract obtained. Methods involving this principle have been employed by Parker,[4] by Schollenberger and Dreibelbis[5] and others. These methods depend on the fact that hydrogen ion adsorbed by the colloidal material of the soil can be replaced by the basic ion of a salt solution, the completeness of the replacement depending primarily on the nature of the salt used. Since at least a part of the adsorbed hydrogen is very slightly dissociated it is apparent that fairly complete replacement can be obtained only when the concentration of hydrogen ions in the extracting solution is maintained at a minimum. This may be accomplished by the use of a highly buffered solution and by continuous removal of the solution after it has reacted with the soil. Although complete removal may not be accomplished by the procedure of extraction, it is likely that measurement of the readily replaceable hydrogen may more nearly represent that part of the total adsorbed hydrogen which is active in underground corrosion than values for the total hydrogen present in the soil. Whether this assumption is valid, however, can not be stated at this time.

A normal solution of barium acetate was used for extracting the adsorbed hydrogen. Before use the normally alkaline solution was adjusted to "neutrality" (pH 7) with acetic acid in order to minimize the adsorption of hydroxyl ions which, as has already been pointed out, is likely to occur in the case of highly absorptive soils. It is probable, however, that barium acetate solution adjusted to about pH 8.3, at which point phenolphthalein shows a sharp color change, would give equally satisfactory extractions and would involve less uncertainty in the titrations through the magnitude of the blank correction otherwise required. This conclusion has been partially confirmed, since completion of the present study, by comparing the values obtained using barium acetate adjusted to pH 8.3 with those obtained with a neutral solution. However, somewhat higher values were obtained by use of the alkaline solution.

---

[4] Parker, F. W., Methods for Determination of the Amount and Avidity of Exchangeable Hydrogen in Soils, Proc. and Papers of the First Internat. Cong. of Soil Sci., vol. 2, pp. 164–173; 1928.

[5] Schollenberger, C. J., and Dreibelbis, F. R., Analytical Methods in Base Exchange Investigations in Soils, Soil Sci., vol. 30, No. 3, pp. 161–173; 1930.

Titration of the extract was made with phenolphthalein as the indicator. Although the extract was highly buffered a sharp end point was obtained. Titration of several extracts by a differential potentiometric method showed that the end point coincided with the color change of phenolphthalein. Since the barium acetate solution was initially adjusted to neutrality it was necessary to deduct from the titration value the quantity of alkali required to bring the same volume of neutral barium acetate to the color change of phenolphthalein.

The details of the original procedure were as follows: A 50 g sample of soil contained on a 15 cm filter paper was extracted with normal barium acetate solution, which had been adjusted to pH 7, until 100 ml of the solution after having percolated through the soil showed no change in acidity on titration with 0.1 *N* barium hydroxide. Usually 1 liter of solution was required for complete extraction. In determing the acidity of the extracts, 250 ml aliquots were titrated with 0.1 *N* barium hydroxide to the first definite color change of phenolphthalein. From thist itration value was subtracted the volume (approximately 12 ml) of 0.1 *N* alkali required to bring 250 ml of the neutral barium acetate solution to the end point of phenolphthalein.

The quantity of exchangeable hydrogen in the soils at various points along the lines is shown graphically in Figure 1. Comparison of these values with the average percentage pipe replacement of the five lines between intervals of 1,000 feet shows that a general correlation obtains between corrosion and total acidity. In the very corrosive areas between stake Nos. 16,000 and 31,000 and between 156,000 and 164,000 the soils show the highest values for acidity. In certain other areas where few replacements have been made the soils are but slightly acid if at all. In comparing further the data on acidity and replacements it is necessary to take into account the fact previously referred to, that in certain areas replacements have been made necessary by certain incidental factors which are either external to the soil or which were not evaluated by the method used. The lack of correspondence between acidity and replacement between stake Nos. 100,000 and 101,000 would indicate that in this region well drained but highly acid sandy soils are probably not corrosive.

Although the values for acidity may be considered to define the most corrosive areas in a fairly satisfactory manner, it is evident that in small areas of acid soils, the soil at pipe depth frequently shows little if any acidity, indicating a relatively noncorrosive condition. Whether or not marked corrosion has occurred at such points can not be determined, of course, from the replacement data since these data represent the average corrosion which has occurred over intervals of 1,000 feet in which several small noncorrosive areas may occur. In order that the actual corrosiveness of similar areas might not be obscured by variations in acidity at isolated points within the area, it would seem preferable to collect samples of soil from the same stratum or horizon of the soil profile rather than arbitrarily at pipe depth. This procedure would insure that samples of similar soil material would be tested and would probably decrease the number of samples necessary to represent the area.

In testing the corrosiveness of acid soils it is often an advantage to employ methods adapted to the rapid estimation of acidity in the field. Such methods are of especial value in connection with corrosion surveys prior to pipe-line construction. Since the hydrogen ion

concentration of soils in a neutral salt solution is related in a general way to the total acidity as was recognized by Holler, this relation if sufficiently close in the case of the soils under study would permit the use of an alternate method for indicating soil corrosiveness.

The relation which obtains between the total acidity of soils and the pH values of these neutral salt extracts, depends upon the fact that the basic ion of a neutral salt is able to replace ionic hydrogen present in an adsorbed condition in acid soils with the result that the H ion concentration of the extract is increased in proportion to the quantity of H ions replaced. Several factors, such as ease or difficulty of replacement, render this proportionality somewhat inexact. However, in soils which do not differ fundamentally in their characteristics apart from degree of acidity a fairly satisfactory relation between the pH values of the soils in a neutral salt solution and their values for total acidity may be expected. The nature of this relation in the soils under test was studied by plotting the pH values of the soils, determined colorimetrically in normal potassium chloride extracts, against the corresponding values for total acidity. The data are shown graphically in Figure 2.

It will be seen from the figure that the pH values in potassium chloride are fairly closely related to the total acidity of the samples except, of course, in the case of the slightly buffered sands indicated on the diagram by the letter S. In view of this relation, the hydrogen ion concentrations of the potassium chloride extracts should define the corrosive areas along the lines about as well as the total acidity. A figure prepared by plotting these pH values with the average percentage replacement between 1,000-foot intervals showed that this method indicated the corrosive areas about as well as the total acidity method. In areas of well-drained sandy soils, which are generally noncorrosive, the acidity values by either method possess little significance.

IV. RELATION BETWEEN CORROSION LOSSES FROM AN ACCELERATED CORROSION TEST AND CORROSION OF PIPE LINES

Soils which are inherently corrosive toward pipe materials might be expected to produce degrees of corrosion in the laboratory which would bear some relation to their actual corrosiveness in the field. This assumption is the basis of an accelerated test for soil corrosiveness which has been devised by V. A. Grodsky, research associate of the Cast Iron Pipe Research Association, at the National Bureau of Standards. This test, which has been studied in a general way only, was employed in the present investigation to bring out certain of the factors on which the test depends. The data obtained are reported at this time merely because they are in general agreement with the data obtained from the acidity determinations and with the record of pipe replacements.

The method consists in determining the extent to which a steel disk is corroded in moist soil in a period of two weeks. The disk used was cut from cold-rolled sheet steel 0.1 mm (0.004 inch) in thickness, and was of such a size as to fit exactly when placed in a straight-side crystallizing dish about 44 mm (1¾ inches) in diameter. The bottom of the crystallizing dish was covered with a sheet of filter paper

over which was spread a thin layer of soil. After moistening the soil with ½ to 1 ml of water, the previously weighed disk was placed in the dish, and covered with 10 g of soil which had passed a 2 mm

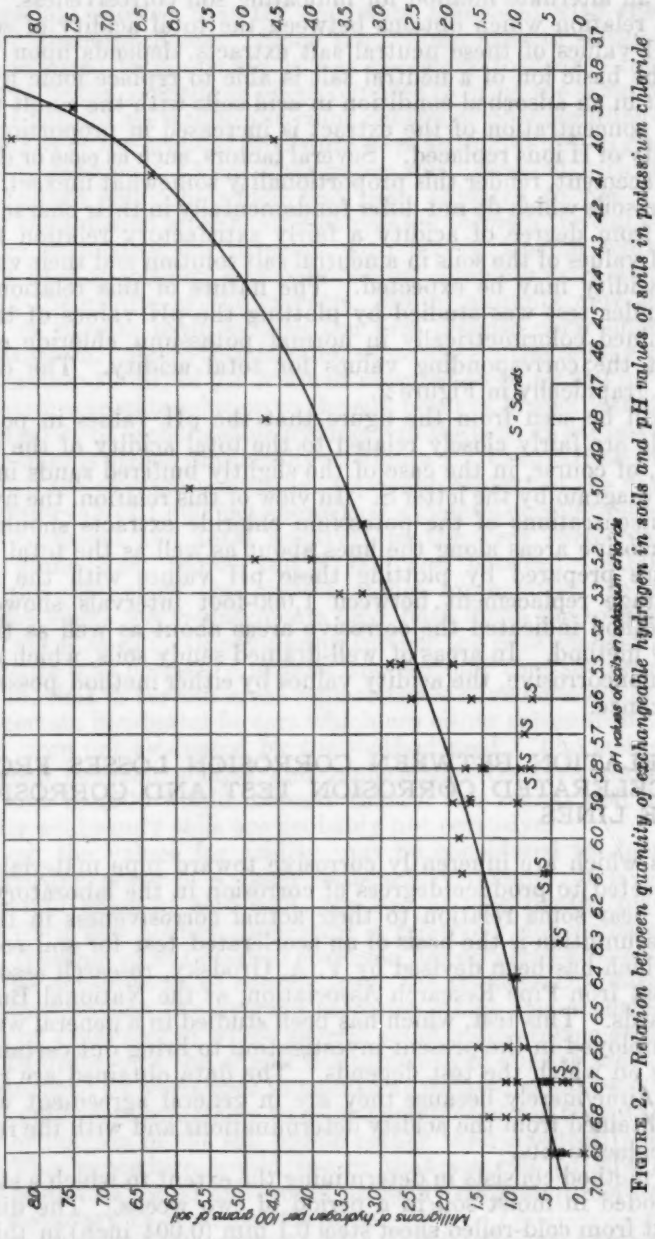

FIGURE 2.—*Relation between quantity of exchangeable hydrogen in soils and pH values of soils in potassium chloride*

sieve. The soil was compacted by rotating on the surface a solid brass cylinder weighing about 500 g. A piece of filter paper was then placed on the soil and the soil was moistened with a definite

quantity of distilled water. A second 10 g portion of soil was added, compacted, and moistened as before. The dish was then placed in a 500 ml (1-pint) preserving jar to which a small quantity of water had been added to maintain a saturated atmosphere, and the jar was sealed and kept at an average temperature of about 30° C. for two weeks. At the end of this period the disk was removed, washed thoroughly, and the rust removed by immersing the disk in a 10 per cent solution of ammonium citrate made alkaline with ammonia. The disk was allowed to remain 5 to 10 minutes in the solution at a temperature of 75° C. Rust which remained in pits was carefully removed by the point of a knife blade. The disk was then wiped dry and weighed. The rate of loss of weight was calculated as penetration in microns per day.

One of the most important factors to be controlled in carrying out the method is the moisture content of the soil, since preliminary studies showed that corrosion of the disks varied markedly with moisture content. In order that the degrees of corrosion caused by soils of different textures would be comparable, it was necessary to add to each soil an amount of water which was determined by the texture of the particular soil. The amount added was that given by the moisture equivalent, which is the percentage of water retained by a soil under a centrifugal force of 1,000 times the force of gravity. The physical significance of the moisture equivalent is that it represents the moisture-holding capacity of field soils when their moisture content is in equilibrium with gravitational and capillary forces. Owing to lack of suitable equipment, the values for the moisture equivalent were directly determined only for a representative group of the soils. In the case of the remaining samples this value was estimated for each soil on the basis of its texture.

In carrying out tests according to this method, a few special precautions were taken. The disks before being weighed were carefully cleaned with emery paper and then with a cloth moistened with ether. In order to avoid abnormal corrosive action from the rapid evolution of carbon dioxide as the result of bacterial activity, a small quantity of toluene was added to each sample. This precaution is probably necessary only in the case of soils containing considerable quantities of calcium carbonate and organic matter.

The data obtained from the accelerated test are shown graphically in Figure 3, together with the data on pipe replacements. It is apparent from the figure that the loss of weight values indicate fairly satisfactorily the corrosive areas except in the area between stake Nos. 26,000 and 31,000 in the soil mapped as Wauseon fine sandy loam. The failure of the accelerated test to indicate corrosiveness in this area may be explained by assuming that relatively coarse-textured soils with a given acidity do not corrode the metal disks to the same extent as heavy-textured soils, such as those of the Brookston and Nappanee series. A further illustration of this possibility is seen in the sandy loam soil at stake No. 100,500. In the presence of relatively high acidity, corresponding to 4.1 mg of hydrogen and pH 5.2 in potassium chloride, the metal disk has been corroded to only a slight extent, namely 1.1 per cent. The fact that the sandy loam soils referred to showed a marked tendency to preserve their state of aggregation when moistened suggests that this effect may also have tended to diminish their corrosive action in the accelerated test.

In order to study further the influence of the acidity and texture on the corrosion of the metal disks, the rates of penetration were plotted

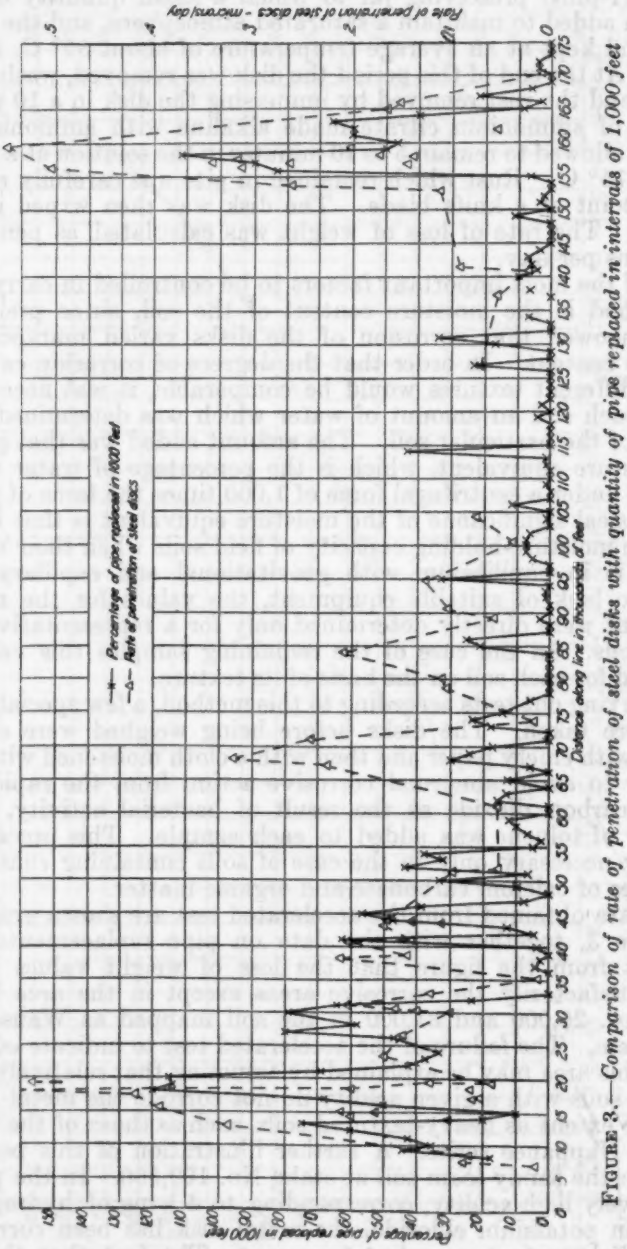
Rate of penetration of steel discs - microns/day
Percentage of pipe replaced in 1000 feet
Rate of penetration of steel discs
Distance along line in thousands of feet
Percentage of pipe replaced in 1000 feet

FIGURE 3.—*Comparison of rate of penetration of steel disks with quantity of pipe replaced in intervals of 1,000 feet*

against the pH values of the soil samples in potassium chloride. The data are shown in Figure 4.

In considering the figure it can be seen that a simple relation does not obtain between the values for rate of penetration and the pH

values in potassium chloride. However, if the texture of the soils is considered, it can be seen that in the case of the fine-textured soils, namely, the clays and clay loams, a rough relation obtains between the rate of penetration and the pH values in potassium chloride; whereas in the case of the coarse soils, the sands and sandy loams, rate of penetration appears to be only slightly influenced by acidity. The distribution of the points between the two trend lines suggests that loss of weight of metal in soils of intermediate texture is influenced by acidity in proportion to the content of fine soil particles.

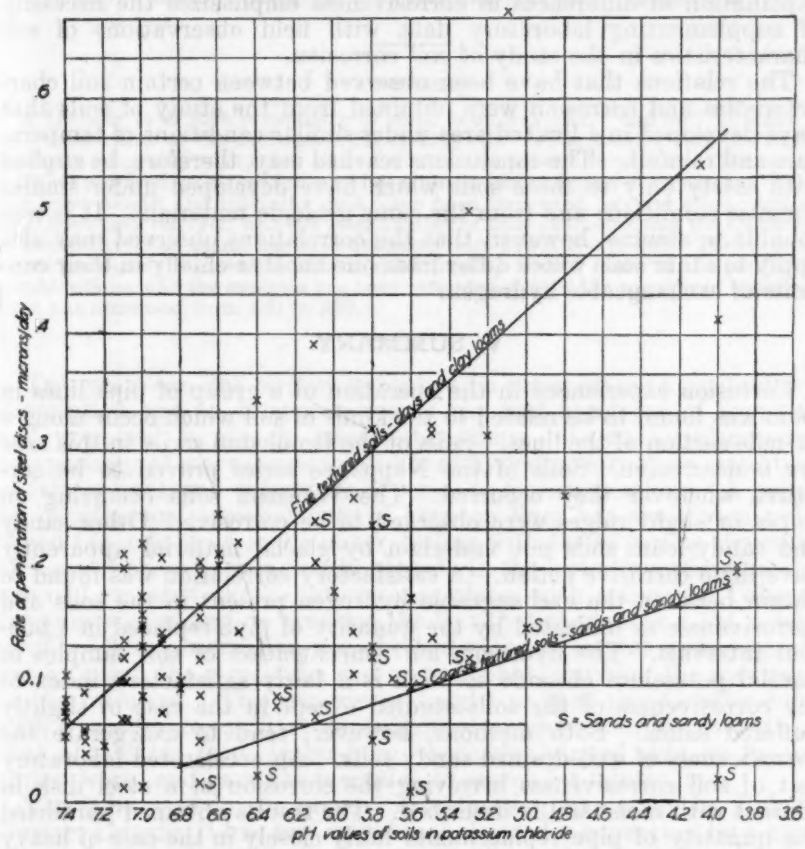
Rate of penetration of steel discs - mm/day
6
5
4
3
2
0.1
0
Fine textured soils - clays and clay loams
Coarse textured soils - sands and sandy loams
S = Sands and sandy loams
7.4 7.2 7.0 6.8 6.6 6.4 6.2 6.0 5.8 5.6 5.4 5.2 5.0 4.8 4.6 4.4 4.2 4.0 3.8 3.6
pH values of soils in potassium chloride

FIGURE 4.—*Relation between rate of penetration of steel disks in soils and pH values of soils in potassium chloride*

Although the acidity methods and the accelerated corrosion tests were equally satisfactory in indicating the corrosiveness of the heavy glacial soils, it has been seen that neither type of test was always dependable in the case of the coarser, sandy soils. It will be recalled that at stake No. 100,500 the acidity methods indicated corrosiveness although few if any replacements have been necessary in this area. Similarly, the loss-of-weight method proved inadequate in the corrosive area between stake Nos. 26,000 and 31,000. Since the soils at both of these locations are equally acid and of about the same texture, it is evident that a third factor in corrosion must be sought.

The essential difference between the corrosive and noncorrosive areas which are not well defined by the laboratory tests is one of drainage. In the noncorrosive area at stake No. 100,500 the soil is well drained. Between stake Nos. 26,000 and 31,000, however, the sandy loam soil overlies at about 30 inches glacial material of a peculiarly dense, compact nature. Owing to its impenetrability to water this material retards drainage to a considerable extent. The combination of the two factors—poor drainage and relatively high acidity—is probably responsible for corrosion in this area. This explanation of differences in corrosiveness emphasizes the necessity of supplementing laboratory data with field observations of soil characteristics in the study of soil corrosion.

The relations that have been observed between certain soil characteristics and corrosion were obtained from the study of soils that have developed in a limited area under similar conditions of temperature and rainfall. The conclusions reached may, therefore, be applied with safety only to those soils which have developed under similar climatic conditions and from the same geologic materials. It is reasonable to assume, however, that the correlations observed may also apply to other soils which differ from one another chiefly in their contents of exchangeable hydrogen.

V. SUMMARY

Corrosion experienced in the operation of a group of pipe lines in Ohio was found to be related to the kinds of soil which occur along a 32-mile section of the lines. Soils of the Brookston series in this area are noncorrosive. Soils of the Nappanee series proved to be corrosive wherever they occurred. The Wauseon soils occurring on slopes or slight ridges were observed to be corrosive. Other sandy and sandy-loam soils not underlain by glacial material apparently have little corrosive action. A satisfactory correlation was found to obtain between the exchangeable hydrogen present in the soils and corrosiveness as indicated by the quantity of pipe replaced in 1,000-foot intervals. The hydrogen ion concentration of soil samples in normal potassium chloride solution is a fairly satisfactory index to the corrosiveness of the soils studied except in the case of slightly buffered sands. Both methods, however, tend to exaggerate the corrosiveness of well-drained sandy soils. An accelerated laboratory test of soil corrosiveness involving the corrosion of a steel disk in contact with moist soil is described. The results obtained paralleled the quantity of pipe replacements fairly closely in the case of heavy soils. The degree of corrosiveness indicated by the test is influenced by the acidity, texture, and probably by the structure of the soils studied. Since only a qualitative study of the factors influencing the test has been made, the test can not at this time be considered a reliable index of soil corrosiveness except in the case of soils similar to those tested. The methods described for identifying corrosive soils which involve determinations of acidity are probably most reliable in the case of related soils which differ from one another chiefly in their contents of exchangeable hydrogen. The data obtained from the tests are probably insufficient to indicate the relative corrosiveness of soils having widely different physical and chemical characteristics.

WASHINGTON, June 17, 1931.

RP364

FURTHER DESCRIPTION AND ANALYSIS OF THE FIRST SPECTRUM OF KRYPTON

By William F. Meggers, T. L. deBruin,[1] and C. J. Humphreys

ABSTRACT

A Geissler tube with a capillary of small bore was used "end on" to make a new description of the first spectrum of krypton. On account of the increased intensity compared with tubes viewed side on this procedure permitted the use of a higher powered spectrograph, and has added a large number of new lines. Thus the wave length and intensity data have been improved, several close pairs of lines have been resolved, and the total number of lines characterizing the spectrum of neutral krypton atoms has been extended from about 200 to 460. The spectral terms previously reported have been confirmed by finding many of the predicted combinations, and the analysis has been extended so that the number of classified lines has increased from 180 to 350.

Two years ago the writers published [2] a paper giving a preliminary description and an interpretation of the first spectrum of krypton, and promised to give in later publications data on interferometer comparisons of wave lengths, studies of hyperfine structure, detection of fainter lines, and extensions of series to higher members. A paper on interference measurements of krypton lines has since been published [3] by one of us, and a paper dealing with the hyperfine structure of some of these lines is now in press.[4] In the latter investigation the use of Lummer-Gehrcke interference plates with a Geissler Tube of krypton viewed end on revealed the fact that the line at 8,104 A was double. This observation was checked with our largest concave grating by using the same tube end on and photographing the spectrum in the infra-red. This experience taught us that this Geissler tube with a small-bore capillary emits light of much greater intensity than that obtainable from larger-bore capillaries viewed side on in our earlier work, and gave the incentive to search for fainter lines.

The tube used in the present investigation was made by Robert Goetze, Leipzig; it has two cylindrical electrodes connected by a capillary of 11 cm length and about 1 mm bore, the viewing end being inclosed in a thin-walled glass bulb of 2.5 cm diameter. To emit the arc spectrum this tube was operated with a. c. transformers in exactly the same manner as described in our first paper. (RP89.) The capillary was placed in position on the axis of the spectrograph with the viewing end directed at the slit, and a condensing lens was interposed to image the capillary bore on the slit. When the discharge passes through the tube a brilliant spot is thus projected on the spectrograph.

[1] Laboratory, "Physica," of the University of Amsterdam.
[2] Meggers, deBruin, and Humphreys, B. S. Jour. Research, vol. 3 (RP89), p. 129; 1929.
[3] Humphreys, B. S. Jour. Research, vol. 5 (RP245), p. 1041; 1930.
[4] Humphreys, B. S. Jour. Research, vol. 7 (RP351), p. —; 1931.

The great increase in light intensity obtained with this end-on tube resulted in a twofold improvement in the description of the Kr I spectrum; it made possible the observation of a large number of fainter lines and permitted their observation with a more powerful spectrograph. Whereas our preliminary description (RP89) was based almost entirely on spectrograms made in the first order of a concave grating with 7,500 lines per inch giving a scale of 10.4 A/mm, the new observations have been made from 3,200 to 9,000 A with a similar grating ruled 20,000 lines per inch giving a scale of 3.7 A/mm in the first order spectrum. Increasing the dispersion and resolving power by a factor of 3 has made it possible to obtain greater accuracy in the wave-length measurements, and has, furthermore, permitted the separation of close lines. These observations with the larger grating were supplemented by exposures to the spectrographs described in our first paper (RP89); the Hilger E_1 quartz spectrograph being used in the ultra-violet, and the Anderson grating in the infra-red. The duration of exposure for making spectrograms ranged from 4 to 24 hours.

Wave-length measurements were made relative to international secondary standards in the arc spectrum of iron. The values from each spectrogram were compared with the interference measurements (RP245), and in a few cases where systematic differences were noted corrections of 0.01 or 0.02 A were applied to the grating values to bring them to the same scale as the interferometer values. When the results were compiled we had more than 1,000 lines ranging in wave length from 3,064 to 9,856 A, but less than half of these are recognized as characteristic of neutral krypton atoms, the remainder being ascribable to ionized atoms and to impurities. Although the Geissler tube was filled with krypton gas of high purity, 50 lines due to argon were recognized in the spectrum, and 5 faint lines were identified with xenon. By far the most troublesome impurity was a trace of water vapor which gives several hundred lines ranging in wave length from 3,064 to about 4,000 A, making it especially difficult to find the fainter members of the principal series of Kr I having a theoretical limit near 3,100 A. These same fine lines were encountered in our earlier work (RP89) and it was suspected that the group beginning at 3,064 A might be identifiable with water vapor. This suspicion has now been confirmed by measurements which agree with those of Grebe and Holtz [5] who remark that the appearance of water vapor bands is a common occurrence in Geissler tubes. The bands are ascribed to the OH molecule by Watson[6] who has analyzed their structure.

A considerable number of lines observed with the end-on krypton tube were found to be greatly enhanced when the tube was operated with a condensed discharge and series spark gap, thus proving that they belong to ionized krypton atoms. In this respect the end-on tube is at a disadvantage; the side-on tubes used in our earlier work showed hardly a trace of spark lines when operated with uncondensed discharges.

Still another difficulty was met with in preparing a new list of true Kr I lines. When an imperfect grating is used to record long exposures to an intense source of sharp spectral lines it is not unusual

[5] Grebe and Holtz. Annalen der Physik. 39, p. 1243; 1912.
[6] Watson, Astrophys. J. 60, p 145; 1924.

to find a family of Rowland ghosts accompanying each strong line, and sometimes obscuring real lines. The Anderson grating is almost completely free from this trouble, but the Rowland grating used for making most of the new observations showed from 2 to 16 symmetrically placed ghosts on all lines ranging from 20 to 2,000 in our scale of estimated intensities.

After all spurious and impurity lines were removed about 460 lines remain to describe the first spectrum of krypton. These are presented in Table 3, in which the measured wave length, estimated intensity, vacuum wave number, and term combination appear in successive columns. Wave lengths of the stronger lines which have been measured by interferometer comparisons with neon standards are quoted from the paper already referred to. (RP245.) Since this new list contains more than twice the number of lines given in our preliminary description (RP89) and includes more than 200 fainter lines it has been necessary to revise the earlier estimates of relative intensity. For lines common to both lists, the present intensity estimates are from 5 to 10 times greater than before.

An entirely new term table has been prepared. The numerical values of terms already reported remain essentially unchanged, but the increased precision of the measurements, the fact that most of the series have been extended and several new series discovered, and new interpretations placed upon a few of the terms has made advisable this revision of the term table. Table 2 contains the new term values and effective quantum numbers. The absolute value of the terms was fixed as before by determining the limit of the series $2p_0 - md'_4$. The calculation is presented in Table 1. The Rydberg constant for krypton has been recalculated using the value of R_∞, 109,737.42, given by Birge,[7] and is now given as 109,736.695. The use of this value in connection with the new wave length measurements leads to a value of $1s_5$ equal to 32,943.165 as against 32,943.47 given in the previous paper. As far as possible the relative term values were fixed by interferometer measurements. The term values given in the report on the interference measurements (RP245) have been incorporated in the new term table with the displacement necessary to make them conform to the new value of $1s_5$. These include the $1s$, $2p$, and $3p$ terms and can be given to three decimal places. A number of additional terms for which the relative values can be completely determined from combination lines measured by interference methods are given to the thousandth of a wave number unit.

[7] Birge, Phys. Rev. Supplement 1, p. 49; 1929.

TABLE 1.—*Determination of absolute term values in Kr I*

$2p_9 - md'_4$ $(5p^5D_3 - 5d^5F_4)$

$$\nu = A - \frac{R}{[m+\mu+\alpha(A-\nu)]^2}$$

$R_{Kr} = 109{,}736.695$
$A = 20{,}620.504$
$\mu = +0.5985937937$
$\alpha = +0.000004625591474$

m	Int.	λ_{obs}	ν_{obs}	$\nu_{calc.}$	$\nu_{calc.} - \nu_{obs}$
2				5, 225. 061	
3	30	8, 104. 02	12, 336. 17	12, 324. 425	−11. 74
4	200	6, 456. 293	15, 484. 493	15, 484. 493	00
5	100	5, 832. 85	17, 139. 54	17, 139. 54	00
6	40	5, 520. 52	18, 109. 22	18, 109. 073	−. 15
7	20	5, 339. 13	18, 724. 45	18, 724. 307	−. 14
8	5	5, 223. 57	19, 138. 68	19, 138. 652	−. 03
9	2*h*	5, 145. 04	19, 430. 80	19, 430. 80	00
10	2*h*	5, 089. 12	19, 644. 30	19, 644. 424	+1. 12

$1s_5 - 2p_9 = 12{,}322.661$
$2p_9 = 20{,}620.504$
$\therefore 1s_5 = 32{,}943.165$

TABLE 2.—*Terms and effective q*

Electron	j	Term, Paschen notation		1		2		3		4		5
p	0	p_0	112, 914. 17 =13. 930 volts									
s	2	s_5		32, 943. 165	1. 8252	(13, 500±)		7, 267. 421	3. 8858	4, 589. 89	4. 8896	3, 162. 96
	1	s_4		31, 998. 139	1. 8519	13, 023	2. 9028	7, 144. 21	3. 9192	4, 541. 83	4. 9154	3, 135. 59
	0	s_3		27, 723. 281	1. 8221	8, 393. 307	2. 8278					
	1	s_2		27, 068. 192	1. 8404	8, 027. 588	2. 8662					
p	1	p_{10}				21, 746. 389	2. 2464	10, 027. 695	3, 3081	5, 909. 57	4. 3092	3, 832. 19
	3	p_9				20, 620. 503	2. 3069	9, 799. 251	3. 3464	5, 773. 85	4. 3596	3, 811. 84
	2	p_8				20, 607. 524	2. 3076	9, 793. 745	3. 3474	5, 774. 13	4. 3595	3, 809. 12
	1	p_7				19, 950. 507	2. 3453	9, 601. 415	3. 3807	5, 693. 60	4. 3902	3, 765. 35
	2	p_6				19, 791. 563	2. 3547	9, 552. 277	3. 3894	5, 668. 23	4. 4000	3, 754. 04
	0	p_5				18, 822. 039	2. 4146	9, 153. 252	3. 4625	5, 504. 54	4. 4649	3, 618. 73
	1	p_4				15, 318. 979	2. 3053	4, 476. 620	3. 3452			
	1	p_3				14, 995. 746	2. 3236	4, 400. 695	3. 3582			
	2	p_2				14, 969. 727	2. 3250	4, 347. 112	3. 3675			
	0	p_1				14, 059. 824	2. 3790	4, 093. 310	3. 4125			
f	1	X								6, 949. 58	3. 9737	4, 434. 16
	2	Y								6, 893. 56	3. 9898	4, 443. 788
	2	Z								6, 950. 38	3. 9735	4, 411. 23
d	0	d_6								8, 841. 431	3. 5230	5, 311. 28
	1	d_5						13, 267	2. 8760	9, 113. 135	3. 4701	5, 238. 73
	4	d'_4								8, 284. 33	3. 6395	5, 136. 010
	2	d_3								7, 907. 660	3. 7252	5, 117. 98
	3	d_4								7, 998. 424	3. 7040	5, 037. 988
	2	d_1''								7, 751. 41	3. 7626	4, 922. 09
	3	d_1'								9, 213. 47	3. 4512	4, 868. 55
	1	d_2								7, 266. 47	3. 8861	4, 656. 11
	1	s_1'						7, 768. 55	2. 8944	2, 811. 65	3. 6712	
	2	s_1''						9, 472. 21	2. 7228	2, 792. 82	3. 6756	
	3	s_1'''						9, 648. 50	2. 7067	2, 884. 61	3. 6550	
	2	s_1''''								3, 609. 76	3. 5036	

quantum numbers of Kr I

m = 6			7		8		9		10		11	
5. 8902	2, 306. 57	6. 8975	1, 760. 51	7. 8951	1, 387. 08	8. 8946						
5. 9158	2, 295. 92	6. 9135	1, 744. 08	7. 9322	1, 374. 03	8. 9367						
5. 3512	2, 734. 83	6. 3345	2, 042. 48	7. 3299								
5. 3655	2, 705. 35	6. 3689	2, 019. 12	7. 3722	1, 564. 98	8. 3738						
5. 3674	2, 705. 06	6. 3692										
5. 3984	2, 680. 06	6. 3989										
5. 4066	2, 672. 08	6. 4084	1, 998. 84	7. 4095	1, 550. 40	8. 4131						
5. 5068	2, 606. 77	6. 4882	1, 958. 67	7. 4851	1, 524. 57	8. 4840						
4. 9747	3, 078. 62	5. 9703	2, 259. 64	6. 9688	1, 727. 10	7. 9711						
4. 9693	3, 105. 74	5. 9442										
4. 9877	3, 062. 61	5. 9859	2, 249. 49	6. 9845								
4. 5455	3, 583. 95	5. 5334	2, 624. 55	6. 4662	1, 981. 54	7. 4417	1, 502. 47	8. 5462	1, 206. 59	9. 5367		
4. 5768	3, 571. 95	5. 5427	2, 579. 23	6. 5228	1, 911. 91	7. 5760	1, 486. 34	8. 5925	1, 196. 75	9. 5758		
4. 6224	3, 480. 96	5. 6147	2, 511. 28	6. 6104	1, 896. 05	7. 6077	1, 481. 82	8. 6055	1, 189. 70	9. 6041	976. 20	10. 6024
4. 6305	3, 539. 56	5. 5680	2, 402. 13	6. 7589	1, 867. 81	7. 6650	1, 469. 52	8. 6415	1, 183. 77	9. 6281		
4. 6671	3, 443. 43	5. 6452	2, 444. 00	6. 7008			1, 464. 48	8. 6564	1, 178. 05	9. 6515	968. 00	10. 6472
4. 7215	3, 387. 34	5. 6918	2, 418. 23	6. 7364	1, 843. 46	7. 7154	1, 447. 56	8. 7068				
4. 7476	3, 335. 88	5. 7355	2, 406. 81	6. 7527	1, 835. 85	7. 7314	1, 440. 83	8. 7271	1, 160. 56	9. 7239		
4. 8547	3. 226. 14	5. 8322	2, 400. 86	6. 7607	1, 810. 54	7. 7852						

TABLE 3.—*List of Kr I lines*

Intensity	Wave length	Wave number	Comb.
1	3, 184. 53	31, 392. 76	$1s_5$–$8p_6$
1	3, 186. 01	31, 378. 18	$1s_5$–$8p_{8,9}$
2	3, 230. 68	30, 944. 33	$1s_5$–$7p_6$
2	3, 232. 80	30, 924. 04	$1s_5$–$7p_{8,9}$
1	3, 257. 10	30, 693. 34	$1s_5$–$7Z$
$1h$	3, 258. 00	30, 684. 86	$1s_5$–$7X$
1	3, 280. 59	30, 473. 57	$1s_4$–$8p_5$
10	3, 302. 54	30, 271. 04	$1s_5$–$6p_6$ $1s_4$–$8X$
7	3, 306. 17	30, 237. 81	$1s_5$–$6p_{8,9}$
2—	3, 328. 00	30, 039. 47	$1s_4$–$7p_5$
1—	3, 332. 47	29, 999. 17	$1s_4$–$7p_6$
1—	3, 334. 47	29, 981. 18	$1s_4$–$7p_8$
1	3, 337. 17	29, 956. 92	$1s_4$–$7p_{10}$
4	3, 345. 73	29, 880. 28	$1s_5$–$6Z$
2	3, 347. 50	29, 864. 48	$1s_5$–$6X$
2	3, 361. 74	29, 737. 98	$1s_4$–$7X$
5	3, 401. 40	29, 391. 25	$1s_4$–$6p_5$
2	3, 408. 97	29, 325. 99	$1s_4$–$6p_6$
2	3, 409. 89	29, 318. 08	$1s_4$–$6p_7$
1	3, 412. 80	29, 293. 08	$1s_4$–$6p_8$
15	3, 424. 97	29, 189. 00	$1s_5$–$5p_6$
2	3, 426. 27	29, 177. 92	$1s_5$–$5p_7$
2	3, 431. 45	29, 133. 88	$1s_5$–$5p_8$
20	3, 431. 75	29, 131. 33	$1s_5$–$5p_9$
8	3, 434. 16	29, 110. 89	$1s_5$–$5p_{10}$
1	3, 454. 90	28, 936. 14	$1s_4$–$6Z$
3	3, 456. 87	28, 919. 65	$1s_4$–$6X$
2	3, 460. 13	28, 892. 40	$1s_4$–$6Y$
10	3, 495. 99	28, 596. 05	$1s_5$–$3p_2$
20	3, 502. 56	28, 542. 41	$1s_5$–$3p_3$
15	3, 503. 90	28, 531. 50	$1s_5$–$5Z$
3	3, 506. 66	28, 509. 04	$1s_5$–$5X$
3	3, 507. 84	28, 499. 45	$1s_5$–$5Y$
4	3, 511. 91	28, 466. 42	$1s_5$–$3p_4$
15	3, 522. 68	28, 379. 39	$1s_4$–$5p_5$
5	3, 539. 55	28, 244. 14	$1s_4$–$5p_6$
5	3, 540. 97	28, 232. 81	$1s_4$–$5p_7$
3	3, 546. 46	28, 189. 10	$1s_4$–$5p_8$
1	3, 549. 44	28, 165. 44	$1s_4$–$5p_{10}$
20	3, 615. 48	27, 650. 99	$1s_4$–$3p_2$
1	3, 622. 53	27, 597. 18	$1s_4$–$3p_3$
1	3, 623. 84	27, 587. 20	$1s_4$–$5Z$
2	3, 626. 91	27, 563. 85	$1s_4$–$5X$
10	3, 628. 17	27, 554. 28	$1s_4$–$5Y$
4	3, 632. 51	27, 521. 36	$1s_4$–$3p_4$
80	3, 665. 33	27, 274. 93	$1s_5$–$4p_6$
10	3, 668. 74	27, 249. 58	$1s_5$–$4p_7$
100	3, 679. 58	27, 169. 31	$1s_5$–$4p_{8,9}$
6	3, 698. 05	27, 033. 61	$1s_5$–$4p_{10}$

TABLE 3.—*List of Kr I lines*—Continued

Intensity	Wave length	Wave number	Comb.
50	3, 773. 43	26, 493. 59	$1s_4$–$4p_5$
20	3, 796. 88	26, 329. 97	$1s_4$–$4p_6$
30	3, 800. 55	26, 304. 54	$1s_4$–$4p_7$
20	3, 812. 22	26, 224. 02	$1s_4$–$4p_8$
30	3, 837. 81	26, 049. 16	$1s_5$–$4Y$
15	3, 845. 98	25, 993. 82	$1s_5$–$4X$
2	3, 846. 12	25, 992. 88	$1s_5$–$4Z$
1	3, 892. 69	25, 681. 92	$1s_3$–$7p_{10}$
1	3, 915. 16	25, 534. 53	
1	3, 926. 05	25, 463. 71	$1s_3$–$7X$
1	3, 953. 60	25, 286. 27	
6	3, 982. 18	25, 104. 73	$1s_4$–$4Y$
20	3, 991. 08	25, 048. 81	$1s_4$–$4X$
10	3, 991. 25	25, 047. 75	$1s_4$–$4Z$
3	3, 994. 82	25, 025. 34	$1s_2$–$7p_{10}$
2	4, 000. 72	24, 988. 46	$1s_3$–$6p_{10}$
1	4, 028. 03	24, 819. 04	$1s_3$–$7Z$
2	4, 029. 66	24, 809. 00	$1s_3$–$7X$
3	4, 056. 57	24, 644. 43	$1s_3$–$6X$
2	4, 086. 90	24, 461. 54	$1s_3$–$6p_5$
1	4, 097. 84	24, 396. 24	$1s_3$–$6p_6$
3	4, 108. 43	24, 333. 36	$1s_3$–$6p_{10}$
1	4, 139. 04	24, 153. 40	
2	4, 164. 48	24, 005. 85	$1s_3$–$6Z$
5*d*	4, 167. 28	23, 989. 73	$1s_3$–$6X$
3	4, 172. 83	23, 957. 82	$1s_3$–$5p_7$
20	4, 184. 48	28, 891. 12	$1s_3$–$5p_{10}$
20	4, 263. 29	23, 449. 48	$1s_3$–$5p_5$
1, 000	4, 273. 9705	23, 390. 8876	$1s_5$–$3p_6$
100	4, 282. 9686	23, 341. 7469	$1s_5$–$3p_7$
40	4, 286. 4875	23, 322. 5849	$1s_3$–$3p_3$
5	4, 288. 02	23, 314. 25	$1s_2$–$5p_6$
4	4, 290. 78	23, 299. 25	
6	4, 292. 64	23, 289. 16	$1s_3$–$5X$
1	4, 295. 82	23, 271. 92	
50	4, 300. 4877	23, 246. 6602	$1s_3$–$3p_4$
10	4, 302. 45	23, 236. 06	$1s_2$–$5p_{10}$
400	4, 318. 5523	23, 149. 4203	$1s_5$–$3p_8$
1, 000	4, 319. 5798	23, 143. 9137	$1s_5$–$3p_9$
1	4, 340. 84	23, 030. 56	
2	4, 349. 55	22, 984. 44	
1	4, 349. 84	22, 982. 91	
100	4, 351. 3605	22, 974. 8824	$1s_2$–$3p_1$
2	4, 353. 90	22, 961. 48	
2	4, 354. 23	22, 959. 74	
500	4, 362. 6429	22, 915. 4670	$1s_5$–$3p_{10}$
800	4, 376. 1217	22, 844. 8870	$1s_4$–$3p_5$
2	4, 380. 11	22, 824. 09	
200	4, 399. 9675	22, 721. 0802	$1s_2$–$3p_2$
1	4, 406. 76	22, 686. 06	

TABLE 3.—*List of Kr I lines*—Continued

Intensity	Wave length	Wave number	Comb.
50	4, 410. 369	22, 667. 498	$1s_2$–$3p_3$
6	4, 412. 39	22, 657. 11	$1s_2$–$5Z$
20	4, 416. 88	22, 634. 08	$1s_2$–$5X$
1	4, 417. 58	22, 630. 49	
50	4, 418. 769	22, 624. 404	$1s_2$–$5Y$
1	4, 421. 30	22, 611. 45	
100	4, 425. 1909	22, 591. 5728	$1s_2$–$3p_4$
600	4, 453. 9183	22, 445. 8618	$1s_4$–$3p_6$
800	4, 463. 6897	22, 396. 7266	$1s_4$–$3p_7$
600	4, 502. 3546	22, 204. 3931	$1s_4$–$3p_8$
3	4, 538. 06	22, 029. 69	$1s_3$–$4p_7$
40	4, 550. 298	21, 970. 446	$1s_4$–$3p_{10}$
20	4, 636. 14	21, 563. 65	$1s_3$–$4p_5$
10	4, 671. 61	21, 399. 92	$1s_2$–$4p_6$
1	4, 677. 16	21, 374. 53	$1s_2$–$4p_7$
4	4, 694. 84	21, 294. 04	$1s_2$–$4p_8$
3	4, 722. 16	21, 170. 84	
20	4, 724. 89	21, 158. 61	$1s_2$–$4p_{10}$
3	4, 810. 51	20, 782. 03	
40	4, 812. 607	20, 772. 971	$1s_3$–$4X$
4*h*	4, 861. 31	20, 564. 86	
2*h*	4, 861. 84	20, 562. 62	$2p_{10}$–$10d_3$
2*h*	4, 864. 91	20, 549. 64	$2p_{10}$–$10d_5$
1*h*	4, 867. 24	20, 539. 80	$2p_{10}$–$10d_6$
2	4, 910. 39	20, 359. 31	$2p_{10}$–$8s_5$
4*h*	4, 930. 38	20, 276. 77	$2p_{10}$–$9d_3$
4*h*	4, 934. 48	20, 259. 92	$2p_{10}$–$9d_5$
2*h*	4, 938. 38	20, 243. 92	$2p_{10}$–$9d_6$
15	4, 955. 27	20, 174. 92	$1s_2$–$4Y$
20	4, 969. 08	20, 118. 85	$1s_2$–$4X$
15	4, 969. 36	20, 117. 72	$1s_2$–$4Z$
2	5, 002. 14	19, 985. 88	$2p_{10}$–$7s_5$
5	5, 029. 15	19, 878. 55	$2p_{10}$–$8d_3$
7	5, 040. 34	19, 834. 52	$2p_{10}$–$8d_5$
4	5, 058. 08	19, 764. 85	$2p_{10}$–$8d_6$
2*h*	5, 089. 12	19, 644. 30	$2p_9$–$11d_4'$
1*h*	5, 090. 36	19, 639. 52	$2p_8$–$11d_4$
2	5, 109. 81	19, 564. 76	
1	5, 139. 9	19, 450. 23	$2p_{10}$–$6s_4$
4	5, 142. 7	19, 439. 64	$2p_{10}$–$6s_5$
2*h*	5, 145. 04	19, 430. 80	$2p_9$–$10d_4'$
1*h*	5, 145. 39	19, 429. 47	$2p_8$–$10d_4$
1	5, 167. 73	19, 345. 48	$2p_{10}$–$7d_2$
4	5, 168. 06	19, 344. 25	$2p_{10}$–$7d_3$
2	5, 172. 36	19, 328. 16	$2p_{10}$–$7d_1''$
1*h*	5, 197. 82	19, 233. 49	$2p_9$–$8s_5$ $2p_8$–$8s_4$
1	5, 212. 41	19, 179. 66	$2p_9$–$9d_1'$
8	5, 215. 81	19, 167. 16	$2p_{10}$–$7d_5$
1	5, 217. 78	19, 159. 92	$2p_8$–$9d_1''$

TABLE 3.—*List of Kr I lines*—Continued

Intensity	Wave length	Wave number	Comb.
1	5, 218. 84	19, 156. 03	$2p_9$–$9d_4$
3	5, 222. 38	19, 143. 04	$2p_8$–$9d_4$
5	5, 233. 57	19, 138. 68	$2p_9$–$9d_4'$
20	5, 228. 18	19, 121. 84	$2p_{10}$–$7d_6$
2	5, 232. 06	19, 107. 63	
4	5, 274. 61	18, 953. 49	$2p_{10}$–$4s_1''$
9	5, 279. 84	18, 934. 71	$2p_{10}$–$4s_1'$
1	5, 290. 76	18, 895. 63	
2*h*	5, 299. 79	18, 863. 44	$2p_8$–$7s_4$
3	5, 300. 74	18, 860. 06	$2p_9$–$7s_5$
1	5, 304. 43	18, 846. 94	$2p_8$–$7s_5$
2	5, 322. 02	18, 784. 65	$2p_9$–$8d_1'$
1–	5, 325. 70	18, 771. 67	$2p_8$–$8d_1'$
2	5, 327. 87	18, 764. 02	$2p_8$–$8d_1''$
2	5, 331. 08	18, 752. 72	$2p_9$–$8d_3$
10	5, 334. 78	18, 739. 72	$2p_8$–$8d_3$
1	5, 337. 72	18, 729. 40	
20	5, 339. 13	18, 724. 45	$2p_9$–$8d_4'$
2	5, 347. 37	18, 695. 60	$2p_8$–$8d_5$
1*h*	5, 365. 91	18, 631. 00	$2p_6$–$10d_1'$
2	5, 371. 74	18, 610. 78	$2p_{10}$–$5s_4$
15	5, 379. 64	18, 583. 45	$2p_{10}$–$5s_5$
2*h*	5, 403. 03	18, 503. 00	$2p_7$–$9d_1''$
1*h*	5, 409. 44	18, 481. 08	$2p_7$–$9d_3$
1–	5, 445. 43	18, 358. 93	$2p_{10}$–$6d_1''$
3*h*	5, 447. 86	18, 350. 75	$2p_6$–$9d_1'$
2*h*	5, 456. 39	18, 322. 06	$2p_6$–$9d_3$
7	5, 458. 80	18, 313. 97	$2p_9$–$6s_5$
4	5, 459. 47	18, 311. 72	$2p_8$–$6s_4$
1	5, 461. 37	18, 305. 35	$2p_6$–$9d_5$
2	5, 462. 65	18, 301. 06	$2p_8$–$6s_5$
2	5, 476. 58	18, 254. 51	
1	5, 487. 46	18, 218. 32	$2p_9$–$7d_3$
5	5, 488. 86	18, 213. 67	$2p_9$–$7d_1'$
50	5, 490. 94	18, 206. 77	$2p_{10}$–$6d_3$ $2p_7$–$7s_4$
2*h*	5, 491. 33	18, 205. 48	$2p_8$–$7d_2$
1	5, 492. 77	18, 200. 71	$2p_8$–$7d_1'$
3	5, 496. 21	18, 189. 31	$2p_8$–$7d_1''$
50	5, 500. 71	18, 174. 43	$2p_{10}$–$6d_5$
15	5, 504. 02	18, 163. 50	$2p_8$–$7d_4$
20	5, 504. 34	18, 162. 45	$2p_{10}$–$6d_6$
1	5, 511. 16	18, 139. 97	$2p_7$–$8d_2$
20	5, 516. 66	18, 121. 89	$1s_3$–$3p_7$
40	5, 520. 52	18, 109. 22	$2p_9$–$7d_4'$
3	5, 521. 17	18, 107. 09	$2p_7$–$8d_1''$
1	5, 522. 18	18, 103. 78	
2–	5, 528. 63	18, 082. 66	$2p_7$–$8d_3$
1*h*	5, 539. 4	18, 047. 50	$2p_8$–$7s_4$
1*h*	5, 544. 4	18, 031. 22	$2p_5$–$7s_5$
500	5, 562. 2251	17, 973. 4381	$1s_5$–$2p_2$

TABLE 3.—*List of Kr I lines*—Continued

Intensity	Wave length	Wave number	Comb.
2, 000	5, 570. 2890	17, 947. 4190	$1s_5$–$2p_3$
2	5, 573. 13	17, 938. 27	$1s_4$–$2p_1$
10	5, 575. 6	17, 930. 32	
3*h*	5, 577. 64	17, 923. 77	$2p_6$–$8d_3$
80	5, 580. 39	17, 914. 93	$1s_2$–$3p_5$
1*h*	5, 581. 34	17, 911. 88	
2	5, 591. 41	17, 879. 62	$2p_6$–$8d_5$
1	5, 606. 74	17, 830. 74	
1	5, 607. 72	17, 827. 62	$2p_9$–$4s_1''$
3	5, 608. 37	17, 825. 56	
4	5, 611. 82	17, 814. 60	$2p_8$–$4s_1''$
1	5, 643. 04	17, 716. 04	
100	5, 649, 5627	17, 695, 5863	$1s_3$–$3p_{10}$
3	5, 662. 67	17, 654. 63	$2p_7$–$6s_4$
1	5, 666. 09	17, 643. 97	$2p_7$–$6s_5$
50	5, 672. 45	17, 624. 19	$1s_5$–$2p_4$
3—	5, 696. 54	17, 549. 66	$2p_7$–$7d_2$
1	5, 696. 95	17, 548. 39	$2p_7$–$7d_3$
10	5, 702. 19	17, 532. 27	$2p_7$–$7d_1''$
40	5, 707. 51	17, 515. 93	$1s_2$–$3p_6$
2	5, 714. 11	17, 495. 70	$2p_6$–$6s_4$
3	5, 717. 61	17, 484. 99	$2p_6$–$6s_5$
10	5, 721. 88	17, 471. 94	$2p_5$–$5s_4$
15	5, 723. 56	17, 466. 81	$1s_2$–$3p_7$
20	5, 726. 59	17, 457. 57	$2p_9$–$5s_5$
4	5, 730. 86	17, 444. 56	$2p_5$–$5s_5$
5	5, 749. 02	17, 389. 46	$2p_6$–$7d_3$
10	5, 750. 57	17, 384. 77	$2p_6$–$7d_1'$
1	5, 754. 33	17, 373. 41	$2p_6$–$7d_1''$
2	5, 755. 04	17, 371. 27	$2p_7$–$7d_5$
4	5, 762. 90	17, 347. 58	$2p_6$–$7d_4$
2	5, 775. 56	17, 309. 55	
10	5, 783. 89	17, 284. 62	$2p_9$–$6d_1$
6	5, 787. 29	17, 274. 47	$1s_2$–$3p_8$
7	5, 788. 24	17, 271. 63	$2p_6$–$6d_1'$
2	5, 801. 17	17, 233. 13	$2p_9$–$6d_1''$
20	5, 805. 53	17, 220. 19	$2p_8$–$6d_1''$
8	5, 810. 80	17, 204. 58	$2p_{10}$–$4s_4$
1	5, 814. 29	17, 194. 25	
1	5, 818. 97	17, 180. 42	
15	5, 820. 10	17, 177. 08	$2p_9$–$6d_4$
3	5, 823. 51	17, 167. 03	$2p_6$–$7d_6$
40	5, 824. 50	17, 164. 11	$2p_5$–$6d_4$
20	5, 827. 07	17, 156. 54	$2p_{10}$–$4s_5$
100	5, 832. 85	17, 139. 54	$2p_9$–$6d_4'$
1	5, 843. 29	17, 108. 92	
1	5, 849. 12	17, 091. 86	
2	5, 849. 66	17, 090. 28	$2p_{10}$–$5d_2$
5	5, 852. 86	17, 080. 94	$2p_9$–$6d_3$
1	5, 857. 32	17, 067. 93	$2p_6$–$6d_3$

TABLE 3.—*List of Kr I lines*—Continued

Intensity	Wave length	Wave number	Comb.
50	5, 866. 74	17, 040. 53	$1s_2$–$3p_{10}$
3, 000	5, 870. 9153	17, 028. 4108	$1s_4$–$2p_2$
50	5, 879. 89	17, 002. 42	$1s_4$–$2p_3$
2	5, 881. 18	16, 998. 69	$2p_6$–$4s_1''$
3	5, 887. 68	16, 979. 92	$2p_8$–$4s_1'$
2	5, 942. 13	16, 824. 33	$2p_{10}$–$5d_1''$
5	5, 945. 44	16, 814. 97	$2p_7$–$5s_4$
2	5, 955. 14	16, 787. 59	$2p_7$–$5s_5$
4	5, 977. 65	16, 724. 36	$2p_7$–$6d_2$
60	5, 993. 8500	16, 679. 1585	$1s_4$–$2p_4$
3	6, 002. 19	16, 655. 98	$2p_8$–$5s_4$
50	6, 012. 111	16, 628. 499	$2p_{10}$–$5d_3$ $2p_8$–$5s_5$
15	6, 035. 82	16, 563. 18	$2p_8$–$6d_1''$
60	6, 056. 11	16, 507. 69	$2p_{10}$–$5d_5$
20	6, 075. 24	16, 455. 71	$2p_8$–$6d_1'$
40	6, 082. 85	16, 435. 12	$2p_{10}$–$5d_3$
2	6, 088. 00	16, 421. 22	$2p_5$–$7d_2$
6	6, 091. 81	16, 410. 95	$2p_7$–$6d_3$
2	6, 094. 31	16, 404. 22	$2p_8$–$6d_1''$
1	6, 103. 86	16, 378. 55	$2p_8$–$6d_5$
3	6, 108. 34	16, 366. 54	$2p_7$–$6d_6$
3	6, 115. 23	16, 348. 10	$2p_8$–$6d_4$
20	6, 151. 38	16, 252. 02	$2p_6$–$6d_3$
7	6, 163. 65	16, 219. 68	$2p_8$–$6d_5$
2	6, 172. 08	16, 197. 52	$2p_5$–$7d_6$
20	6, 222. 71	16, 065. 73	$2p_5$–$4s_4$
30	6, 236. 34	16, 030. 62	$2p_9$–$4s_5$
10	6, 241. 39	16, 017. 65	$2p_5$–$4s_5$
2	6, 267. 33	15, 951. 36	$2p_5$–$5d_2$
20	6, 346. 66	15, 751. 97	$2p_9$–$5d_1'$
8	6, 351. 90	15, 738. 98	$2p_5$–$5d_1'$
4	6, 368. 26	15, 698. 55	$2p_9$–$5d_1''$
1	6, 373. 19	15, 686. 40	$2p_5$–$5s_4$
30	6, 373. 58	15, 685. 44	$2p_5$–$5d_1''$
5	6, 410. 17	15, 595. 91	$2p_5$–$6d_2$
20	6, 415. 65	15, 582. 59	$2p_9$–$5d_4$
100	6, 421. 028	15, 569. 536	$2p_5$–$5d_4$
10	6, 448. 78	15, 502. 53	$2p_9$–$5d_3$
1	6, 454. 19	15, 489. 54	$2p_5$–$5d_3$
200	6, 456. 293	15, 484. 493	$2p_9$–$5d_4'$
15	6, 488. 07	15, 408. 65	$2p_7$–$4s_4$
10	6, 504. 89	15, 368. 81	$2p_5$–$5d_5$
3	6, 508. 37	15, 360. 59	$2p_7$–$4s_5$
8	6, 536. 55	15, 294. 37	$2p_7$–$5d_2$
2	6, 555. 56	15, 250. 02	$2p_6$–$6d_5$
6	6, 555. 69	15, 249. 72	$2p_6$–$4s_4$
20	6, 576. 42	15, 201. 65	$2p_7$–$4s_5$
2	6, 605. 12	15, 135. 60	$2p_6$–$5d_2$
2–	6, 612. 38	15, 118. 98	

TABLE 3.—*List of Kr I lines*—Continued

Intensity	Wave length	Wave number	Comb.
40	6, 652. 24	15, 028. 39	$2p_7$–$5d_1''$
1	6, 691. 43	14, 940. 37	
60	6, 699. 23	14, 922. 98	$2p_6$–$5d_1'$
4	6, 723. 36	14, 869. 42	$2p_6$–$5d_1''$
20	6, 740. 10	14, 832. 49	$2p_7$–$5d_3$
3	6, 776. 15	14, 753. 56	$2p_6$–$5d_4$
4	6, 795. 40	14, 711. 78	$2p_7$–$5d_5$
50	6, 813. 10	14, 673. 56	$2p_6$–$5d_3$
8	6, 829. 09	14, 639. 21	$2p_7$–$5d_6$
20	6, 846. 40	14, 602. 19	$2p_{10}$–$3s_4$
2	6, 853. 32	14, 587. 45	
1	6, 860. 04	14, 573. 16	
3	6, 862. 82	14, 567. 26	
1	6, 866. 89	14, 558. 62	
20	6, 869. 63	14, 552. 82	$2p_6$–$5d_5$
15	6, 904. 22	14, 479. 91	$2p_{10}$–$4d_2$
100	6, 904. 68	14, 478. 94	$2p_{10}$–$3s_5$
1*h*	6, 935. 30	14, 415. 02	
1	6, 988. 51	14, 305. 26	
2	6, 993. 05	14, 296. 98	
1	6, 995. 52	14, 290. 93	
7	7, 000. 79	14, 280. 17	$2p_5$–$4s_4$
2	7, 001. 62	14, 278. 47	
1	7, 004. 29	14, 273. 03	
2	7, 008. 62	14, 264. 21	
1	7, 011. 31	14, 258. 74	
1	7, 041. 86	14, 198. 25	
1	7, 048. 89	14, 182. 72	
10	7, 057. 27	14, 165. 88	$2p_5$–$5d_2$
1	7, 085. 47	14, 109. 51	
1*h*	7, 089. 51	14, 101. 47	
8	7, 143. 45	13, 994. 99	$2p_{10}$–$4d_1''$
5	7, 152. 21	13, 977. 84	$2p_{10}$–$3s_1'$
3	7, 180. 47	13, 922. 83	
2*h*	7, 200. 59	13, 883. 93	
100	7, 224. 109	13, 838. 729	$2p_{10}$–$4d_3$
2	7, 227. 34	13, 832. 55	
2	7, 234. 58	13, 818. 70	
1	7, 252. 70	13, 784. 18	
1	7, 259. 95	13, 770. 41	
80	7, 287. 262	13, 718. 801	$2p_{10}$–$2s_2$
5	7, 301. 25	13, 692. 52	
1	7, 316. 01	13, 664. 89	
1	7, 319. 69	13, 658. 02	
1	7, 322. 03	13, 653. 66	
5	7, 327. 00	13, 644. 40	
1	7, 333. 82	13, 631. 71	
4	7, 334. 33	13, 630. 76	
2	7, 341. 16	13, 618. 08	
1	7, 341. 66	13, 617. 15	

TABLE 3.—*List of Kr I lines*—Continued

Intensity	Wave length	Wave number	Comb.
1	7, 344. 41	13, 612. 05	
1	7, 345. 34	13, 610. 33	
1	7, 348. 10	13, 605. 22	
4	7, 355. 48	13, 591. 57	
5	7, 359. 96	13, 583. 29	$2p_5$–$5d_5$
1	7, 360. 65	13, 582. 02	
4	7, 362. 83	13, 578. 00	
2*h*	7, 366. 80	13, 570. 68	
2*h*	7, 367. 02	13, 570. 28	
1	7, 370. 18	13, 564. 46	
1	7, 373. 86	13, 557. 69	
1	7, 392. 39	13, 523. 70	
1	7, 399. 82	13, 510. 12	
1*h*	7, 402. 70	13, 504. 87	
60	7, 425. 54	13, 463. 33	$2p_8$–$3s_4$
1*h*	7, 427. 61	13, 459. 58	
3*h*	7, 465. 01	13, 392. 14	
100	7, 486. 850	13, 353. 082	$2p_{10}$–$2s_3$ $2p_9$–$3s_5$
20	7, 493. 58	13, 341. 09	$2p_8$–$4d_2$
30	7, 494. 15	13, 340. 07	$2p_8$–$3s_5$
3	7, 543. 10	13, 253. 50	
3	7, 550. 63	13, 240. 29	
1, 000	7, 587. 4135	13, 176. 0999	$1s_6$–$2p_5$
2, 000	7, 601. 5465	13, 151. 6027	$1s_5$–$2p_6$
1	7, 615. 64	13, 127. 27	$2p_4$–$4s_1''$
1	7, 620. 63	13, 118. 67	
1	7, 628. 24	13, 105. 58	
1	7, 639. 55	13, 086. 18	
3*h*	7, 652. 16	13, 064. 61	
2	7, 663. 75	13, 044. 86	
400	7, 685. 2472	13, 008. 3682	$1s_2$–$2p_1$
500	7, 694. 5401	12, 992. 6577	$1s_5$–$2p_7$
2	7, 703. 35	12, 977. 79	
10	7, 741. 37	12, 914. 06	
50	7, 746. 831	12, 904. 958	$2p_{10}$–$4d_5$
1	7, 767. 29	12, 870. 97	
2	7, 768. 42	12, 869. 09	$2p_9$–$4d_1''$
2	7, 772. 42	12, 862. 47	
15	7, 776. 27	12, 856. 10	$2p_8$–$4d_1''$
1	7, 786. 65	12, 838. 96	$2p_8$–$3s_1'$
15	7, 806. 52	12, 806. 29	$2p_7$–$3s_4$
1	7, 830. 22	12, 767. 53	
3*h*	7, 840. 17	12, 751. 32	
200	7, 854. 823	12, 727. 535	$1s_3$–$2p_3$
3	7, 863. 91	12, 712. 82	$2p_9$–$4d_3$
1	7, 871. 92	12, 699. 89	$2p_8$–$4d_3$
5	7, 881. 77	12, 684. 02	$2p_7$–$4d_2$
2	7, 882. 36	12, 683. 07	$2p_7$–$3s_5$
4	7, 904. 63	12, 647. 34	$2p_6$–$3s_4$

TABLE 3.—*List of Kr I lines*—Continued

Intensity	Wave length	Wave number	Comb.
50	7, 913. 443	12, 633. 254	$2p_{10}$–$4d_5$
6	7, 920. 46	12, 622. 06	$2p_9$–$4d_4$
40	7, 928. 602	12, 609. 100	$2p_8$–$4d_4$
1	7, 938. 69	12, 593. 07	$2p_9$–$2s_2$
3	7, 946. 98	12, 579. 94	$2p_8$–$2s_2$
1	7, 981. 26	12, 525. 91	$2p_8$–$4d_2$
10	7, 982. 37	12, 524. 17	$2p_6$–$3s_5$
1	7, 993. 17	12, 507. 25	$2p_4$–$4s_1'$
2	8, 026. 38	12, 455. 50	
100	8, 059. 5053	12, 404. 3030	$1s_3$–$2p_4$
30	8, 104. 02	12, 336. 17	$2p_9$–$4d_4'$
200	8, 104. 3660	12, 335. 6408	$1s_5$–$2p_8$
500	8, 112. 9023	12, 322, 6615	$1s_5$–$2p_9$
2	8, 132. 96	12, 292. 27	
1*h*	8, 144. 99	12, 274. 12	$2p_{10}$–$3s_1''$
1*h*	8, 175. 04	12, 229. 00	
300	8, 190. 0570	12, 206. 5759	$1s_4$–$2p_6$
2	8, 192. 31	12, 203. 22	$2p_8$–$4s_1''$
15	8, 195. 08	12, 199. 09	$2p_7$–$4d_1''$
1	8, 199. 39	12, 192. 68	
1	8, 205. 14	12, 184. 14	$2p_3$–$4s_1'$
2	8, 206. 59	12, 181. 98	$2p_7$–$3s_1'$
1	8, 209. 54	12, 177. 61	$2p_5$–$4s_1''$
2	8, 218. 39	12, 164. 49	
1	8, 222. 68	12, 158. 15	$2p_2$–$4s_1'$
1	8, 228. 83	12, 149. 06	
400	8, 263. 2412	12, 098. 4676	$1s_2$–$2p_2$
20	8, 272. 37	12, 085. 12	$2p_5$–$4s_1'''$
1	8, 277. 41	12, 077. 76	
200	8, 281. 06	12, 072. 43	$1s_3$–$2p_3$
1	8, 287. 56	12, 062. 96	
500	8, 298. 1091	12, 047. 6312	$1s_4$–$2p_7$
5	8, 301. 38	12, 042. 88	$2p_7$–$4d_3$
2	8, 303. 18	12, 040. 27	$2p_6$–$4d_1''$
1	8, 351. 42	11, 970. 73	
2	8, 384. 87	11, 922. 97	$2p_7$–$2s_2$
1	8, 386. 61	11, 920. 50	
10	8, 412. 45	11, 883. 88	$2p_6$–$4d_3$
2	8, 498. 18	11, 764. 00	$2p_6$–$2s_2$
200	8, 508. 8736	11, 749. 2128	$1s_3$–$2p_4$
3	8, 537. 92	11, 709. 24	$2p_4$–$4s_1''''$
3	8, 560. 88	11, 677. 84	$2p_5$–$3s_4$
2	8, 568. 94	11, 666. 86	
2	8, 605. 83	11, 616. 84	
1	8, 651. 29	11, 555. 80	$2p_5$–$4d_2$
1	8, 667. 94	11, 533. 60	
3	8, 697. 54	11, 494. 35	$2p_5$–$4d_5$
1	8, 755. 15	11, 418. 72	
8	8, 764. 11	11, 407. 04	$2p_9$–$4d_1'$
1	8, 773. 02	11, 395. 46	

TABLE 3.—*List of Kr I lines*—Continued

Intensity	Wave length	Wave number	Comb.
10	8, 774. 10	11, 394. 05	$2p_8$–$4d_1'$
300	8, 776. 7898	11, 390. 6150	$1s_4$–$2p_8$
2	8, 780. 33	11, 385. 97	$2p_3$–$4s_1''''$
200	8, 928. 6934	11, 196. 7764	$1s_5$–$2p_{10}$
1	8, 967. 52	11, 148. 30	$2p_9$–$3s_1''$
3	8, 977. 95	11, 135. 35	$2p_8$–$3s_1''$
2	8, 999. 11	11, 109. 16	$2p_7$–$4d_6$
1	9, 111. 66	10, 971. 94	$2p_9$–$3s_1'''$
1	9, 243. 62	10, 815. 31	
2	9, 352. 12	10, 689. 83	
2	9, 362. 10	10, 678. 44	$2p_6$–$4d_5$
5	9, 751. 71	10, 251. 84	$1s_4$–$2p_{10}$
1	9, 856. 19	10, 143. 13	$2p_6$–$3s_1'''$

The term sequences formerly designated by md_2 and ms are now interpreted as the extensions of the ms_4 and ms_5 series, respectively. The term 8,393.307 is now designated as $2s_3$ instead of $4d_6$. This choice makes the difference $2s_3-2s_2$ smaller than $1s_3-1s_2$ as it should be. The new term 8,841.431 at first thought to be $2s_3$ is interpreted as $4d_6$. This assignment makes the md_6 series run more smoothly.

The p terms are left unchanged except for the extensions to higher series members permitted by the measurement of newly observed lines in the ultra-violet region. The identification of $2p_1$ which was somewhat doubtful in the original investigation (RP89, p. 147) due to the fact that it was assigned from only one combination, $1s_2-2p_1$, 13,008.368 cm^{-1}, has now been confirmed by the observation of $1s_4-2p_1$, 17,938.27 cm^{-1}. The higher members of the series mp_8, and mp_9 are merged together. The peculiar analogy between the discontinuities in the mp_5 and mp_{10} sequences (RP89, fig. 5, p. 154) may be noted from the effective quantum numbers as far as both series can be traced. A new sequence of f terms with inner quantum number 2 have been found. The series has been designated by mZ.

The reality of all the d terms reported in the previous paper has now been confirmed, due to improved measurements and the observation of practically all expected combinations. The series have also been extended by the discovery of some 20 new terms. A new sequence with j equal to 1 has been found. This series is designated by md_2. It should not be confused with the old md_2 series now interpreted as ms_4. There is some uncertainty as to the higher members of the d_3 and d_4 series. The term 1,867.81 now assigned to $8d_3$ since it combines with $2p_7$ and $2p_{10}$ as well as with $2p_9$, $2p_8$, and $2p_6$ was formerly interpreted as $8d_4$. With the present assignment no completely satisfactory value for $8d_4$ can be found unless it is coincident with $8d_3$, a possibility favored by the intensities of the combination lines. It may be seen that the 8 series of d terms predicted by the Hund theory have all been observed.

The $3d_5$ term is found from far ultra-violet data. (RP89, p. 153.) The other $3d$ terms have not been found. Possibly some of the unclassified lines between 13,000 and 14,000 cm^{-1} are combinations of these terms with higher p terms.

Four sequences of non-Ritzian d terms are predicted by the Hund theory. Three of the lowest group with values close to 9,000 cm^{-1} have been found, and all four of the next group ranging around 3,000 cm^{-1}. These sequences are designated by ms_1', ms_1'', ms_1''', and ms_1''''. Altogether 48 new terms have been added to the original list.

A contribution worth special mention is found in the resolution of close pairs of lines which are not separated heretofore. Such lines occur at 3,431 A, 3,846 A, 3,991 A, 4,969 A, 5,504 A, 6,555 A, 6,904 A, and 8,104 A. In our first analysis of the Kr I spectrum (RP89) it was assumed that 8,113 was a double line so as to obtain a starting point for the $2p_9-4d'_4$ series. The duplicity is now definitely assigned to 8,104 A and the line at 8,104.02 A is to be considered as the first member of the subordinate series mentioned.

The data presented in Table 3 of the present paper being so much superior to those given in our preliminary description, should be regarded as entirely superseding Table 12 of the earlier paper.

WASHINGTON AND AMSTERDAM, July 9, 1931.

(R P 365)

A CORRELATED COLOR TEMPERATURE FOR ILLUMINANTS

By Raymond Davis

ABSTRACT

As has long been known, most of the artificial and natural illuminants do not match exactly any one of the Planckian colors. Therefore, strictly speaking, they can not be assigned a color temperature. A color of this type may, however, be correlated with a representative Planckian color.

The method of determining correlated color temperature described in this paper consists in comparing the relative luminosities of each of the three primary red, green, and blue components of the source with similar values for the Planckian series.

With such a comparison three component temperatures are obtained; that is, the red component of the source corresponds with that of the Planckian radiator at one temperature, its green component with that of the Planckian radiator at a second temperature, and its blue component with that of the Planckian radiator at a third temperature. The average of these three component temperatures is designated as the correlated color temperature of the source. The mean deviation of the component temperatures from the average temperature is used as a basis for specifying the color (chromaticity) departure of the source from that of the Planckian radiator at the correlated color temperature. The conjunctive wave length indicates the kind of color departure.

CONTENTS

	Page
I. Introduction	659
II. The proposed method	662
III. Procedure	665
1. The Planckian radiator evaluated in terms of relative luminosity of the primary components	665
2. Computation of the correlated color temperature	670
3. Calculation of color departure in terms of sensation steps	672
4. Determination of the conjunctive wave length	674
IV. Characteristics of correlated color temperatures	674
1. Color departure and the isotemperature line	674
2. Conjunctive wave length as a function of correlated color temperature	677
V. Correlated color temperature data for Davis-Gibson filters 2,450° to 3,500° K. and 2,450° to 6,500° K	678
VI. Bibliography	680

I. INTRODUCTION

The method of describing the color of an illuminant in terms of the temperature at which a black body will have the same color was apparently first used by Hyde (1)[1] in 1911. Since that time, this method of assigning "color temperatures" to incandescent bodies has

[1] Numbers in parentheses, followed occasionally by page references, refer to the bibliography at the end of the paper.

come into general use. It furnishes a much simpler description of the chromaticity than a table giving spectral energy values. A definition of color temperature which is in accord with the common usage of the term is that of Priest (2) which follows. The color temperature of a light source is "the temperature at which a Planckian radiator [2] would emit radiant energy competent to evoke a color of the same quality as that evoked by the radiant energy from the source in question." This definition is seldom strictly applicable because probably none of the common illuminants evokes a color matching exactly any of those evoked by the Planckian radiator; therefore, under this definition artificial and natural illuminants can not strictly be assigned color temperatures. In such cases the specification aims to fix upon that Planckian temperature which furnishes the minimum difference in color; that is, that color temperature is specified which most nearly matches the given source. For a satisfactory specification the color difference involved must then be evaluated in readily appreciable terms.

In this paper are considered particularly illuminants which do not match exactly any of the Planckian colors, but whose color may be definitely correlated with a Planckian color. The above definition of color temperature may then be extended as follows: The "ideal correlated color temperature" of a light source is the absolute temperature at which the Planckian radiator emits radiant energy competent to evoke a color which, of all Planckian colors, most closely approximates the color evoked by the source in question. Strictly speaking, ideal correlated color temperatures can not be computed because at the present time no computational method can be successfully defended on theoretical grounds. Ideal correlated color temperatures may be approximated by direct observation under certain specific conditions; that is, the values may differ from the ideal correlated color temperature by the observational uncertainty. Accordingly, we shall call all color-temperature values representing non-Planckian colors "correlated color temperatures" regardless of the method by which they were obtained provided they are intended to approximate the ideal correlated color temperature.

The correlated color temperature derived by the method described in this paper is believed to give a Planckian temperature which is at least very close to the nearest match with the given source. The description is then completed by giving the kind and magnitude of the color difference. The correlated color temperature by this method approaches the true color temperature as a limit, as an exact color match between the Planckian radiator and the given source is approached; hence, in this respect there can be no question as to the applicability of the method. The degree of color departure [3] of the given source from that of the Planckian radiator at the correlated temperature is then expressible definitely in terms of trilinear coor-

[2] By defining color temperature in terms of a Planckian radiator, Planck's distribution formula, as given in B. S. Misc. Pub. No. 56, is used as an energy basis irrespective of the question as to whether or not it perfectly describes black body radiation. See also the footnote 3.

[3] In accord with the definition of "chromaticity" given in the Report of Committee on Colorimetry for 1920-21, ((5) p. 535) "chromaticity" departure should be used instead of color departure since brightness is not to be included in this concept. But by the same token "chromaticity temperature" should then be used instead of "color temperature." The same reservation, of course, applies to the definition of color temperature and of the ideal correlated color temperature. Throughout this paper it will be understood that when the terms color departure, color match, color difference, etc., are used, chromaticity departure, chromaticity match, chromaticity difference, etc., are meant.

dinates; or, proportionately in terms of the Planckian termperature scale in the immediate vicinity; or, by the number of sensation steps (least perceptible differences) involved. The kind of color departure of the source in question from that of the Planckian radiator at the correlated temperature is given in terms of the wave length of homogeneous light which added to or subtracted from the given source will furnish a perfect match with the Planckian radiator at the correlated temperature.

To evaluate the colors of illuminants in terms of color temperature it is necessary to adopt as a reference basis, a set of spectral energy distributions as a function of the temperature of the radiator. For this purpose it is customary to use the energy distributions calculated by Planck's well-known formula. For each of these energy distributions a single variable is usually derived which serves to represent the Planckian distribution. The corresponding quantity is then computed for the energy distribution of the illuminant. By comparing this value with the series of Planckian values the color temperature of the given distribution may be estimated. Single variables which have been used are (*a*) the slope of the relative spectral energy curve in the visual part of the spectrum, (*b*) the wave-length coordinate of the maximum of the energy curve (Wien's displacement law), and (*c*) the wave-length coordinate of the center of gravity of the luminosity curve of the source (λ_c method) (2). Forsythe (3) has used the red-blue ratio, which in effect is equivalent to slope; and the method involving Wien's law is commonly used for assigning stellar temperatures. The first two of these methods are suitable only for grading energy distributions giving smooth curves similar to those of the Planckian radiator. They are not at all suitable for grading irregular or non-Planckian energy distributions in terms of color temperatures. The λ_c method employed by Priest has been used at the National Bureau of Standards and by others for some time. The proposed method appears satisfactory from the standpoint of accuracy and recommends itself through its relative completeness.

Among the light filters designed by Davis and Gibson (4) are two which were intended to duplicate more or less accurately a series of Planckian colors by varying the color temperature of the light source from 2,000° to 3,100° K. With one of the filters the color temperature range is from 2,650° to 5,000° K. and with the other, from 4,000° to 18,600° K. The locus of colors evoked by the lamp-and-filter combination crosses the Planckian locus of colors at a small angle, the point of intersection being in one case at 3,500° K., and in the other at 6,500° K. In both of these instances the light source, is, by design, at 2,450° K. Thus, at one point in each case the filter combined with the source at 2,450° K. evokes a color which coincides with a Planckian color, and for all other color temperatures of the light source the agreement is more or less imperfect, the imperfection increasing with the departure of the light source from 2,450° K. If these two filters are to serve the purpose for which they were designed, not only the correlated color temperatures obtainable therewith at the various light-source temperatures should be specified, but also the degree of the approximation. This was the immediate spur to the present undertaking.

II. THE PROPOSED METHOD

The method of correlating a non-Planckian source with a Planckian source followed here, may be described by plotting (trilinear coordinates) the locus of Planckian colors, and inscribing on this curve the corresponding temperature scale. The color of the Planckian radiator at any given temperature is then specified equally definitely by the trilinear coordinates or by the temperature.

Colors off the Planckian locus are correlated with this temperature scale by averaging the three temperatures (primary component tem-

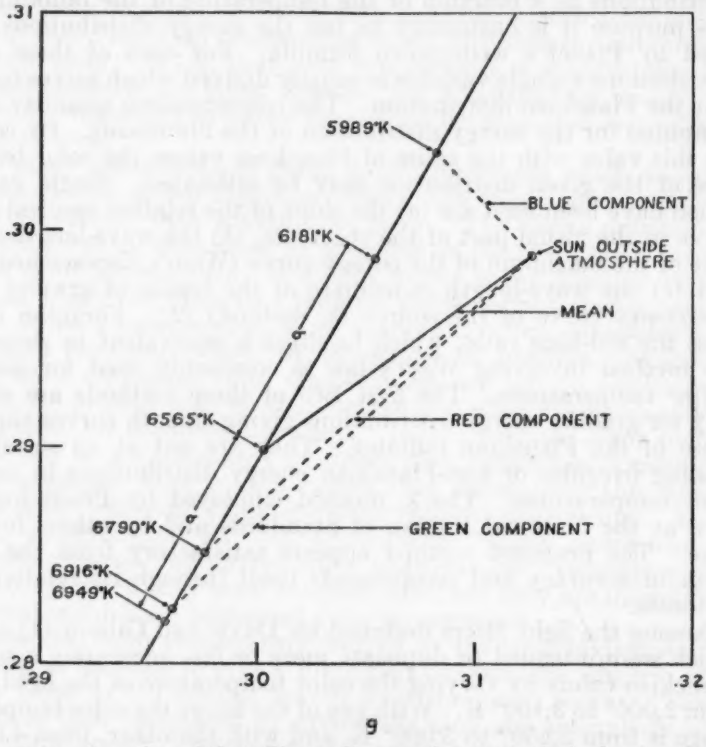

FIGURE 1.—*A section of the trilinear diagram (r-g projection) showing the colorimetric positions of the component temperatures, the mean temperature, and the mean deviation (σ) for sunlight outside the earth's atmosphere computed from Abbot's 1917 data (4)*

peratures) at which the Planckian color has, respectively, in terms of luminosity the same fractional part of primary "red," "green," and "blue" as the non-Planckian color. This average temperature (correlated color temperature) is used to associate non-Planckian colors with some definite color temperature. Points representing colors having the same correlated color temperature form lines on the trilinear diagram (isotemperature lines) intersecting the Planckian locus at the point where the temperature of the Planckian radiator and the correlated color temperature of the source are identical. The system of isotemperature lines fills the color area with nonintersecting lines which, sufficiently near the Planckian locus, may be treated as parallel

straight lines. These are more widely spaced at lower temperatures (2,000° K.) crowding closely at the higher temperatures (20,000° K.). See for example Figure 3.

Figure 1 is a restricted plot which shows the correlation of the color of the sun outside the earth's atmosphere with that of the Planckian radiator at 6,565° K. As indicated, the sun's red component corresponds in luminosity to that of a Planckian radiator at 6,790°, its green component to that of a Planckian radiator at 6,916°, and its blue component to that of a Planckian radiator at 5,989° K. By the

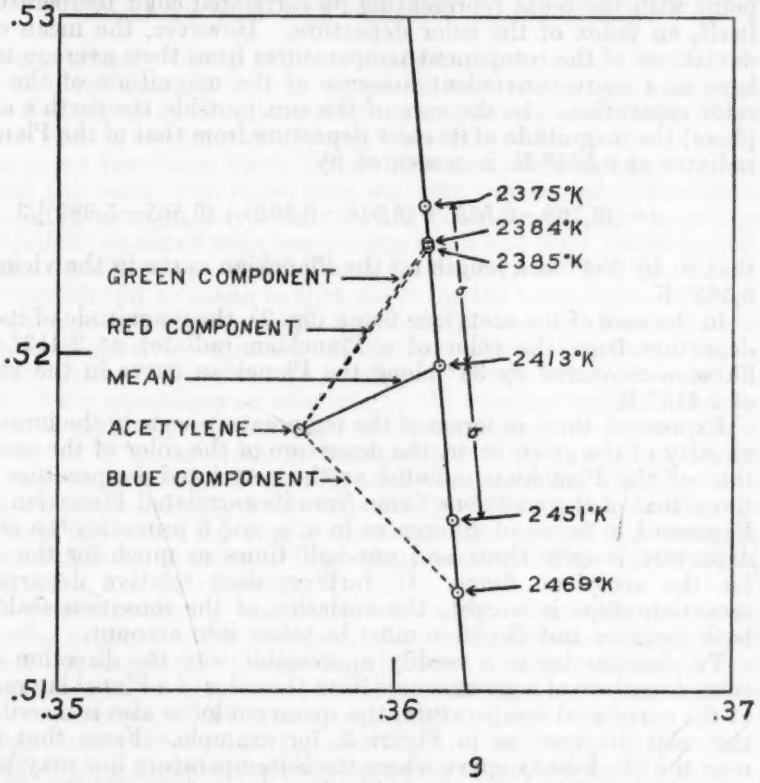

FIGURE 2.—*A section of the trilinear diagram (r-g projection) showing the colorimetric positions of the component temperatures, the mean temperature and the mean deviation (σ) for the energy distribution of the acetylene flame computed from Coblentz's data*

present method the mean of these three temperatures, 6,565° K., is the correlated color temperature of the sun. The line which joins the sun's colorimetric position with that of the Planckian radiator at 6,565° is an isotemperature line along which the color changes by magnitudes approximately proportional to distance. Likewise, Figure 2 illustrates the correlated color temperature (2,413° K.) of the acetylene flame and its color departure from the correlated Planckian color.

If these magnitudes of color departure in the specific direction and for the specific locations be evaluated once in terms of sensation units,

they may be used as a basis for evaluating like directed color changes in the immediate neighborhood. There is, however, no a priori reason for applying the evaluation of sensation magnitudes in one direction to those in another direction, in fact, they are known to be different. The same reservation applies to points in different neighborhoods even though the direction of the departure be the same.

We may now consider expressing the degree of color departure of a given source from that of the Planckian radiator at the correlated temperature. The length of the line connecting the non-Planckian point with the point representing its correlated color temperature is, itself, an index of the color departure. However, the mean of the deviations of the component temperatures from their average is used here as a more convenient measure of the magnitude of the given color separation. In the case of the sun (outside the earth's atmosphere) the magnitude of its color departure from that of the Planckian radiator at 6,565° K. is measured by

$$\sigma = [(6{,}790 - 6{,}565) + (6{,}916 - 6{,}565) + (6{,}565 - 5{,}989)]/3$$

that is, by 384° as a length on the Planckian curve in the vicinity of 6,565° K.

In the case of the acetylene flame (fig. 2), the magnitude of its color departure from the color of a Planckian radiator at 2,413° K. is likewise measured by 38° along the Planckian curve in the vicinity of 2,413° K.

Expressed, then, in terms of the temperature scale in the immediate vicinity of the given color, the departure of the color of the sun from that of the Planckian radiator at the correlated temperature is ten times that of the acetylene flame from its correlated Planckian point. Expressed in terms of differences in r, g, and b primaries the relative departure is only three and one-half times as much for the sun as for the acetylene flame. If, further, their relative departure in sensation steps is sought, the variation of the sensation scale with both location and direction must be taken into account.

To characterize in a readily appreciable way the direction of the color departure of a given source from the color of a Planckian radiator at the correlated temperature, the spectrum locus also is inscribed on the color diagram, as in Figure 3, for example. From that region near the black-body curve where the isotemperature line may be considered as straight it is extended in direction to intersect the spectrum locus. This intersection gives the wave length of the homogeneous light (conjunctive wave length) which must be added to, or subtracted from, as the case may be, the given source in order to make it match exactly in chromaticity the Planckian radiator at the correlated temperature. In the case of the sun, this conjunctive wave length is about 565 mμ; for the acetylene flame it is slightly more than 580 mμ. For a color temperature of 1,800°, it is 586 mμ; and for 15,000°, it is near 560 mμ. These limits correspond to only a moderate deviation of the conjunctive wave-length lines from parallelism.

Color points beyond the region in which the isotemperature lines are practically straight are specified in exactly the same way as those falling within this region. The conjunctive wave length serves just as definitely in these cases to specify the direction of the color departure of the source in question from the color of the Planckian radiator

at the correlated color temperature; but this direction is slightly different from that for nearer color points, hence could not be expected to coincide with the direction of least color difference in terms of sensation change if it does for nearer points. However, the range of colors expressible in terms of correlated color temperature should obviously be restricted to near-Planckian colors

III. PROCEDURE

1. THE PLANCKIAN RADIATOR EVALUATED IN TERMS OF RELATIVE LUMINOSITY OF THE PRIMARY COMPONENTS

As a necessary basis, trilinear coordinates, r, g, and b, for the Planckian radiator at various temperatures were computed by the method described in the report of the committee on colorimetry of the Optical Society of America (5) and elsewhere (Abney, Ives, Guild). In the paper describing Davis-Gibson filters (4) colorimetric computations on this basis, with mean noon sunlight represented at the center of the color triangle, have been carried out not only for the energy distributions obtained with the various lamp and filter combinations, but also for Planckian distributions between 1,600° and 20,000° K. Reference should be made to that paper for the basic data used here.

It is the generally accepted view that the products of the excitations by their respective luminosity coefficients should sum to yield the visibility curve. Because the luminosity coefficients given in the report of the committee on colorimetry (5) were not considered satisfactory in this respect, new ones were computed, by least squares, from the O. S. A. excitations, extrapolated (6), adjusted to "mean sun" and the standard Gibson-Tyndall recommended visibility data (7) in a manner differing from that used by Judd (8) only in that the equations contained the requirement that the sum of the three coefficients shall equal unity. The values so obtained are $L_r = 0.45014$, $L_g = 0.54417$, and $L_b = 0.00569$.

The products of r, g, and b for any energy distribution by their respective luminosity coefficients L_r, L_g, and L_b give the three relative primary luminosities. Computing in this manner values for the Planckian series, it is seen that the sum of these three varies with the color temperature; which is to be expected. To give them on a basis of equal luminosities rL_r, gL_g, and bL_b are, for each temperature, multiplied by a factor ω such that the sum is one-third.

In Table 1 are given then ωrL_r, ωgL_g, and ωbL_b for Planckian energy distributions obtained by computation and by graphical interpolation from their respective r, g, and b values.

TABLE 1.—*Table to facilitate the computation of correlated color temperatures*

The r, g, and b values of the energy distribution (computed as illustrated in B. S. Mis. Pub. No. 114, Figure 12) are multiplied by the respective luminosity coefficients (L_r=0.45014, L_g=0.54417, L_b=0.00569). The resulting values are adjusted by a factor (ω) so that their sum is 0.33333.

Color temperature	$\omega r L_r$	$\omega g L_g$	$\omega b L_b$	Color temperature	$\omega r L_r$	$\omega g L_g$	$\omega b L_b$
° K				° K			
1,600	0.20788	0.12530	0.000152	2,500	0.17895	0.15382	0.000571
10	.20741	.12577	.000156	20	.17854	.15421	.000582
20	.20693	.12624	.000159	40	.17813	.15461	.000593
30	.20646	.12672	.000162	60	.17773	.15500	.000604
40	.20599	.12718	.000166	80	.17733	.15539	.000616
1,650	.20552	.12765	.000169	2,600	.17693	.15577	.000627
60	.20505	.12812	.000173	20	.17654	.15614	.000639
70	.20459	.12857	.000176	40	.17615	.15652	.000650
80	.20413	.12902	.000180	60	.17578	.15688	.000661
90	.20369	.12946	.000183	80	.17541	.15725	.000673
1,700	.20324	.12990	.000187	2,700	.17505	.15760	.000684
10	.20281	.13034	.000191	20	.17470	.15794	.000696
20	.20237	.13077	.000194	40	.17435	.15828	.000707
30	.20194	.13120	.000198	60	.17401	.15861	.000719
40	.20152	.13161	.000202	80	.17368	.15893	.000730
1,750	.20110	.13203	.000206	2,800	.17334	.15925	.000742
60	.20069	.13244	.000210	20	.17301	.15957	.000753
70	.20028	.13284	.000214	40	.17268	.15989	.000765
80	.19988	.13324	.000218	60	.17236	.16020	.000777
90	.19948	.13363	.000222	80	.17203	.16051	.000788
1,800	.19909	.13402	.000226	2,900	.17172	.16081	.000800
10	.19870	.13440	.000230	20	.17142	.16111	.000812
20	.19831	.13478	.000234	40	.17112	.16140	.000824
30	.19793	.13516	.000238	60	.17082	.16168	.000835
40	.19755	.13554	.000243	80	.17053	.16196	.000847
1,850	.19716	.13591	.000247	3,000	.17023	.16225	.000859
60	.19679	.13628	.000251	20	.16994	.16252	.000871
70	.19643	.13664	.000255	40	.16965	.16280	.000883
80	.19606	.13700	.000259	60	.16937	.16307	.000895
90	.19570	.13736	.000264	80	.16908	.16334	.000907
1,900	.19535	.13772	.000268	3,100	.16880	.16361	.000919
10	.19499	.13807	.000272	20	.16853	.16387	.000930
20	.19464	.13842	.000277	40	.16827	.16413	.000942
30	.19429	.13877	.000281	60	.16800	.16438	.000954
40	.19395	.13910	.000286	80	.16773	.16464	.000966
1,950	.19361	.13944	.000290	3,200	.16747	.16488	.000977
60	.19327	.13977	.000295	20	.16722	.16512	.000989
70	.19293	.14010	.000299	40	.16697	.16537	.001001
80	.19260	.14043	.000304	60	.16672	.16560	.001013
90	.19227	.14075	.000308	80	.16648	.16583	.001024
2,000	.19195	.14107	.000313	3,300	.16623	.16607	.001036
20	.19129	.14171	.000322	20	.16599	.16629	.001048
40	.19066	.14233	.000332	40	.16576	.16652	.001059
60	.19004	.14294	.000342	60	.16553	.16674	.001071
80	.18944	.14354	.000351	80	.16529	.16696	.001082
2,100	.18885	.14412	.000361	3,400	.16507	.16718	.001094
20	.18827	.14470	.000371	20	.16484	.16739	.001106
40	.18770	.14525	.000381	40	.16462	.16759	.001117
60	.18714	.14579	.000391	60	.16440	.16780	.001129
80	.18659	.14634	.000401	80	.16419	.16800	.001141
2,200	.18606	.14686	.000411	3,500	.16398	.16820	.001152
20	.18553	.14738	.000421	20	.16377	.16841	.001164
40	.18499	.14790	.000432	40	.16355	.16860	.001176
60	.18447	.14841	.000442	60	.16335	.16879	.001187
80	.18397	.14891	.000452	80	.16315	.16898	.001199
2,300	.18347	.14939	.000463	3,600	.16295	.16917	.001210
20	.18298	.14987	.000473	20	.16274	.16937	.001222
40	.18252	.15033	.000484	40	.16255	.16955	.001233
60	.18204	.15080	.000494	60	.16236	.16973	.001245
80	.18157	.15124	.000505	80	.16217	.16991	.001256
2,400	.18112	.15169	.000516	3,700	.16197	.17009	.001268
20	.18068	.15212	.000527	20	.16178	.17027	.001280
40	.18024	.15255	.000538	40	.16160	.17044	.001291
60	.17980	.15298	.000549	60	.16141	.17062	.001303
80	.17937	.15340	.000560	80	.16123	.17079	.001314

TABLE 1.—*Table to facilitate the computation of correlated color temperatures*—Con.

Color temperature	$\omega r L_r$	$\omega g L_g$	$\omega b L_b$	Color temperature	$\omega r L_r$	$\omega g L_g$	$\omega b L_b$
° K				° K			
3, 800	0. 16104	0. 17096	0. 001326	5, 100	0. 15232	0. 17900	0. 002007
20	.16086	.17113	.001337	20	.15222	.17908	.002017
40	.16068	.17130	.001348	40	.15213	.17917	.002027
60	.16050	.17147	.001360	60	.15203	.17926	.002036
80	.16033	.17163	.001371	80	.15193	.17935	.002046
3, 900	.16016	.17179	.001382	5, 200	.15184	.17943	.002055
20	.15998	.17196	.001394	20	.15174	.17952	.002064
40	.15981	.17212	.001405	40	.15165	.17960	.002073
60	.15964	.17227	.001416	60	.15156	.17968	.002083
80	.15947	.17243	.001427	80	.15147	.17977	.002093
4, 000	.15931	.17258	.001438	5, 300	.15138	.17986	.002102
20	.15914	.17274	.001450	20	.15128	.17994	.002111
40	.15898	.17288	.001461	40	.15119	.18002	.002120
60	.15882	.17304	.001472	60	.15111	.18010	.002129
80	.15866	.17318	.001483	80	.15102	.18018	.002138
4, 100	.15850	.17334	.001494	5, 400	.15093	.18026	.002148
20	.15834	.17349	.001505	20	.15084	.18034	.002157
40	.15818	.17363	.001516	40	.15075	.18042	.002166
60	.15803	.17377	.001527	60	.15066	.18050	.002175
80	.15788	.17391	.001538	80	.15057	.18058	.002184
4, 200	.15773	.17405	.001549	5, 500	.15049	.18065	.002193
20	.15758	.17419	.001560	20	.15041	.18073	.002203
40	.15743	.17433	.001571	40	.15032	.18081	.002212
60	.15729	.17446	.001581	60	.15023	.18088	.002221
80	.15715	.17459	.001592	80	.15016	.18095	.002229
4, 300	.15701	.17472	.001603	5, 600	.15007	.18102	.002237
20	.15687	.17485	.001613	20	.14999	.18110	.002246
40	.15673	.17498	.001624	40	.14991	.18117	.002255
60	.15659	.17511	.001635	60	.14983	.18124	.002264
80	.15646	.17523	.001645	80	.14975	.18132	.002273
4, 400	.15632	.17536	.001656	5, 700	.14967	.18138	.002282
20	.15618	.17548	.001666	20	.14959	.18145	.002289
40	.15605	.17560	.001677	40	.14951	.18152	.002297
60	.15593	.17572	.001687	60	.14943	.18159	.002306
80	.15579	.17584	.001698	80	.14936	.18166	.002315
4, 500	.15568	.17595	.001708	5, 800	.14928	.18173	.002324
20	.15554	.17607	.001718	20	.14920	.18179	.002333
40	.15542	.17618	.001729	40	.14913	.18186	.002341
60	.15529	.17630	.001739	60	.14906	.18193	.002349
80	.15517	.17641	.001749	80	.14899	.18199	.002357
4, 600	.15504	.17653	.001759	5, 900	.14891	.18205	.002366
20	.15493	.17663	.001770	20	.14884	.18211	.002374
40	.15481	.17674	.001780	40	.14877	.18218	.002382
60	.15468	.17686	.001790	60	.14869	.18224	.002390
80	.15456	.17697	.001800	80	.14863	.18230	.002398
4, 700	.15445	.17707	.001810	6, 000	.14856	.18237	.002407
20	.15433	.17718	.001820	20	.14848	.18243	.002415
40	.15422	.17728	.001830	40	.14841	.18249	.002423
60	.15410	.17739	.001840	60	.14834	.18255	.002430
80	.15398	.17750	.001850	80	.14827	.18261	.002438
4, 800	.15387	.17760	.001860	6, 100	.14821	.18267	.002446
20	.15377	.17770	.001870	20	.14814	.18273	.002454
40	.15366	.17779	.001880	40	.14807	.18279	.002462
60	.15355	.17789	.001890	60	.14801	.18285	.002470
80	.15344	.17799	.001900	80	.14794	.18291	.002478
4, 900	.15333	.17809	.001910	6, 200	.14788	.18297	.002486
20	.15323	.17818	.001920	20	.14782	.18302	.002494
40	.15312	.17828	.001930	40	.14775	.18309	.002502
60	.15302	.17837	.001940	60	.14768	.18314	.002509
80	.15292	.17846	.001950	80	.14762	.18320	.002517
5, 000	.15282	.17855	.001960	6, 300	.14755	.18326	.002525
20	.15272	.17864	.001969	20	.14749	.18332	.002533
40	.15262	.17873	.001978	40	.14743	.18337	.002541
60	.15252	.17882	.001988	60	.14737	.18342	.002549
80	.15242	.17891	.001998	80	.14731	.18347	.002556

TABLE 1.—*Table to facilitate the computation of correlated color temperatures*—Con.

Color temperature	$\omega r L_r$	$\omega g L_g$	$\omega b L_b$	Color temperature	$\omega r L_r$	$\omega g L_g$	$\omega b L_b$
° K				° K			
6,400	0.14724	0.18353	0.002563	7,700	0.14398	0.18635	0.003001
20	.14718	.18358	.002570	20	.14394	.18638	.003007
40	.14712	.18363	.002577	40	.14391	.18642	.003013
60	.14706	.18369	.002586	60	.14387	.18645	.003019
80	.14701	.18374	.002593	80	.14383	.18648	.003025
6,500	.14695	.18379	.002600	7,800	.14379	.18652	.003030
20	.14689	.18384	.002607	20	.14375	.18655	.003036
40	.14683	.18390	.002615	40	.14371	.18658	.003042
60	.14677	.18395	.002623	60	.14367	.18662	.003048
80	.14671	.18400	.002630	80	.14363	.18665	.003053
6,600	.14666	.18404	.002637	7,900	.14359	.18668	.003059
20	.14659	.18410	.002644	20	.14356	.18671	.003065
40	.14654	.18415	.002652	40	.14352	.18674	.003070
60	.14648	.18420	.002659	60	.14348	.18678	.003076
80	.14643	.18424	.002666	80	.14345	.18681	.003082
6,700	.14637	.18429	.002673	8,000	.14341	.18684	.003087
20	.14632	.18434	.002680	20	.14337	.18687	.003093
40	.14626	.18439	.002687	40	.14333	.18691	.003098
60	.14621	.18444	.002694	60	.14330	.18694	.003104
80	.14616	.18448	.002701	80	.14326	.18697	.003109
6,800	.14610	.18453	.002708	8,100	.14322	.18700	.003115
20	.14604	.18458	.002715	20	.14319	.18703	.003120
40	.14599	.18462	.002722	40	.14315	.18706	.003126
60	.14594	.18467	.002729	60	.14311	.18709	.003131
80	.14588	.18471	.002736	80	.14308	.18712	.003137
6,900	.14583	.18476	.002743	8,200	.14304	.18715	.003142
20	.14578	.18481	.002750	20	.14300	.18718	.003147
40	.14573	.18485	.002756	40	.14297	.18721	.003153
60	.14568	.18490	.002763	60	.14293	.18724	.003158
80	.14563	.18494	.002770	80	.14290	.18727	.003163
7,000	.14558	.18498	.002777	8,300	.14286	.18730	.003168
20	.14553	.18502	.002784	20	.14283	.18733	.003174
40	.14548	.18506	.002790	40	.14279	.18736	.003179
60	.14543	.18510	.002797	60	.14276	.18739	.003184
80	.14538	.18515	.002804	80	.14272	.18742	.003189
7,100	.14533	.18519	.002810	8,400	.14269	.18745	.003194
20	.14528	.18523	.002817	20	.14265	.18748	.003200
40	.14523	.18527	.002824	40	.14262	.18751	.003205
60	.14518	.18531	.002830	60	.14258	.18753	.003210
80	.14513	.18536	.002837	80	.14255	.18756	.003215
7,200	.14509	.18540	.002844	8,500	.14252	.18759	.003220
20	.14504	.18544	.002850	20	.14249	.18762	.003225
40	.14499	.18548	.002857	40	.14245	.18765	.003230
60	.14494	.18552	.002863	60	.14242	.18767	.003235
80	.14490	.18556	.002870	80	.14239	.18770	.003240
7,300	.14485	.18560	.002876	8,600	.14236	.18773	.003245
20	.14480	.18564	.002883	20	.14233	.18775	.003250
40	.14476	.18568	.002889	40	.14229	.18778	.003255
60	.14471	.18572	.002896	60	.14226	.18781	.003260
80	.14467	.18576	.002902	80	.14223	.18783	.003265
7,400	.14462	.18580	.002907	8,700	.14220	.18786	.003270
20	.14458	.18584	.002915	20	.14217	.18788	.003275
40	.14453	.18588	.002921	40	.14214	.18791	.003280
60	.14449	.18591	.002928	60	.14211	.18794	.003285
80	.14444	.18595	.002934	80	.14208	.18796	.003290
7,500	.14440	.18599	.002940	8,800	.14205	.18799	003295
20	.14436	.18603	.002946	20	.14202	.18801	.003300
40	.14431	.18606	.002952	40	.14199	.18804	.003304
60	.14427	.18610	.002959	60	.14196	.18806	.003309
80	.14423	.18614	.002965	80	.14193	.18809	.003314
7,600	.14419	.18617	.002971	8,900	.14190	.18811	.003319
20	.14415	.18621	.002977	20	.14187	.18814	.003324
40	.14411	.18624	.002983	40	.14184	.18817	.003329
60	.14407	.18628	.002989	60	.14181	.18819	.003334
80	.14402	.18631	.002995	80	.14178	.18821	.003338

TABLE 1.—*Table to facilitate the computation of correlated color temperatures*—Con.

Color temperature	$\omega r L_r$	$\omega g L_g$	$\omega b L_b$	Color temperature	$\omega r L_r$	$\omega g L_g$	$\omega b L_b$
° K				° K			
9,000	0.14175	0.18824	0.003343	10,300	0.14016	0.18956	0.003616
20	.14172	.18826	.003348	20	.14013	.18958	.003620
40	.14169	.18829	.003352	40	.14011	.18959	.003624
60	.14167	.18831	.003357	60	.14009	.18961	.003627
80	.14164	.18833	.003361	80	.14007	.18963	.003631
9,100	.14161	.18835	.003364	10,400	.14005	.18965	.003634
20	.14158	.18837	.003370	20	.14003	.18966	.003638
40	.14156	.18840	.003375	40	.14001	.18968	.003641
60	.14153	.18842	.003380	60	.13999	.18970	.003645
80	.14150	.18844	.003384	80	.13997	.18971	.003649
9,200	.14148	.18846	.003389	10,500	.13995	.18973	.003652
20	.14145	.18849	.003393	20	.13993	.18975	.003656
40	.14142	.18851	.003398	40	.13991	.18976	.003659
60	.14139	.18853	.003402	60	.13989	.18978	.003663
80	.14137	.18855	.003406	80	.13987	.18980	.003666
9,300	.14134	.18857	.003411	10,600	.13985	.18981	.003670
20	.14131	.18860	.003415	20	.13983	.18983	.003673
40	.14129	.18862	.003420	40	.13981	.18985	.003677
60	.14126	.18864	.003424	60	.13979	.18986	.003680
80	.14123	.18866	.003429	80	.13977	.18988	.003684
9,400	.14121	.18868	.003433	10,700	.13975	.18990	.003688
20	.14118	.18871	.003438	20	.13973	.18991	.003691
40	.14116	.18873	.003442	40	.13971	.18993	.003695
60	.14113	.18875	.003446	60	.13969	.18994	.003698
80	.14110	.18877	.003451	80	.13967	.18996	.003702
9,500	.14108	.18879	.003455	10,800	.13965	.18998	.003705
20	.14105	.18881	.003459	20	.13963	.18999	.003709
40	.14103	.18883	.003464	40	.13961	.19001	.003712
60	.14100	.18885	.003468	60	.13959	.19003	.003716
80	.14098	.18887	.003472	80	.13957	.19004	.003719
9,600	.14095	.18889	.003477	10,900	.13955	.19006	.003723
20	.14093	.18891	.003481	20	.13953	.19008	.003726
40	.14090	.18893	.003486	40	.13951	.19009	.003730
60	.14088	.18896	.003490	60	.13949	.19011	.003733
80	.14085	.18898	.003494	80	.13947	.19012	.003737
9,700	.14083	.18900	.003498	11,000	.13945	.19014	.003740
20	.14081	.18902	.003503	20	.13943	.19015	.003744
40	.14078	.18904	.003507	40	.13941	.19017	.003747
60	.14076	.18906	.003511	60	.13939	.19019	.003750
80	.14073	.18908	.003515	80	.13938	.19020	.003754
9,800	.14071	.18910	.003519	11,100	.13936	.19022	.003757
20	.14069	.18912	.003524	20	.13934	.19023	.003761
40	.14066	.18914	.003528	40	.13932	.19025	.003764
60	.14064	.18916	.003532	60	.13930	.19026	.003768
80	.14062	.18917	.003536	80	.13928	.19028	.003771
9,900	.14059	.18919	.003540	11,200	.13927	.19029	.003774
20	.14057	.18921	.003544	20	.13925	.19030	.003778
40	.14055	.18923	.003548	40	.13923	.19032	.003781
60	.14052	.18925	.003552	60	.13921	.19033	.003784
80	.14050	.18927	.003556	80	.13920	.19035	.003788
10,000	.14048	.18929	.003560	11,300	.13918	.19036	.003791
20	.14046	.18931	.003564	20	.13916	.19038	.003794
40	.14043	.18933	.003568	40	.13914	.19039	.003798
60	.14041	.18935	.003572	60	.13913	.19040	.003801
80	.14039	.18936	.003576	80	.13911	.19042	.003804
10,100	.14037	.18938	.003579	11,400	.13909	.19043	.003807
20	.14035	.18940	.003583	20	.13908	.19045	.003810
40	.14033	.18942	.003587	40	.13906	.19046	.003814
60	.14030	.18944	.003591	60	.13904	.19047	.003817
80	.14028	.18945	.003595	80	.13903	.19049	.003820
10,200	.14026	.18947	.003598	11,500	.13901	.19050	.003823
20	.14024	.18949	.003602	20	.13899	.19051	.003826
40	.14022	.18951	.003606	40	.13898	.19053	.003829
60	.14020	.18952	.003609	60	.13896	.19054	.00383 *2*
80	.14018	.18954	.003613	80	.13894	.19055	.00383 *5*

TABLE 1.—*Table to facilitate the computation of correlated color temperatures*—Con.

Color temperature	wrL_r	wgL_g	wbL_b	Color temperature	wrL_r	wgL_g	wbL_b
° K				° K			
11,600	0.13893	0.19057	0.003838	15,000	0.13684	0.19223	0.004248
20	.13891	.19058	.003841	100	.13680	.19227	.004257
40	.13889	.19059	.003844	200	.13675	.19231	.004267
60	.13888	.19060	.003847	300	.13671	.19234	.004276
80	.13886	.19062	.003850	400	.13666	.19238	.004284
11,700	.13884	.19063	.003853	15,500	.13662	.19241	.004293
20	.13883	.19064	.003856	600	.13658	.19245	.004302
40	.13881	.19066	.003860	700	.13653	.19248	.004311
60	.13880	.19067	.003863	800	.13649	.19251	.004318
80	.13878	.19068	.003866	900	.13645	.19255	.004327
11,800	.13877	.19069	.003869	16,000	.13641	.19258	.004337
20	.13875	.19071	.003872	100	.13637	.19261	.004343
40	.13873	.19072	.003874	200	.13633	.19264	.004352
60	.13872	.19073	.003877	300	.13630	.19267	.004360
80	.13870	.19074	.003880	400	.13626	.19270	.004368
11,900	.13869	.19076	.003883	16,500	.13622	.19273	.004377
20	.13867	.19077	.003886	600	.13618	.19276	.004384
40	.13866	.19078	.003889	700	.13615	.19279	.004392
60	.13864	.19079	.003892	800	.13611	.19282	.004400
80	.13862	.19081	.003895	900	.13608	.19285	.004407
12,000	.13861	.19082	.003898	17,000	.13604	.19288	.004414
100	.13854	.19088	.003911	100	.13601	.19290	.004422
200	.13847	.19093	.003925	200	.13597	.19293	.004429
300	.13839	.19099	.003938	300	.13594	.19296	.004437
400	.13832	.19105	.003952	400	.13591	.19298	.004444
12,500	.13825	.19111	.003966	17,500	.13587	.19301	.004451
600	.13819	.19116	.003978	600	.13584	.19303	.004458
700	.13812	.19122	.003992	700	.13581	.19306	.004464
800	.13805	.19127	.004004	800	.13578	.19308	.004471
900	.13799	.19132	.004017	900	.13575	.19311	.004478
13,000	.13792	.19137	.004029	18,000	.13572	.19313	.004484
100	.13786	.19142	.004042	100	.13569	.19315	.004491
200	.13780	.19147	.004054	200	.13566	.19318	.004497
300	.13774	.19152	.004067	300	.13563	.19320	.004503
400	.13768	.19157	.004078	400	.13561	.19322	.004510
13,500	.13762	.19162	.004090	18,500	.13558	.19324	.004516
600	.13756	.19166	.004102	600	.13555	.19326	.004522
700	.13751	.19171	.004113	700	.13553	.19328	.004528
800	.13745	.19175	.004124	800	.13550	.19330	.004533
900	.13740	.19180	.004135	900	.13547	.19332	.004540
14,000	.13734	.19184	.004146	19,000	.13545	.19334	.004546
100	.13729	.19188	.004157	100	.13542	.19336	.004552
200	.13724	.19192	.004167	200	.13540	.19338	.004556
300	.13718	.19196	.004177	300	.13537	.19340	.004563
400	.13713	.19200	.004188	400	.13535	.19342	.004568
14,500	.13708	.19204	.004198	19,500	.13532	.19344	.004573
600	.13703	.19208	.004208	600	.13530	.19346	.004579
700	.13699	.19212	.004218	700	.13527	.19348	.004584
800	.13694	.19216	.004228	800	.13525	.19349	.004590
900	.13689	.19220	.004238	900	.13522	.19351	.004595
				20,000	.13520	.19353	.004600

2. COMPUTATION OF THE CORRELATED COLOR TEMPERATURE

To make the directions more specific the correlated color temperature of sunlight outside the earth's atmosphere will be computed. Using Abbot's 1917 data (4, Table 1) and following the form given in (4, fig. 12) the values of r, g, and b were calculated.

Thus

$$r=0.29883;\ L_r=0.45014;\ rL_r=0.134515$$
$$g=0.31261;\ L_g=0.54417;\ gL_g=\ .170113$$
$$b=0.38856;\ L_b=0.00569;\ bL_b=\ .002211$$

$$rL_r+gL_g+bL_b=\ .306839$$

$$\omega=\frac{0.333333}{0.306839}=1.08635$$

$$\omega rL_r=\ .14613$$
$$\omega gL_g=\ .18480$$
$$\omega bL_b=\ .002402$$

(Check:— $\omega rL_r+\omega gL_g+\omega bL_b=\ .33333$)

Seeking these values of ωrL_r, ωgL_g, and ωbL_b in the respective columns of Table 1 we obtain the following component temperatures:

For

	°K
ωrL_r,	6,790
ωgL_g,	6,916
ωbL_b,	5,989
Correlated color temperature (mean)	6,565

Table 2 gives for a number of sources a comparison of the values calculated by the λ_c method, the present method and also what may be designated as observed magnitudes.

TABLE 2.—*Comparison of correlated color temperatures obtained by computation and observation*

Energy distribution used in computation	Correlated color temperatures					
	Computed values			Observed values		
	Reference	λ_c method	Present method	Reference	Time observed	Value
		°K.	°K.			°K.
Mean noon sun	(4)	5,578	5,394	(12)	2/20/20 noon	[1] 5,200
Mean noon sun summer solistice	(4)	5,918	5,740	(12)	6/26/22 12:30 p. m.	[1] 5,300
Mean noon sun winter solstice	(4)	5,275	5,077	(12)	1/24/25 1:30 p. m.	[1] 5,212
Sun outside earth's atmosphere		6,724	6,565			
Abbot-Priest sun	(12)	5,323	5,229	(12)		5,323
						5,216
Equal energy spectrum		5,212	5,357			
Acetylene flame	(4)	2,388	2,413	(4)		[2] 2,420
B. S. lamp No. 1717	(11)	2,848	2,860	(11)		2,848
Blue glass R4-28 (source at 2,077° K.)		2,358	2,386			
Blue glass R4-28 (source at 2,080° K.)			2,389			[3] 2,390
Blue glass R4-28 (source at 2,360° K.) [4]			2,779			

[1] These values are isolated measurements, and are not necessarily representative of "mean" atmospheric conditions. Furthermore, the days on which these measurements were made are not wholly consistent with the dates assumed for the computation.

[2] For a discussion of the color of the acetylene flame, see B. S. Misc. Pub. No. 114, Secs. III, 4; V, 6, (*a*); VIII, 6.

[3] Quoting from National Physical Laboratory's Report dated January, 1930 (International Comparison of the Transmissions of Four Blue Glasses): "It was found by color matching experiments at the National Physical Laboratory that the glasses would change the light from a tungsten lamp operating at a color temperature of 2,080° K. to light having a color temperature of 2,390° K."

[4] Quoting again the National Physical Laboratory Report: "By calculation it was then found that the same glasses would change the light from a tungsten lamp operated at a color temperature of 2,360° K. to light having a color temperature of 2,770° K. which corresponds to about 13 lumens per watt for a gas filled lamp."

TABLE 3.—*Correlated color temperature data for well-known energy distributions* [1]

Source of energy	Correlated color temperture (θ_i)	Mean deviation (σ)	Sensation steps $\frac{\sigma}{\delta}$	Conj. wave length (λ_i)
	°K.	°K.		μ
Mean noon sun	5,394	347	11.9	566.8
Mean noon sun, summer solstice	5,740	365	11.1	566.3
Mean noon sun, winter solstice	5,077	345	13.4	567.6
Abbot-Priest sun	5,229	219	8.0	567.0
Acetylene, from Coblentz' data	2,413	38	6.6	[2] −580.5
Lamp 1717 (bib. ref. 11), from Coblentz data	2,860	18	2.2	576.7
Equal energy spectrum	5,357	291	10.1	[2] −565.7

[1] The specific energy distributions for which these values apply may be found in B. S. Misc. Pub. No. 114 (4)—the noon sun data in Table 1, the acetylene data in Table 3, Abbot-Priest sun in fig. 3, and Lamp 1717 in fig. 7.

[2] The negative sign indicates that light of the conjunctive wave length must be added to the stimulus in question in order to match the Planckian color.

3. CALCULATION OF COLOR DEPARTURE IN TERMS OF SENSATION STEPS

Within any small region near the Planckian locus the ratio of the color departure to the mean deviation should be constant. Since, as is well known, the perceptibility of a unit increment in color temperature decreases rapidly with increase in temperature, it is desirable to express mean deviation in "sensation" steps rather than in degrees of temperature.

Priest (2) has shown that between 3,000° and 20,000° K. the probable error of a single observation in color matching is between 0.1 and 0.2 $m\mu$ as expressed on the λ_c scale, without showing any systematic variation with color temperature. The reasonable assumption is made that the number of degrees just perceptibly different in color (a sensation step) at any color temperature, corresponds to a constant difference in λ_c values.

An attempt made to obtain a more convenient method resulted in the discovery that the number of degrees represented by a constant difference in λ_c over the range 2,000° to 24,000° K. varies quite closely as the square of the color temperature.[4]

Hence, a "sensation step" in degrees along the Planckian locus for any color temperature, may be calculated approximately from the relation

$$\delta = K\Theta^2$$

where:

θ = a sensation step measured in degrees, along the Planckian locus.
K = a constant evaluated by experiment.
Θ = the color temperature in degrees Kelvin.

At 2,360° K., a point much used in color matching of incandescent electric lamps, a difference of 5° or 6° in color temperature of the two fields of the photometer is roughly the magnitude of the "least perceptible difference" in color under the best observing conditions (9). Substituting 5.6° for δ and 2,360° for Θ gives $K = 1 \times 10^{-6}$.[5]

[4] Verification of this statement may be obtained by utilizing the λ_c data in Tables 1, 2, 3, and 4 of the Appendix to Priest's paper (2).

[5] A value of $K = 1 \times 10^{-6}$ corresponds to $\delta = 0.07$ $m\mu$ on the λ_c scale. Footnote 15 of Priest's paper (2), gives the values 0.1 and 0.2 $m\mu$ as representing on the λ_c scale the probable error of a single observation, stating however: "These values apply only to certain experimental conditions. Absolutely smaller probable errors can probably be obtained under improved conditions of observation."

The above relation permits the calculation of δ (the magnitude of one "sensation step") in degrees along the Planckian locus at any temperature. The ratio $\frac{\sigma}{\delta}$, then, expresses mean deviation in "sensation steps" whose size must necessarily be constant for sufficiently restricted regions near the Planckian locus. Whether the size of these "sensation steps" varies appreciably with temperature is not known; however, we assume in what follows that their size may be considered constant within the limits 1,600° to 20,000° K. Whether this assumption proves to be wholly justified or not is of little practical importance because accurate comparisons in terms of "sensation steps" are of interest chiefly within restricted ranges of correlated color temperature.

These steps are considerably smaller than the satron as defined by Priest (4; p. 121). For example, it is estimated that Abbot-Priest sunlight is about 1.6 satrons from 5,229° K., the correlated color temperature of Abbot-Priest sunlight. This compared with 8 steps $\left(\frac{\sigma}{\delta}\right)$ as given in Table 3 shows that a satron at this point is approximately equivalent to five of the units used in this paper for describing the magnitude of the color difference. While these units may seem quite small compared with the satron it should be pointed out that an absolutely smaller satron locus could be obtained under improved observing conditions. For the purpose used in this paper the size of the unit is of little consequence.

In the example of the correlated color temperature of sunlight outside the earth's atmosphere, given at the end of the previous section, we had obtained component temperatures of 6,790°, 6,916°, and 5,989° K., respectively. The average of these is 6,565° K. Taking the mean of the deviations of the component temperatures from the average we have

$$\sigma=\frac{(6{,}790°-6{,}565°)+(6{,}916°-6{,}565°)+(6{,}565°-5{,}989°)}{3}=384°$$

To determine the divergence of the color match in least perceptible differences in color, we find from the relation

$$\delta=K\theta^2$$

That

$$\delta=\frac{6{,}565^2}{1{,}000{,}000}=43.1° \text{ (a sensation step at 6,565° K).}$$

$\frac{\sigma}{\delta}=\frac{384}{43.1}=8.9$ sensation steps (a measure of the color departure of sunlight outside the earth's atmosphere from the Planckian radiator at 6,565° K).

Table 3 gives for a number of sources the correlated color temperatures, the values of mean deviation σ, their color departure $\frac{\sigma}{\delta}$ in sensation steps, together with the conjunctive wave length λ_j.

4. DETERMINATION OF THE CONJUNCTIVE WAVE LENGTH

In homo-hetero-analysis, a color stimulus is specified by giving its dominant wave length and its purity. The dominant wave length may be computed or it may be found graphically from the trilinear diagram by drawing a straight line through the center of the color triangle and that point representing the color of the stimulus to be specified and extending it until it cuts the spectrum locus.

In the present case, it is desired to specify a non-Planckian stimulus, not with reference to a fixed "neutral" standard, but rather with reference to a particular Planckian distribution as standard; that is, we wish to find the homogeneous stimulus which, when added to or subtracted from (as the case may be) the non-Planckian stimulus will produce a perfect color match. This is found graphically from the familiar trilinear diagram as the intersection of the spectrum locus and a straight line passing through the points representing the two energy distributions. It would appear that this color difference between two light qualities, neither of which is the "neutral" standard, has been so seldom used that it has not been given a name to distinguish it from dominant wave length. The term conjunctive wave length (λ_j) is used in the present discussion.[6] Conjunctive wave lengths for several non-Planckian colors are given in Table 3 and are considered in more detail below.

IV. CHARACTERISTICS OF CORRELATED COLOR TEMPERATURES

1. COLOR DEPARTURE AND THE ISOTEMPERATURE LINE

The work involved in carrying out the computations necessary to make a large-scale graph showing the system of isotemperature lines on the trilinear diagram is so great that a less laborious procedure illustrating the characteristics of the method was adopted. These data are given in Tables 4 and 5. A group of colors representing hypothetical energy distributions were selected as follows: The r, g, and b coordinates for 2,000°, 3,000°, and 10,000° K. were changed to represent non-Planckian colors by adding an increment, 0.0070, to the g coordinate and subtracting a similar value from the b coordinate in each case. The r coordinate was, of course, unchanged since r, g, and b sum to unity by definition. In this way colors were selected which fall on a curve approximately parallel to the Planckian locus on the spectrum-locus side. Correlated color temperatures were then computed for the colors represented by these new r, g, and b coordinates. The values were 2,011°, 3,053°, 6,359°, and 11,587° K. The r, g, and b coordinates were then obtained by interpolation from a previously published table (4, Table 11) for each of these color temperatures. The differences were obtained between the

[6] The term conjunctive wave length need not be restricted to the particular use made of it in this paper, but can be employed in all cases where an expression of the chromaticity difference between any two stimuli (neither of which is the "neutral" standard) is desired in terms of the addition (or subtraction) of a certain amount of homogenous light to (or from) one of the stimuli so that it will match the other. It may frequently happen that a line passing through the 2 points (r_1, g_1, b_1; r_2, g_2 and b_2) representing the given stimuli will intersect the spectrum locus at 2 points, then each stimulus may be said to have 2 conjunctive wave lengths with respect to the other. However, this condition will not be found in any case where a non-Planckian stimulus is correlated by the present method with a Planckian stimulus. Conjunctive wave length approaches dominant wave length as a limit as the trilinear coordinates (r_1, g_1, b_1, or r_2, g_2, b_2) of one of the colors approach those corresponding to the "neutral" stimulus for which $r=g=b=\frac{1}{3}$.

respective r coordinates, g coordinates, and b coordinates of each of the non-Planckian colors and those of the corresponding correlated color temperatures. By adding 0. 5 1, 2, 4, and in two instances, 8 times these differences, according to sign, to the Planckian coordinates new r, g, and b coordinates were obtained for a series of colors which plot on a straight line; that is, the original conjunctive wave-length line. Those colors at the same number of increments away from their respective Planckian color plot on a locus approximately paralleling the Planckian locus. With these new coordinates the data given in Tables 4 and 5 for both sides of the Planckian locus were obtained.

TABLE 4.—*Illustrating the characteristics of the method for computing correlated color temperature*

The colors chosen for these examples are on the spectrum side of the Planckian locus

	Trilinear coordinates			Component temperatures			Component temperature differences	Correlated color temperature	Conjunctive wave length	Mean deviation	Sensation steps in °K along Planckian locus at θ_j	Sensation steps in mean deviation (a measure of color departure)
	r	g	b	θ_r	θ_g	θ_b	$\theta_r-\theta_b$	θ_j	λ_j	σ	δ	$\frac{\sigma}{\delta}$
				°K.	°K.	°K.	°K.	°K.	$m\mu$	°K.		
1/2 increment	0. 5749	0. 3537$_5$	0. 0713$_5$	2, 030	2, 031	1, 972	58	2, 011	584. 2	26. 0	4. 0	6. 5
1 increment	. 5757	. 3570	. 0673	2, 050	2, 052	1, 930	120	2, 011	584. 2	53. 7	4. 0	13. 4
2 increments	. 5773	. 3635	. 0592	2, 090	2, 094	1, 845	245	2, 010	584. 1	109. 7	4. 0	27. 4
4 increments	. 5805	. 3765	. 0430	2, 175	2, 183	1, 667	508	2, 008	584. 1	227. 7	4. 0	56. 9
1/2 increment	. 4547	. 3636	. 1817	3, 081	3, 086	2, 992	89	3, 053	575. 5	40. 7	9. 3	4. 4
1 increment	. 4572	. 3674	. 1754	3, 110	3, 118	2, 930	180	3, 053	575. 5	81. 7	9. 3	8. 8
2 increments	. 4622	. 3750	. 1628	3, 167	3, 183	2, 809	358	3, 053	575. 5	162. 7	9. 3	17. 5
4 increments	. 4722	. 3902	. 1376	3, 282	3, 318	2, 575	707	3, 058	575. 7	322. 3	9. 4	34. 3
8 increments	. 4922	. 4206	. 0872	3, 519	3, 602	2, 112	1, 407	3, 078	575. 7	643. 7	9. 5	67. 8
1/2 increment	. 2988$_5$	. 3090	. 3921$_5$	6, 457	6, 516	6, 082	375	6, 352	564. 0	179. 7	40. 3	4. 5
1 increment	. 3033	. 3150	. 3817	6, 567	6, 684	5, 825	742	9, 359	564. 8	355. 7	40. 4	8. 8
2 increments	. 3122	. 3270	. 3608	6, 783	7, 035	5, 373	1, 410	6, 397	565. 1	682. 7	40. 9	16. 7
4 increments	. 3300	. 3510	. 3190	7, 216	7, 795	4, 624	2, 592	6, 545	565. 7	1, 281. 0	42. 8	29. 9
8 increments	. 3656	. 3990	. 2354	8, 100	9, 653	3, 522	4, 578	7, 092	565. 9	2, 380. 0	50. 3	47. 3
1/2 increment	. 2371$_5$	. 2701	. 4927$_5$	11, 870	12, 283	10, 450	1, 420	11, 534	560. 0	723. 0	133. 0	5. 4
1 increment	. 2428	. 2776	. 4796	12, 186	13, 060	9, 515	2, 671	11, 587	561. 0	1, 381. 0	134. 0	10. 3
2 increments	. 2541	. 2926	. 4533	12, 800	14, 825	8, 093	4, 707	11, 906	561. 5	2, 542. 0	142. 0	17. 9
4 increments	. 2767	. 3226	. 4007	14, 080	19, 950	6, 270	7, 810	13, 433	562. 5	4, 776. 0	180. 0	26. 5

TABLE 5.—*Illustrating the characteristics of the method for computing correlated color temperature*

The colors chosen for these examples are on the purple side of the Planckian locus

	Trilinear coordinates			Component temperatures			Component temperature differences	Correlated color temperature	Conjunctive wave length	Mean deviation	Sensation steps in °K along Planckian locus at θ_j	Sensation steps in mean deviation (a measure of color departure)
	r	g	b	θ_r	θ_g	θ_b	$\theta_r-\theta_b$	θ_j	λ_j	σ	δ	$\frac{\sigma}{\delta}$
				°K.	°K.	°K.	°K.	°K.	$m\mu$	°K.		
½ increment	0.5732$_5$	0.3472$_5$	0.0795	1,991	1,991	2,050	59	2,011	584.1	26.3	4.0	6.6
1 increment	.5725	.3440	.0835	1,972	1,970	2,090	118	2,011	584.1	53.0	4.0	13.2
2 increment	.5710	.3375	.0915	1,933	1,929	2,166	233	2,009	584.3	104.3	4.0	26.1
4 increment	.5680	.3245	.1075	1,858	1,852	2,316	458	2,009	584.2	205.0	4.0	51.2
8 increment	.5620	.2985	.1395	1,715	1,704	2,615	900	2,011	584.1	402.3	4.0	100.6
½ increment	.4496	.3560	.1944	3,027	3,024	3,116	89	3,056	575.5	40.3	9.3	4.3
1 increment	.4472	.3522	.2006	2,998	2,990	3,178	180	3,055	575.4	81.7	9.3	8.8
2 increment	.4424	.3446	.2130	2,939	2,923	3,310	371	3,057	575.3	168.3	9.3	18.1
4 increment	.4328	.3294	.2378	2,822	2,794	3,584	762	3,067	574.9	345.0	9.4	36.7
8 increment	.4136	.2990	.2874	2,594	2,546	4,211	1,617	3,117	573.8	729.3	9.7	75.2
½ increment	.2896$_5$	.2968	.4135$_5$	6,254	6,197	6,680	426	6,377	564.1	202.0	40.7	5.0
1 increment	.2855	.2910	.4235	6,134	6,033	7,000	866	6,389	563.7	407.3	40.8	10.0
2 increment	.2772	.2794	.4434	5,903	5,714	7,733	1,830	6,450	562.5	855.3	41.6	20.6
4 increment	.2606	.2562	.4832	5,451	5,124	9,860	4,409	6,812	558.4	2,032.0	46.4	43.8
½ increment	.2241$_5$	.2540$_5$	.5218	11,620	11,260	13,483	1,863	12,121	557.0	908.0	147.0	6.2
1 increment	.2202	.2479	.5319	11,080	10,450	15,100	4,020	12,210	555.3	1,927.0	149.0	12.9
2 increment	.2123	.2356	.5521	10,090	9,080	20,260	10,170	13,143	548.2	4,744.0	173.0	27.4

The first column of these tables serves to identify the points chosen by the increments as described; the next three columns contain their trilinear coordinates; columns 5, 6, and 7 headed θ_r, θ_g, θ_b, respectively, are the component temperatures; column 8, $\theta_r-\theta_b$, shows that the separation of the component temperatures along the black body locus is roughly proportional to the increments given in column 1; column 9 gives the correlated color temperatures for colors having the coordinates given in columns 2, 3, and 4; column 10 gives the conjunctive wave length, column 11, the mean deviations of the component temperatures from the correlated color temperature (θ_j); column 12, the number of degrees the Planckian radiator would have to be increased or decreased in temperature to give a difference in color which would be just perceptible, as given by the expression $\delta=K\theta^2$; and column 13, the mean deviation divided by δ. Note that these last values also increase roughly by powers of 2.

These tables show that the spread of the component temperatures along the Planckian locus, the mean deviation, and $\frac{\sigma}{\delta}$ are approximately proportional to the difference between the trilinear coordinates of the Planckian and the non-Planckian colors. In Table 4 the λ_j values increase slightly with the number of "increments" indicating that the isotemperature line is slightly curved. Furthermore, the curvature becomes more pronounced as the temperature

increases, and λ_f changes with θ_f. In Table 5, referring to colors on the purple side of the Planckian locus, the conjunctive wave length decreases as the distance from the Planckian locus increases; indicating that the isotemperature line continues to curve in the same direction as on the spectrum side of the Planckian locus.

2. CONJUNCTIVE WAVE LENGTH AS A FUNCTION OF CORRELATED COLOR TEMPERATURE

If the conjunctive wave lengths corresponding to a series of given Planckian colors be marked on the spectrum locus, (on a r–b diagram) lines joining these points with the corresponding Planckian points

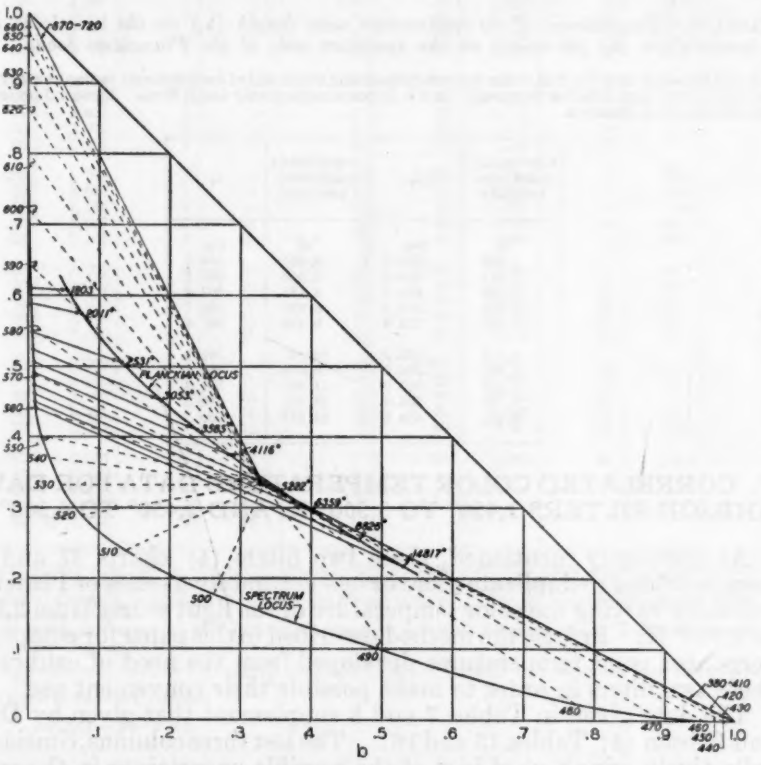

FIGURE 3.—*Illustrating the variation of conjunctive wave length* (λ_f) *with correlated color temperature using the data in Table 6 and plotted on a r-b diagram with mean sun as the "neutral" stimulus*

will indicate roughly the direction of color departure. A diagram of this type (shown in fig. 3) is of practical utility because, since these lines on the plot are nearly parallel, one may obtain, graphically, an approximate value of the correlated color temperature of any color lying in the neighborhood of one of these lines and near the Planckian locus.

To obtain this relation a series of non-Planckian colors was selected (by the method previously described for Table 5) the locus of which parallels the Planckian locus at a distance of "one increment."

From the equation of the line joining the points, representing respectively the Planckian and the non-Planckian colors, the intercept on the r axis is found. Drawing a line from this point through the two given points, its intersection with the spectrum locus is found graphically. From the coordinates of this intersection the corresponding spectrum wave length (conjunctive wave length) is found by way of a table (not published) containing values of $\frac{g-b}{r-b}$, $\frac{g-r}{b-r}$ or $\frac{r-g}{b-g}$ for each millimicron of wave length. In this way the values given in Table 6 were found. The material of Table 6 is applied in figure 3, an r–b projection of the trilinear diagram.

TABLE 6.—*Dependence of the conjunctive wave length* (λ_i) *on the correlated color temperature* (θ_i) *for colors on the spectrum side of the Planckian locus*

It will be noted that the hue of the color corresponding to the added homogeneous radiant energy does not vary greatly (green yellow to orange); that is, λ_i has a range of only about 30mμ. These values are further illustrated in Figure 3.

θ correlated color temperature	λ_i	θ correlated color temperature	λ_i
°K	mμ	°K	mμ
1,803	586.5	6,945	564.0
2,011	584.2	7,549	563.2
2,532	579.5	8,181	562.6
3,053	575.5	8,826	562.1
3,585	572.9	9,483	561.4
4,116	570.2	10,187	561.0
4,663	568.8	10,876	561.2
5,222	567.0	11,587	561.0
5,781	565.8	13,161	560.3
6,359	564.8	14,817	560.3

V. CORRELATED COLOR TEMPERATURE DATA FOR DAVIS-GIBSON FILTERS 2,450° TO 3,500° K. AND 2,450° TO 6,500° K.

As previously mentioned, these two filters (4; charts 37 and 38) were intended to duplicate more or less accurately a series of Planckian colors by varying the color temperature of the light source from 2,000° to 3,100° K. In fact, the method described in this paper for computing correlated color temperatures developed from the need of calibrating these two filters in order to make possible their convenient use.

The data given in Tables 7 and 8 supplement that given by Davis and Gibson (4; Tables 15 and 16). The last three columns, considered collectively, give a good idea of the possible uncertainty in the correlated color temperatures given in the second column.

TABLE 7.—*Correlated color temperature data as functions of the light-source temperature of the Davis-Gibson filter (chart No. 37 and Table 14 of B. S. Misc. Pub. No. 114) designed to convert 2,450° to 3,500° K*

Color temperature of light source	Correlated [1] color temperature of source and filter combination	σ (mean [2] deviation)	δ ($K\theta$ [3])	$\frac{\sigma}{\delta}$ sensation steps [3]	Color temperature of light source	Correlated [1] color temperature of source and filter combination	σ (mean [2] deviation)	δ ($K\theta$ [3])	$\frac{\sigma}{\delta}$ sensation steps [3]
° *K*	° *K*	° *K*			° *K*	° *K*	° *K*		
2,000	2,649	8	7.0	1.1	2,600	3,817	7	14.6	.5
20	2,685	7	7.2	1.0	20	3,859	8	14.9	.5
40	2,721	7	7.4	.9	40	3,903	9	15.2	.6
60	2,757	6	7.6	.8	60	3,947	9	15.6	.6
80	2,793	5	7.8	.7	80	3,992	10	15.9	.6
2,100	2,829	5	8.0	.7	2,700	4,038	10	16.3	.6
20	2,865	4	8.2	.6	20	4,082	11	16.7	.6
40	2,901	4	8.4	.5	40	4,126	11	17.0	.7
60	2,939	3	8.6	.5	60	4,171	12	17.4	.7
80	2,976	3	8.9	.4	80	4,216	13	17.8	.7
2,200	3,012	3	9.1	.4	2,800	4,262	14	18.2	.7
20	3,051	3	9.3	.4	20	4,309	14	18.6	.7
40	3,088	3	9.5	.3	40	4,356	15	19.0	.8
60	3,127	2	9.8	.3	60	4,404	16	19.4	.8
80	3,165	2	10.0	.3	80	4,453	17	19.8	.9
2,300	3,202	2	10.3	.2	2,900	4,502	18	20.3	.9
20	3,242	2	10.5	.2	20	4,551	18	20.7	.9
40	3,281	1	10.8	.2	40	4,600	19	21.2	.9
60	3,320	1	11.0	.1	60	4,650	20	21.6	1.0
80	3,359	1	11.3	.1	80	4,700	21	22.1	1.0
2,400	3,398	1	11.5	.1	3,000	4,751	22	22.6	1.0
20	3,439	0	11.8	.1	20	4,803	23	23.1	1.0
40	3,480	0	12.1	.0	40	4,855	25	23.6	1.0
60	3,521	0	12.4	.0	60	4,908	28	24.1	1.1
80	3,563	1	12.7	.1	80	4,961	31	24.6	1.2
2,500	3,605	2	13.0	.1	3,100	5,015	34	25.2	1.3
20	3,647	3	13.3	.2					
40	3,688	4	13.6	.3					
60	3,730	5	13.9	.4					
80	3,773	6	14.2	.5					

[1] The values in the second and third columns were obtained from large-scale graphs plotted from data computed for every 100° color temperature of the light source. It is impossible at this time to state the accuracy of the color temperatures given in the second column. They are given to the nearest degree to facilitate interpolation.

[2] The mean deviations (σ) plot somewhat irregularly and their accuracy is not, in general, considered to be better than ±1°.

[3] To preserve continuity of the values $\frac{\sigma}{\delta}$, the mean deviations (σ) used were smoothed to an extent beyond those given in the third column.

74280—31——5

TABLE 8.—*Correlated color temperature data as functions of the light source temperature of the Davis-Gibson filter (chart No. 38 and Table 15 of B. S. Misc. Pub. No. 114) designed to convert 2,450° to 6,500° K.*

Color temperature of light source	Correlated [1] color temperature of source and filter combination	σ (mean [2] deviation)	δ (K^0)	$\frac{\sigma}{\delta}$ sensation step	Color temperature of light source	Correlated [1] color temperature of source and filter combination	σ (mean [2] deviation)	δ (K^0)	$\frac{\sigma}{\delta}$ sensation step
° K.	° K.	° K.			° K.	° K.	° K.		
2,000	4,031	47	16	2.9	2,600	7,773	66	60	1.1
20	4,116	47	17	2.8	20	7,976	78	64	1.2
40	4,201	47	18	2.6	40	8,185	91	67	1.4
60	4,289	47	18	2.6	60	8,404	105	71	1.5
80	4,378	46	19	2.4	80	8,632	121	75	1.6
2,100	4,468	45	20	2.2	2,700	8,869	139	79	1.8
20	4,560	45	21	2.1	20	9,123	160	83	1.9
40	4,656	44	22	2.0	40	9,387	183	88	2.1
60	4,752	42	23	1.8	60	9,665	211	93	2.3
80	4,853	41	24	1.7	80	9,957	244	99	2.5
2,200	4,956	39	25	1.6	2,800	10,252	278	105	2.6
20	5,060	37	26	1.4	20	10,600	318	112	2.8
40	5,168	35	27	1.3	40	10,956	360	120	3.0
60	5,279	32	28	1.1	60	11,320	404	128	3.2
80	5,393	28	29	1.0	80	11,696	450	137	3.3
2,300	5,511	25	30	.8	2,900	12,090	500	146	3.4
20	5,632	23	32	.7	20	12,517	559	157	3.6
40	5,757	21	33	.6	40	12,979	624	168	3.7
60	5,884	18	35	.5	60	13,482	700	182	3.8
80	6,014	16	36	.4	80	14,030	789	197	4.0
2,400	6,143	13	38	.3	3,000	14,631	892	214	4.2
20	6,286	8	40	.2	20	15,299	1,020	234	4.4
40	6,430	2	41	.0	40	16,032	1,169	257	4.5
60	6,578	4	43	.1	60	16,844	1,346	284	4.7
80	6,728	11	45	.2	80	17,737	1,557	315	4.9
2,500	6,884	16	47	.3	3,100	18,667	1,778	348	5.1
20	7,047	23	50	.5					
40	7,217	32	52	.6					
60	7,394	43	55	.8					
80	7,580	54	57	.9					

[1] The values in the second and third columns were obtained from large-scale graphs plotted from data computed for every 100° color temperature of the light source. It is impossible at this time to state the accuracy of the color temperatures given in the second column. They are given to the nearest degree to facilitate interpolation.

[2] The mean deviations (σ) plot somewhat irregularly and their accuracy is not, in general, considered to be better than ±1°.

VI. BIBLIOGRAPHY

1. Hyde, Edward P., A New Determination of the Selective Radiation from Tantalum (abstract), Phys. Rev., vol. 32 p. 632; 1911.
2. Priest, I. G., The Colorimetry and Photometry of Daylight and Incandescent Illuminants by the Method of Rotatory Dispersion, J. Opt. Soc. Am. and Rev. Sci. Inst., vol. 7 No. 12, pp. 1175–1209; 1923.
3. Forsythe, W. E., Color Match and Spectral Distribution, J. Opt. Soc. Am. and Rev. Sci. Inst., vol. 7 No. 12, pp. 1115–1121; 1923.
4. Davis, Raymond, and Gibson, K. S., Filters for the Reproduction of Sunlight and Daylight and the Determination of Color Temperature B. S. Mis. Publication No. 114 (45 cents). [7]
5. Troland, L. T. report of O. S. A. Committee on Colorimetry for 1920–21, J. Opt. Soc. Am. and Rev. Sci. Inst., vol. 6 No. 6, pp. 527–596; 1922.
6. Gibson, K. S., report of O. S. A. Committee on Spectrophotometry for 1922–23, J. Opt. Soc. Am. and Rev. Sci. Inst., vol. 10, pp. 169–241; 1925.

[7] National Bureau of Standards official publications may be obtained from the Superintendent of Documents, Government Printing Office, Washington, D. C., postpaid at the prices given.

7. Proceedings, International Commission on Illumination, Sixth Meeting, Geneva, 1924, pp. 67 and 232–238; Cambridge University Press, 1926, *see also* Gibson, K. S. and Tyndall, E. P. T., The Visibility of Radiant Energy, B. S. Sci. Paper No. 475 (15 cents). [7]
8. Judd, Deane B., Chromatic Visibility Coefficients by the Method of Least Squares, J. Opt. Soc. Am. and Rev. Sci. Inst., vol. 10 No. 6, pp. 635–651; 1925.
9. Judd, D. B., Precision of Color Temperature Measurements under Various Observing Conditions; A New Color Comparator for Incandescent Lamps, B. S. Jour. Research; vol. 5, p. 1175; 1930. [7]
10. Priest, I. G., and Brickwedde, F. G., The Minimum Perceptible Colorimetric Purity as a Function of Dominant Wave Length with Sunlight as Neutral Standard, J. Opt. Soc. Am. and Rev. Sci. Inst., vol. 13, p. 306; 1926.
11. Priest, I. G., Measurements of the Color Temperature of the More Efficient Artificial Light Sources by the Method of Rotatory Dispersion, B. S. Sci. Paper No. 443; 1922. [7]
12. Priest, I. G., Standard Artificial Sunlight for Colorimetric Purposes, J. Opt. Soc. Am., and Rev. Sci. Inst., vol. 12 No. 5, p. 480; 1926.

WASHINGTON, November 1, 1930.

[7] National Bureau of Standards official publications may be obtained from the Superintendent of Documents, Government Printing Office, Washington, D. C., postpaid at the prices given.

QUARTZ PLATE MOUNTINGS AND TEMPERATURE CONTROL FOR PIEZO OSCILLATORS

By Vincent E. Heaton and E. G. Lapham

ABSTRACT

In this paper are described a number of representative types of mountings for rectangular and circular quartz plates to be used as frequency standards. Unless the movement of the quartz plate in the holder is restricted, the frequency will change with each slight jar. A satisfactory holder for mounting a long rectangular quartz plate to oscillate in its extensional mode may be made by clamping the plate centrally perpendicular to its length between two keys, one in the face of each electrode. The electrodes are spaced by quartz washers. A plate mounted in such a holder will be constant in frequency to 1 part in 300,000. Such a mounting has not been found satisfactory for frequencies above 100 kc as the damping caused by the pressure of the keys is too great.

A very satisfactory holder for mounting a cylindrical quartz plate for "thickness oscillation" may be made by clamping the plate between three screws, mounted radially 120° apart in a ring so that they press into a V-shaped groove cut around the cylindrical surface of the quartz plate midway between the faces. The electrodes are spaced on either side of the quartz plate by pyrex washers. Mounted in such a way, the plate has been found to be constant in frequency to 1 part in 1,000,000 in a portable frequency standard with the addition of temperature control of the oscillating circuit. Some discussion is given the subject of temperature control of the piezo oscillator.

CONTENTS

	Page
I. Introduction	683
II. The quartz plate and its mounting	684
III. Temperature control	688

I. INTRODUCTION

During the past few years an extensive study of certain phases of piezo oscillator construction and performance has been made at the National Bureau of Standards. The piezo oscillators have come from two chief sources—those sent in for calibration and those built at the bureau to serve as frequency standards. There has been no opportunity for long-continued observations on the former class of piezo oscillators, but the latter have yielded information of considerable value based on measurements which were made daily over a period of a year. These piezo oscillators differed in the manner of temperature control, method of mounting the quartz plate, type and number of tubes used, and type of oscillating circuit. Each of these factors affect the frequency constancy of the piezo oscillator. The material presented herewith deals chiefly with the quartz plate mountings and temperature control units, and is given with the hope that it may be of assistance to those interested in constructing piezo oscillators of greater reliability or in judging the probable merits of a given piezo oscillator.

II. THE QUARTZ PLATE AND ITS MOUNTING

At the present time piezo oscillators are in use which range in frequency from 25 to 5,000 kc. The quartz plates commonly used in covering this range of frequencies are rectangular bars, circular disks, and thin rectangular plates. Mountings for these plates differ greatly in outward appearance but the principles involved are much the same. The mounting must be so made that: (1) The air-gap will not change with ageing of the component parts, (2) the air-gap changes in a definite, predictable manner with variation in temperature; and (3) the unessential electrical capacity is minimized. The freedom of the quartz plate to move about between the electrodes must be restricted as much as possible without damping the desired mechanical vibration of the quartz plate. Any forces which tend to damp the vibration should be constant. The particular use for which the piezo oscillator is intended should determine the type of mounting. If the piezo oscillator is to be used as a primary standard, it will probably be kept in one position, protected from shock as far as possible, and be in continuous operation so that its frequency may be measured in terms of standard time. If the piezo oscillator is to be used as a secondary standard, it should be built so that it may be moved from place to place wherever it is needed and maintain a constant frequency over relatively short intervals of time. The frequency will change abruptly with a shift in the position of the plate within the mounting, and will drift more or less slowly with changes in damping depending on the magnitude of and rate at which the damping changes. It is very difficult, if not impossible, to maintain a constant damping factor for a quartz plate holder for an extended period of time. Therefore, it would appear that primary standards should use a mounting which possesses a minimum amount of damping, maintained, of course, as constant as possible. For secondary standards, the type of holder which allows a minimum of shifting in the position of the quartz plate is to be preferred.

The usual commercial piezo oscillator utilizes a rectangular quartz plate. The extensional mode of oscillation is customarily used for frequencies below 200 to 400 kc. For frequencies above this limit, the "thickness mode" is employed. These quartz plates are usually "Y cut" or "30° cut" quartz plates.[1]

A simple type of holder, which is often used for rectangular quartz plates, consists essentially of two brass electrodes with a celluloid or bakelite ring to limit the shifting of the quartz plate.[2] The upper electrode may be adjustable as to air gap or may rest on the quartz plate. (See fig. 1(*A*) and (*B*).) In another holder are used pins of bakelite or hard rubber mounted in the lower electrode to hold the quartz plate in place. The frequencies of piezo oscillators that incorporate mountings of this type change considerably when jarred, due to the shifting of the plate between the electrodes, and the varying of the damping as the plate touches the pins or a supporting ring, at different points. The constancy of frequency for a quartz plate mounted in this way is ordinarily 1 part in 10,000 to 30,000.

[1] Walter G. Cady, "Piezo-Electric Terminology," Proc. I. R. E., vol. 18, p. 2136; December, 1930.
[2] A. Hund, "Uses and possibilities of piezo-electric oscillators," Proc. I. R. E., vol. 14, August, 1926.
R. C. Hitchcock, "Mounting quartz oscillator crystals," Proc. I. R. E., vol. 15, p. 902, November, 1927.

If the two faces of the quartz plate are cleaned thoroughly, platinum electrodes may be sputtered directly on them. Connection to each electrode may be made by a piece of tin foil which is held in place by amberoid cement. The quartz plate may then be suspended by threads in a suitable position. A plate mounted in this manner will oscillate readily, but the frequency will drift continuously, usually toward a higher frequency. The sputtering on the surface of the plate changes the decrement and frequency of the plate. A quartz plate mounted in such a way gives a constancy of frequency of 1 part in 20,000 during a period of two or three months.

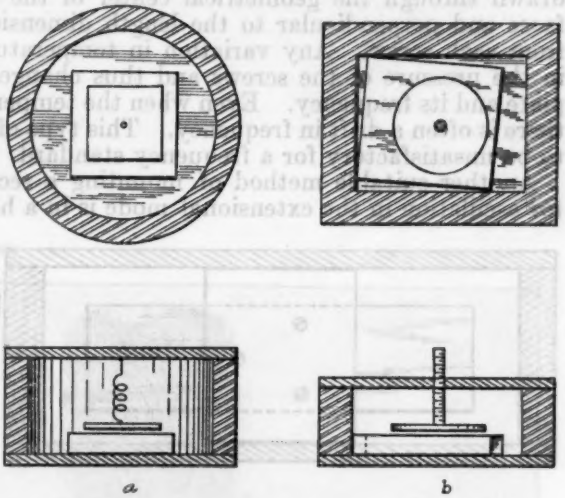

FIGURE 1.—*Types of simple quartz plate holder*

For rectangular plates which have one dimension large with respect to the other two, generally termed bars, there are other methods of mounting which may be used. In order to hold the quartz plate in position, a slot may be made in each edge of the quartz plate, midway between the two ends. These points are approximately at rest when the plate is oscillating in its extensional mode. Two screws are mounted on the lower electrode in such a way that they engage in the slots, and thus hold the quartz plate in position as it rests on the lower electrode. (See fig. 2.) The screws are made to fit the slots very neatly, and are adjusted as tight as possible without producing binding at any normal temperature. If the electrodes cover only the central portion of the quartz plate the damping is considerably reduced. A quartz plate mounted in such a holder will be constant in frequency to 1 part in 300,000.

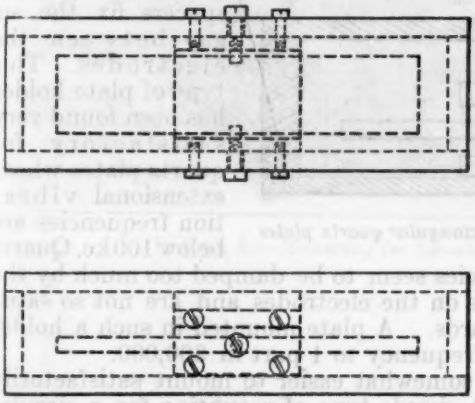

FIGURE 2.—*Mounting for long rectangular quartz plates*

In another piezo oscillator tested, the quartz bar is clamped between screws that project through the electrodes. The screws are

located at the vertices of an equilateral triangle; three screws in each electrode are so placed that each screw is directly opposite a screw in the other electrode. (See fig. 3.) The position of the points of support with respect to the quartz plate must be such that a line drawn through the geometrical center of the plate, parallel to the faces and perpendicular to the length dimension, is equally distant from each screw. Any variation in temperature causes a variation in the pressure of the screws and thus changes the damping of the plate and its frequency. Even when the temperature is held constant there is often a drift in frequency. This type of mounting has proved to be unsatisfactory for a frequency standard.

Another suitable method of mounting a rectangular quartz plate for oscillation in the extensional mode is in a holder having a narrow raised portion across the middle of the lower electrode, and a flat key directly opposite in the upper electrode, which is pressed against the quartz plate by a spring. (See Fig. 4.) The spring in the upper electrode is a stiff phosphor-bronze helix, which gives a small change in pressure with changes in temperature. Quartz spacers fix the air gap between the electrodes. This type of plate holder has been found very satisfactory for quartz plates whose extensional vibration frequencies are below 100 kc. Quartz plates giving higher frequencies seem to be damped too much by the width of the pressing surfaces on the electrodes and are not so satisfactory as frequency standards. A plate mounted in such a holder has been found constant in frequency to 1 part in 300,000.

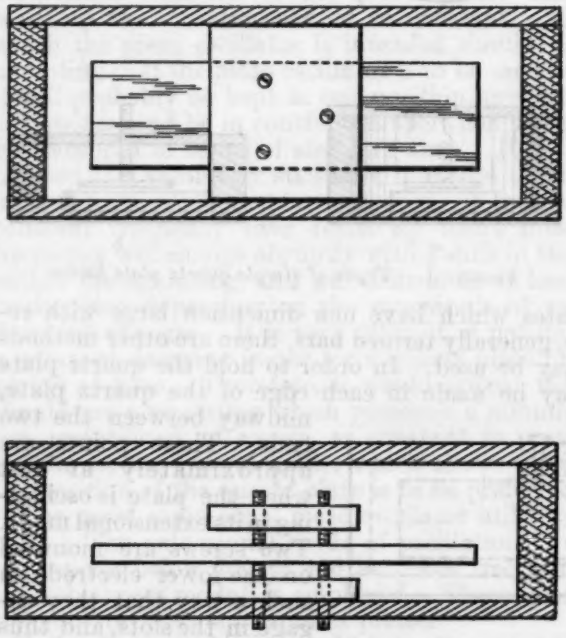

FIGURE 3.—*Mounting for long rectangular quartz plates*

A circular quartz plate is somewhat easier to mount satisfactorily than a rectangular plate. A simple type of mounting for a circular plate utilizes a piece of pyrex tubing, slightly larger in diameter than the quartz plate, to serve as the spacer between the electrodes as well as to hold the quartz plate in place.[3] (See fig. 5.) This type of mounting is found more advantageous for a "thickness mode" rather than for any other mode of oscillation as there is less variation in damping for this mode. The pyrex ring must be of such a size that

[3] V. E. Heaton and W. H. Brattain, Design of a Portable Temperature-Controlled Piezo Oscillator, Proc. I. R. E., vol. 18, p. 1239; July, 1930. B. S. Jour. Research, vol. 4, p. 345; March, 1930.

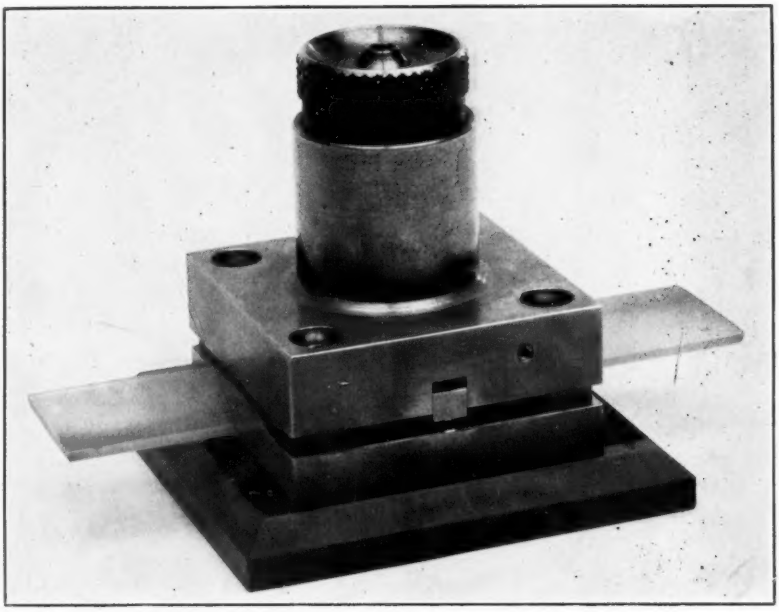

FIGURE 4.—*Mounting for bar-shaped quartz plates*

it will not clamp the quartz plate at any temperature at which the piezo oscillator will be operated. The greatest possible constancy of frequency of a plate in such a holder is 1 part in 200,000 for a portable standard as the quartz plate is able to shift slightly in the plate holder as well as rotate.

Another dependable method of mounting a circular quartz plate involves the cutting of a tapered hole along the axis of a "30°" or Y cut disk. The hole is cut so that the diameter decreases from both faces toward the center. The damping is small when the quartz plate is mounted on a horizontal rod of bakelite, or similar material, passed through the hole.[4] (See fig. 6.) It has been found that the temperature coefficient of frequency may be greatly reduced for such "doughnut-shaped" plates by suitably proportioning the various dimensions. A pyrex ring serves as spacer for the electrodes. If the quartz plate moves so as to come in contact with either electrode, the decrement is increased. Therefore, such a mounting is not reliable as a portable standard, although in a fixed position the piezo oscillator is reliable to 1 part in 1,000,000 with the extension of temperature control to the oscillator circuit. If the temperature and barometric pressure of the air surrounding the quartz plate and if filament and plate voltages of the oscillator tube are maintained very accurately at a constant value, the accuracy of such a piezo oscillator is 1 part in 10,000,000 according to Marrison. Experience obtained at the bureau with similar piezo oscillators verifies this statement.

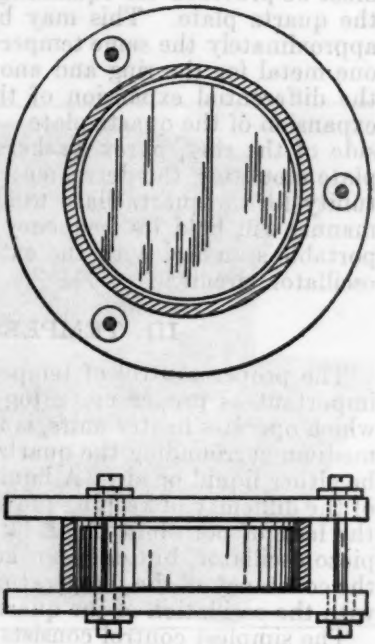

FIGURE 5.—*Simple mounting for cylindrical quartz plates*

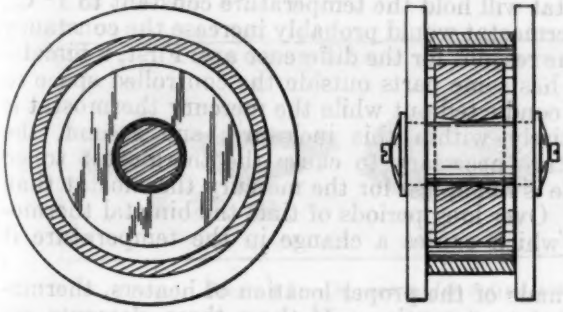

FIGURE 6.—*A satisfactory quartz plate mounting for a stationary frequency standard*

It is possible to mount a cylindrical quartz plate so that it will be reliable as a portable standard. About the cylindrical surface a V-shaped groove is cut halfway between the two plane faces of the quartz plate. The quartz plate is

[4] W. A. Marrison, A High Precision Standard of Frequency, Proc. I. R. E., vol. 17, p. 1103; July, 1929 Bell System Tech. J.; July, 1929.

then mounted within a ring of metal by three screws, 120° apart, whose tapering points fit in the groove in the quartz plate so that it is gripped only at the bottom of the groove. (See fig. 7.) Some means must be provided for equalizing the expansion of the mounting and the quartz plate. This may be done by choosing a metal having approximately the same temperature coefficient as quartz or by using one metal for the ring and another for the mounting screws so that the differential expansion of the two metals will be the same as the expansion of the quartz plate. The electrodes are mounted on either side of the ring, pyrex washers serving to space them. In such a plate mounting the decrement is very small and there is no opportunity for the quartz plate to shift. A quartz plate mounted in this manner will hold its frequency constant to 1 part in 1,000,000 as a portable standard with the extension of temperature control to the oscillator circuit.

III. TEMPERATURE CONTROL

The proper control of temperature in a piezo oscillator is just as important as proper mounting of the quartz plate. A thermostat, which operates heater units, is used to control the temperature of the medium surrounding the quartz plate mounting. This medium may be either liquid or air. A liquid bath is less satisfactory on account of the difficulty of keeping the liquid away from the quartz plate, and the lack of portability.[5] A large air bath increases the bulk of the piezo oscillator, but does not add excessive weight and does increase the constancy of the temperature. The air bath in no way interferes with the oscillation of the quartz plate.

The simplest control consists of a small box of wood or of similar material, containing a thermostat, the quartz plate mounting and a lamp or electric heater. The constancy of temperature depends on the type of thermostat used and the relative locations of the various pieces in the temperature-controlled space. The room temperature will probably affect the temperature at which the quartz plate is maintained. If the thermostat and heaters are properly located, a good bimetal thermostat will hold the temperature constant to 1° C., whereas a mercury thermostat would probably increase the constancy by a factor of 10. The reasons for the difference are: First, a bimetal thermostat ordinarily has some parts outside the controlled space so that the heat may be conducted out while the mercury thermostat is usually mounted entirely within this inclosure; and second, the variation of temperature necessary to cause the thermostat to go through one heat cycle is much less for the mercury thermostat than for the bimetal type. Over long periods of time the bimetal thermostat shows an aging which causes a change in the temperature it maintains.[6]

Mention has been made of the proper location of heaters, thermostat, and the quartz plate mounting. If these three elements are located without any consideration or knowledge of probable results, the temperature may be found to vary several degrees within the so-called temperature-control cabinet, assuming that heat is applied to the thermostat and quartz plate by conduction through air alone.

[5] R. C. Hitchcock, Mounting Quartz Oscillator Crystals, Proc. I. R. E., vol. 15, p. 902; November, 1927.
[6] W. A. Marrison, Thermostat Design for Frequency Standards, Proc. I. R. E., vol., 16, p. 976; July, 1928.

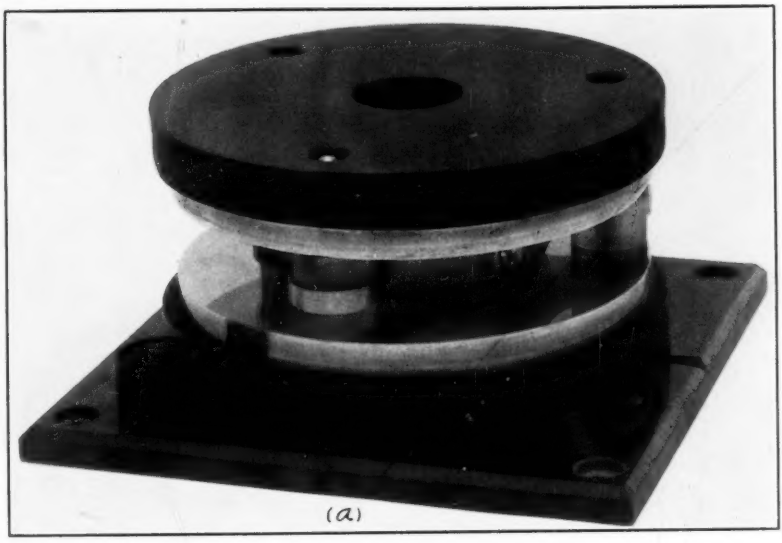

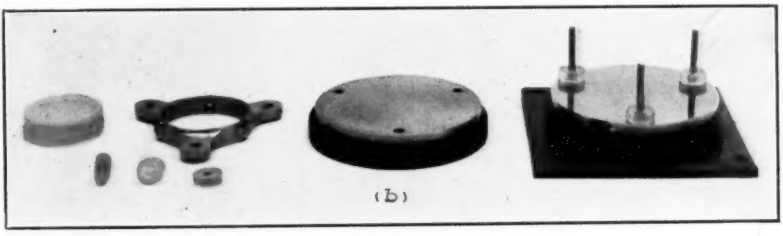

FIGURE 7.—*Mounting for cylindrical quartz plate*

a, Assembled; *b*, disassembled.

However, if the heater unit warms a large metallic body which carries the quartz plate mounting and the thermostat, the metallic body acts as a heat reservoir and distributor and effectively reduces the temperature variation required to actuate the thermostat, with a resulting reduction in temperature change of the quartz plate. Such a system, if suitably designed, using a bimetallic thermostat may be expected to hold a given temperature much better than indicated above for such thermostats.

Another method of improving the temperature control of the quartz plate consists in placing the plate holder inside a heat-attenuating box. This box may consist of a single layer of metal, wood, or other material. It is better, however, to make the compartment of alternate layers of metal and felt or asbestos, using metal as the outside layer. The metal should be brass, copper, or aluminum so as to distribute the heat readily over the entire surface of the attenuator. The poor heat conductor between the metal walls slows down the heat transfer to the plate holder.[7] Such an attenuating cabinet of 3 or 5 layers of material may reduce the variations of temperature inside to 1 per cent of that in the temperature-controlled compartment.

Still better control may be obtained if the thermostat is placed in a well in the outer layer of metal in the attenuation box. Variations of room temperature then have a negligible effect on the temperature of the quartz plate as long as the heaters are not overtaxed.

If portability is not required, the temperature-controlled compartment may be made larger with a fan to force the air to circulate about the attenuating cabinet containing the plate holder. This arrangement is very little superior to the smaller box described above in which heat is supplied on all six sides of the attenuating cabinet.

In any temperature control system, the thermostat operates more satisfactorily if it controls the heater current through the agency of a relay rather than directly. Either direct current or alternating current may be used for the heater current. If direct current is used, a potential divider will supply the necessary current for operating the relay. If a. c. is used, the relay may be operated on the output of a small rectifier.

Where great constancy of frequency is required, the oscillator circuit also must be maintained at a constant temperature. It is very desirable to have a double temperature-control on the quartz plate, putting the oscillator circuit in the outer temperature-control compartment.[8] The quartz plate is mounted in an attenuating box in the outer wall of which is placed a mercury thermostat. This attenuator is in a constant-temperature compartment whose walls are of alternate layers of metal and insulating material and whose temperature is controlled by the thermostat in the wall of the quartz plate attenuator. This temperature-control unit is then placed within another compartment, whose temperature is controlled by a thermostat of either the mercury type or bimetal type. This outer compartment has walls of insulating material. In the outer compartment are placed the oscillator tube, and coil. The inner compart-

[7] V. E. Heaton and W. H. Brattain, Design of a Portable Temperature-Controlled Piezo Oscillator, Proc. I. R. E., vol 18, p. 1239; July, 1930. B. S. Jour. Research, vol. 4, p. 345; March, 1930.
J. W. Horton and W. A. Marrison, Precision Determination of Frequency, Proc. I. R. E., vol. 16, p. 137; February, 1928.

[8] J. K. Clapp, Temperature Control for Frequency Standards, Proc. I. R. E., vol. 18, p. 2003; December, 1930.

ment operates at a temperature a few degrees above that of the outer one. The outer compartment contains enough heaters to maintain a constant temperature, regardless of room temperature. Such a unit will maintain a constant temperature at the quartz plate under all conditions except for small drifts in the operating temperature of the thermostat.

WASHINGTON, July 8, 1931.

AN IMPROVED AUDIO-FREQUENCY GENERATOR

By E. G. Lapham

ABSTRACT

This paper describes in detail the construction of an audio-frequency generator for use in making radio-frequency measurements. The variable audio-frequency output is the beat note between two sources of radio-frequency; the one a piezo oscillator, and the other a variable oscillator. The output is continuously variable from 50 to 1,500 cycles per second. The entire unit is assembled very compactly and the essential parts are mounted in a temperature-controlled compartment. The calibration curve is practically linear over a range of 50 cycles per second, and repeated calibrations indicate that it is constant to better than 0.1 cycle per second over the entire range.

An audio-frequency oscillator is an essential part of radio-frequency measuring equipment. The last step in such a measurement is the determination of the frequency of the audio beat note between the reference standard and the unknown frequency. If the frequency of the beat note is between 0 and 200 cycles per second, an audio-frequency bridge [1] provides a very accurate means of making the measurement. However, if the frequency is greater than 200 cycles per second, the most convenient method is to match the note with a known audio-frequency. A variable audio-frequency generator is ordinarily used for this purpose.

The beat-frequency oscillator [2] provides a very convenient audio-frequency source. The audio-frequency note is the beat between two radio-frequency oscillators; a piezo oscillator and a variable oscillator. The beat note is received by a detector and amplified to the desired energy level by means of an audio-frequency amplifier.

A very satisfactory audio-frequency generator of this type has been constructed for use in measuring the standard frequency transmissions from the National Bureau of Standards radio station, WWV. The complete unit can be seen in Figure 1. It is a very compact unit, mounted in an aluminum case, 18¾ inches long, 12⅝ inches high, and 12¾ inches deep. This case is rigidly constructed of three-sixteenths-inch sheet aluminum with all joints fitted neatly to provide an effective radio-frequency shield. In the upper left-hand corner of the front panel is the filament voltmeter and rheostat. At the right of the rheostat is a light which indicates the operation of the heater. The meter in the upper center indicates the current in the piezo oscillator plate circuit, and the one in the upper right, the plate voltage applied to the oscillator tubes. A small toggle switch is seen on either side of the plate milliammeter. The one on the left is connected in the

[1] N. P. Case, A Precise and Rapid Method of Measuring Frequencies from 5 to 200 Cycles per Second, B. S. Jour. Research, vol 5 (RP. 195); August, 1930.
[2] A. Hund, Piezo-electric Generator for Audio-Frequencies, B. S. Jour. Research, vol. 2 (RP. 40); February, 1929

plate circuit of the piezo oscillator, and the one on the right in the plate circuit of the variable oscillator. The outlets directly below the switches provide the corresponding radio-frequency outputs, by means of which either oscillator can be measured separately against a radio-frequency standard, or the piezo oscillator can be used as a secondary standard. A switch, directly below the plate milliammeter, disconnects the filament battery. The audio-frequency output terminals and volume control are located in the lower right-hand corner of the front panel. In the extreme left a door is provided which gives access to a compartment containing a relay, rectifier, and resistors in the heater circuits. The battery cable and the 110-volt a. c. line are connected by means of suitable outlets at the left end of the box.

By unsoldering seven leads that are connected to the circuits in the temperature-controlled compartment, and removing as many screws, the front panel may be removed. The heater control equipment can be seen in Figure 2 at the left. On the right is a condenser dial with a vernier, which allows a slow, smooth adjustment of the frequency of the variable oscillator.

Figure 3 shows the arrangement of tubes and circuits as seen from the rear of the front panel. The two tubes on the right are the oscillator and coupling amplifier in the piezo oscillator circuits. The three tubes in the center are, from right to left, detector, first and second audio-frequency amplifiers. The two tubes on the left are the oscillator and coupling amplifier in the variable oscillator circuits.

Replacing the front panel and removing the top gives a view, as seen in Figure 4, of the interior of the temperature-controlled cabinet. This compartment is 18¼ inches long, 12 inches high, and 7¾ inches deep, outside dimensions. The side and end walls, as shown in the drawing (fig. 5), consist of a three-eighths inch layer of hardwood, one-half inch layer of hair-felt, and an inner wall of one-half inch balsa wood. The top and bottom of the cabinet consist of an outer wall of three-eighths inch hardwood and a double layer of one-half inch balsa wood.

The quartz plate and mounting can be seen in the aluminum attenuating box at the left end of the temperature-controlled cabinet. Directly in front, mounted on the balsa wood, is the coil in the piezo oscillator plate circuit. An attenuating cover is placed over this coil to reduce the temperature changes which take place as the heaters operate. The aluminum attenuating box on the right contains the condensers and coils of the variable radio-frequency oscillator. The flexible connection on the condenser shaft is in view between the front of the aluminum box and the balsa wood wall. One of the heaters, which maintain the box at a constant temperature, can be seen at each end of the cabinet. Similar heaters, extending the full length of the cabinet, are placed above and below the attenuating boxes. The thermostat is mounted between the boxes in an aluminum well directly attached to the end of the box containing the quartz plate.

The temperature-controlled cabinet is maintained at 40.5° C. by means of four electric heaters. The heaters are made of No. 28 nichrome wire which is wound into a long helical spring and then stretched over the forms. The wire is insulated from the metal supports by one-eighth inch porcelain tubing. A sensitive polarized relay is used to operate the heaters. The relay works positively on 2 milliamperes d. c., which is obtained from the a. c. line by means of a copper-oxide

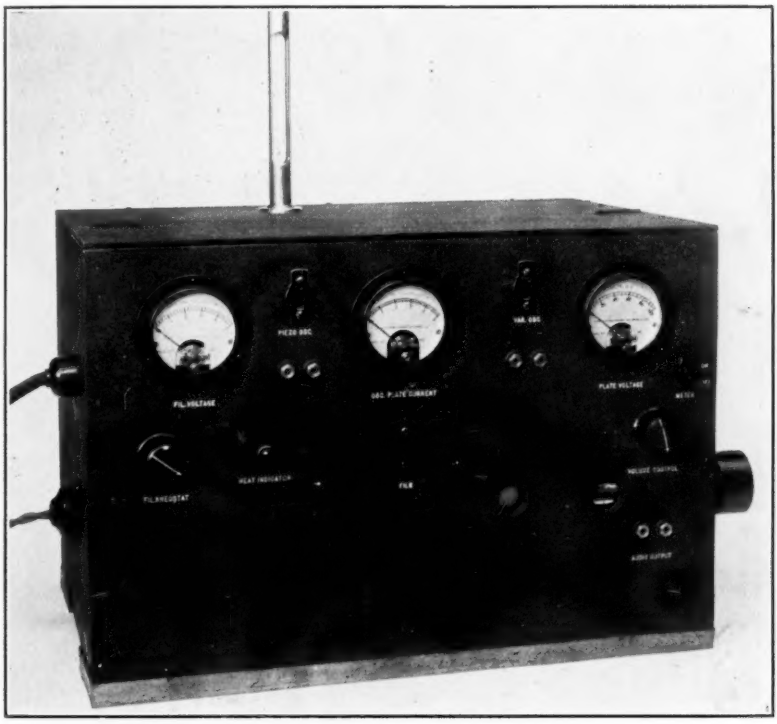

FIGURE 1.—*Front view of audio-frequency generator*

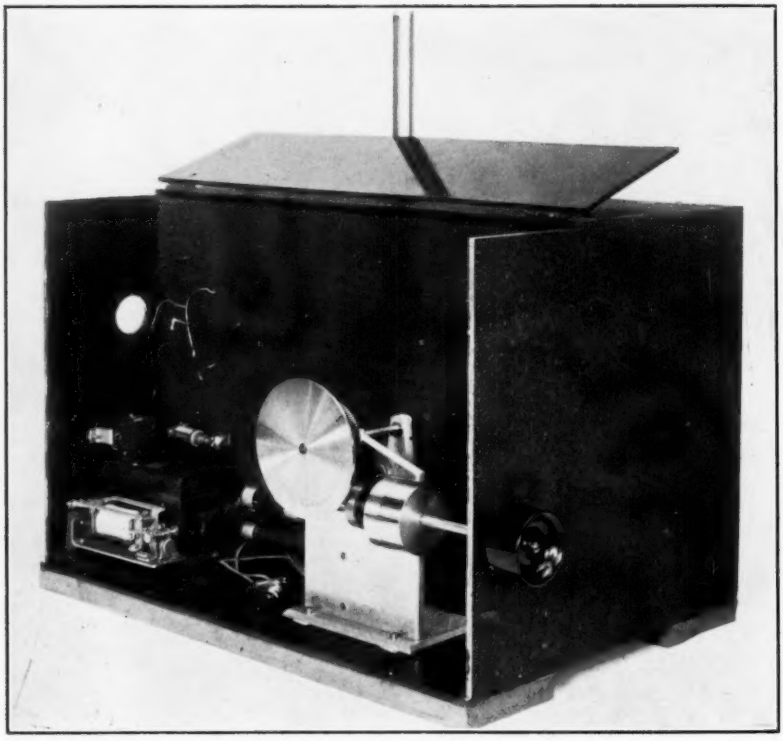

FIGURE 2.—*View of audio-frequency generator with front panel removed*

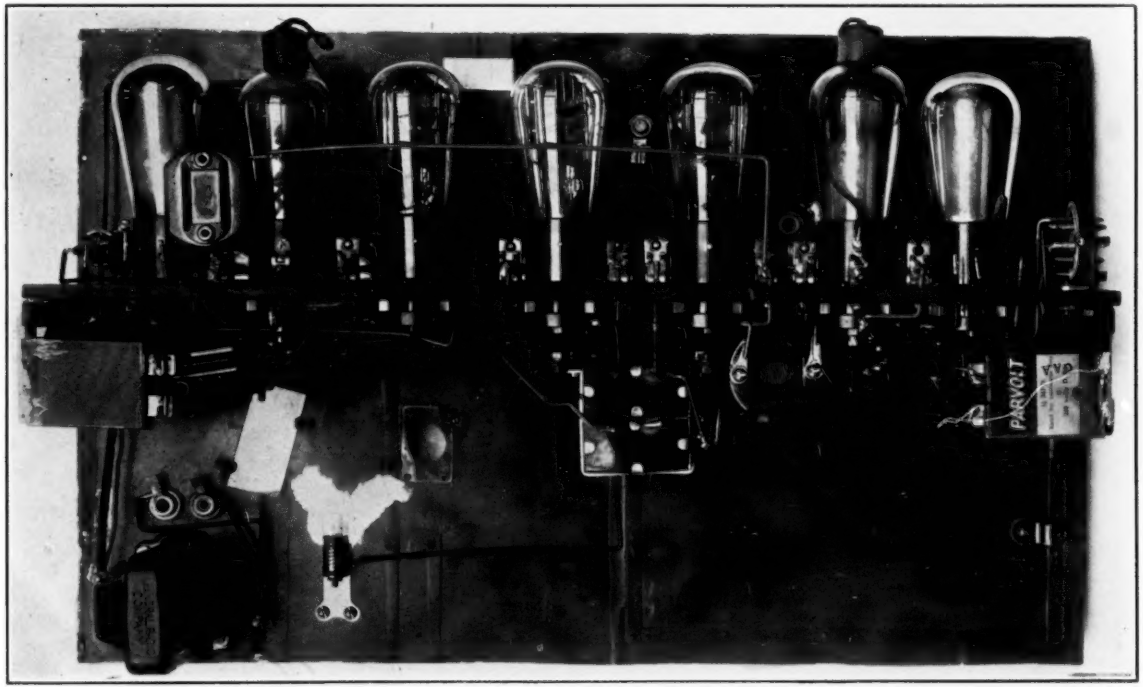

FIGURE 3.—*Tubes and circuit arrangement as seen from rear of front panel*

UNIV. OF ILL.

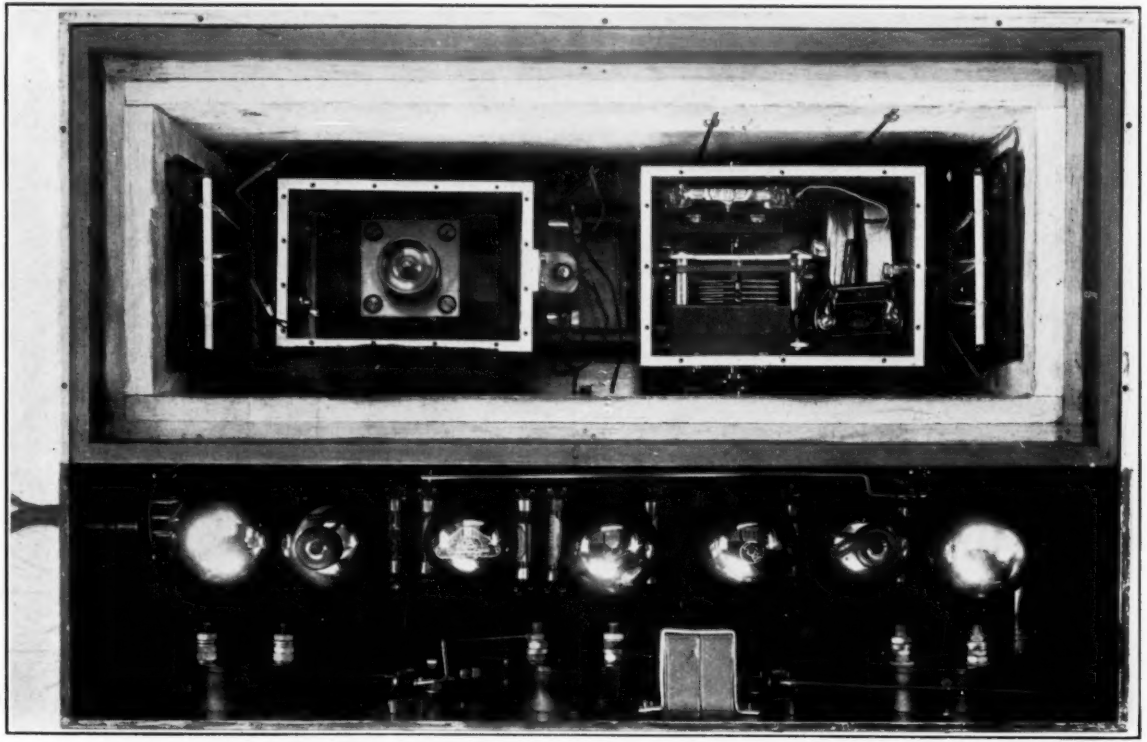

FIGURE 4.—*Interior of temperature-controlled cabinet*

rectifier. This unit has been in continuous operation for four months, and in that time has not required any attention whatever.

The piezo electric element is a 30 kc rectangular bar, 30° or Y cut.[3] It is mounted in a special mounting (fig. 7) in such a way that its

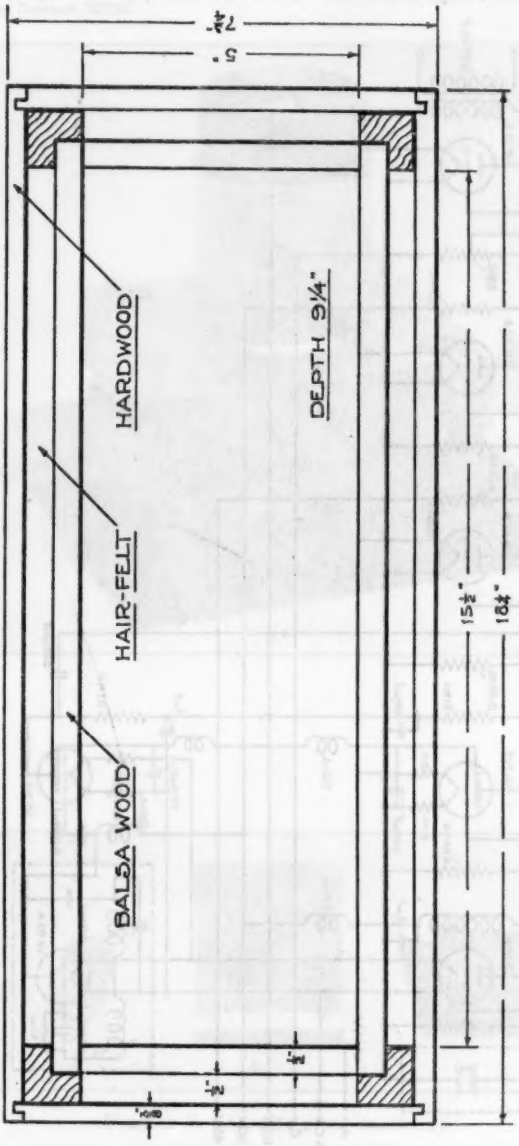

FIGURE 5.—*Plan of temperature-controlled cabinet, showing layers of hair felt and balsa wood*

frequency is practically free from any changes due to jarring. A spring and key in the upper electrode presses the quartz plate against a narrow, raised surface on the lower electrode. As shown in the

[3] W. G. Cady, Piezo-electric Terminology, Proc. I. R. E., vol. 18, p. 2136; December, 1930.

figure, the central portion of the contacting areas are ground away so that pressure is applied only near the edges of the plate. The spring is a phosphor-bronze helix so designed that the pressure is as nearly independent of temperature as possible. In this way the quartz plate is held midway between the electrodes, and is quite free to vi-

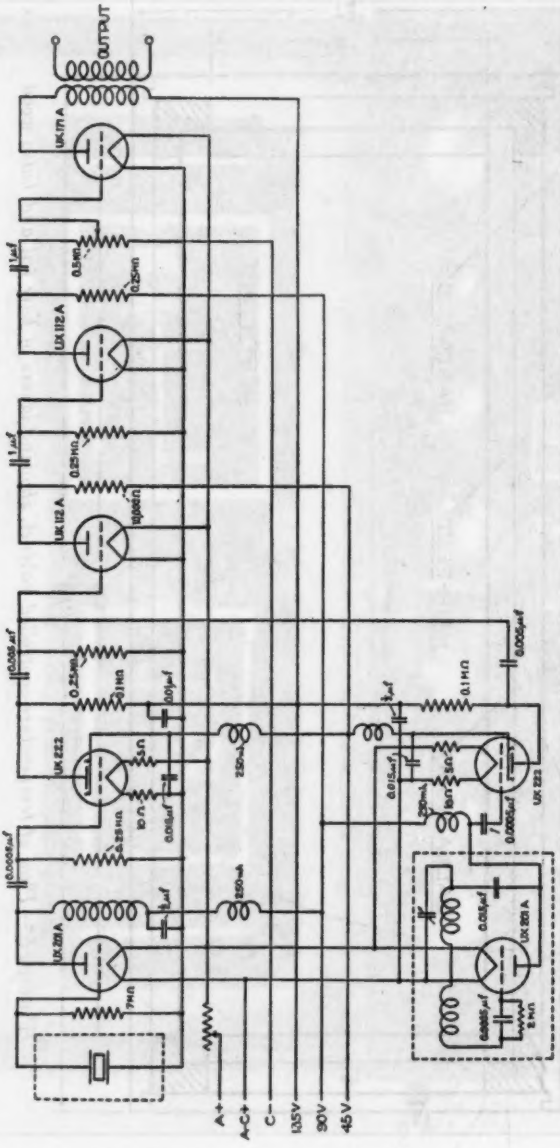

FIGURE 6.—*Complete circuit diagram of audio generator*

brate at its extensional mode. The electrodes are spaced with doughnut-shaped pyrex insulators. The piezo oscillator circuits (see fig. 6) are the same as those used in the secondary standards.[4]

[4] V. E. Heaton and W. H. Brattain, Design of a Portable Temperature-controlled Piezo Oscillator, Proc. I. R. E., vol. 18, p. 345; July, 1930. B. S. Jour. Research, vol. 4, (RP153); March, 1930.

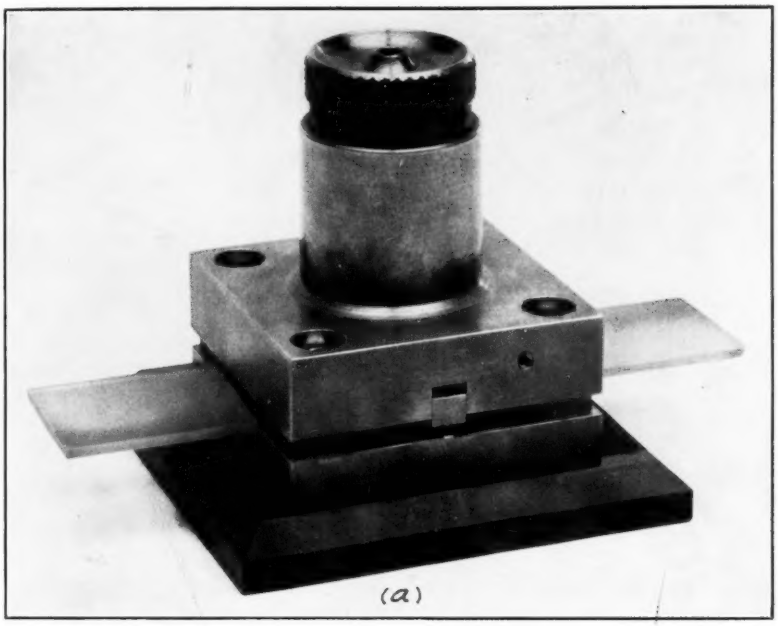

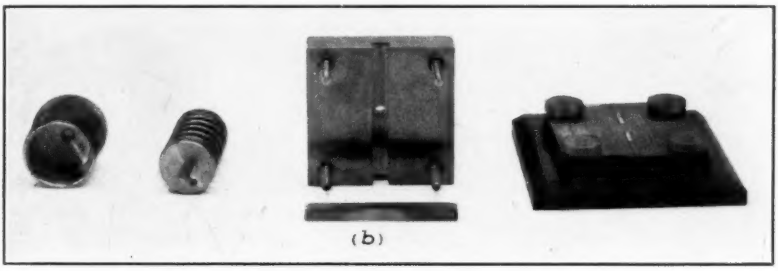

FIGURE 7.—*Quartz plate mounting*

a, Assembled; *b*, Disassembled.

The variable oscillator is a modified Hartley circuit (fig. 6), the frequency of which can be varied from approximately 28.50 to 30.00 kc. The tuning capacity is a 250 $\mu\mu$f, straight-line frequency, receiving condenser connected in parallel with a 200 $\mu\mu$f mica condenser. The hard rubber insulation which was used in the variable condenser has been replaced by pyrex insulation in order that the oscillator might maintain its calibration over a longer period of time. A 15 $\mu\mu$f variable condenser is connected in parallel with the other tuning capacities in order that the audio output may be adjusted to zero cycles per second when the main tuning condenser is set on the zero position. If some other audio-frequency standard is available, the output can be adjusted to exact agreement with that point on the calibration curve instead. The adjustment for this condenser is a bakelite rod brought out through the back of the case. The range of the audio-frequency generator, which, in this case, is only from 50 to 1,500 cycles per second, can be extended as desired by adjusting the capacities of the fixed and variable condensers.

The outputs of the two 30-kc oscillators are amplified separately and fed into a common detector. The resulting audio-frequency note is passed through a two-stage resistance-coupled amplifier. The resistance-capacity coupling is used in order to obtain approximately constant amplification over the entire audio-frequency range. A transformer is used in the output circuit to prevent any change in beat note due to a change in external connections.

The quality of the audio-frequency note which is obtained is largely dependent on the audio-frequency amplifier. If a pure sinusoidal wave-form were required it is probable that some refinements in the amplifier would have to be made. However, no attempt has been made to determine the exact wave-form under the present conditions. For the purpose for which the audio-frequency generator was designed, the quality of the note is entirely satisfactory.

The calibration of the audio-frequency generator has been checked repeatedly for some time. The original calibration and all recalibrations are made against harmonics of the 100-cycle-per-second output of the primary frequency standard. These measurements are made in the following manner. The condenser is set on the setting for 100 cycles per second, which is obtained from the original calibration curve. The audio-frequency note is then adjusted to exact agreement with the standard by means of the small auxiliary condenser previously described. The settings for harmonics of the 100 cycles are then determined. For any setting of the condenser the frequency has been found to vary less than 0.1 cycle per second. Furthermore, if the plate voltage is maintained at a constant value, the auxiliary condenser will not have to be readjusted for several hours at a time, which permits one to make measurements over an extended period without interruption.

WASHINGTON, July 8, 1931.

74280—31——6

THE POROSITY OF ELECTROPLATED CHROMIUM COATINGS

By W. Blum, W. P. Barrows,[1] and A. Brenner

ABSTRACT

Various methods for detecting porosity of chromium coatings were found to yield consistent results. Very thin deposits contain round pores. As the thickness is increased the porosity decreases to a minimum, after which an increase in thickness is usually accompanied by the formation of cracks, either parallel or random.

The well-known copper deposition method for detecting the porosity depends upon the fact that copper will deposit only in pores or cracks and not on the chromium. This test was made semiquantitative by measuring either the average apparent current density or the weight of copper deposited in two minutes at 0.2 v. The following conclusions are based on such measurements. Their practical significance will be determined by exposure tests now in progress.

The porosity usually increases on standing. This increase is accelerated by heating to 200° C. Changes in the composition of the solution have no marked effect on the porosity. An increase in the temperature of deposition, for example to 65° C., instead of the usual temperature of 45° C., greatly decreases the porosity, especially of thick coatings. At any given temperature the porosity is increased by raising the current density.

Deposits on nickel are less porous than those on other base metals. This difference is at least partly due to the greater ease of securing a bright finish on nickel prior to the chromium plating.

CONTENTS

	Page
I. Introduction	698
II. Methods of detecting porosity	698
1. Chemical methods	698
(*a*) On iron	698
(1) Ferroxyl test	698
(2) Copper sulphate immersion test	699
(*b*) On copper and brass	699
(*c*) On nickel	699
2. Copper deposition	699
3. Comparison of methods	700
4. Types of porosity	700
III. Evaluation of the porosity	701
IV. Factors governing porosity	702
1. Preparation of samples	702
2. Effect of time on porosity at room temperature	702
3. Effect of elevated temperature	704
4. Effect of conditions of deposition	705
(*a*) Composition of plating bath	705
(*b*) Operating conditions	706
(1) Thickness of deposits	707
(2) Temperature	707
(3) Current density	710
(*c*) The base metal	710
(1) Composition	710
(2) Surface condition	710
V. Conclusions	710
VI. Bibliography	711

[1] Formerly Research Associate of the American Electroplaters' Society.

I. INTRODUCTION

Although chromium plating is very extensively applied to automobiles and other metal products, it is now generally recognized that these deposits are porous and do not furnish much protection against the corrosion of a base metal such as steel. It is therefore the custom to first apply to the steel relatively thick layers of copper and nickel, followed by a thin film of chromium. The chromium serves more for resistance to tarnish than for the protection of the base metal against corrosion.

If the chromium deposits could be made more nearly impervious, their protective value would probably increase, and a smaller thickness of copper and nickel might then be adequate. This paper represents a study of the methods of detecting and evaluating the porosity of chromium coatings, and of the effects of different conditions upon the porosity. The results show that it is possible to produce less permeable deposits at high temperatures. Further observations, including exposure tests, will be required to determine whether this decrease in porosity has any marked effect upon the behavior of the plated metals when in service. This factor will be included in extensive exposure tests that are being conducted by cooperation of this bureau with the American Electroplaters' Society and the American Society for Testing Materials. Pending the completion of such tests, any conclusions based on the results of this investigation must be considered as tentative.

II. METHODS FOR DETECTING POROSITY

The porosity of chromium coatings may be detected by various methods.

1. CHEMICAL METHODS

In principle it is possible to detect pores or cracks in a metal coating by applying some reagent that will not attack the coating, but will act upon any exposed base metal and yield visible evidence of such action. The composition and concentration of the reagent will vary with the metals involved.

(a) ON IRON

(1) FERROXYL TEST.—This well-known test has been extensively used to detect porosity of metal coatings, such as copper, nickel, lead, and tin, upon iron or steel. The corrosive agent is usually sodium chloride and attack of the iron is detected by the formation of a blue color with the ferricyanide present in the reagent. This test is applicable only when the metal coating is, under the conditions used, more noble than the iron. It is therefore not applicable to steel coated with zinc or cadmium.

Although chromium in its "active" state is less noble than iron, under most conditions of exposure chromium becomes "passive," and is more noble. Hence the ferroxyl reagent serves to detect pores in chromium coatings on steel. In this work it was found that a reagent containing 10 g/l of sodium chloride and 1 g/l of potassium ferricyanide yielded within 30 minutes well-defined lines and spots wherever the steel was exposed. If the reagent contains a colloid, such as agar, which is often used in this test, less sharply defined

patterns are secured. At best the definition is not as good as in some of the other methods to be described.

(2) COPPER SULPHATE IMMERSION TEST.—When ordinary iron or steel is placed in an acidified copper sulphate solution, copper is deposited "by immersion." It was found that this reaction can be used to detect porosity of chromium coatings on steel, and that well-defined lines or spots appear within 30 minutes.

(b) ON COPPER AND BRASS

It has been reported by many authors that the ferroxyl test produces red spots wherever copper is exposed through a metal coating. As the red spots are probably due to the formation of cupric ferrocyanide, it seems more logical to apply a ferrocyanide than to depend upon partial reduction of the ferricyanide. Dilute nitric acid attacks copper and brass, but not chromium. A suitable reagent was prepared by dissolving 2 g/l of potassium ferrocyanide in dilute nitric acid (10 per cent by volume). Nitric acid of this concentration does not rapidly oxidize ferrocyanide, but it is preferable to add the latter to the nitric acid just before the mixture is used. This reagent produces well-defined spots or lines within 15 minutes wherever copper is exposed.

(c) ON NICKEL

It was not found possible to develop any reagent that will attack nickel rapidly and not affect chromium. A solution containing 2 g/l of dimethylglyoxime in ammonium hydroxide (1–1) slowly produces a pink color wherever nickel is exposed through chromium. As, however, the test requires 12 to 24 hours it is not suitable for inspection purposes.

2. COPPER DEPOSITION

It was observed independently by Kyropoulos (1)[2] and Dubpernell, as quoted by Baker and Pinner (2), that copper does not readily deposit upon chromium. This fact was used by Baker and Pinner (2) and by Baker and Rente (3) as a means of detecting porosity of chromium coatings. They found that when a chromium-plated surface was made the cathode in an acidified copper sulphate solution, copper was deposited only where there were pores or cracks in the chromium. This method was used by them to compare and classify the porosities of various chromium deposits.

In experiments at this bureau it was found that copper can be deposited upon electrodeposited chromium, though it requires a higher potential than to deposit copper on other metals. In order to insure that the copper will deposit only on the exposed base metal and not upon the chromium, it is therefore desirable to control the applied voltage and not the apparent current density as was done by the above authors. The actual current density is indeterminate, as the area upon which the copper is deposited is not known.

It was found that copper is deposited in sharply defined spots or lines within two minutes when a potential of 0.1 to 0.2 volt is applied between a copper anode and a chromium plated cathode that are about 5 cm (2 inches) apart. It is conceivable that copper may deposit in cracks in the chromium that do not extend through to the base

[2] Numbers in parentheses in the text refer to the bibliography at the end of the paper.

metal. If so, the formation of the copper deposits would not be a true criterion of porosity. To test this possibility a piece of chromium-plated copper was subjected to copper deposition, and the resulting spots and lines of copper were observed and photographed. The chromium was then dissolved off with dilute hydrochloric acid, after which, examination showed the same pattern, which now consisted of ridges of copper adhering to the base metal. The copper deposition test therefore appears to be a reliable measure of the porosity. Subsequently it was found that relatively thick chromium deposits may contain cracks, visible under a microscope, in which copper does not deposit. Presumably such cracks do not extend through to the base metal.

Numerous observations indicate that the resistance of a chromium surface to copper deposition is caused by its passivity. This may be destroyed by treatment with hydrochloric acid, by cathodic pickling or cleaning, or even by vigorous scratching or buffing. Within a short time after such treatments, copper will readily deposit on the chromium itself. On standing in air the passivity slowly returns. This restoration of passivity can be accelerated by making the articles anodic in the acid copper bath for one minute or less with a potential of not more than 0.8 volt. Under these conditions no measurable current passes. The copper deposition method for detecting porosity is valid only on passive chromium. The deposits as removed from the chromium bath and rinsed are in this condition, and the following results apply to such coatings.

3. COMPARISON OF METHODS

In order to determine whether the above methods, so far as they are applicable, yield comparable results, deposits of chromium of different thicknesses were made on different base metals and tested by appropriate methods. The results showed similar patterns for companion plates, and hence proved that each of the above methods may be used to detect porosity. As, however, the deposition method is applicable to all base metals and can be made at least semiquantitative, it was employed in all subsequent experiments.

4. TYPES OF POROSITY

Figures 1, 2, and 3 illustrate the results obtained by copper deposition. In general thin deposits (up to 0.5 micron or 0.00002 inch) of chromium contain fine holes, roughly circular, which are similar to those in most other electroplated coatings. (Fig. 1.) Thicker deposits (for example 0.5 to 25 microns, or 0.00002 to 0.0001 inch) usually contain cracks, which have also been observed in deposits of other metals, such as platinum, which absorb much hydrogen during deposition. It was observed that the initial cracks in the chromium, especially when deposited upon copper and nickel, are parallel to each other, and perpendicular to the direction in which the base metal was last polished. (Fig. 2.) No satisfactory explanation can be offered for this curious phenomenon, which is probably associated with strains set up in the metal surface during the buffing of the base metal. In thick, badly cracked deposits (fig. 3) the lines are random and show no preferred orientation. The various types of porosity in chromium deposits have been described by different authors (2), (3), (4).

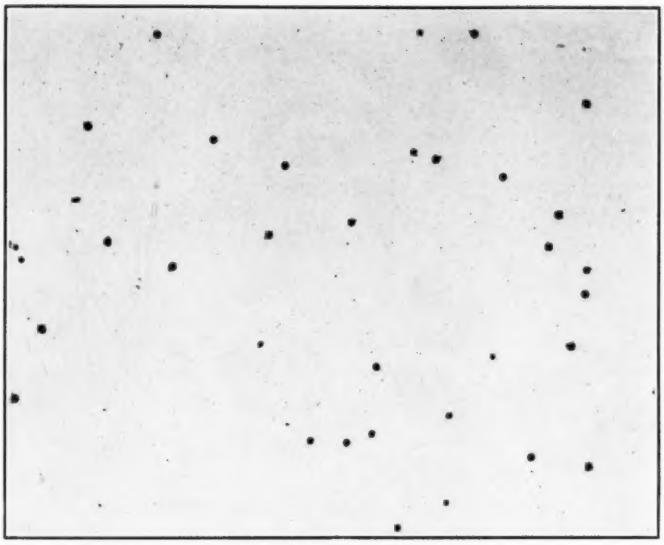

FIGURE 1.—*Pores in thin chromium coatings on nickel* (× *40*)

Thickness=0.14 micron (0.000006 inch). Porosity (expressed in this and other figures as current density in the copper deposition test); = 25 ma/dm².

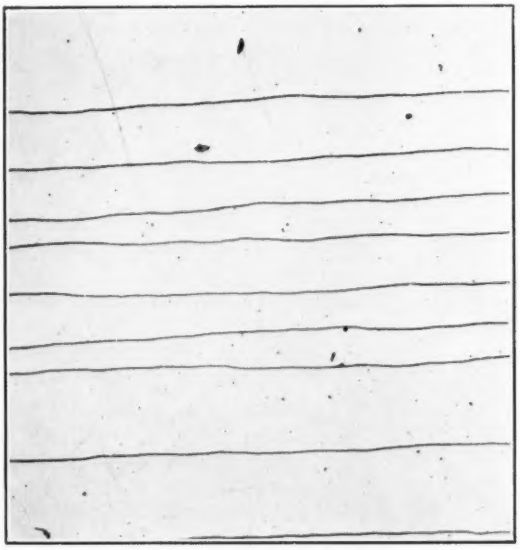

FIGURE 2.—*Parallel cracks in moderately thick chromium coatings on nickel* (× *40*)

The cracks are perpendicular to the direction of last polishing of base metal. Thickness=1.25 microns (0.00005 inch); porosity=180 ma/dm².

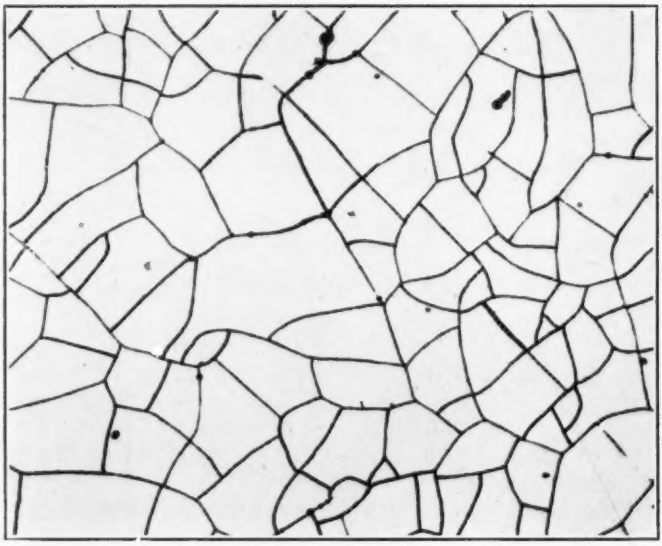

FIGURE 3.—*Random cracks in thick chromium coatings on nickel* (× *100*)

Thickness=2.75 microns (0.00011 inch); porosity=215 ma/dm².

UNIV. OF MICH.

III. EVALUATION OF THE POROSITY

As the discontinuities in the coatings may consist of either pores or cracks and may vary greatly in number, size, and orientation, it is difficult from visual examination to determine whether better protection would be afforded by one type of chromium coating than by another. Such a method of test might be more valid if it were possible to measure, or at least to compare, the areas of base metal exposed.

If two electrodes are immersed in an electrolyte at a fixed distance from each other and a constant voltage is applied, the current that passes will increase, but not linearly, if the area of one or both electrodes is increased. In depositing copper at a low potential upon a chromium-plated cathode, the chromium surface is in effect insulated, and current passes only to the exposed base metal, which latter, therefore, represents the effective cathode surface. A change in this area will produce a corresponding change in the current and in the weight of copper deposited in a specified time.

TABLE 1.—*Evaluation of porosity of chromium coatings by copper deposition at 0.2 v for two minutes*

Cr. thickness		Type of porosity	Average current density	Copper deposition		
Microns	inch / 100,000			Calculated	Found	Cathode efficiency
			ma/dm²	*g*	*g*	*Per cent*
0.13	0.5	Many pores	365	0.0145	0.0146	101
.13	.5	do	346	.0137	.0140	102
.25	1.0	do	249	.0099	.0100	101
.25	1.0	do	205	.0081	.0073	90
.5	.2	Pores and short cracks	81	.0032	.0036	112
.5	.2	do	100	.0039	.0036	92
1.0	4	Long cracks	116	.0046	.0052	113
1.0	4	do	101	.0040	.0042	105
5.0	20	Network	70	.0028	.0030	107
5.0	20	do	85	.0034	.0032	95
25.0	100	do	54	.0021	.0025	119
25.0	100	do	40	.0016	.0016	100

In the experiments recorded in Table 1, the chromium-plated copper cathodes were 5 by 10 cm (2 by 4 inches) and had a total surface of 1 dm^2 (16 square inches). Each plate was suspended between two copper anodes of the same size, 5 cm (2 inches) away, in a small glass jar in which the electrodes almost filled the cross section of the copper solution. This contained 200 g/l (27 oz./gal.) of copper sulphate and 75 g/l (10 oz./gal.) of sulphuric acid. A constant bath voltage of 0.20 v. was applied, and the current was read on a milliammeter at intervals of 30 seconds for two minutes. As in most experiments the increase in current from zero was approximately linear, the average current was equal to one-fifth of the sum of the four readings. For practical purposes this is equal to the current at the end of one minute. For longer periods than two minutes, the results were less reproducible. The weight of copper deposited in two minutes was determined from the increase in weight of the cathodes.

The data in Table 1 show that the cathode efficiency for the copper deposition approaches 100 per cent as closely as may be expected from an average current computed from four increasing values.

Hence either the current (apparent current density) or the weight of copper per unit area may be used as a measure of the porosity. The subsequent results for porosity represent "average current density in milliamperes per square decimeter for a period of two minutes at 0.2 v."

As shown in Table 1, the results are fairly reproducible. In general, the greatest proportional variations were found in deposits in which the cracking had just started, and in which the metal coating was no doubt in a state of strain. Naturally under such conditions the extent of the cracking would vary in different samples. All subsequent results in this paper represent the average of two or more specimens.

A few efforts were made to estimate microscopically the areas of the copper deposits, and thus to obtain the actual and not merely the relative porosities. The results were not consistent or reproducible. It was evident that even in two minutes' deposition the copper extended considerably beyond the original width of the cracks, sometimes to form a nearly cylindrical wire attached to the copper in the crack. If the deposition was conducted for less than two minutes, some of the finest cracks were not revealed, while deposition for more than two minutes disclosed few, if any, additional cracks, but simply made the copper deposits larger and less distinct. The results of this method of test must therefore be considered as merely semiquantitative, and comparable with each other only when the conditions for the copper deposition are carefully defined and controlled.

IV. FACTORS GOVERNING POROSITY

1. PREPARATION OF SAMPLES

All the specimens used in this phase of the study were flat strips having a total area of 1 dm^2 (16 square inches). Each was plated with chromium in a small glass jar, in which the specimen almost completely filled the cross section of the solution. A lead anode of the same size was placed about 5 cm (2 inches) from each side of the cathode. The currents through the two anodes were kept equal, so as to obtain uniform deposits on each side of the cathode. The bath was kept at the specified temperatures to $\pm 1°$ C. The "standard" solution was prepared from 250 g/l of CrO_3 and 2.5 g/l of H_2SO_4. This solution was frequently renewed, and hence did not contain much trivalent chromium.

The cathodes were all buffed or polished before being chromium plated. The nickel plated copper had a coating of nickel about 0.01 mm (0.0004 inch) thick, which was also polished. The cathodes were introduced into the chromium bath in such a way as to close the circuit. Copper and brass cathodes are likely to be etched and to show increased porosity if this procedure is not followed. The thickness of each deposit was computed from the current density, plating period, and previously determined cathode efficiency.

2. EFFECT OF TIME ON POROSITY AT ROOM TEMPERATURE

Preliminary observations showed that the porosity and especially the cracking of chromium deposits increases with time. Hence measurements of porosity made soon after the chromium is deposited

may not represent the properties of the coatings in service. Corresponding samples were allowed to stand at room temperature in clean air and were tested at intervals. The results in Table 2 show that the most rapid increase in porosity occurs within 24 hours, although the porosity of thick deposits continues to increase for two weeks or more. Thin deposits, which contain pores rather than cracks, do not increase in porosity on standing.

TABLE 2.—*Effect of time on porosity of chromium deposits exposed to air at room temperature*

[Porosities expressed as apparent average current densities.]

Experiment	Base metal	Cr. thickness		Elapsed time, days			
		Microns	Inch / 100,000	¼	1	7	14
				ma/dm²	*ma/dm²*	*ma/dm²*	*ma/dm²*
1	Copper	5.0	20	49	118	123	148
2	Brass	5.0	20	20	73	83	108
3	Nickel plated	5.0	20	94	126	165	136
4	Copper	.5	2	29	15	21	25

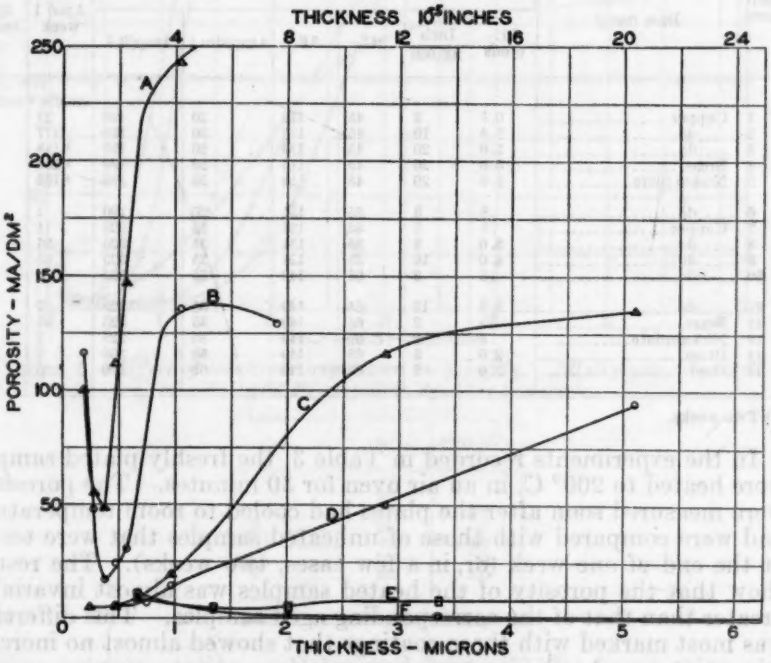

FIGURE 4.—*Effect of time on porosity*

A, 1 week; on Cu, 45°C., 10 amp/dm²
B, 1 hour; on Cu, 45°C., 10 amp/dm²
C, 1 week; on Ni, 45°C., 20 amp/dm²
D, 1 hour; on Ni, 45°C., 20 amp/dm²
E, 1 week; on Cu, 65°C., 60 amp/dm²
F, 1 hour; on Cu, 65°C., 60 amp/dm²

Except as otherwise noted, the subsequent tests were all made after the deposits had aged for one week. The difference in results for one hour and one week is illustrated in Figure 4 for deposits produced

under widely different conditions. Coatings with low porosity show little difference with time in the actual values, though the proportional change in porosity may be much greater than for more porous samples.

3. EFFECT OF ELEVATED TEMPERATURE

It might be expected that heating chromium deposits would accelerate the evolution of hydrogen and the cracking. Heating chromium deposits to change their properties has been suggested by Enos (5) and by Ollard (6). Wirshing (7) recently recommended the heating of chromium-plated metals to 200° C., and reported that this treatment produced an increased resistance to corrosion in a calcium chloride spray. Herschman (8) found that chromium plated gages heated to 300° C. showed a marked increase in resistance to wear.

TABLE 3.—*Effect of heating upon the porosity of chromium deposits*

Heated 30 minutes at 200° C. (392° F.)

Experiment	Conditions of deposition							Porosity	
	Base metal	Cr. thickness		Temperature		Current density		Aged 1 week	After heating
		Microns	Inch 100,000	°C.	°F.	Amp/dm²	Amp/ft²		
								ma/dm²	*ma/dm²*
1	Copper	0.5	2	45	113	20	190	21	319
2	do	2.5	10	45	113	20	190	177	221
3	do	5.0	20	45	113	20	190	[1] 148	146
4	Brass	5.0	20	45	113	20	190	[1] 108	142
5	Nickel plate	5.0	20	45	113	20	190	[1] 136	128
6	do	.8	3	55	131	20	190	1	12
7	Copper	.8	3	55	131	35	325	11	192
8	do	2.0	8	55	131	35	325	24	165
9	do	4.0	16	55	131	35	325	55	118
10	do	.5	2	65	149	35	325	4	54
11	do	3.3	13	65	149	35	325	2	38
12	Brass	.5	2	65	149	35	325	13	120
13	Nickel plate	.5	2	65	149	35	325	2	8
14	Brass	2.0	8	65	149	60	560	2	108
15	Steel	2.0	8	65	149	60	560	6	45

[1] Two weeks.

In the experiments recorded in Table 3, the freshly plated samples were heated to 200° C. in an air oven for 30 minutes. The porosities were measured soon after the plates had cooled to room temperature, and were compared with those of unheated samples that were tested at the end of one week (or, in a few cases, two weeks). The results show that the porosity of the heated samples was almost invariably greater than that of the corresponding aged samples. This difference was most marked with those coatings that showed almost no increase in porosity on standing.

From these results it appears that the reported increase in corrosion resistance produced by heating is not due to a decrease in porosity. Wirshing's results may be due to a change in the specific action of calcium chloride on the chromium coating, for example, through an increase in the passivity of the chromium when it was heated in air. The reported increase in abrasion resistance after heating bears no necessary relation to the porosity. It is probably caused by a decrease in brittleness of the chromium when the hydrogen is expelled.

4. EFFECT OF CONDITIONS OF DEPOSITION

(a) COMPOSITION OF PLATING BATH

The most important variables in a chromium bath are the content of chromic acid and the ratio of chromic acid to sulphate. Figure 5 shows that on nickel at 45° C. (113° F.) and 20 amp/dm ^{2} (186 amp/sq. ft.), with a CrO_3/SO_4 ratio of 100, a change in CrO_3 content from 250 to 400 g/1 (33 to 55 oz./gal.) has a slight beneficial effect upon the

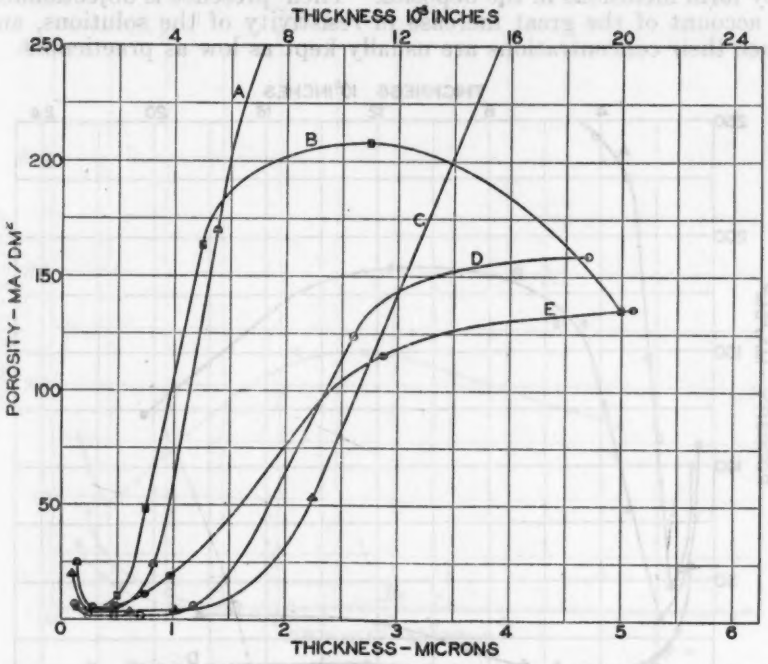

FIGURE 5.—*Effect of solution composition on porosity. All deposits on nickel at 45°C. and 20 amp/dm², aged for one week*

	CrO_3	CrO_3/SO_4
	g/l	
A [1]	150	100
B	250	50
C [1]	400	100
D	250	150
E	250	100

[1] Includes points beyond the diagram.

porosity of thin coatings. Baker and Rente (3) also found a decrease in porosity when the concentration was increased. More dilute solutions, such as 150 g/1 (20 oz./gal.) of CrO_3 yield slightly more porous thin deposits and a more sharply defined minimum porosity.

As the reproductility is only about 25 per cent, no high accuracy should be attributed to individual points on these and succeeding curves. Their shapes and relative positions have merely a semi-quantitative significance.

An increase in the "sulphate ratio" to 150 produces a decrease in the porosity of thin deposits, while a decrease in the ratio to 50 increases the porosity. It was not found practicable to produce uniformly bright, thin deposits on nickel with a higher sulphate ratio, such as 200, as then some brown spots invariably formed.

No experiments were made upon the effects of trivalent chromium or of iron. It is at least probable that high concentrations of either of these in the plating bath will increase the porosity, especially if they form inclusions in the deposits. Their presence is objectionable on account of the great increase in resistivity of the solutions, and hence their concentrations are usually kept as low as practicable.

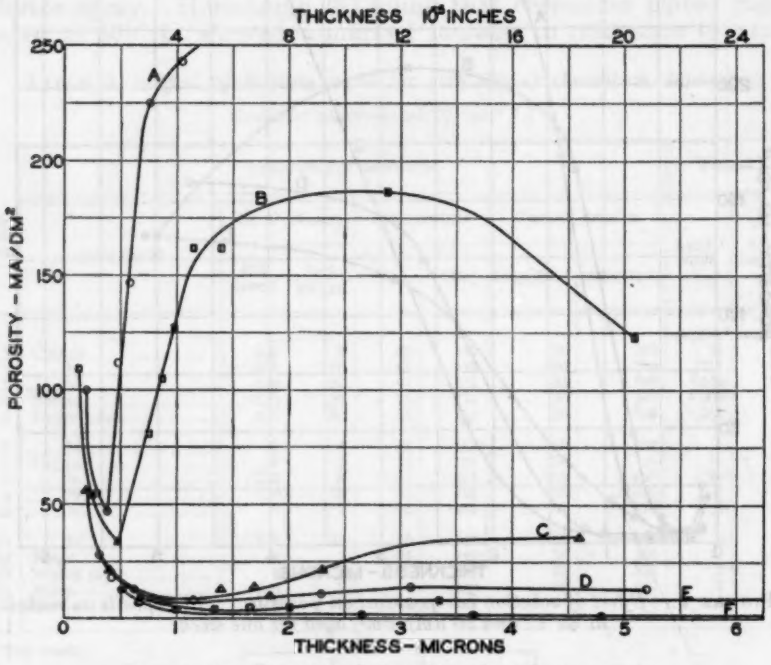

FIGURE 6.—*Porosity of chromium deposits on copper*

Solution containing 250 g/l CrO_3 and $CrO_3/SO_4=100$.

	Temperature	Current density
	°C.	amp/dm²
A	45	10
B	45	20
C	55	35
D	55	20
E	65	60
F	65	35

(b) OPERATING CONDITIONS

As the temperature and current density must be coordinated in order to obtain bright deposits, and as their effects vary greatly with the thickness, these three factors were simultaneously investigated. The results are shown in Figures 6 to 9 in which all the deposits were bright or nearly so.

(1) THICKNESS OF DEPOSITS.—The most striking feature of these curves is the pronounced minimum in each curve for deposits made at 45° C. or lower. The existence of a minimum porosity at a certain thickness has been reported by Baker and Rente (3), and is no doubt partly responsible for the present extensive use of chromium deposits with an average thickness of about 0.0005 mm (0.00002 inch). It should be noted, however, that the minimum porosity under certain conditions may be much greater than that under some other con-

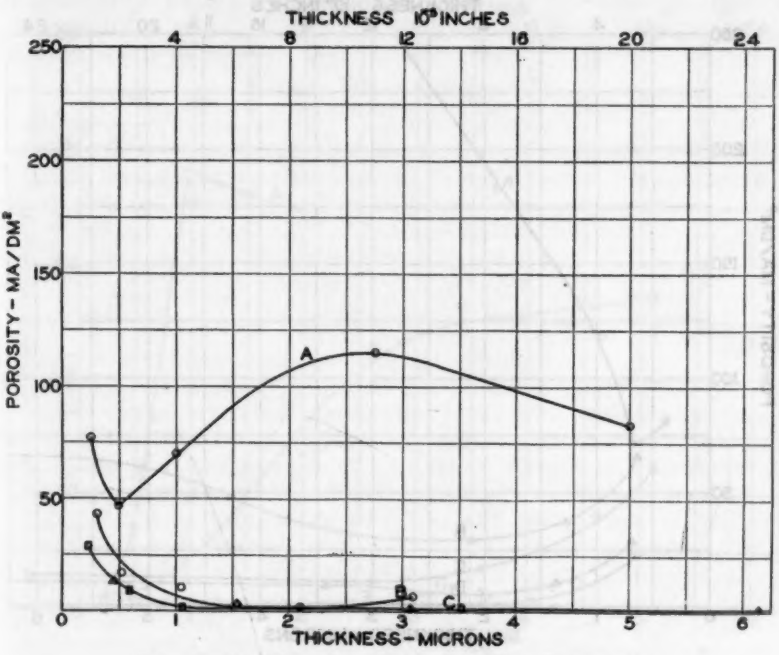

FIGURE 7.—*Porosity of chromium deposits on brass*

Solution containing 250 g/l CrO_3 and CrO_3/SO_4=100.

	Temperature	Current density
	°C.	amp/dm²
A	45	20
B	55	20
C [1]	65	60
C [1]	65	35

[1] Curves practically coincident.

ditions, and that it does not necessarily occur at the same thickness. In general, the porosity to the left of the minimum is caused by pores and to the right by cracks. The minimum, therefore, corresponds to the thickness at which most of the pores have been "sealed" and few cracks have appeared.

(2) TEMPERATURE.—In general, it was observed that an increase in bath temperature, accompanied by an appropriate current density to produce bright deposits, yields a minimum porosity that is lower and less sharply marked than at lower temperatures. The curves to

the left of the minimum are very similar; that is, the conditions of deposition do not greatly change the extent of the pores. The large differences caused by higher temperature become evident in the decreased tendency toward cracking as the thickness is increased. On all the base metals, at 65° C. (149° F.) and 35 amp./dm.^{2} (325 amp./ft.^{2}) the porosity decreases to a negligible value, which persists as the thickness is increased, even beyond that shown in the figures.

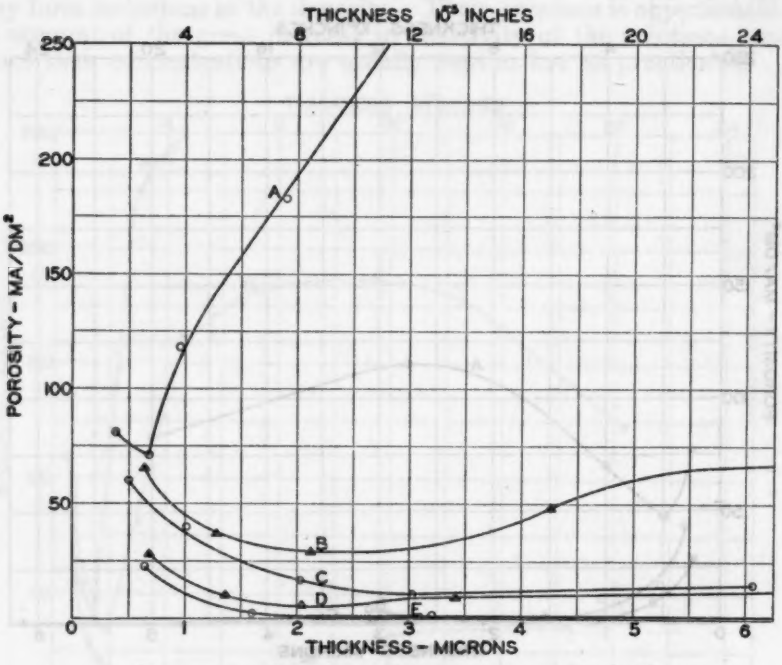

FIGURE 8.—*Porosity of chromium deposits on steel*

Solution containing 250 g/l CrO_3 and CrO/SO_4=100.

	Temperature	Current density
	°C.	amp/dm^2
A [1]	45	10
B [1]	55	35
C	55	20
D [1]	65	60
E [1]	65	35

[1] Includes points beyond the diagram.

Baker and Rente (3) obtained "nearly perfect" plates at 55° C. (131° F.). Recently Willink (9) reported that at still higher temperatures (probably approaching 100° C. or 212° F.) and current densities exceeding 100 amp./dm.^{2} (930 amp./ft.^{2}) dense deposits were obtained on tools and dies. He did not, however, measure the porosity of the coatings. In this investigation no temperatures above 65° C. (149° F.) were used, as most of the deposits produced at that temperature were practically impervious.

If the cracking of the chromium deposits is due to the evolution of hydrogen that is included in them during deposition, it is reasonable to suppose that the least cracked deposits, for example, those produced at a high temperature, have initially a lower content of hydrogen than the more cracked deposits. No quantitative data are available upon the relation between conditions of deposition and the hydrogen content of chromium. Any lower hydrogen content of the deposits

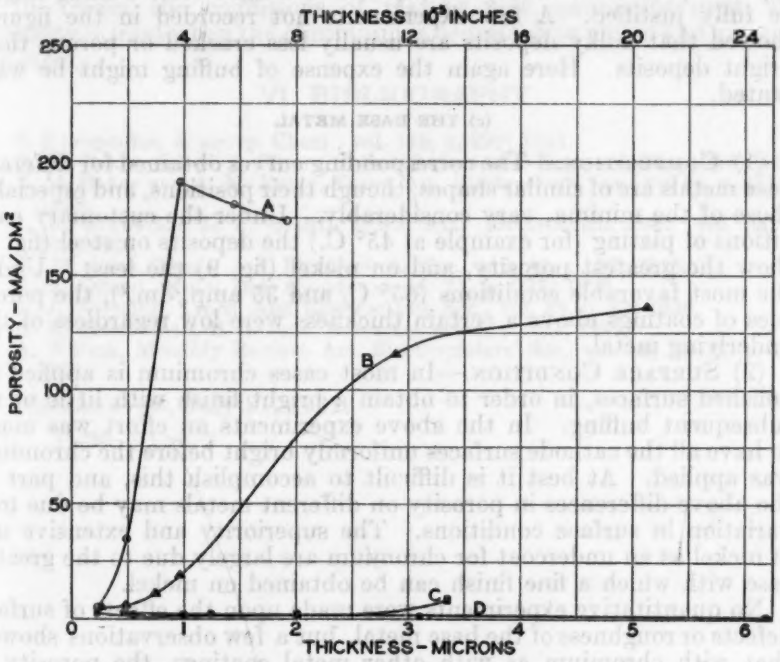

FIGURE 9.—*Porosity of chromium deposits on nickel*

Solution containing 250 g/l CrO_3 and CrO_3/SO_4=100.

	Temperature	Current density
	°C.	amp/dm²
A	45	5
B	45	20
C [1]	55	20
C [1]	65	60
D	65	35

[1] Curves practically coincident.

made at higher temperatures is probably caused by lower solubilities of hydrogen in the chromium at the higher temperatures. It certainly is not caused by a change in the cathode efficiency, as the latter is nearly uniform (from about 10 to 15 per cent) for bright deposits. In all cases a large volume of hydrogen is evolved, so that the chromium always has the opportunity to become saturated with hydrogen during its deposition.

(3) CURRENT DENSITY.—An increase in current density at a given temperature usually increases the tendency toward cracking. As low a current density as will produce bright deposits should, therefore, be used. It was difficult to obtain at 65° C. (149° F.) as bright deposits as the best at 45° C. (113° F.), although fairly bright deposits were obtained at 65° C. over a wide current range. If experience shows that deposits produced at a high temperature have a superior protective value, the expense of a light color buffing might be fully justified. A few experiments not recorded in the figures showed that milky deposits are usually less cracked or porous than bright deposits. Here again the expense of buffing might be warranted.

(c) THE BASE METAL

(1) COMPOSITION.—The corresponding curves obtained for different base metals are of similar shapes, though their positions, and especially those of the minima, vary considerably. Under the customary conditions of plating (for example at 45° C.) the deposits on steel (fig. 8) show the greatest porosity, and on nickel (fig. 9) the least. Under the most favorable conditions (65° C. and 35 amp./dm.^{2}), the porosities of coatings above a certain thickness were low regardless of the underlying metal.

(2) SURFACE CONDITION.—In most cases chromium is applied to polished surfaces, in order to obtain a bright finish with little or no subsequent buffing. In the above experiments an effort was made to have all the cathode surfaces uniformly bright before the chromium was applied. At best it is difficult to accomplish this, and part of the above differences in porosity on different metals may be due to a variation in surface conditions. The superiority and extensive use of nickel as an undercoat for chromium are largely due to the greater ease with which a fine finish can be obtained on nickel.

No quantitative experiments were made upon the effects of surface defects or roughness of the base metal, but a few observations showed that with chromium as with other metal coatings, the porosity is thereby increased.

V. CONCLUSIONS

1. Copper deposition at a low potential serves to detect pores and cracks in chromium coatings on all base metals.

2. If all the conditions during the copper deposition are controlled, either the average apparent current density or the weight of copper per unit area may serve as a semiquantitative measure of porosity.

3. The porosity, and especially the cracking of the chromium coatings, increase rapidly during the first 24 hours' standing, and more slowly for the following few weeks.

4. If the deposits are heated to 200°C. (392°F.) for a short time, the cracking is much more pronounced than on specimens aged at room temperature.

5. The porosity of thin coatings is slightly decreased by an increase in the content of chromic acid.

6. The porosity of thin coatings is slightly decreased by an increase in the CrO_3/SO_4 ratio to the maximum value that will yield bright deposits.

7. Chromium deposits produced at or below 45°C. (113°F.) show a marked minimum in porosity at a thickness of about 0.5 micron (0.00002 inch).

8. Deposits produced at higher temperatures, such as 55° or 65°C. (131° or 149°F), have a lower minimum porosity, and the porosity does not increase greatly as the thickness is increased.

9. At any given temperature the porosity is increased by an increase in current density.

10. Under the conditions of plating now commonly used, the porosity is least when the chromium is deposited on nickel and greatest on steel.

VI. BIBLIOGRAPHY

1. S. Kyropoulos, Z. anorg. Chem., vol. 119, p. 299; 1921.
2. E. M. Baker and W. L. Pinner, J. Soc. Automotive Eng., vol. 22, p. 331; 1928.
3. E. M. Baker and A. M. Rente, Trans. Am. Electrochem. Soc., vol 54, p. 337; 1928.
4. L. E. Grant and L. F. Grant, Trans. Am. Electrochem. Soc., vol. 54, p. 509; 1928
5. G. M. Enos, Trans. Am. Electrochem. Soc., vol. 48, p. 37; 1925.
6. E. A. Ollard, Metal Ind. (London), vol. 27, p. 235; 1925.
7. R. J. Wirshing, Trans. Am. Electrochem. Soc., vol. 58, p. 89; 1930.
8. H. K. Herschman, B. S. Jour. Research, vol. 6, p. 295; 1931.
9. A. Willink, Monthly Review, Am. Electroplaters' Soc., vol. 18, No. 4, p. 32; 1931.

WASHINGTON, July 21, 1931.

74280—31——7

THE USE OF SATURATED AMMONIUM CHLORIDE[1] IN THE ELIMINATION OF CONTACT POTENTIALS

By C. N. Murray and S. F. Acree

ABSTRACT

In the electrometric measurement of the concentrations of various ions in plant extracts and other organic mixtures the potential of the junction between two electrode liquids is a source of error unless this contact potential is calculated, measured, or eliminated. The study of various concentrations of ammonium chloride up to saturated (5.66 *N*) gives a practical method for annulling the contact potential to within ± 1.0 m .v.

CONTENTS

	Page
I. Introduction	713
II. Experimental work on contact potentials and their elimination	716
III. Discussion	720

I. INTRODUCTION

In the use of e. m. f. measurements for the determination of *H*-ion and other ionic concentrations or more exactly the ionic activities in xylan, lignin and other plant extracts, a source of serious error may be found in the potential of the junction between electrode liquids of different composition.[2] This potential may at times amount to 35 m. v. or more, and failure to correct for it would then cause an error of at least 0.5 pH.

There are three types of methods available for treating contact potentials. Of these, the first is that of calculation by formulas devised by Planck[3] and simplified later by Henderson,[4] Abegg and Cumming,[5] Lewis,[6] and more recently from newer points of view by MacInnes,[7] and Smith.[8] These formulas can be applied to specified simple cases for which they have been verified experimentally but can not be used with complex unknown mixtures, such as plant extracts and culture media.

[1] Presented in part at the Baltimore meeting of the American Chemical Society, April, 1925.

[2] Desha, L. J., and Acree, S. F., On Difficulties in the Use of the Hydrogen Electrode in the Measurement of the Concentration of Hydrogen Ions in the Presence of Organic Compounds, presented at Baltimore Meeting of the Am. Chem. Soc., 1908; Science, vol. 30, p. 624; 1909. Am. Chem. J., vol. 46, p. 638; 1911.

[3] Planck, M., On the Potential Difference between Two Dilute Solutions of a Binary Electrolyte, Wied. Ann., vol. 39, p. 178; vol. 40, p. 561; 1890. Ann. Physik, vol. 4, p. 581; 1890.

[4] Henderson, P., Thermodynamics of Liquid Chains, Z. Physik. Chem., vol. 59, p. 118; 1907: vol. 63, p. 325; 1908.

[5] Cumming, A. C., The Elimination of Potential Due to Liquid Contact, Trans. Faraday Soc., vol. 2, p. 213; 1906: vol. 8, p. 86; 1912: vol. 9, p. 174; 1913: Zt. Elektrochem, vol. 13, p. 17; 1907.

[6] Lewis, G. N., and Sargent, L. W., Potentials Between Liquids, J. Am. Chem. Soc. vol. 31, p. 363; 1909.

[7] MacInnes, D. A., and Parker, Karr, Potassium Chloride Concentration Cells, J. Am. Chem. Soc., vol. 37, p. 1445; 1915: MacInnes, D. A., Liquid Junction Potentials, Ibid., vol. 37, p. 2301; 1915: MacInnes, D. A., and Yeh, Y. L., The Potentials at the Junctions of Monovalent Chloride Solutions, Ibid; vol. 43, p. 2652; 1921.

[8] Smith, E. R., Potential Differences across the Boundaries between Solutions of Mixed Univalent Chlorides, B. S. Jour. Research, vol. 2, p. 1137; 1929.

The second type is the direct measurement of the contact potential by a more or less absolute procedure which gives both the contact potential and the electrode potential. Only four of these methods are available, and they are limited to special cases. One used by MacInnes and Yeh with simple solutions and by Smith with mixtures is cited above. Another by Elliott, Duschak and Acree [9] depends upon the use of negative (calomel or silver chloride) electrodes, and of positive (hydrogen or quinhydrone) electrodes in two different concentrations of a solute (such as hydrochloric acid), whose anions and cations, respectively, are in equilibrium with the electrodes. The e. m. f. across the negative (calomel) electrodes is the algebraic sum of the contact potential and the electrode potentials, $cp+E=a$. The e. m. f. across the positive (hydrogen) electrodes is the algebraic difference between the contact potential and the electrode potentials, $cp-E=b$. These two equations give the values of cp and E. The ratios $a/(a+b)$ and $b/(a+b)$ are the transference numbers Nc and Na. A third method of this type involves the two e. m. f. readings given by the two contacted solutions containing two pairs of electrodes, one set giving an e. m. f. corresponding to the known a power of the ratio of the activities of an ion common to the two solutions and the other set giving an e. m. f. involving the known b power of the same ratio of the activities of that or another ion. In both cases the e. m. f. involves also the contact potentials and the equations may be written as follows for hydrogen-ion activities:

$$E=cp+(RT/F)\log(H/H')^a \quad (1)$$

and

$$E'=cp+(RT/F)\log(H/H')^b \quad (2)$$

By difference we get

$$E'-E=(b-a)(RT/F)\log(H/H').$$

From this equation (H/H'), the ratio of the hydrogen-ion activities may be calculated and substituted in either (1) or (2) to give cp. The hydrogen electrode functions through the first power of the ratio of the hydrogen-ion activities and the manganese dioxide electrode [10] involves the second power of the same ratio of the hydrogen-ion activities in the presence of M/1,000 Mn salts in both acid solutions. Within the experimental errors of about 1 m. v. the hydrogen and manganese dioxide electrodes have been found to give the contact potentials and electrode potentials calculated and observed by other methods for solutions of HNO_3 and HCl. They may prove to be generally useful below pH 7.0 in complex organic solutions when the necessary salt errors are taken into consideration. By the addition of M/1,000 Mn salt to any unknown solution surrounding both a manganese dioxide electrode and a hydrogen (or other equivalent) electrode, the measured e. m. f. can be employed to calculate the pH without directly involving H-ion standards and contact potentials. A fourth method applicable to two different

[9] Article presented by Elliott, F., Duschak, E., and Acree, S. F., at the St. Louis meeting of the Amer. Chem. Soc.; 1920.

[10] Tower, O. F., Studies of Superoxide Electrodes, Zt. physik. chem., vol. 18, p. 17; 1895, on the Potential Differences at the Junctions of Dilute Solutions, Ibid, vol. 20, p. 198; 1896. Hill, J. R., The Oxidation-Reduction Potential of the Manganese Dioxide Mangan Ion Electrode, Diss., Catholic University of America; 1929.

concentrations of a uni-univalent electrolyte in contact, such as dilute (0.1*N*–0.001*N*) solutions of potassium chloride or hydrochloric acid, is the use of two pairs of electrodes reversible to both ions (for example, AgCl or HgCl electrodes for chloride ions), and measurement of the e. m. f. values with and without transference. The electrode potential is just one-half of the e. m. f. without transference. As the e. m. f. with transference is equal to the algebraic sum of the electrode potential and the contact potential, the subtraction of the electrode potential (obtained as above) therefrom gives the contact potential. The transference numbers can be calculated from the value of *cp*. This method can be modified for other types of electrolytes and complex solutions.

The third type is a practical general method of elimination or reduction of the contact potential to very small values by inserting between the electrode liquids concentrated solutions of salts whose ions have nearly equal mobilities. This method may be advantageously used in connection with the four preceding ones to see whether the elimination is complete. It may be said in advance that the efficiency of each respective contact potential eliminator varies with the junction liquids and hence that the method is only approximate. The following abstracts [11] give a résumé of the previous work on elimination of contact potentials.

Planck, cited above, and Nernst [12] proved in 1889 that two solutions of a substance with nearly equal ionic mobilities have low contact potentials. In 1895, Tower, cited above, discovered that the insertion of potassium chloride (*N*/128 to *N*/1) or of other salts between solutions of acids tends to eliminate contact potentials. In 1905, Bjerrum [13] measured the two e. m. f. produced when he interposed first 1.75 *N* KCl, which he called "half saturated," and then 3.5 *N* KCl, called "saturated," between two solutions of a given chloride containing calomel electrodes. He subtracted the difference between these two e. m. f. values from that found with the 3.5 *N* KCl solution, and called the resulting extrapolated e. m. f. the correct value for the electrode potentials. Although he clearly pointed out that the extrapolation must not amount to more than 1 or 2 m. v. his method has frequently been used incorrectly by other workers having larger corrections in their *H*-ion investigations. Confusion also arises because saturated KCl at 25° C. is 4.1 *N* and not 3.5 *N*.

The use of varying concentrations of ammonium nitrate up to saturated by Cumming [14] and Abegg in 1906 nearly completely eliminated the contact potential between different solutions of silver nitrate or of other salts. Desha, Loomis, Myers, Clarke, and Acree found in 1907–1914 that ammonium nitrate is not so efficient for hydrochloric acid, [15] and showed that 4.1 *N* KCl nearly completely

[11] All of the above methods and the data were discussed in a lecture before the chemical staff of the National Bureau of Standards on December 14, 1929.

[12] Nernst, W., The Electromotive Activity of Ions. Z. physik. Chem., vol. 4, p. 165, 1889.

[13] Bjerrum, N., Elimination of Contact Potential Between Two Dilute Aqueous Solutions by Interposition of a Concentrated Solution of Potassium Chloride. Z. physik. Chem., vol. 53, p. 428, 1905; vol. 59, pp. 336, 581, 1907. Z. Elektroch., vol. 17, pp. 58, 389, 1911.

[14] Cumming, A. C., The Elimination of Potential Due to Liquid Contact, Trans. Far. Soc., vol. 2, p. 213, 1906; vol. 8, p. 86, 1912; vol. 9, p. 174, 1913. Z. Electrochem., vol. 13, p. 18, 1907.

[15] Desha, loc. cit.; Loomis, N. E., and Acree, S. F. A study of the Hydrogen Electrode and of Contact Potential, Amer. Chem. J., vol. 46, pp. 585, 621; 1911. Loomis, J. Phys. Chem., vol. 19, p. 660; 1915. Loomis and Acree, J. Am. Ch. Soc., vol. 38, p. 2391; 1916. Loomis and Meacham, Ibid, vol. 38, p. 2310; 1916. Loomis, Essex, and Meacham, Ibid, vol. 39, p. 1193; 1917. Myers, C. N., Clark, W. F., and Acree, S. F. A study of the Hydrogen Electrode, of the Calomel Electrode, and of Contact Potential, V., J. Phys. Chem., vol. 20, 243; 1916. Myers and Acree, J. Phys. Chem., vol. 21, p. 334; 1917.

eliminates the usual contact potentials. This method is now widely used.

Meacham and Acree [16] used 0.1 *N*, 1.75 *N*, 3.5 *N*, and 4.1 *N* KCl between 0.1 *N* KCl–HgCl and 0.1 *N* HCl–H_2 electrodes in 1916 and found the Bjerrum extrapolation too large in this case.

Fales and Vosburgh [17] in 1918 used various concentrations of KCl from 0.1 *N* to 4.1 *N* between KCl–HgCl and HCl–H_2 electrodes, proved Planck's formula inadequate, and confirmed the conclusion of Loomis, Myers, and Acree that 4.1 *N* KCl substantially eliminates contact potentials.

This article deals with further work on the elimination of contact potentials by means of ammonium chloride.

II. EXPERIMENTAL WORK ON CONTACT POTENTIALS AND THEIR ELIMINATION

In order to learn more about the magnitude and cause of various contact potentials, especially in systems which may also give data on the individual electrode potentials, and to study the actual reversal or over-annulment of contact potentials by the interposition of salts with highly mobile cations between solutions with very mobile anions and vice versa,[18] we have undertaken further studies with potassium and ammonium chlorides and other very soluble salts with nearly equal ionic mobilities. It was believed that the higher solubility of ammonium chloride, and the nearly equal ionic mobilities would make its saturated solution perhaps a better practical contact potential eliminator than potassium chloride. Its use with hydrochloric acid was tried with the idea that if it effectively annuls the contact potential of about 28 m. v. for 0.1 *N* HCl, the saturated ammonium chloride should certainly eliminate the 5 to 10 m. v. formed at junctions between the usual well buffered organic solutions and standard calomel electrodes.

In order to make a comparison of the relative merits of KCl and NH_4Cl as contact potential eliminators in such potentiometric *H*-ion measurements, NH_4Cl solutions having about the same concentrations as the KCl solutions used by Tower, Bjerrum, Fales and Vosburgh, Meacham and Acree, and Duschak, Elliott, and Acree, cited above, were prepared, a dye being added to make the junctions easily observable. This series of concentrations makes possible an extension of the curve secured by Meacham and Acree in their attempt to approach asymptotically the maximum elimination of contact potentials by these salts. The solutions of NH_4Cl used were 0.1 *N*, 0.5 *N*, 1 *N*, 1.75 *N*, 2.5 *N*, 3.5 *N*, 4.1 *N* (corresponding to saturated KCl) and saturated (about 5.66 *N*). Only 4.1 *N* KCl was employed in this series of experiments.

The double hydrogen electrode (fig. 1), without the traps *T* and *T'*, was used to form either fixed or flowing sharp liquid junctions. The gold electrodes were coated with palladium black. All readings were taken in an air bath at 25° C. The electrodes were first standardized with 0.1 *N* sodium acid phthalate in both electrode chambers.

---

[16] Mecham, M. R., Dissertation, Syracuse University; 1918. Work presented at the St. Louis meeting of the American Chemical Society, 1920.

[17] Fales, H. A., and Vosburgh, W. C., Planck's Formula for the Potential Difference Between Solutions and the Values of Certain Important Cells. J. Amer. Chem. Soc., vol. 40, p. 1291; 1918.

[18] Cumming, loc. cit. p. 215, vol. 16.

Measurements were then taken directly between 0.1 *N* sodium acid phthalate and 0.1 *N* HCl, without a contact potential eliminator. The barrel or U tube *B* of the apparatus was filled with the sodium acid phthalate solution, which usually contained a dye to facilitate the observation of the junctions *J* and *J'*. In some cases no dye was used, but a satisfactory liquid junction was nevertheless formed

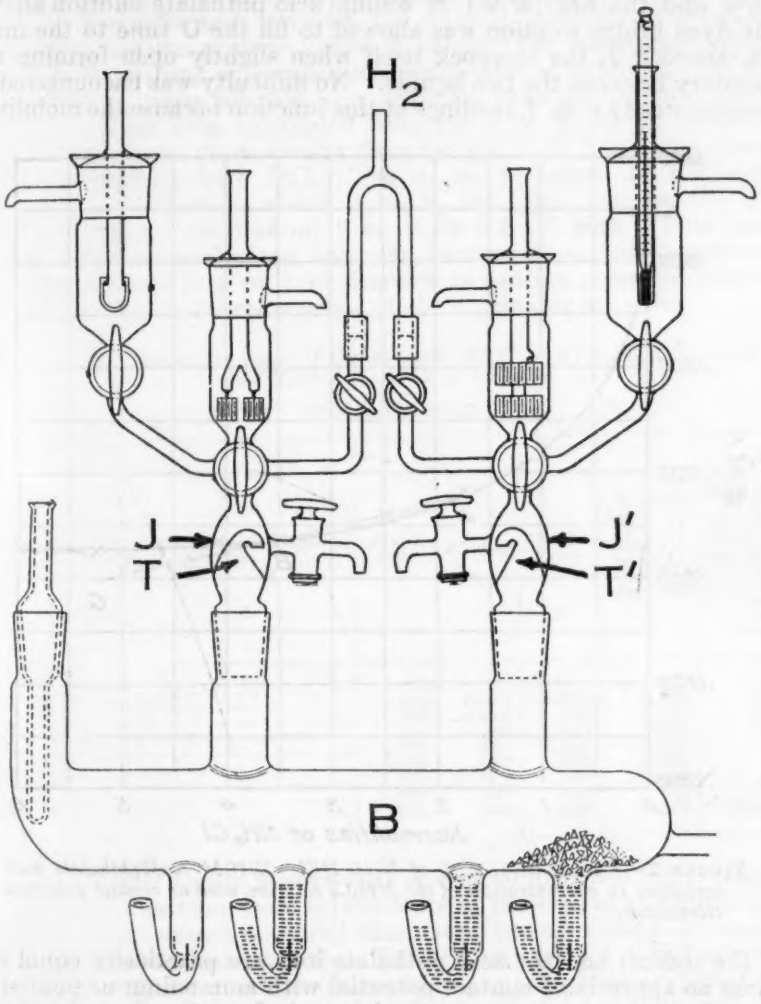

FIGURE 1.—*Double hydrogen electrode*

without difficulty. The barrel was then filled successively with the different solutions of the ammonium or potassium chloride as "bridges" or "links," junctions were made with the 0.1 *N* sodium acid phthalate and 0.1 *N* HCl, and the e. m. f. values measured for each "bridge." The liquid junctions are very sharp with links whose concentrations are above *N*/1 ammonium or potassium chloride. Other accessories to this apparatus involving the principle of the

traps T and T' for joining (heavier or) lighter liquids, such as the very dilute ammonium chloride solution, and (lighter or) heavier solutions, such as 0.1 N sodium acid phthalate, to form good junctions were not available in this work. Consequently, at the lower concentrations of NH_4Cl (normal and below) difficulty was experienced in making the liquid junction between the lighter bridge solution below and the heavier 0.1 N sodium acid phthalate solution above. The dyed bridge solution was allowed to fill the U tube to the main left stopcock 2, the stopcock itself when slightly open forming the boundary between the two liquids. No difficulty was encountered in securing steady e. m. f. readings at this junction because the mobilities

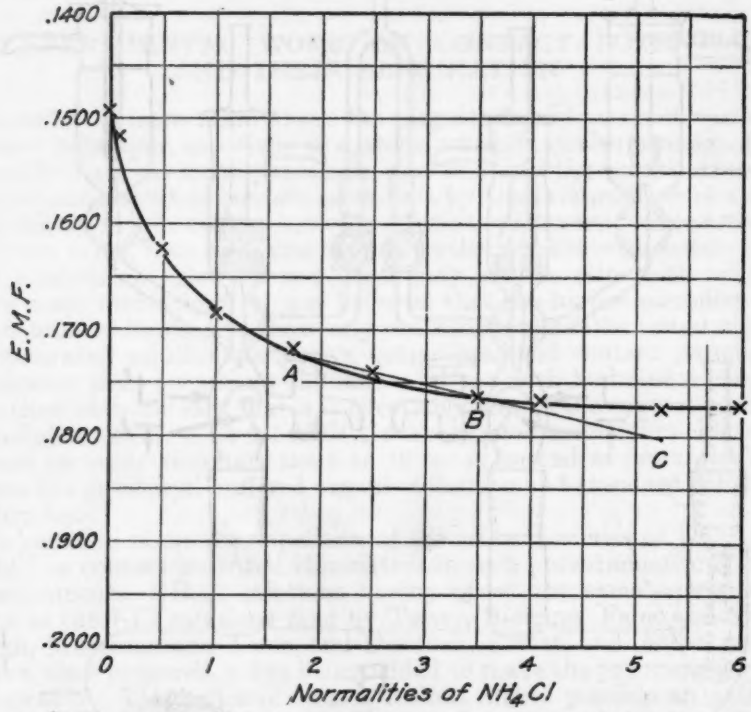

FIGURE 2.—*Change in e. m. f. of N/10 HCl—N/10M NaHphthalate with variation in concentration of the NH_4Cl solution used as contact potential eliminator.*

of the sodium and the acid phthalate ions are practically equal and cause no appreciable contact potential with ammonium or potassium chlorides in either sharp or mixed boundaries. On the other hand, the contact potential at the junction with the 0.1 N hydrochloric acid drifted as much as one millivolt unless a sharp, new junction was made before each e. m. f. reading.

The accompanying Table 1 and Figure 2 show the change in e. m. f. readings obtained with the several concentrations of NH_4Cl used between 0.1 N HCl and 0.1 N sodium acid phthalate (NaHPh). These are compared in column 6 with some average values for the same concentrations of KCl used between 0.1 N HCl and 0.1 N

KCl–HgCl by Bjerrum, Sörensen, Lewis and Sargent, Fales and Vosburgh, Meacham and Acree, and Duschak, Elliott, and Acree, cited above. In Table 1 the first column gives the concentration of the ammonium or potassium chloride solution used as the contact potential eliminator between the electrode solutions; the second column gives the e. m. f. reading; the third column gives as "Δ values" the difference between the e. m. f. readings of column 2; the fourth column gives as "total Δ values" the differences between the e. m. f. reading with saturated ammonium chloride and the reading with any other solution of ammonium chloride; the fifth column gives the same data calculated from the e. m. f. for 4.1 *N* NH_4Cl; the sixth column gives similar data for 4.1 *N* KCl and the systems *N*/10 KCl–*x*KCl–*N*/10 HCl. The e. m. f. values in the second column are uniformly about 6 m. v. too large because the *N*/10 NaHPh was adjusted about 6 m. v. or 0.1 pH high. This has no bearing on our conclusions, however, because we are really concerned with the change in e. m. f. or decrease in contact potential produced when the various concentrations of the eliminator are used.

TABLE 1.—*Electromotive force of the systems N/10 NaHPh–xNH₄Cl–N/10 HC and N/10 KCl–xKCl–N/10 HCl*

(Temperature 25° C.)

Concentration (*x*) of NH_4Cl used as contact potential eliminator	E. m. f. volts	Δ Values	Total Δ values	Deviation from e. m. f. for 4.1 *N* NH_4Cl as contact potential eliminator	Average difference between e. m. f. for *N*/10 KCl–*x*KCl–*N*/10 HCl and e.m.f. for *N*/10 KCl–4.1 *N* KCl–*N*/10 HCl observed by other workers
Saturated (5.66 *N*)	0.1773				
4.1	.1769	0.0004	0.0000	0.0000	0.0000
3.5	.1763	.0006	.0010	.0006	.0006
2.5	.1740	.0023	.0033	.0029	.0022
1.75	.1719	.0021	.0054	.0050	.0047
1.00	.1685	.0034	.0088	.0084	.0076
.50	.1625	.0060	.0148	.0144	
.10	.1518	.0107	.0255	.0251	
.00	.1493	.0025	.0280	.0276	0.0270–0.0284

Table 1 and Figure 2 show that the curve for the e. m. f. readings with NH_4Cl starting from 0.1493 volts in the case of the direct junction with no contact potential eliminator, becomes less steep as saturation is approached, until the difference between 4.1 *N* and saturated NH_4Cl is only 0.4 m. v., the curve at last approaching asymptotically a horizontal straight line in the neighborhood of 0.1774 volt. An average of five readings with 4.1 *N* KCl gave 0.1766 v. instead of 0.1769 v. with 4.1 *N* NH_4Cl. This e. m. f. curve for NH_4Cl may be taken either as showing complete elimination of contact potential or elimination of the same to the greatest extent possible by the saturated NH_4Cl. The line *ABC* gives at *C* the electrode e. m. f. obtained by the Bjerrum method. These curves show that the wrong use of Bjerrum's extrapolation gives an e. m. f. postulating complete elimination of contact potential which is 3 m. v. too high in this type of case. As the figures for maximum elimination of contact potential in-

dicated by this method agree within limits of usual experimental errors with those obtained by the Loomis-Acree 4.1 *N* KCl method in routine tests, it is reasonable to assume that NH_4Cl more nearly approaches an ideal contact potential eliminator for precision work than does KCl because of its greater (38 per cent larger) molar solubility. MacInnes and his coworkers showed furthermore that these two salts have nearly identical transference numbers in dilute solutions, and that in the case of KCl these values do not change appreciably between 0.005 *N* and 2 *N*. Comparative data are greatly needed for more concentrated solutions up to 4.1 *N* or 5.66 *N*, respectively, for KCl and NH_4Cl. The work of E. R. Smith[19] is a recent contribution in this field. It seems probable that NH_4Cl may conveniently replace KCl in potentiometric measurements of contact potentials of solutions of sufficiently low pH to avoid any possible errors due to the liberation of NH_3.

III. DISCUSSION

We have carried on further experiments with various types of buffer solutions of known pH value for the purpose of determining: (*a*) The lowest and highest pH at which NH_4Cl can still be used to replace KCl as a contact potential eliminator; (*b*) the relative values of other salt bridges having nearly the same mobilities of anion and cation for the elimination of contact potential, such as rubidium bromide, lithium iodate, and ammonium perchlorate; and (*c*) the effect of the addition of sufficient amounts of ammonium and potassium nitrates, respectively, to saturated ammonium and potassium chlorides to counterbalance the effect of the slightly higher mobility of the chloride ion.

It seems that a molar ratio of 1:3 for these nitrate-chloride mixtures should form an approximately isoelectric contact potential eliminator capable of annulling liquid junction potentials of buffer solutions with pH values between 3 and 10. The molar ratio and the nature of the salt mixture can be changed for more acid and alkaline solutions, respectively. We have found that these mixed ammonium and potassium nitrates and chlorides form very stable standard calomel electrodes.

The possible practical advantage of using such chloride-nitrate mixtures as contact potential eliminators may be illustrated as follows. By use of the Henderson equation for mixed boundaries cited above and the accepted conductivity data we have made the following calculations. Whereas 4.0 *N* potassium or ammonium chloride gives the contact potentials 0.9, 1.1, and 1.4 m. v., respectively, with 0.1 *N*, 0.01 *N* and 0.001 *N*, sodium acetate-acetic acid standards, the corresponding 1:3 nitrate-chloride 4 *N* mixture gives the contact potentials 0.2, 0.03, and 0.01 m. v., respectively: Whereas 5 *N* NH_4Cl gives the contact potentials 4.4, 1.5, and 1.3 m. v., respectively, with 0.1 *N*, 0.01 *N*, and 0.001 *N* HCl, the corresponding 1:3 nitrate-chloride 5 *N* mixture gives the values 4.0, 0.7, and 0.1 m. v. Consequently, the calculated contact potentials for the 1:3 nitrate-chloride 4 *N* mixture in junctions with the usual well-buffered solutions with pH 3 to 10 are apparently less than 0.2 m. v., whereas the 4 *N* KCl or NH_4Cl may leave a residual error of around ± 1

[19] E. R. Smith, B. S. Jour. Research, vol. 6, p. 917; 1931.

m. v. Another error of 1 to 2 m. v. in saturated calomel electrodes may be caused by the customary use of potassium chloride crystals over the calomel and resulting hysteresis in solubilities and e. m. f. when the temperature fluctuates. The authors urge the use of 4 *N* KCl without any solid potassium chloride if the calomel electrode is used in the open room instead of in a thermostat. All these conclusions should be considered tentative pending further experimental work outlined above because of the uncertainties regarding the properties of the concentrated contact potential eliminators. The ionization, ionic mobilities, transference numbers, diffusion of the molecules, interionic effects, and other properties concerned with contact potentials need further investigation and new equations must be devised if errors and uncertainties are to be reduced to ± 0.1 m. v.

WASHINGTON, July 1, 1931.

A BALANCED THERMOCOUPLE AND FILTER METHOD OF ULTRA-VIOLET RADIOMETRY, WITH PRACTICAL APPLICATIONS

By W. W. Coblentz, R. Stair, and J. M. Hogue

ABSTRACT

This paper is a further contribution (see RP318) to the investigation of filter radiometry, as applied to the measurement of ultra-violet radiation used for therapeutic purposes.

The experimental procedure consisted in exposing both receivers of a thermocouple simultaneously to radiation. On covering one receiver with a filter that excludes the ultra-violet, and the other receiver with a window that freely transmits these ultra-violet rays and exactly balances the transmission losses of the exclusion filter, throughout the remaining part of the spectrum, the galvanometer deflection obtained on exposure of the two thermocouple receivers to the source is a direct measurement of the ultra-violet emitted.

Data are given on the amount of ultra-violet in sunlight at midday in summer and in winter in Washington.

An experimental procedure is described for testing the performance and for the standardization of photo-electric cells, for use as ultra-violet dosage meters; also for using measured amounts of ultra-violet in physiological experiments using spectrally homogeneous ("monochromatic") and heterogeneous ultra-violet radiation.

CONTENTS

	Page
I. Introduction	724
II. Apparatus and methods of observation	725
1. The balanced thermocouples	725
2. The filters	728
(*a*) The exclusion filter	728
(*b*) Exclusion filter corrections	729
(*c*) Comparison of a cell of water and a thick plate of quartz for excluding the infra-red	730
3. Calibration of the thermocouple	731
4. Experimental procedure	731
III. Reduction of observations on ultra-violet solar radiation	732
1. Reduction of data obtained by Method I	733
2. Reduction of data obtained by Method II	735
3. Summary comparison of experimental procedure and results obtained	737
IV. Integration of ultra-violet radiation by spectroradiometric and by filter methods	737
1. The spectroradiometric method	738
2. The balanced thermopile and exclusion filter method	740
V. Calibration of a photo-electric cell in absolute units by radiometric filter methods	742
VI. Physiological tests	743
VII. Summary	747
VIII. Bibliography	748

I. INTRODUCTION

The balanced thermocouple method of measuring ultra-violet radiation was described in a previous paper (1).[1] The method is based upon the simple physical principle that when both receivers are simultaneously exposed to the sun, or to a uniform flux of radiation from an artificial source, practically no electric current flows through the galvanometer—it is "balanced" radiometrically.

On covering one receiver with a filter (for example, of barium flint glass) that excludes the ultra-violet which it is desired to measure, and the other receiver with a window (for example, crystalline quartz or, Corex G980A glass) that freely transmits the ultra-violet, and has the same transmissive properties as the exclusion filter for the remaining part of the spectrum, the galvanometer deflection obtained on exposure of the two thermocouple receivers through this combination of filters is a direct measure of the ultra-violet emitted by the source under investigation.

This method was considered a year or so ago; but only recently was it given a thorough trial, the results of which are reported in this paper.

The most difficult problem that has confronted radiometricians in recent years is the exact evaluation of ultra-violet radiation, particularly of wave lengths less than 313 $m\mu$ (millimicrons, 3,130 Å), recognized by biologists as having a specific healing value, particularly in preventing rickets.

The logical procedure would be to place the source at a known distance from the entrance slit of a spectroradiometer and measure the spectral intensity of the radiation emitted.

Correcting these spectral radiation intensities for absorption losses in the spectroradiometer gives the intensities incident upon the entrance slit, and hence, the intensity (the radiant flux) at a given distance from the lamp. Recent measurements by this method have been described by Barnes (2).

This method requires an exact knowledge of the size of the entrance and the exit slits, and of the transmission losses in the spectroradiometer, including the losses in the window (if any is used) of the thermopile or other radiometer receiver. The spectrometer slits being small (only about 5 by 0.5 mm) large errors may be introduced. The lens material, whether of fluorite or of fused quartz, absorbs some of the short wave length ultra-violet. Hence, if the absorption in the spectroradiometer has been determined, using a uniform irradiation over the whole lens, then it will be necessary to irradiate the whole lens uniformly with the source under investigation. This is impracticable in an investigation of an extended source; for example, a carbon arc lamp in a large reflector, or a small mercury arc in a quartz bulb, in which the lamp is so placed that both the bulb and the arc irradiate the lenses and the prism. In the latter source only about 5 per cent of the total ultra-violet is contributed by reflection and scattering by the outer portion of the bulb.

Unless the investigator can have the transmission of his spectroradiometer determined in another laboratory, he is obliged to have an extra monochromator to isolate the spectral lines used in deter-

[1] Figures in parenthesis here, and throughout the text indicate references given in the bibliography at the end of this paper.

mining the absorption in his spectroradiometer. In view of the scarcity of lens and prism material, and the difficulty in using such apparatus, particularly on extended sources, substitute methods are urgently needed.

In this connection filter methods (1) using a nonselective (thermopile) radiometer appear promising in view of the fact that the receiver does not deteriorate on exposure to ultra-violet radiation (5), and it can be easily calibrated in absolute units by exposure to a standard of radiation (3).

As will be shown presently the filter radiometer offers a ready means of calibrating a photo-electric radiometer in absolute value, and thus provides a convenient dosage meter of ultra-violet radiation.

In connection with the balanced thermocouple and exclusion filter method of radiometry the spectroradiometer is used as a secondary instrument to obtain the approximate spectral energy distribution of the source, which information is necessary in order to obtain the conversion factors for each type of source; for example, the sun, the mercury arc, etc. However, from the limited number of lamps examined, of a given type (for example, the tungsten mercury arc lamp in a quartz bulb) the conversion factor is a constant value; hence, lamps can be tested on a large scale of production by the filter method, while only a relatively limited number can be tested by the tedious spectroradiometric method. Laboratories which do not possess ultra-violet spectroradiometers can calibrate their filter radiometers by interchange of ultra-violet lamps or by having the radiometer calibrated in some laboratory possessing complete equipment.

II. APPARATUS AND METHODS OF OBSERVATION

The writers have always adhered to the policy of using the simplest and least complicated auxiliary apparatus in connection with the radiometer. Electron-tube amplifying devices have been tried and automatic recording apparatus has been considered; but since these devices increase the complexity of the procedure without markedly increasing the precision of the measurements the writers use a well-shielded, quick-acting, ironclad Thomson (4) (or a quick-acting d'Arsonval) galvanometer. The Thomson galvanometer is far more sensitive than required, but by inserting 500 to 30,000 ohms in series, it is readily adapted for measuring either intense or weak sources of ultra-violet radiation.

Aside from occasional disturbances by radio waves which happen to tune into the thermopile circuit, the writers are favorably situated as regards mechanical and electromagnetic disturbances and hence, can control their measurements more easily than workers less favorably situated.

1. THE BALANCED THERMOCOUPLES

The thermocouple is a simple device mounted upon an insulated base as indicated in Figure 1, *B* and *E*. The rear of the thermocouple container, *E*, is painted with lampblack, which absorbs the radiation entering through the openings surrounding the receivers, and, by scattering and reradiation, assists in establishing uniform temperature conditions within the container. As described in the previous paper

(1) the latter is wrapped in white cotton batting in order to prevent heating in sunlight.

The thermocouples used consisted of copper and bismuth wire (the latter 0.1 mm in diameter, pressed flat) or copper and constantan ("Advance," No. 40, thickness 0.075 mm) wire rolled flat, and having a thickness of 0.018 mm. The copper wire has a thickness of 0.037 mm. The receivers are of pure tin; thickness 0.018 mm; bright on the rear, and painted with lampblack, then smoked, on the front surface. For further details concerning construction, reference is made to earlier papers (6).

The distance between the receivers is determined by the size of the water cell used in front of the thermocouple, and also by the fact that, if the two junctions are too widely separated, there may be difficulty in maintaining uniformity of temperature conditions within the container, which determines the steadiness of the zero reading of the

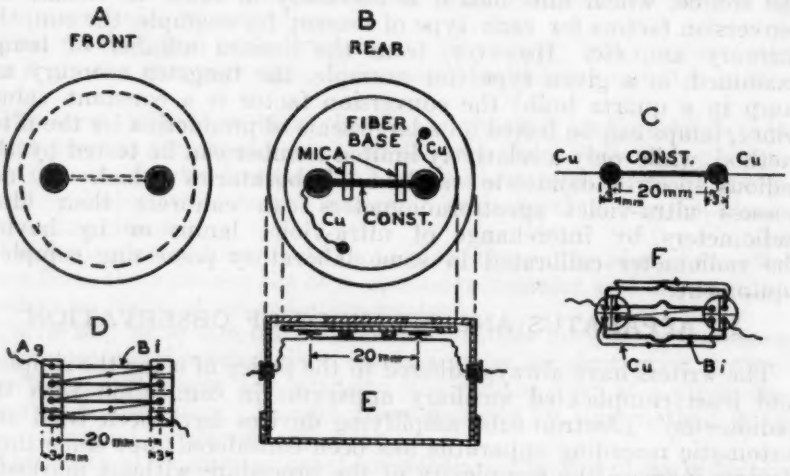

FIGURE 1.—*Thermocouple mounting, also designs of thermopiles*

galvanometer or other indicating device. The experimental data reported in this paper were obtained on thermocouples in which the centers of the receivers were separated by 18 mm. As indicated in Figure 1, a separation of 20 to 25 mm should prove satisfactory.

A separation of 30 to 40 mm between the centers of the receivers would permit the use of larger filters of barium flint and quartz, as illustrated in Figure 2, *A*, thus increasing the ability to keep them free from dust. But this increases the expense of the water cell, and may decrease the temperature uniformity within the thermocouple container.

Using widely separated receivers requires two window covers of fluorite (or quartz) instead of a single window as used in the present work.

Using the single thermocouple receiver and filter method previously employed (1), comparisons were made of the accuracy of various forms of balanced thermocouples (fig. 1, *C*) in measuring the ultraviolet in sunlight.

Thermocouple No. 233 of copper constantan, having a resistance of 2.6 ohms and receivers 3 mm in diameter, blackened on front and rear, was used in a mounting with windows 3.3 mm in diameter. Thermocouple No. 234 of copper constantan with receivers 3 mm in diameter, painted black on the front, and left unpainted on the rear, was tested in an inclosure having, first, the window openings 3.3 mm, and then with openings 3.5 mm in diameter, to determine the effect of heating the interior by direct solar radiation. No unequal heating of the interior that was attributable to the larger window was observed.

Thermopile No. 235, consisting of four junctions, of bismuth-copper, and having a resistance of 12.3 ohms, was constructed as indicated in Figure 1, *F*. The receivers were about 5 mm in diameter. It was tested back of window openings that were a little less than 5 mm in diameter in order to prevent solar radiation from entering the rear of the inclosure. It was tested also with the windows 5.7 mm in diameter.

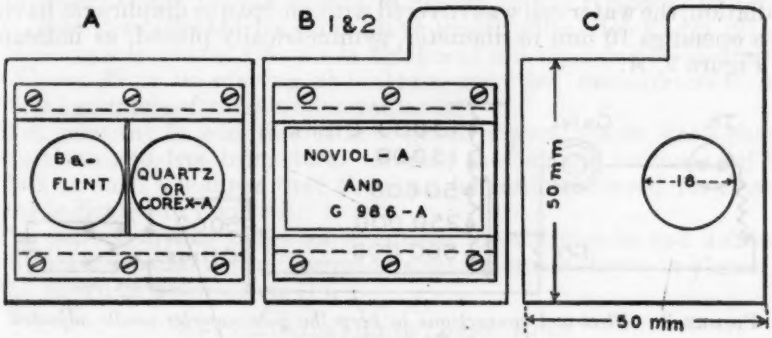

FIGURE 2.—*Filter mountings*

Aside from the fact that when the window opening was larger than the radiometer receiver, less refinement was required in exposing the instrument to the sun, within the errors of observation, no appreciable difference was found in the measurements made with the various arrangements of the radiometer receivers and sizes of windows.

The use of a 4-junction thermopile as depicted in Figure 1, *F*, increased the radiation sensitivity about eightfold. This is useful for measuring weak sources of ultra-violet radiation, but it is too sensitive for use in measuring solar radiation without 1,000 ohms resistance in the Thomson galvanometer circuit.

Another form of balanced thermopile arrangement is depicted in Figure 1, *D*. It was used in measuring the radiation from the solar corona (7).

As already mentioned, the trial of this type of radiometer was delayed owing to the fear that exposure of the device to a source so intense as the sun would introduce unsteadiness. It was, therefore, an agreeable surprise to find that, although a small difference in the radiation sensitivity of the two thermopile receivers produced a permanent zero shift of 1 to 15 cm of the galvanometer reading, there was little or no shifting of the zero while making the readings.

To eliminate the error that may result from this zero shift a small current from a dry battery is maintained through the galvanometer circuit, in a direction opposite to that causing the zero shift, and of sufficient strength to maintain the same zero reading when making the measurements on the sun and when calibrating the thermopile against the standard of radiation (3). This arrangement is depicted in Figure 3. It is easily assembled by employing resistors in common use in radio installations.

2. THE FILTERS

The balanced thermopile method of ultra-violet filter radiometry was tested by two methods:

1. The front of the thermopile container (fig. 1, *A*) was covered with cell of water, 1 cm in thickness, and 3 cm in diameter, with windows of crystal quartz about 3 mm in thickness, attached to the glass container by means of Chatterton wax, or Picein, melted around the outer edge. To reduce the heating of the water by the intense solar radiation, the water cell was covered with an opaque diaphragm having two openings 10 mm in diameter, symmetrically placed, as indicated in Figure 2, *A*.

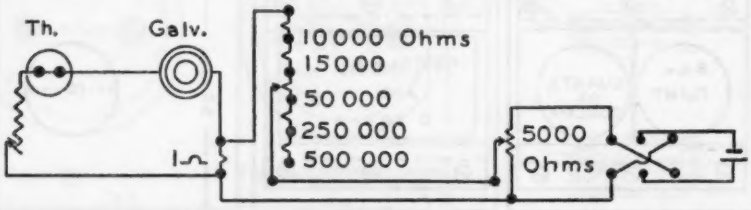

FIGURE 3.—*Electrical connections to keep the galvanometer needle adjusted to the zero reading*

2. The thermocouple receivers were covered with a 1 cm cell of water and also a purple glass filter, G986A, which reduces the heating of the water by sunlight.

For artificial sources emitting ultra-violet radiation of wave lengths less than 270 mμ, where the purple glass begins to absorb considerably (8), also owing to the fact that this glass decreases in transmission on exposure to ultra-violet radiation, it seems preferable to use only the cell of water, or a plate of quartz 1 to 2 cm in thickness to absorb the infra-red rays. Since fused quartz may absorb considerable ultra-violet of wave lengths less than 250 mμ (8) it is desirable to use windows of crystalline quartz. If the outer walls of the cell are of glass, which is dissolved by distilled water, thus decreasing the ultra-violet transmission, (9) it is desirable to renew the water daily.

(a) THE EXCLUSION FILTER

This combination is depicted in Figure 2, *A*. It consists of a barium-flint glass that shuts out the ultra-violet, and a plate of crystalline quartz or Corex-G980A glass that freely transmits the ultra-violet to be evaluated. Both should have the same spectral transmission throughout the rest of the spectrum of wave lengths longer than about 400 mμ.

Since it was desired to evaluate the ultra-violet radiation of wave lengths less than and including 313 mμ the barium-flint glass filter was selected of such a thickness (about 3.1 mm) that the transmission at 313 mμ is small (about 0.5 per cent), so as to provide an easily determined end point of transparency. Such a filter transmits 49 to 50 per cent at 334 mμ, 84 to 85 per cent at 365 mμ, and 89 to 90 per cent at 405 mμ. This kind of glass has the sharpest cut-off yet found. It does not decrease in transparency on exposure to ultra-violet radiation (exposure test of 30 hours at 15 cm from a 110-volt quartz mercury arc), hence, the transmission does not require redetermination.

Throughout the visible and near infra-red spectrum the barium-flint and the Corex-G980A glasses, used in the present work, had closely (within 0.3 per cent) the same transmission, and hence, on exposing this combination to sunlight there was but little unbalancing of the thermopile caused by the difference in transparency of these two glasses for radiation of wave lengths longer than 400 mμ.

However, Corex G980A begins to absorb in the region of 250 mμ and, since it is affected by short wave length ultra-violet rays (8), a plate of crystal quartz 1.5 mm in thickness was used in preference to the Corex filter in making the herein recorded measurements on artificial sources of ultra-violet radiation.

It is relevant to add that it is of great importance to keep these filters clean and free from dust. Hence, they should be mounted in holders in such a manner that they can be easily removed for cleaning, as indicated in Figure 2.

The general arrangement for mounting the thermopile and holding the filters when making measurements on the sun is shown in Figure 1 of the previous publication (1).

(b) EXCLUSION FILTER CORRECTIONS

Since the exclusion filter of barium flint glass and its long wave length radiation-balancing filter of quartz, or of Corex G980A glass, do not have exactly the same transmission throughout the spectral range from about 400 to 1,400 mμ (when using the water cell, or to 3,000 mμ when using a thick quartz plate instead of a cell of water) the amount of unbalancing (the thermopile deflection produced) by the radiation in this spectral range is determined experimentally by temporarily covering the thermopile (fig. 1, *A*) with a filter of Noviol–A glass, that has a transmission of 1 per cent or less at 405 mμ, 55 to 60 per cent at 436 mμ (12), and completely absorbs the ultra-violet of wave lengths less than 400 mμ. (See fig. 2, *B*.) The exclusion filters (fig. 2, *A*) are inserted under this filter and the galvanometer deflections noted. This deflection, after correction for absorption by the Noviol filter, is deducted from the observed galvanometer deflection produced by inserting only the barium flint and quartz combination of exclusion filter. (See Table 3.)

Since this correction is a secondary matter and is practically negligible when making the measurements through the purple filter G986A, an exact determination of the transmission of the Noviol filter is not necessary. For example, the transmission of a Noviol-C filter for sunlight of all wave lengths to 1,400 mμ was 69 per cent, whereas by using only radiation of wave lengths 365 to 1,400 mμ (by covering the thermocouple receiver with a plate of Cruxite glass)

the transmission was increased to 71 per cent, a difference of only 2 per cent to be applied to a correction that is less than 10 per cent of the total value measured.

For determining the transmission of the Corning Noviol–A filter (82 per cent) the diaphragm (fig. 2, *C*) is inserted in front of the thermocouple receiver which is covered with a plate of Cruxite glass, a shutter is provided, and the galvanometer deflection is noted with and without the Noviol glass inserted in the path of the incident radiation.

(c) COMPARISON OF A CELL OF WATER AND A THICK PLATE OF QUARTZ FOR EXCLUDING THE INFRA-RED

Although the thermocouple is well balanced radiometrically, it is desirable to exclude from it as much of the infra-red and the visible radiation as possible. Furthermore, since the barium flint glass and the balancing filter of quartz or Corex G980A glass do not have the same transmission beyond 2μ in the infra-red it may be simpler for interpreting the data, to exclude the infra-red by means of a 1-cm cell of water, which is opaque to wave lengths longer than 1.4μ.

However, since the water cell can not be exposed to the sun continuously without overheating and the consequent formation of bubbles on the windows, conditions may arise where it is desirable to replace the water cell by a thick plate of crystal quartz, which, in thicknesses of 1 to 2 cm, is practically opaque to radiation of wave lengths longer than 4μ.

The accuracy in measuring ultra-violet solar radiation of wave lengths less than 313 $m\mu$, when the water cell was replaced (alternately) by a plate of crystal quartz 1 cm in thickness was tested by direct measurement (on July 8, 1931) following the "experimental procedure" described in the second following caption.

The day was extremely hot and sultry and the measurements were terminated by cirrus clouds, which decreased the accuracy of the work. Furthermore, the greater transparency of the plate of quartz to infra-red rays produced a greater heating of the thermopile container, and consequently a greater unsteadiness of the galvanometer reading. Nevertheless, in spite of these hindrances, as shown in the central part of Figure 5 (for July 8, 1931), the data obtained (*a*) with the water cell and (*b*) with the 1 cm plate of quartz (in both cases with and without the additional purple filter of G986A glass) are in good agreement. This shows that, in spite of theoretical objections, a thick plate of quartz appears to be a good substitute for the water cell in apparatus that is to be exposed continuously to solar radiation.

It is relevant to add that one reason for the successful operation of the device is probably owing to the fact only a very small amount of the total incident solar radiation is of wave lengths longer than 2 μ, whereas the great deviations in transparency of the exclusion filters occur at wave lengths longer than 2 μ. Another item of interest is that the correction for infra-red radiation (as determined with the Noviol filter) is practically the same when using the thick quartz plate as for the water cell. This is owing to the fact that the quartz plate transmits appreciably more of the ultra-violet than the water cell. This leaves the relative proportions of solar radiation transmitted and excluded by the barium flint glass filter about the same for the quartz plate as when the water cell is used.

3. CALIBRATION OF THE THERMOCOUPLE

To calibrate the balanced thermocouple radiometer the cell of water is removed from the holder, the diaphragm (fig. 2, *C*) is inserted and the galvanometer deflection (plus or minus) is noted when one thermocouple receiver is exposed to a standard of radiation (3). The diaphragm is then reversed and the other receiver is exposed to the radiation standard.

The radiant flux of the standard lamp (in microwatts per cm ^{2}) divided by the average of the two deflections gives the calibration in microwatts per cm ^{2} for 1 cm deflection of the galvanometer.

As described in the previous publication (1) the evaluation of the measurements in absolute value, when using the single thermocouple receiver, Method I was obtained from a knowledge of the total solar radiation intensity, Q, amounting to some 90,000 μw (microwatts) per cm ^{2}, which data were supplied by the United States Weather Bureau.

In the herein described balanced thermocouple method of measuring ultra-violet solar radiation (Method II) the calibration is obtained by exposure to a standard of radiation of 300 μw/cm ^{2}. This is a three hundredfold difference in intensity involved in the energy evaluation in absolute measure. Nevertheless, as will be seen on a subsequent page, the concordance of the data seems to indicate that the methods are reliable.

4. EXPERIMENTAL PROCEDURE

The method of operation of the balanced thermocouple device is extremely simple. No shutter is used. The balanced thermopile (with (*a*) the water cell or (*b*) with the water cell and the purple glass filter, G986A) is exposed to the source of radiation and the zero position of the galvanometer reading is noted.

If the zero position is markedly displaced from that used in calibrating the thermocouple against the standard of radiation, it is adjusted to the latter zero reading by means of the current balancing device illustrated in Figure 3, which procedure is essentially the same as balancing a bolometer. By changing the circuit slightly the device might be used as a null instrument, reading the current from the dry battery through a milliammeter or microammeter, instead of the direct galvanometer deflection. For low intensities of ultra-violet radiation the writers prefer to use the direct galvanometer deflection.

The exclusion filter (fig. 2, *A*) is then inserted with the barium flint glass over, say, the left receiver and the galvanometer deflection (positive or negative) caused by the excess ultra-violet radiation passing through the quartz (or Corex G980A glass) is noted. The filter is then withdrawn and the galvanometer deflection is corrected for the zero shift, if any has occurred.

The exclusion filter is then inserted in the reverse position so that the barium flint glass covers the right-hand receiver, and the galvanometer deflection (now in the opposite direction) is again noted and corrected for zero shift if any has occurred. The average of these two deflections is a measure of the total radiation shut out by the barium flint glass filter, including a few per cent of wave lengths longer than 400 mμ.

To eliminate the radiation of wave lengths longer than about 400 mμ the Noviol filter is inserted and a set of measurements, similar to the preceding one, is obtained, using the barium flint glass, first over the one, then over the other receiver, as already described. This value corrected for incomplete transparency of the Noviol glass is then deducted from the first set of measurements, giving the total ultra-violet shut out. To determine the amount of radiation of wave lengths less than 313 mμ it is necessary to observe the relative spectral ultra-violet energy distribution of the source.

As already noted, the balanced thermopile of bismuth-copper, illustrated in Figure 1, *F*, requires an insensitive d'Arsomal galvanometer, when making measurements of the ultra-violet in direct sunlight. By using the ironclad Thomson galvanometer on a short period, with 1,000 ohms in series (30,000 ohms for making the transmission measurements of the Noviol glass) with this thermopile, it is possible to make measurements of the high intensity ultra-violet radiation in direct sunlight. Similarly by decreasing the resistance in series with the galvanometer it is possible to measure the low intensity (amounting to only a few microwatts per cm^2) emitted from certain artificial sources.

III. REDUCTION OF OBSERVATIONS ON ULTRA-VIOLET SOLAR RADIATION

Under this caption data are presented on the amount of ultra-violet of wave lengths less than 313 mμ in sunlight as measured by a single thermocouple receiver and two exclusion filters of barium flint glass, designated Method I, previously described (1), and by a balanced thermocouple with a single exclusion filter of barium flint glass, designated Method II mentioned in the previous paper (1) and more fully described in the present paper. The concordance of the results obtained by these two methods is impressive when we consider the widely different methods of making the measurements and evaluating the results in absolute value.

In Method I, the purple glass filter transmits about 8 per cent of the total incident solar radiation amounting to about 90,000 μw (microwatts) per cm^2. This 8 per cent consists of violet and ultra-violet radiation of wave lengths less than 400 mμ (also some near infra-red radiation).

The total galvanometer deflection that can be conveniently used, without encumbering the work by changing the sensitivity, is 20 to 25 cm. By inserting the filters of barium flint glass the amount of ultra-violet of wave lengths less than 365 mμ, which is excluded, amounts to only a few per cent (a few millimeters) of the total observed galvanometer deflection. Nevertheless, as shown in previous papers (1) and (8), comparison of this deflection with the standard of radiation gives values which are in good agreement with data calculated by using the total solar radiation data, *Q*, obtained from the United States Weather Bureau.

In Method II the total galvanometer deflection observed is from 12 to 15 cm (or larger by changing the galvanometer sensitivity), and, depending upon the solar altitude, the amount of ultra-violet of wave lengths less than about 365 mμ (in which we are particularly interested,

as in Method I), is 90 to 95 per cent of this value when using the purple glass filter G986A, and 60 to 70 per cent of this value when purple glass filter is not used.

1. REDUCTION OF DATA OBTAINED BY METHOD I

The general procedure in reducing the observations, using the single thermocouple receiver and two barium flint exclusion filters, remains the same as previously described (1). An important change is introduced by a recalculation of the reduction factors, F, depicted

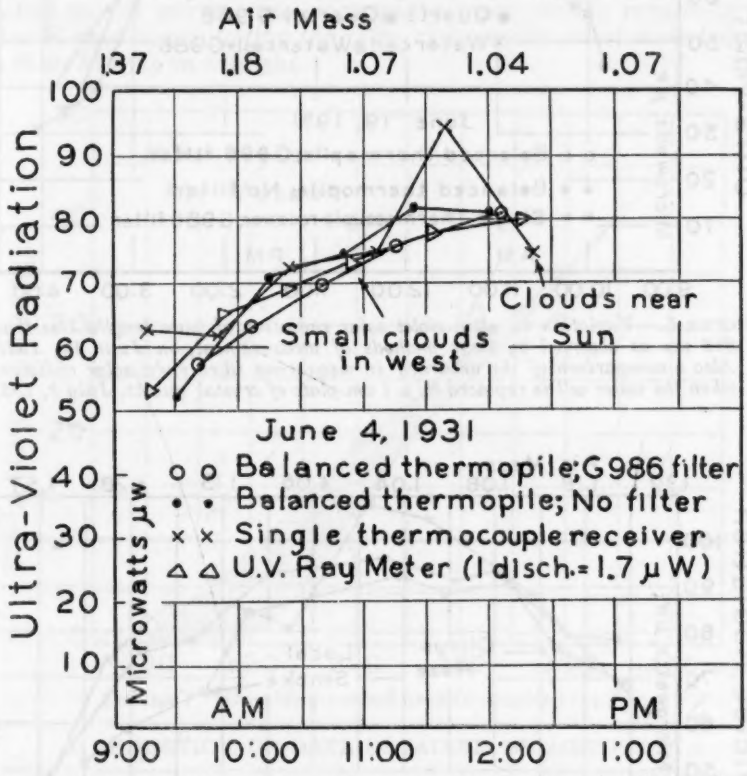

FIGURE 4.—*Variation in ultra-violet solar radiation of wave lengths less than 313 mμ as observed by four methods of measurement*

in Figure 5 of the previous publication (1). This change is introduced by using an observed solar spectral energy curve that represents more closely the observed per cent transmissions of the barium flint glass filters (a/I_o and $a+b/a$) than the calculated values depicted in Figures 3 and 4 of the previous publication (1). The new factors, F, are on an average, about 20 to 25 per cent higher than previously used.

New factors are introduced for eliminating the absorption at 290 to 313 mμ by the water cell and the purple glass filter G986A, amounting to 15 and 21 per cent, respectively.

As shown in Figures 4, 5, and 6, the average amount of ultra-violet solar radiation of wave lengths less than 313 mμ, for midlatitude sea

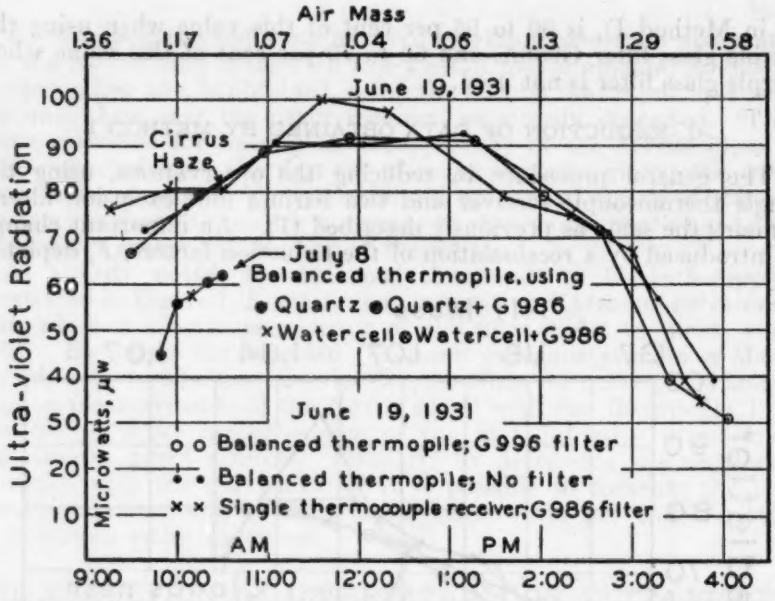
Air Mass
1.36 1.17 1.07 1.04 1.06 1.13 1.29 1.58
June 19, 1931
Cirrus Haze
July 8
Balanced thermopile, using
● Quartz ● Quartz + G 986
× Water cell ⊗ Water cell + G986
June 19, 1931
o o Balanced thermopile; G 996 filter
• • Balanced thermopile; No filter
× × Single thermocouple receiver; G 986 filter
Ultra-violet Radiation
Microwatts, μw
100 90 80 70 60 50 40 50 20 10
AM
PM
9:00 10:00 11:00 12:00 1:00 2:00 3:00 4:00

FIGURE 5.—*Variation in ultra-violet solar radiation of wave lengths less than 313 mμ as observed by three methods of measurement, on June 19, 1931. Also a comparison of the accuracy in measuring ultra-violet solar radiation when the water cell is replaced by a 1 cm plate of crystal quartz, July 8, 1931*

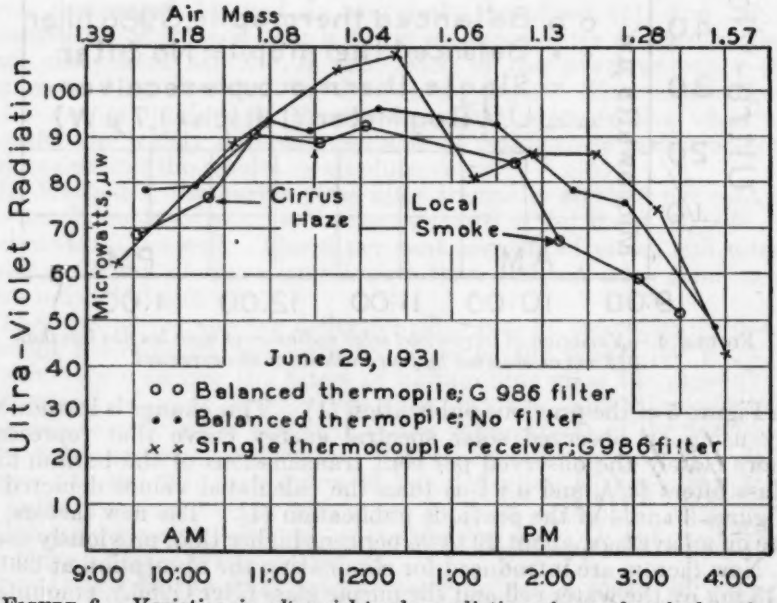
Air Mass
1.39 1.18 1.08 1.04 1.06 1.13 1.28 1.57
Cirrus Haze
Local Smoke
June 29, 1931
o o Balanced thermopile; G 986 filter
• • Balanced thermopile; No filter
× × Single thermocouple receiver; G 986 filter
Ultra-Violet Radiation
Microwatts, μw
100 90 80 70 60 50 40 30 20 10
AM
PM
9:00 10:00 11:00 12:00 1:00 2:00 3:00 4:00

FIGURE 6.—*Variation in ultra-violet solar radiation of wave lengths less than 313 mμ as observed by three methods of measurement*

level stations, during the clearest weather, during midday in midsummer, averages about 90 $\mu w/cm^2$ instead of 55 $\mu w/cm^2$ as previously published (1).

In the absence of an exact knowledge of the spectral energy curve of the sun, at the time of making the observations, it remains uncertain as to which values, obtained by Method I, are the more nearly correct. However, fortified with the data obtained by Method II, described in the next section, it appears that on the basis of the present work, the previously published data, using Method I should be increased by perhaps 50 per cent, instead of 10 to 20 per cent, previously estimated (1). Until a better knowledge is obtained of the solar spectral energy curve some uncertainty must remain regarding the factor F, used in evaluating the ultra-violet radiation of wave lengths less than 313 mμ in sunlight.

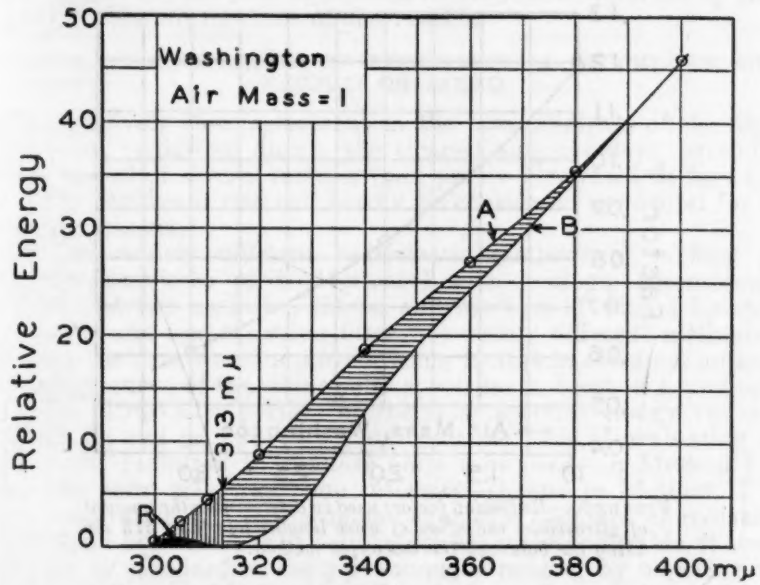

FIGURE 7.—*Graphical method used in reducing the data*

2. REDUCTION OF DATA OBTAINED BY METHOD II

The reduction factor, F, for obtaining the amount of ultra-violet radiation of wave lengths less than 313 mμ, when using the balanced thermocouple and single barium flint glass exclusion filter, is obtained as illustrated in Figure 7, in which A is the observed solar spectral energy curve (1) and B is the spectral transmittance curve of the barium-flint glass filter, on the assumption that both the flint glass and the nonabsorbing screen (quartz or Corex G980A) have the same transparency to wave lengths longer than 400 mμ. The procedure given in the previous paper (1) is followed in obtaining the factor, F, for different air masses. These factors are given in Figure 8. They indicate that the amount of ultra-violet of wave lengths less than, and including 313 mμ (which wave length is important in integrating the spectrum of the quartz mercury arc) ranges from about 6 per cent

of the total shaded area in Figure 7, for air mass, $m=3$, to 12 per cent for air mass, $m=1$.

The reduction of the data is relatively simple. A sample illustration of the method is given in Table 1 in which column *d* gives the average observed deflection on insertion of the barium-flint glass exclusion filter. (Fig. 2, *A*.)

Column *e* gives the galvanometer deflection indicating the amount of radiation of wave lengths longer than 400 mμ, obtained by covering the thermocouple with the Noviol filter, and corrected by dividing the observed deflection by the transmission (71 per cent) of the filter. Column *f* (which is column *d* minus column *e*) gives the observed ultra-violet excluded by the barium flint glass filter.

Column *g* gives the factor, *F*, to reduce the amount of the total radiation measured (column *f*) to that of wave lengths less than 313 mμ.

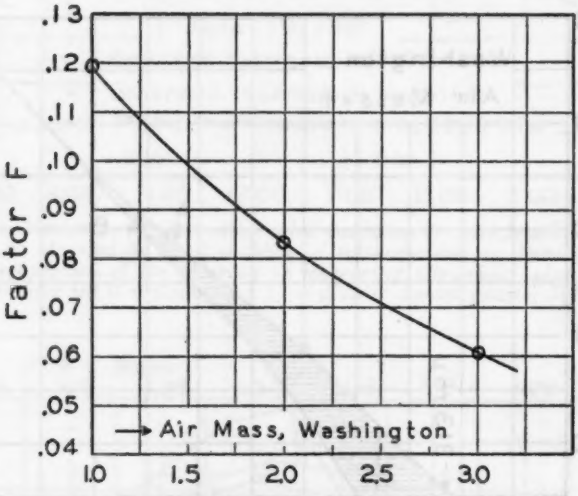

FIGURE 8.—*Reduction factors used in determining the amount of ultra-violet radiation of wave lengths less than 313 mμ using the balanced thermocouple method.*

Column *h* is the experimentally observed factor that must be applied to column *f*, because of absorption of radiation of wave lengths less than 313 mμ by the water cell, the Corex G980A glass, and the fluorite window which covers the thermocouple receivers.

Column *i* is the radiation sensitivity of the thermopile in microwatts per cm² for 1 cm deflection, observed by exposure to the standard of radiation.

Column *j*, which is the product of columns *f*, *g*, *h*, and *i*, is the total amount of ultra-violet solar radiation of wave lengths less than 313 mμ available at 10.50 to 10.59 a. m., June 29, 1931.

On this day, sky conditions were as follows:

Clear at 9 a. m.; cirrus clouds east of the sun at 10.30 a. m.; sky mottled near the sun at 11.30 a. m.; sky relatively clear during the afternoon, except a local fire of short duration with smoke rising southwest of the sun, which did not appear to be in the line of sight, but which may have caused the depression in the curve at 2.15 p. m. (See fig. 6.)

TABLE 1.—*Reduction of data observed on June 29, 1931*

Time	Filter	Air mass	Observed galv. deflection	Infra-red correction	Difference	Factor F	Filter factor	Thermopile sensitivity	$\mu w/cm^2$ below 313 mμ
a	b	c	d	e	f	g	h	i	j
a. m.			*cm.*	*cm.*	*cm.*			$\mu w/cm^2$	
10.50	Water cell and G986	1.09	5.51	0.37	5.14	0.115	0.172	88.5	90.0
10.59	Water cell	1.08	11.15	4.24	6.91	.116	.132	88.5	93.6

Some of the other observations of ultra-violet solar radiation, made on the same day using Method I and the two modifications of Method II (practically three methods in all) are illustrated in Figures 4 and 5, showing the close agreement in the results obtained by these markedly different methods of observation.

3. SUMMARY COMPARISON OF EXPERIMENTAL PROCEDURE AND RESULTS OBTAINED

The relatively close agreement in the measurements of the ultra-violet solar radiation, during the clearest summer days, extending over a period of several months (and partly illustrated in figs. 4, 5, and 6) is significant and can hardly be considered accidental for the following reasons:

(*a*) Two widely different radiometric methods of making the measurements were used—Method I with a single thermocouple receiver and two exclusion filters, and Method II with a balanced thermopile and one exclusion filter; (*b*) widely different methods of reducing the data were employed, using factors based upon an average energy curve of the whole solar spectrum in Method I, and upon only the ultra-violet portion of the solar spectral energy curve in Method II; and (*c*) two widely different methods of evaluating the ultra-violet radiation in absolute units were used—in Method I by using the total solar radiation intensity, Q, and in Method II by direct calibration of the thermopile against a standard of radiation. While these two methods of calibration are interchangeable, it seems desirable to standardize the galvanometer reading by exposing the thermopile to a standard source that emits radiation comparable in intensity with the total (ultra-violet) measured.

From these data it appears that the average amount of ultra-violet solar radiation of wave lengths less than, and including 313 mμ, for mid-latitude sea-level stations, during the clearest weather, during midday, in midsummer, amounts to about 90 $\mu w/cm^2$, decreasing to about 20 $\mu w/cm^2$ on the clearest days in December.

IV. INTEGRATION OF ULTRA-VIOLET RADIATION BY SPECTRORADIOMETRIC AND BY FILTER METHODS

As indicated in the introductory part of this paper, the élite method of measuring the intensity of ultra-violet radiation is by means of a spectroradiometer, with the source at a known distance from the entrance slit. However, the method is beset with difficulties, especially when the problem is presented to measure the radiation from an extended source. Hence, it is desirable to obtain some filter

method for quickly and accurately measuring the integrated ultra-violet radiation from sources used for therapeutic purposes.

Under this caption comparative data are given of the ultra-violet radiation emitted by a tungsten mercury arc lamp, in a quartz bulb, as observed (1) with a spectroradiometer, and (2) with a balanced thermopile and a barium flint glass exclusion filter already described.

1. THE SPECTRORADIOMETRIC METHOD

The spectroradiometer consisted of two uncemented quartz fluorite achromatic lenses 33 mm in diameter and 30 cm focal length, and a prism of quartz 6 cm in height. The fluorite used in the lenses was of the yellow variety, and, while it appeared quite colorless in the thickness used, it had a small absorption in the blue and violet, followed by a relatively high transmission in the ultra-violet.

To facilitate setting on a spectral line, the slit was given a thin coat of turpentine upon which was dusted a thin deposit of anthracene, which was then rubbed smooth. Starting with the slit closed, this method of applying the fluorescent material produces a sharp knife-edge, which, on opening the slit permits an accurate isolation of closely adjoining emission lines.

The size of the entrance slit was 5.0 by 0.50 mm, and the exit slit was 5.3 by 0.60 mm. The radiation sensitivity of the thermopile back of the exit slit was obtained by exposing the exit slit to the standard of radiation. Since the area of the exit slit was 1.283 times larger than the entrance slit, and since, for small variations in slit opening, the galvanometer deflection is proportional to the size of the thermopile receiver that is exposed to radiation, this slit factor, f, must be applied in Table 2.

The factor, h, for reducing the data in Table 2, to a distance of 1 m is 0.01613.

The radiation sensitivity of the thermopile, corrected by the transmission (91.6 per cent) of the fluorite window, was 1 cm deflection = 12.05 μw/cm^2. At each spectrometer setting the galvanometer deflection is multiplied by this factor, e, in Table 2, to reduce the data to absolute units.

The galvanometer deflections must be corrected also for the loss in transmission through the spectroradiometer. (Column c in Table 2.) The transmission of the quartz-fluorite spectroradiometer (2) was determined by isolating spectral lines with a quartz monochromator and measuring the intensities by means of two thermopiles, one placed at the entrance slit and the other at the exit slit of the spectroradiometer. As a check on the accuracy when using two thermopiles, the vacuum thermopile (usually employed at the exit slit) was used to measure the intensity of the 365 mμ line, at both the entrance and the exit slit. The same transmissions, within 0.5 per cent, was observed by the two methods.

In these measurements, at each wave length the apparatus was adjusted so that the lenses and prism were uniformly irradiated with monochromatic light. To trace the ultra-violet beam of radiation through the spectrometer, it was made luminous by inserting in the path a piece of white cardboard covered with a thin film of turpentine upon which anthracene was dusted and rubbed smooth.

In order to correct for scattered radiation when making measurements at wave lengths longer than 313 mμ a red or amber glass shutter

was used. For wave lengths 313 to 280 mμ the shutter was of clear window glass, and for wave lengths less than 280 mμ, Helioglass was used.

The source was a new type of tungsten mercury arc (2) in which the ultra-violet radiation from a V-shaped helical filament of tungsten wire is supplemented by the radiation from a mercury vapor arc across two tungsten electrodes at the top of the V-shaped filament.

The measurements were made with a vacuum thermopile described in previous papers. The ultra-violet spectral transmission of the fluorite window is given in column *d* of Table 2.

In order to obtain sufficient intensity, and in order to uniformly irradiate the whole lens, the lamp was operated at a distance of 12.7 cm from the entrance slit. This is important, since, in measuring the transmission of the spectroradiometer, the whole lens was irradiated. The radiation from the whole lamp including the bulb is 4.4 per cent larger. This is factor *g* in Table 2.

The observed intensities (the galvanometer deflections) of the strong emission lines and of the continuous spectrum, are given in column *b* of Table 2; also the absolute values of these intensities, deduced as just described.

The sum of the intensities of all the radiation shorter than and including the emission lines at 313 mμ, amounts to 23.9 μw/cm², which is somewhat lower than the value obtained by the filter method. This is to be expected in view of the fact that no spectroradiometric measurements were made on the weak radiation between 365 and 436 mμ, and at the wave lengths shorter than 230 mμ.

TABLE 2.—*Ultra-violet spectral intensities, in microwatts/cm² at 1 m, from a tungsten mercury arc in a quartz bulb*

[The correction factors, *e* for the radiation sensitivity of the thermopile, *f* for difference in areas of the slits, *g* for size of lamp image on prism, and *h* for distance of lamp from the entrance slit, are described in the text]

Wave length	Observed galvanometer deflection	Spectrometer transmission	Transmission, fluorite window on thermopile	Absolute intensity at 1 m; Cols. $\frac{b \times e \times f \times g \times h}{c \times d}$
a	b	c	d	i
mμ	cm			μw/cm²
365	12.75	0.398	0.900	9.27
365–334	1.04	.390	.895	.77
334	.98	.377	.890	.76
334–313	.49	.360	.885	.40
313	10.39	.344	.880	8.94
302	2.98	.322	.875	2.76
297	2.33	.310	.871	2.25
289	.56	.292	.869	.57
280	.95	.261	.861	1.10
275	.37	.245	.859	.46
270	.38	.231	.854	.50
265	1.98	.218	.850	2.78
258	.25	.201	.843	.39
254	1.13	.194	.840	1.80
248	.59	.180	.835	1.02
241	.25	.162	.830	.48
238	.25	.155	.825	.51
234	.09	.145	.820	.19
230	.06	.135	.815	.14
Total shorter than and including 313 mμ.....				23.89 μw/cm²

2. THE BALANCED THERMOPILE AND EXCLUSION FILTER METHOD

The same procedure was followed in measuring the undispersed ultra-violet radiation from the tungsten mercury arc as was used in measuring the ultra-violet radiation from the sun, except that the balancing filter (fig. 2, *A*) was of quartz instead of Corex-A glass, which appreciably absorbs the wave lengths less than about 260 mμ.

The data are assembled in Table 3 in which column *a* gives the observed galvanometer deflection. Column *c* is column *a* after correction for the amount of infra-red present (column *b*) determined by means of the Noviol filter as already described. Column *e* is the radiation sensitivity of the galvanometer in microwatts per cm^2, obtained by exposure to a standard of radiation, and corrected for transmission (91.6 per cent) of the fluorite window.

TABLE 3.—*Integrated ultra-violet radiation of wave lengths less than, and including 313 mμ, at 1 m from a tungsten mercury arc in a quartz bulb, as determined by a balanced thermopile and exclusion filter radiometer*

Observed galvanometer deflection	Infra-red correction	Difference; $a-b$	Factor F, Table 4	Thermopile sensitivity, 1 cm = μw/cm^2	Total ultra-violet radiation, in μw/cm^2; Cols. $c\times d\times e$
a	b	c	d	e	f
cm 2.70	*cm* 0.73	*cm* 1.97	1.44	9.89	28.0

An important factor, F, is the amount of ultra-violet of wave lengths less than, and including 313 mμ, relative to the total shutout by the barium flint glass exclusion filter.

The procedure followed in obtaining the factor, F, is given in Table 4 in which column *b* is the spectral energy distribution of the radiation emitted by the lamp (taken from the last column of Table 2). These values need not be determined in absolute units.

Assuming equality of transmission of the barium flint glass and the quartz filters for wave lengths longer than 400 mμ (for which a correction for inequality of transmission is made by means of the Noviol filter) column *c* gives the difference in transmission of these two filters throughout the ultra-violet.

The observed spectral transmission of the water cell (using freshly distilled water) is given in column *d*. The balanced thermopile receivers were covered with a plate of fluorite which had the transmissions given in column *e*. The products of these factors, representing the radiation shut out by the barium flint glass filter are given in column *f* of Table 4. The sum of the intensities (galvanometer deflections) of all the wave lengths represents the observed amount of ultra-violet radiation excluded by the barium flint glass filter.

TABLE 4.—*Determination of the factor, F, for reducing the observed spectral intensity to radiation of wave lengths 313 mμ and less, for a tungsten mercury arc lamp*

[The value of the factor F is 23.89÷16.56=1.44]

Wave length	Relative intensity	Transmission quartz minus barium flint	Transmission water cell	Transmission fluorite on thermopile	Radiation excluded by barium flint glass; cols. $b \times c \times d \times e$
a	b	c	d	e	f
400		0.00	0.880	0.900	0.000
365	9.27	.06	.875	.891	.434
365–334	.77	.17	.871	.885	.102
334	.76	.40	.868	.878	.233
334–313	.40	.64	.865	.875	.192
313	8.94	.895	.862	.873	6.020
302	2.76	.90	.859	.863	1.842
297	2.25	.90	.856	.860	1.491
289	.57	.90	.851	.857	.374
280	1.10	.90	.849	.848	.712
275	.46	.90	.840	.845	.295
270	.50	.90	.843	.840	.319
265	2.78	.90	.841	.837	1.760
258	.39	.90	.839	.830	.243
254	1.80	.90	.837	.825	1.119
248	1.02	.90	.835	.819	.626
241	.48	.90	.832	.810	.291
238	.51	.90	.830	.805	.307
234	.19	.90	.828	.800	.115
230	.14	.90	.827	.795	.085
	[1] 23.89				[2] 16.560

[1] Total present of wave lengths 313 mμ and less.
[2] Total excluded by the barium flint glass.

The sum of the intensities of wave lengths shorter than and including 313 mμ in column *b* represents the total amount emitted; and column *f* is the total amount excluded by the barium flint glass filter. The ratio of these two summations (23.89/16.56) is the factor $F=1.44$.

In other words, owing to the absorption by the water cell and the (fluorite) thermopile window, the observed average galvanometer deflection (representing the ultra-violet radiation shut out by the barium flint glass filter) given in column *c* of Table 3, must be multiplied by the factor 1.44 in order to obtain the radiation of wave lengths less than and including 313 mμ in the tungsten mercury arc.

As given in Table 3, the undispersed ultra-violet radiant flux, of wave lengths less than and including 313 mμ, at a distance of 1 m, from this tungsten mercury arc lamp, as measured with the balanced thermopile and the barium flint glass exclusion filter is 28 μw/cm². The value obtained by summation of the spectral lines is 23.9 μw/cm²—a difference of about 14.6 per cent. Since these data were obtained to illustrate the method, and not as a final crucial test of the ultra-violet efficiency of a particular type of lamp, in which case averages of several series of observations would be taken, the agreement in the two methods of measuring the integrated ultra-violet is satisfactory.

Moreover, a small difference is to be expected in the values obtained by these two widely different methods of making the measurements, because of the difficulty in measuring weak ultra-violet radiation,

when it is resolved into a spectrum, whereas in the undispersed state it is measured as a whole by the filter method.

Using another tungsten mercury arc lamp, the same factor, $F=1.44$, was obtained. From this it appears that the factor, F, for a given type of lamp can be obtained by observing a limited number of samples, using the spectroradiometric method, after which it is possible to rate the performance of these lamps, on a large scale, by means of the balanced thermopile and exclusion filter method.

In conclusion, it is relevant to recall that in order to determine the factor, F, for a source which emits a continuous spectrum, it is necessary to reduce the intensity measurements to a normal spectrum energy distribution (13), then correct these intensities for absorption by the spectroradiometer and thermopile window. This gives the normal spectral energy flux upon the entrance slit. Since only the relative spectral intensities are required, it is unnecessary to calibrate the galvanometer in absolute units. The evaluation of the factor, F, is then made as in the case of sunlight, illustrated in Figure 7.

V. CALIBRATION OF A PHOTO-ELECTRIC CELL IN ABSOLUTE UNITS BY MEANS OF RADIOMETRIC FILTER METHODS

For some years the problem has been presented to calibrate and keep a check on the accuracy of a photo-electric cell, for use as an intensity, or so-called dosage meter of ultra-violet radiation, used in heliotherapy.

With the herein described satisfactory tests of unselective radiometer-filter methods, particularly the balanced thermocouple and filter radiometer, it is believed that a way has been found for calibrating and for testing the constancy of the performance of selective (photo-electric) radiometers for use in measuring ultra-violet radiation.

The particular device studied was a Rentschler "ultra-violet ray meter" (11) consisting of a photo-electric cell connected with a counting device.

As shown in Figure 4 (the triangles $\Delta\Delta\Delta$) the number of discharges of the condenser through the glow relay tube, which is connected with the photo-electric cell, is proportional to the intensity of the ultra-violet radiation (from the sun and a large part of the sky) incident upon the cell. The intensity or flux density of ultra-violet radiation of wave lengths less than 334 mμ (the long wave length limit of sensitivity of the particular cell used) represented by a single discharge through the glow relay tube, in midwinter (air mass, $m=1.6$) was 1 discharge $=2.6$ μw/cm^2, and in midsummer ($m=1.05$ to $m=1.3$) it was 1 discharge $=1.7$ μw/cm^2. Another cell, which had been used only a few times, varied from 1 discharge $=1.9$ μw/cm^2 in winter to 1 discharge $=1.35$ μw/cm^2 in midsummer.

These data are interesting in showing that whereas the rate of discharge appears to be proportional to the intensity (see fig. 4) for small changes in air mass, yet the constant of the instrument (the value of 1 discharge in μw/cm^2) appears to be smaller in summer than that observed in winter. This would occur if, as is generally supposed, the summer sun is richer in short wave length ultra-violet than winter sunlight. The cell intercepts also a large part of the sky, which may affect the constant of the instrument.

In view of the fact that this was an experimental type of cell that is to be superseded by an entirely different mounting of the photo-sensitive surface, the foregoing data are presented merely to illustrate the procedure followed in standardizing, and in testing the performance of selective (photo-electric) radiometers, for use as ultra-violet intensity meters, by means of a nonselective filter radiometer, but they are not to be considered as indicating the performance of a particular make of photo-electric cell. Such variations are to be expected in all selective (photo-electric) radiometers in which the response is not confined to a narrow spectral band, in this case of wave lengths less than 313 mμ. For a more accurate calibration of such a device, the response should be observed with and without a barium-flint glass filter to eliminate the effect of wave lengths longer than 313 mμ.

VI. PHYSIOLOGICAL TESTS

Progress in physiological tests using measured amounts of spectrally pure ("monochromatic") and of spectrally heterogeneous ultra-violet radiation is necessarily slow. Nevertheless such tests will be necessary in order to determine the reliability of an ultra-violet intensity or so-called dosage meter. At the present time there is neither a unit of dosage nor a meter for accurately measuring the amount of ultra-violet radiation used for healing purposes.

The object of the present report is to show the agreement obtained in the erythemic reaction of three sources differing very widely in ultra-violet spectral energy distribution, based upon energy measurements made with the balanced filter radiometer.

These sources are: (*a*) The sun, in which there is practically no radiation of wave lengths shorter than 290 mμ, and the intensity at 313 mμ is a million times that at 290 mμ; (*b*) the low voltage, relatively high vapor pressure, mercury arc, in a quartz tube, which has a group of intense emission lines at the wave lengths 248, 254, 265, 280, 297, 302, and 313 mμ; and (*c*) the high voltage, low vapor pressure mercury arc in a quartz tube, in which 93 to 96 per cent of the radiation, of wave lengths less than, and including 313 mμ, is emitted by the resonance line 254 mμ (2,537 A).

Using spectrally pure radiation, in an erythemic reaction test made on the untanned inner upper arm, during July (high humidity, skin moist) an exposure to the 297 mμ line, having a radiant flux of 316 μw/ per cm^2, produced a minimum perceptible erythema in 60 seconds on J. M. H. and in a little less than 70 seconds on W. W. C. The total incident energy used was, therefore, about 189,600 and 221,000 ergs, respectively. In another publication (10) it was shown that the amount of energy required to produce a minimum perceptible erythema on the average untanned inner forearm (wintertime, low humidity, skin dry) using the wave length of maximum erythemic susceptibility (at 297 mμ), is about 500,000 ergs/cm^2.

The test on spectrally heterogeneous radiation was made on the same day (July 22, 1931) at the noon hour, when two small areas on the same part of the arm (of W. W. C.) were similarly exposed to the sun (through holes 5 by 15 mm, cut in dark cloth) for 20 and 30 minutes, respectively, the ultra-violet radiant flux, of wave lengths less than and including 313 mμ, being 88 μw/cm^2. By 5 p. m. the follow-

ing day the erythema produced by the 20-minute exposure had practically disappeared and the exposed area appeared pigmented. The area that received the 30-minute exposure was still very red and quite sore to the touch, showing the importance of a properly timed exposure. Two additional exposures, of 10 and 15 minute duration, on July 23 (ultra-violet radiant flux, *u. v. Q*, = 79 $\mu w/cm^2$) failed to produce a definite erythema, though the 15-minute exposure showed slight pigmentation.

Similar exposures were made on J. M. H. (July 27, noon hour, hazy *u. v.* $Q = 69$ $\mu w/cm,^2$) for 15, 18, 21, and 25 minutes, the 21-minute exposure giving a well-defined minimum erythema.

In the 20-minute exposure on W. W. C. the total energy used in producting an erythema was about 1,056,000 ergs, as compared with 221,000 ergs using homogeneous radiation of wave length 297 mμ. For J. M. H. the values were 870,000 ergs and 189,600 ergs, respectively. For R. S., on whom the exposures were made on June 3 (solar *u. v.* $Q = 78$ $\mu w/cm^2$ for 45 minutes; 297 mμ line = 395 $\mu w/cm^2$ for 2 minutes) the values were 2,106,000 ergs and 474,000 ergs, respectively.

On this basis the erythemogenic efficiency of Washington midsummer ultra-violet solar radiation, of wave lengths less than and including 313 mμ for W. W. C. was, therefore, 20.9 per cent of that of the wave length of maximum erythemic susceptibility; for J. M. H. it was 21.8 per cent; and for R. S. it was 22.5 per cent.

The erythemogenic efficiency of the ultra-violet in midsummer noon-hour sunlight, calculated from the rubescence curve, *R* (fig. 7) is 22 per cent. The agreement between the observed and the calculated efficiency of solar radiation is probably closer than should be expected, in view of the lack of information on the short wave length ultra-violet solar radiation.

It is to be noted that the erythema resulting from the 20-minute exposure on W. W. C. was followed by distinct pigmentation, which made it difficult to decide when the erythema had ceased. Apparently a shorter exposure to the sun would have produced the desired results, thus increasing the experimentally determined erythemogenic efficiency to a value somewhat higher than 20 per cent. It is to be noted, also, that the 15-minute exposure (total 720,000 ergs) failed to produce an erythema and that the threshold on the inner upper arm of this subject, was about 1,000,000 ergs, showing the importance of closely timing the exposure, especially when the predominating radiation is of wave lengths 310 to 315 mμ, in which a small amount of energy added to the threshold is sufficient to produce a burn (10).

In the second series of tests of the physiological application of measured amounts of spectrally heterogeneous ultra-violet radiation in producing a minimum perceptible erythema, the source was a mercury vapor arc, between two tungsten electrodes, located at the top of a V-shaped helical filament of tungsten, in a quartz bulb, which emits a large amount (see Table 5) of erythemogenic radiation of wave lengths less than 290 mμ, not present in sunlight.

The erythemogenic value (column *d*, Table 5) of the radiation at different wave lengths, is obtained by multiplying the observed spectral intensities (column *b*, Table 5) by the erythemic response (10) given in column *c*, Table 5. The ratio of the sum of these components (in relative or absolute units) to the total emitted (6.42+

23.89 = 0.269) is the erythemogenic efficiency of the spectrally heterogeneous ultra-violet radiation emitted by this particular lamp, operated upon a certain specified voltage.

As shown in Table 3 the ultra-violet intensity, or radiant flux, at 1 m from this particular lamp, as measured with the balanced thermocouple and exclusion filter method, was 28.0 μw/cm^2. Hence, the calculated radiant flux of the erythemogenic ultra-violet radiation at 20 cm from the lamp was (28.0 × 25 × .269) = 188 μw/cm^2.

TABLE 5.—*Showing the spectral erythemogenic efficiency of a certain tungsten mercury arc lamp in a quartz bulb*

Wave length (in mμ)	Intensity at 1 m	Erythemic response	Erythemogenic value
a	b	c	d
	$\mu w/cm^2$		$\mu w/cm^2$
313	8.94	0.03	0.27
302	2.76	.55	1.52
297	2.25	1.00	2.25
289	.57	.19	.11
280	1.10	.06	.07
275	.46	.07	.03
270	.50	.12	.06
265	2.78	.22	.61
258	.39	.29	.11
254	1.80	.32	.58
248	1.02	.34	.35
248–230	1.32	.35	.46
Total..	23.89	----------	6.42

Exposure to the 297 mμ line, having a radiant flux of 395 μw/cm^2 required between 1.0 and 1.2 minutes to produce a minimum perceptible erythema, on the inside of the upper arm of one of the writers (W. W. C.) hence, to produce a minimum perceptible erythema at a distance of 20 cm from this lamp the calculated time of exposure was between 2 minutes 7 seconds, and 2 minutes 39 seconds. The actual exposures (five in all) were varied in 10-second intervals ranging from 1 minute 50 seconds to 2 minutes 40 seconds. The resulting erythemas showed that the 2 minutes 40 seconds exposure was decidedly too long, that the 1 minute 50 seconds was underexposed, and that the 2-minute exposure gave practically a miniumm perceptible erythema.

In another test, with the lamp at 25 cm, the observed time of exposure to produce a minimum perceptible erythema was 3 minutes 20 seconds for W. W. C., and between 2 minutes 50 seconds and 3 minutes for J. M. H., which is in good agreement with the calculated time of 3 minutes 23 seconds and 3 minutes 2 seconds, respectively. In this case the erythema test was made directly after the radiometric evaluation of the intensity (387 × 0.269 = 104 μw/cm^2) of erythemogenic radiation from this lamp.

In the third series of erythema tests, using measured amounts of heterogeneous ultra-violet radiation, as compared with the 297 mμ line, the source was a so-called "cold quartz lamp" (practically the low vapor pressure Geissler tube discharge in quartz) in which the relative intensities of the lines that could be measured (at the wave

lengths 254, 297, and 313 mμ) were 865, 14, and 45, respectively. (See Table 5 for a different type of mercury arc.)

The total ultra-violet radiation of wave lengths less than, and including the 313 mμ line, at a distance of 25 cm from the lamp, as determined with the above-described balanced thermopile and filter method (and the observed factor F = 1.46) was 186 μw/cm².

Irradiation of the inner upper arm (of W. W. C.) for 2, 3, 4, 5 (3 exposures), and 6 minutes (2 exposures) showed slight discoloration of the skin for the 2 and 3 minute exposures. The 6-minute exposures were decidedly overexposed, and the minimum exposure appeared to be between 3 and 4 minutes. The minimum exposure for J. M. H. was 3 minutes.

The spectral erythemic response for equal energy, in the region of 254 mμ is not well established (10). The average value of the various observers is about 45 per cent as compared with 100 per cent at 297 mμ. On this basis the calculated time of exposure to produce a minimum perceptible erythema would have been 3.4 minutes, as compared with observed values of 3 to 4 minutes. Considering the possible errors in the radiation measurements, on this type of lamp and the uncertainty in the spectral erythemic response curve at wave lengths less than and including 254 mμ, the observed and the calculated times of exposure are in good agreement.

An important result of this experiment is that an exposure of two to three times the threshold dosage produced only an intense superficial reddening of the skin, whereas a slight overexposure to the longer wave lengths (at 313 mμ) in the sun produced a painful burn (10), which phenomenon was observed long ago, but only in recent times is being taken into consideration.

In view of the complex correlation between the spectral energy distribution of the source and the spectral erythemic response curve (which is subject to misinterpretation of the effect produced by the short wave lengths), the agreement between the observed time of exposure, using measured amounts of spectrally heterogeneous ultra-violet radiation from three sources differing very markedly in spectral energy distribution, and the calculated time of exposure, based upon the total energy required to produce an erythema by means of the 297 mμ line (the wave length of maximum erythemic susceptibility), is as close as can be expected.

The results of these tests indicate how closely the exposures must be timed in order to obtain consistent results. According to earlier observers a close agreement in erythema tests is not possible. It is to be noted, however, that their observations were not made with accurately measured amounts of spectrally heterogeneous ultra-violet radiation and the effects compared with that of the 297 mμ line. Evidently, tests on a group of observers will be desirable to establish an average.

It is to be noted (10) that the erythemic reaction of the human skin, on short exposure to the very short wave lengths (240 to 280 mμ) of ultra-violet radiation, rises to a maximum and disappears again in the course of a few hours, whereas a similar number of hours elapses before the erythema produced by the longer wave lengths (313 mμ) becomes at all visible and about 5 hours more are required for the reddening to attain a maximum, after which (if pigmentation has not started) some 15 to 20 hours may elpase before the erythema

disappears. But even after the erythema has apparently disappeared it can be restored by wiping the surface with alcohol.

Hence, it can hardly be expected that there will always be an exact agreement between the erythemic efficiency of the wave length (297 mμ) of maximum susceptibility and the efficiency derived from an integration of the rubescence curve R (fig. 7), obtained from the spectral energy curve of the sun, or from an artificial source.

As just noted the total ultra-violet solar energy required to produce a mild erythema may be somewhat larger (exposure longer) than the calculated value; and in artificial sources, emitting considerable ultra-violet of wave lengths less than 270 mμ, the time of exposure may be found to be somewhat shorter than the calculated value. However, it will serve as a guide in determining the safe dosage exposure, which is the purpose of the whole procedure (10).

VII. SUMMARY

The present paper is a further contribution (see RP318) to the investigation of filter radiometry, with special reference to the quantitative measurement of the component of ultra-violet radiation of wave lengths less than 313 mμ in sunlight and in artificial sources, which biologists recognize as of special importance in the prevention and cure of rickets.

The apparatus used was a balanced radiometer, consisting of a thermocouple in which the two receivers are simultaneously exposed to radiation, under which conditions practically no thermoelectric current flows through the galvanometer. A 1 cm cell of water or of crystal quartz was used continuously over the thermocouple receivers.

On covering one receiver with a filter that excludes the ultra-violet which it is desired to evaluate and the other receiver with a window that freely transmits these ultra-violet rays, and exactly balances the transmission losses of the exclusion filter, throughout the remaining part of the spectrum, the galvanometer deflection obtained on exposure of the two thermocouple receivers through this combination of filters is a direct measurement of the ultra-violet emitted by the source under investigation. In order to evaluate the ultra-violet of wave lengths less than 313 mμ, it is necessary to know the relative spectral energy distribution of the source for wave lengths less than 400 mμ.

The ultra-violet exclusion filter was a barium flint glass and the balancing filter was of crystal quartz or Corex G980A glass, depending upon the source of radiation. The lack of complete balance of long wave-length radiation was determined by covering both receivers with a plate of Noviol–A glass, which is opaque to radiation of wave lengths less than 400 mμ, the long wave length endpoint of the barium flint exclusion filter.

Using two arrangements of (*a*) the balanced pair of thermocouple receivers with a single exclusion filter method, and (*b*) a single thermocouple receiver with two exclusion filters (three methods in all), and (*c*) using two methods of calibrating the radiation sensitivity of the thermocouple receivers in absolute units, closely agreeing measurements were made showing that the average amount of ultra-violet radiation of wave lengths less than and including 313 mμ, for mid-latitude sea level stations, during the clearest weather, during midday

in midsummer, amounts to about 90 μw/cm^2, decreasing to about 20 μw on the clearest days in midwinter.

An experimental procedure is described for testing the performance and for standardizing photo-electric cells for use as ultra-violet intensity (so-called dosage) meters.

An experimental procedure is described for using measured amounts of spectrally pure ("monochromatic") ultra-violet radiation in physiological tests, such as, for example, the amount of ultra-violet energy required to produce a minimum perceptible erythema on the untanned human skin. Data are given showing that the erythemogenic efficiency of Washington midsummer ultra-violet solar radiation is only about 21 per cent that of the wave length (297 mμ) of maximum erythemic susceptibility. Using the spectral erythemic response curve, observed by the writers, the calculated erythemogenic efficiency is 22 per cent, which is as close an agreement as can be expected, in view of the uncertainty in the ultra-violet solar spectral energy curve upon which the calculations must be based.

Using an artificial source of radiation in which the ultra-violet spectral energy distribution and the total erythemogenic ultra-violet radiation could be accurately measured, the observed time of exposure to the total radiation from the lamp, required to produce a minimum perceptible erythema, was in good agreement with the time calculated from observations using the wave length (297 mμ) of maximum erythemic susceptibility.

VIII. BIBLIOGRAPHY

1. Measurements of Extreme Ultra-Violet Solar Radiation by a Filter Method, W. W. Coblentz, R. Stair, and J. M. Hogue, B. S. Jour. Research, vol. 6 (RP318), p. 951; 1931. This paper gives an extensive bibliography of previous contributions to the general subject of instruments and methods of radiometry.
2. Spectral Distribution of Energy Radiated from a New Type Tungsten Mercury Arc., B. T. Barnes, Phys. Rev., vol. 36, p. 1468; 1930. Spectral Transmission of Quartz-Fluorite Monochromators, W. E. Forsythe and B. T. Barnes, Rev. Sci. Inst., vol. 1, p. 569; 1930; M. Rosenmüller, Ann. der Phys., (4), vol. 29, p. 355; 1909.
3. Measurements on Standards of Radiation in Absolute Value, W. W. Coblentz, B. S. Bull. No. 227, vol. 11, p. 87; 1914.
4. Sensitivity and Magnetic Shielding Tests of Thomson Galvanometers for Use in Radiometry, W. W. Coblentz, B. S. Bull. No. 282, vol. 13, p. 423; 1916.
5. Disintegration of Metal Surfaces by Ultra-Violet Radiation, W. W. Coblentz and C. W. Hughes, Sci., vol. 60, p. 64; B. S. Sci. Papers vol. 19 (S493), p. 577; 1924; W. W. Coblentz and R. Stair, B. S. Jour. Research, vol. 4 (RP141), p. 189; 1930. This is a problem that must be considered in connection with the use of photo-electric cells.
6. Various Modifications of Bismuth Silver Thermopiles Having a continuous Absorbing Surface, W. W. Coblentz, B. S. Bull. No. 229, p. 131; 1914. Another arrangement to be tested consists of two thin blackened metal strips, in front of the thermocouple receivers, which can be calibrated in absolute measure by electric heating, as in the Ångström pyrheliometer.
7. Measures of The Radiation of The Solar Corona, H. T. Stetson and W. W. Coblentz, Astrophys. J. vol. 62, p. 128; 1925. A photograph of the balanced thermopile is illustrated in Figure 1 of this publication.
8. Data On Ultra-Violet Solar Radiation and the Solarization of Window Materials, W. W. Coblentz and R. Stair, B. S. Jour. Research, vol. 3, (RP113) p. 629; 1929.
9. A Radiometric Investigation of the Germicidal Action of Ultra-Violet Radiation, W. W. Coblentz and H. R. Fulton, B. S. Sci. Papers, vol. 19, (S495), p. 641; 1924. Kreusler, Ann. der Physik, (4), vol. 6, p. 412; 1901.

10. The Spectral Erythemic Reaction of the Human Skin to Ultra-Violet Radiation, W. W. Coblentz, R. Stair and J. M. Hogue, Proc. Nat. Acad. Sci., vol. 17, p. 401; 1931.
11. An Ultra-Violet Light Meter, H. C. Rentschler, Trans. Amer. Inst. Elect. Eng., New York Convention, January 27 to 31, 1930.
12. The Ultra-Violet and Visible Transmission of Eye-Protective Glasses, K. S. Gibson and H. J. McNicholas, BS. Tech. Papers No. 119, issued June 7, 1919. The standard samples complying with the present specifications were prepared by Dr. H. P. Gage, Corning Glass Works Research Laboratory.
13. Constants of Spectral Radiation of a Uniformly Heated Inclosure or so-called Black Body, I, W. W. Coblentz, B. S. Bull. No. 204, vol. 10, p. 44; 1913. This paper describes the method commonly used for reducing the observed data from prismatic to a normal spectrum.

WASHINGTON, JULY 30, 1931.

RADIATION FROM PROBE SURFACES BOMBARDED BY ELECTRONS

By F. L. Mohler and C. Boeckner

ABSTRACT

Metals in the form of small probe surfaces are held at a positive potential in the highly ionized region of a discharge (commonly a cæsium discharge) and under intense electron bombardment emit radiation. Photographic spectrophotometric measurements are made. Radiations at 7 volts from W, Al, Be, Au alloyed with Cs, Th, and Pt are similar in intensity and intensity distribution. The spectral energy distribution on a wave-length scale is nearly constant between 6,400 and 2,400 A with a radiation flux of about 20 ergs for a wave-length range of 1μ and for a current density of 1 ampere per cm^2. J (λ) for Cu has a pronounced increase in the red and for silver a tenfold increase between 3,200 and 3,600 A. Above 6 volts this intensity distribution remains the same while with lower voltages it drops almost linearly to zero with increasing ν. The threshold value of ν agrees with the relation $h\nu = e(V+W)$ where W is 1.45 volts for tungsten and about 2 volts for Cu, Ag, and Al. The voltage variation of intensity is different for each metal. The intensity and intensity distribution of tungsten and silver radiation in a helium discharge are similar to values obtained in cæsium vapor.

The equal energy spectrum common to all metals is probably analogous to continuous X rays. The selective radiation of silver and copper may correspond to characteristic X radiation. The high-frequency edge of the silver emission band has the shape of a Fermi distribution of electrons at 370° C., suggesting that the emission process involves the ionization of an underlying level and the fall of a conduction electron into that level.

CONTENTS

	Page
I. Method and procedure	751
II. Intensity distribution at 7 volts	753
1. Tungsten	753
2. Aluminum	753
3. Beryllium	753
4. Gold-cæsium alloy	754
5. Thorium	754
6. Platinum	754
7. Copper	754
8. Silver	755
III. Intensity distribution at other voltages	755
IV. Intensity as a function of voltage	756
V. Probe radiation in a helium discharge	758
VI. Discussion	759
1. The equal energy spectrum	759
2. Selective radiation of silver and copper	760
3. The variation of intensity with voltage	763

I. METHOD AND PROCEDURE

An earlier paper describes measurements of a continuous spectrum emitted by metals under low voltage electron bombardment.[1] The large currents required to make the radiation measurable were obtained by the device of using the metal in the form of a small

[1] Mohler, F. L., and Boeckner, C., B. S. Jour. Research, vol. 6 (RP297), p. 673 April, 1931. Referred to as "first paper."

probe surface in the highly ionized region of a fairly intense discharge. Measurements by the same method have been extended to other metals and to a larger voltage range, and this paper reports the new results.

In Figure 1 we repeat from the first paper a diagram of the type of tube used. A discharge current of about an ampere is maintained between the hairpin cathode and the cylindrical anode while the probe surface, which is the end of a heavy wire about 2 mm. in diameter, is held at a potential positive with respect to the surrounding space. The current density at the probe surface was commonly from 2 to 5 amperes per cm^2. From the current voltage characteristics of the probe, the voltage drop between the probe and the surrounding space and the average energy of the electrons in the space can be determined. This energy, about 0.4 electron volts, added to the energy derived from the voltage drop gives the average energy

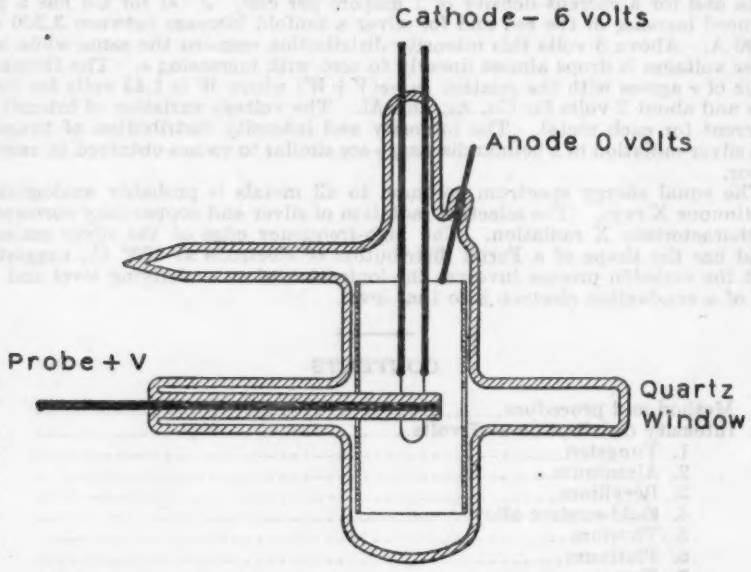

FIGURE 1.—*Type of tube used for observation of probe radiation*

of the electrons striking the surface. The corrected potential is referred to as the applied potential in this paper.

Spectra have been photographed with a Hilger E_2 quartz spectrograph, a small quartz spectrograph, and a 3-prism Zeiss glass spectrograph. Exposure times ranged from 15 minutes to many hours. For comparison of metals two probes have been mounted side by side in the discharge.

Relative intensity measurements were based on densitometer comparisons of two or more exposures with full light and light reduced in a known ratio and one or more exposures under different conditions of intermediate density. Intensity-distribution measurements are based on comparison with spectra of a calibrated tungsten strip lamp in quartz. A correction for failure of the reciprocity law has been applied where exposure times differ, and some results of the first paper have been recomputed on this basis.

An obvious difficulty of the experiments is that the faint continuous spectrum must be viewed in the presence of a brilliant discharge. The cæsium discharge gives the least trouble in this respect and so has been used in most of this work, although conditions of metal surfaces in cæsium vapor are complicated by the fact that a monatomic layer of cæsium is occluded on most metals. With intermediate voltages the ultra-violet spectrum appeared to be free from scattered light except for isolated emission lines. Under other conditions there was a more or less continuous background which could be partially corrected for by making a blank exposure with the probe current off, but since the light in front of the probe is intensified when it is drawing a current, measurements become unreliable when the background correction is large.

Contamination of the probe surface from sputtering or evaporation from the cathode or from a neighboring probe was a serious source of error. The surface could usually be brought back to its initial state by bombarding it with positive ions at -100 volts for a few minutes. Many metals combine with cæsium, but there was no evidence of combination with any of the metals here used except gold which forms a silvery white alloy. The statement in the first paper that silver appeared to combine with cæsium is now judged to be erroneous.

It has been shown in the first paper that the probe radiation is independent of vapor pressure and other discharge conditions and that the intensity is proportional to the probe current. The significant variables to be investigated are the intensity as a function of wave length and voltage.

II. INTENSITY DISTRIBUTION AT 7 VOLTS

The intensity of radiation from tungsten at 7 volts has been taken as a standard—perhaps unfortunately, as there are inconsistencies of the order of twofold between some comparative measurements as compared with direct measurements obtained with the strip lamp. The absolute value here given is about half the value given in the first paper, and is probably uncertain by a factor of 2.

1. TUNGSTEN

Figure 2 gives the intensity distribution of tungsten radiation based on four overlapping series of measurements which show that between 2,600 and 5,200 Å the intensity per unit wave length range, $J(\lambda)$, is nearly constant. The absolute value as given by the mean of the ultra-violet measurements is 20 ergs per cm^2 per sec. for a wave-length range of 1μ and a current density of 1 ampere per cm^2.

2. ALUMINUM

Comparative measurements with tungsten show that from 4,900 to 2,300 Å the intensity per unit current is almost identical with tungsten, while comparison with a strip lamp shows that $J(\lambda)$ remains nearly constant to 6,400 Å.

3. BERYLLIUM

The intensity and intensity distribution are about the same as for tungsten.

4. GOLD-CAESIUM ALLOY. (Silvery in appearance)

The intensity and intensity distribution also resemble tungsten.

5. THORIUM

Thorium radiation is about twice as bright as tungsten with the same intensity distribution.

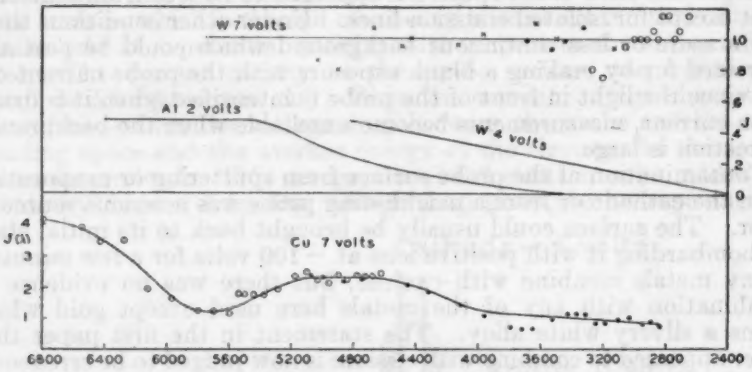

FIGURE 2.—*Intensity distribution of probe radiation*

All curves are on a scale of J (λ) for tungsten at 7 volts as unity with the unit equal approximately to 20 ergs per cm ^{2} for a current of one ampere per cm ^{2}.

6. PLATINUM

For platinum J (λ) dropped regularly from 1.4 times the tungsten intensity at 3,700 A to 0.7 times tungsten at 2,400 A.

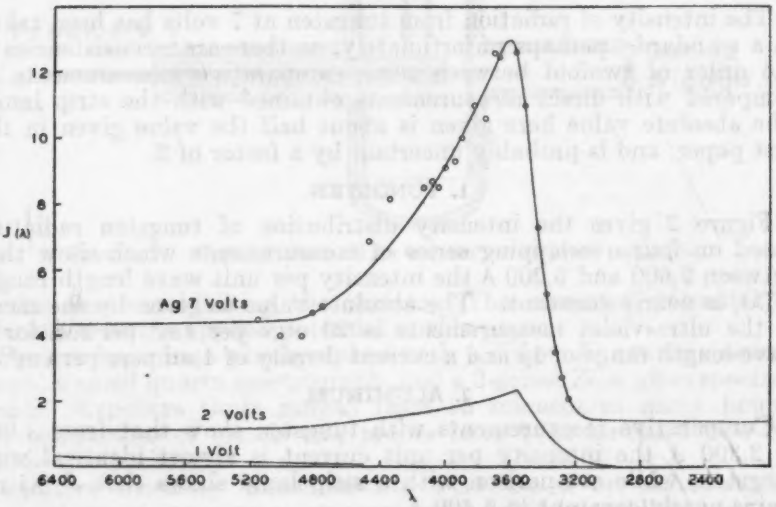

FIGURE 3.—*Intensity distribution of silver radiation with ordinates in units of Figure 2*

7. COPPER

Data in the first paper have been recomputed to include factors neglected before and results are plotted in Figure 2. The intensity for wave lengths shorter than 3,600 A is about the same as for tung-

sten; for longer wave lengths there are marked differences. The experimental uncertainty becomes extreme at the red end of the curve.

8. SILVER

The intensity distribution for silver radiation is in marked contrast to other metals. Several sets of data have been averaged to give the extreme portions of the curve in Figure 3 while a single set has been used near the maximum to avoid a false rounding of the sharp maximum. Ordinates are on the same scale as Figure 2, viz, J (λ) for tungsten equal to unity. J (λ) for wave lengths less than 3,200 A is much the same as for other metals.

III. INTENSITY DISTRIBUTION AT OTHER VOLTAGES

The intensity changes with the voltage in a manner described in the following section, but, in general, the intensity distribution remains nearly the same as the potential is increased above 7 volts. Below 6 or 7 volts J (λ) decreases with decreasing wave length and for most metals with applied voltages below 4 volts J (λ) approaches zero in the range of the quartz spectrograph.

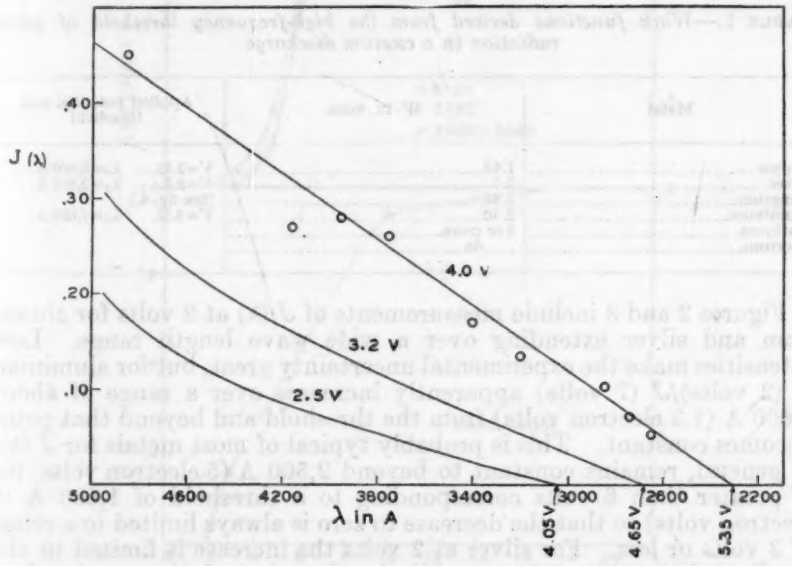

FIGURE 4.—*Intensity distribution of tungsten radiation at low voltage in units of Figure 2*

Below each intercept is given the voltage corresponding to the threshold wave length.

Figure 4 gives the intensity distribution of tungsten spectra at 2.5, 3.2, and 4.0 volts on a scale of J (λ) at 7 volts = 1. As J (λ) is nearly a linear function of λ the extrapolation to zero intensity gives a definite and reproducible value for the high-frequency threshold. The values of these high-frequency thresholds are given in terms of $h\nu/e$ in volts. The three values satisfy the equation.

$$h\nu = e\,(V + W) \qquad W = 1.45 \pm .1 \text{ volts}$$

where V is the applied voltage and W is interpreted to be the work function of the cæsiated metal. In the first paper we report an independent series of measurements leading to an identical value of W.

Figure 3 of the first paper and Figures 2 and 3 of this paper include plots of J (λ) at low voltages for copper, silver and aluminum as well as for tungsten and it is seen that J (λ) approaches zero in a similar manner for all these metals. For thorium and platinum the intensity distribution at 3 volts is practically the same as at 7 volts with no evidence of a threshold in the range of the quartz spectrograph. We conclude that the work function is greater than 3 volts which would give a threshold near 2,100 A. Table 1 summarizes the values of the work functions derived from this work. The values of 2.1 volts or less are of the magnitude to be expected for cæsiated metals, but there is no safe basis for quantitative comparison. Thus, Ives and Olpin [2] find that the photo-electric threshold depends critically on the thickness of the alkali film on a metal and very little on the nature of the underlying metal. For cæsium on silver and platinum the minimum value of the work function was 1.38 volts. It is consistent with their conclusions that all our observed values are somewhat greater than this.

TABLE 1.—*Work functions derived from the high-frequency threshold of probe radiation in a cæsium discharge*

Metal	W in volts	Applied potential and threshold
Copper	1.95	V=2.15. λ_o=3,000 A.
Silver	2.1	V=2.2. λ_o=2,860 A.
Tungsten	1.45	(See fig. 4.)
Aluminum	2.10	V=2.55. λ_o=2,650 A.
Platinum	3 or more	
Thorium	do	

Figures 2 and 3 include measurements of J (λ) at 2 volts for aluminum and silver extending over a wide wave length range. Low intensities make the experimental uncertainty great, but for aluminum J (2 volts)/J (7 volts) apparently increases over a range of about 2,000 A (1.3 electron volts) from the threshold and beyond that point becomes constant. This is probably typical of most metals for J (λ), in general, remains constant to beyond 2,500 A (5 electron volts) for V greater than 6 volts corresponding to a threshold of 1,600 A (8 electron volts) so that the decrease to zero is always limited to a range of 3 volts or less. For silver at 2 volts the increase is limited to the small range 2,800 to 3,200 A while for the relatively intense band on the red side of 3,200, J (2 volts)/J (7 volts) remains constant.

IV. INTENSITY AS A FUNCTION OF VOLTAGE

The foregoing results have shown a marked similarity between most metals, but the voltage variation of intensity is strikingly characteristic of the metal used. A comparison of the intensities at one wave length and different voltages is intrinsically simpler than a

[2] Ives and Olpin, Phys. Rev., vol. 34, p. 117; 1929. Ives, Astrophys. J., vol. 60, p. 4; 1924.

measurement of intensity distribution. Measurements could be reproduced to about 5 per cent though occasionally much greater variations were caused by contamination of the surfaces. Figures 5 and 6 give the results. Data for tungsten, silver, and aluminum were checked by repeated series of measurements. (The tungsten point at 10 volts is probably in error because of surface contamina-

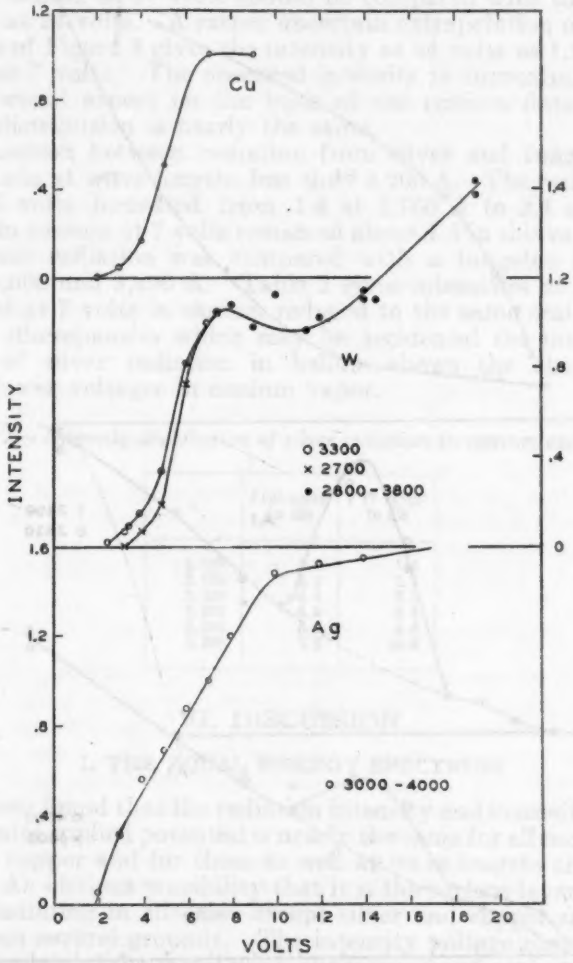

FIGURE 5.—*Voltage variation of monochromatic intensity*

The ordinate at 7 volts on each curve is taken as 1.

tion.) In general, the intensity distribution remains the same within about 10 per cent for voltages above 5 volts and the plotted points are a mean of measurements at many wave lengths between 2,600 and 4,000 A where other wave lengths are not specified. The voltage threshold and the slope of the curve near the threshold depend on the wave length as described in the preceding section.

V. PROBE RADIATION IN A HELIUM DISCHARGE

Some effort has been made to obtain measurements of radiation from probe surfaces in a helium discharge as such radiation could more safely be assumed to be characteristic of a pure metal. Scattered

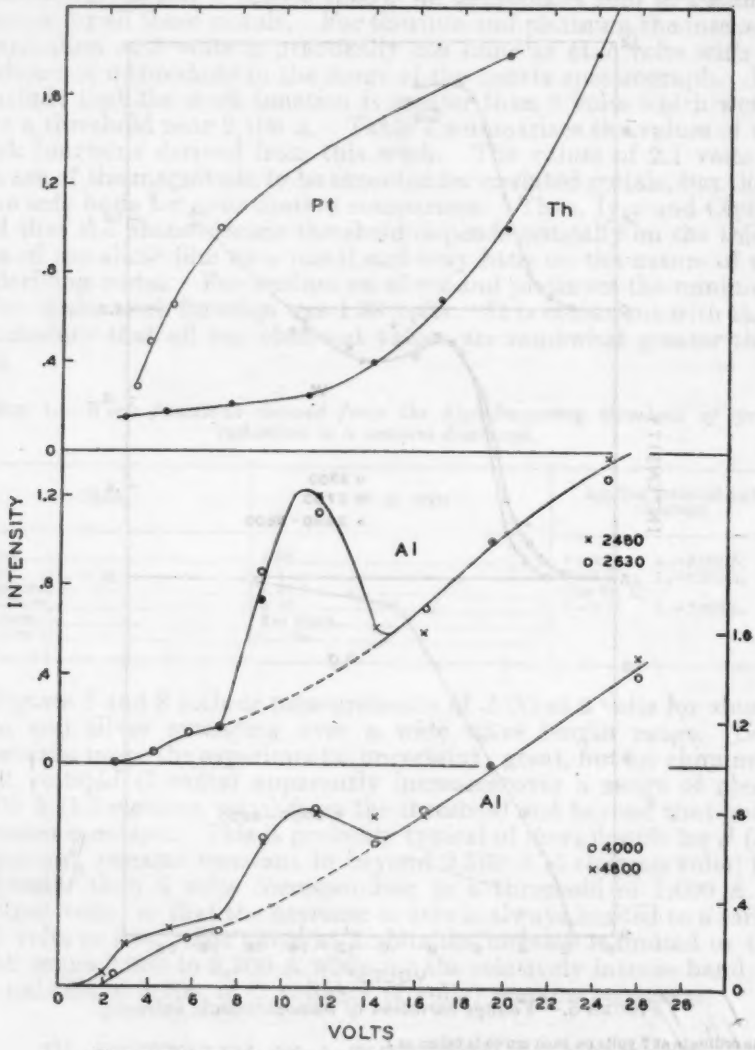

FIGURE 6.—*Voltage variation of monochromatic intensity*

light was usually very much greater than in the cæsium discharge and it was impossible to maintain steady conditions over a long period of time. Because of the high-ionization potential of helium higher probe potentials could be used and were used to increase the intensity and reduce errors from scattered light.

A comparison between radiation from tungsten in a helium discharge at 21 volts and radiation from a similar probe in cæsium at 7 volts gives the following ratio of intensity per unit current. J (helium)/J (cæsium) at 3,270 A, 3.2; 3,100 A, 3.5; 2,900 A, 4.1; 2,680 A, 3.9; 2,600 A, 4.2; mean, 3.8. The variation of the ratio with wave length is no greater than the experimental uncertainty. Since pure tungsten has a work function 3 volts greater than cæsiated tungsten, the intensity in helium at 21 volts should be compared with the intensity in cæsium at 24 volts. A rather uncertain extrapolation of the tungsten curve of Figure 5 gives the intensity at 24 volts as 1.9 times the intensity at 7 volts. The observed intensity is approximately twice what we would expect on the basis of the cæsium data while the intensity distribution is nearly the same.

A comparison between radiation from silver and tungsten could only be made at wave lengths less than 3,200 A. The ratio J (Ag)/J (W) at 28 volts increased from 1.4 at 2,760 A to 2.4 at 3,110 A. The ratio in cæsium at 7 volts remained about 1.5 in this range.

The silver radiation was compared with a tungsten strip lamp between 3,000 and 3,490 A. Table 2 gives intensities at 28 volts in helium and at 7 volts in cæsium reduced to the same scale. Except for minor discrepancies which may be accidental the intensity distribution of silver radiation in helium shows the characteristics found at lower voltages in cæsium vapor.

TABLE 2.—*Intensity distribution of silver radiation in cæsium and helium*

λ	J (28 volts) in He	J (7 volts) in Cs
3,000	1.5	1.4
3,100	2.5	1.5
3,230	4.6	2.0
3,310	4.9	3.4
3,390	6.0	5.6
3,490	8.5	10.0

VI. DISCUSSION

1. THE EQUAL ENERGY SPECTRUM

It has been found that the radiation intensity and intensity distribution at 7 volts applied potential is nearly the same for all metals except silver and copper and for these as well at wave lengths shorter than 3,000 A. An obvious possibility that it is the surface layer of cæsium which is radiating in all cases except silver and copper seems to be ruled out on several grounds. The intensity voltage curves seem to be characteristic of the metal used; the intensity of probe radiation in a helium discharge is of the same magnitude as in cæsium; the cæsium layer is probably monatomic and the incident electrons as well as the emergent light can penetrate 10 to 100 atom diameters. For these reasons it seems safe to assume that most metals give nearly identical spectra.

In the first paper we interpreted this radiation as analogous to the continuous X-ray spectrum and applied the general equation for

intensity of continuous X-rays from a thick target as given by Kramers.[3] The radiation per unit frequency range is

$$J(\nu)\ (\text{ergs}) = i \times 5 \times 10^{-50} Z (\nu_0 - \nu) \qquad (1)$$

where i is the number of electrons striking the surface per second, Z is the atomic number and ν_0 is the threshold frequency given by

$$h\nu_0 = e(V + W) \qquad (2)$$

Our results show J to be quite independent of Z, but this is not entirely unexpected. Equation (1) involves Z because high-frequency radiation is assumed to result from a transition between hyperbolic orbits in the immediate vicinity of the nucleus. For the low frequencies here considered the transition can take place much nearer the atom surface and for all elements beyond some undetermined value of Z the intensity will cease to depend on Z. We found that for $i = 0.63 \times 10^{19}$ per cm^2, $\nu_0 = 2.2 \times 10^{15}$ ($V + W = 9$ volts), $\nu = 1 \times 10^{15}$ (3,000 A), $J(\nu)$ was about 6×10^{-15} ergs per cm^2 ($J(\lambda) = 20$ ergs) for all metals. $J(\nu)$ by equation (1) is $3.8 \times 10^{-16} \times Z$ ergs for the above values of i, ν and ν_0. Dividing the observed value by the coefficient of Z, 3.8×10^{-16}, gives the value of an effective nuclear charge Z_e of about 16. Admitting an uncertainty of at least twofold such a value is not inconsistent with observations except for beryllium for which $Z = 4$. The above reasoning is extremely crude, but any adequate treatment would be very complicated.

In the first paper the continuous spectrum was also compared with theoretical predictions as to the converse of the photo-electric effect. The agreement in order of magnitude for the case of copper holds equally well for the revised values of $J(\lambda)$ and for all of the metals.

2. SELECTIVE RADIATION OF SILVER AND COPPER

The high maximum in silver radiation near 3,600 A is clearly a selective radiation superposed on the equal energy spectrum and of entirely different origin. The anomalies in copper radiation are less striking but presumably of a similar kind. For silver the increase begins at 3,200 A where the optical constants of silver suddenly change. Both reflection and absorption increase in the range in which the emission increases so that loss of radiation by internal reflection and absorption reduces the observed effect. A correction for loss by absorption is impossible, but a correction for reflection can be applied by dividing observed values by $1-R$ where R is the reflection coefficient. For two reasons this correction is uncertain. The probe surfaces were unpolished, and the reflection for light originating close to the surface may be appreciably less than for plane waves. The over correction for reflection is in the direction to compensate for the neglect of absorption. Figure 7 shows the intensity distribution for silver and copper thus corrected for reflection.[4] The form of the silver curve has been entirely changed and instead of a maximum 10 times the usual value of $J(\lambda)$ we have a nearly con-

[3] Kramers, Phil. Mag., vol. 46, p. 836; 1923.
[4] Optical Constants from I. C. T., vol. 5, p. 248, and Landoldt u. Bornstein, Ergänzungsband, vol. 1, p. 471.

stant intensity fifty times the usual value for wave lengths longer than 3,600. Beyond 4,500 A, R is over 0.9 and the correction very large and uncertain. For all other metals in the ultra-violet R is less than 0.5 and a reflection correction is unimportant compared with other uncertainties.

For comparison we include plots of the absorption of silver and copper; that is, the quantity $4\pi nk/\lambda$ from the equation

$$J/J_0 = exp\ (-4\pi nk/\lambda)x$$

It is of interest that k for silver increases at exactly the same wave length and in nearly the same way as the corrected intensity distribution. Evidently the increase in copper radiation in the red is similarly related to the optical constants though the phenomena are less striking.

Houston[5] has suggested that this selective radiation is analogous to a characteristic X-ray emission. The impacting electron ionizes an underlying electron level and one of the "free" conduction elec-

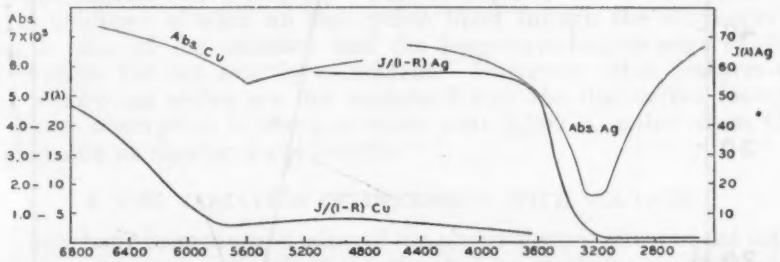

FIGURE 7.—*Intensity distribution of silver and copper radiation corrected for internal reflection in units of Figure 2*

Absorption coefficients of copper and silver in cm⁻¹.

trons falls into the vacant place emitting radiation, with the resulting spectrum a continuous band because of the wide range of energies of the free electrons. High dispersion spectra of soft X-ray emission lines show the broadening and Söderman's[6] densitometer curves of Be $K\alpha$ are the best illustration. This line appears as a band extending from 110 to 125 A with the maximum near the short-wave-length limit. The selective emission of silver is assumed to be such a band with the long-wave-length limit somewhere in the infra-red. This view is supported by the fact that the short-wave-length part of the band between 3,800 and 3,100 A is strikingly like the high velocity end of a Fermi distribution in energy as is borne out by the following computation:

The Sommerfeld equation for this distribution is:[7]

$$F(E) = \frac{c_1 E^{1/2}}{exp(e(E - W_i)/kT) + 1} \qquad (3)$$

where E is the electron energy, W_i the "internal work function," T the absolute temperature, and $e/k = 11{,}600$ for $E - W_i$ in volts.

[5] Houston, Remarks made in presentation of paper No. 61, Washington Meeting of the Physical Society, May 1, 1931.
[6] Söderman, Zeits. f. Phys., vol. 65, p. 656; 1930.
[7] Darrow, Phys. Rev. Supplement (Rev. of Modern Physics), vol. 1, p. 90; 1929.

We will apply equation (3) to a range of values of E small in comparison to E and treat $c_1E^{1/2}$ as a constant, c_2. Then $F(E)$ is equal to $c_2/2$ for $E=W_t$ and it increases to c_2 and decreases to zero symmetrically for E less or greater than W_t. Figure 8 shows that the intensity distribution is of the form

$$J=\frac{c_2}{exp\ x+1} \tag{4}$$

$$x=e(V-V_0)/kT$$

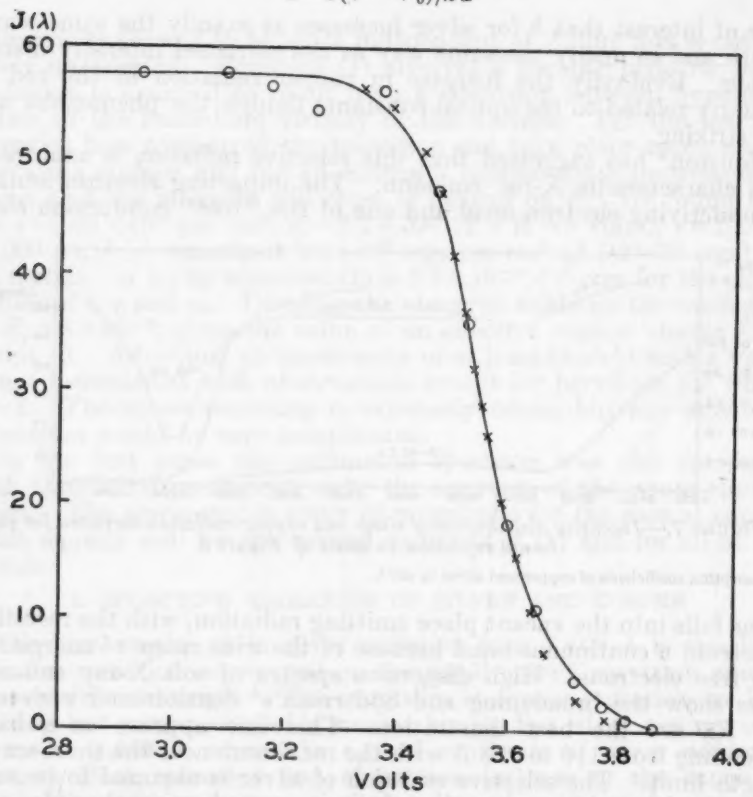

FIGURE 8.—*Circles, silver intensity corrected for internal reflection; crosses, Fermi distribution in energy of electrons at 370° C. on the same scale*

with V_0, the origin of x, at 3.56 volts and $x=1$ for $V-V_0=0.055$ volts. This gives $T=640°$ K or 370° C. As the cæsium tube is held at 200° C. and the probe is considerably heated by electron bombardment the assumed value of x is a reasonable value.

This result supports modern theories of metallic conduction in contrast with classical theories in indicating that the conduction electrons have a wide range of energies with a distribution consistent with equation (3) near the maximum energy. It does not give specific evidence that the entire distribution is like a Fermi distribution. Further V and V_0 of equation (4) are not identical with E and W_t of equation (3) for the origin of V is undetermined. Houston suggested that the underlying level is part of a "Bloch distribution"

of free electrons in which case W_i is greater than $V_0=3.56$ volts. However, the above computation indicates that the lower level is sharply defined and not a diffuse band for the entire spread of the edge of the emission band is accounted for by the temperature effect on the upper energy level. This suggests that the lower level is a discrete atomic level and that the energy range of "free" electrons is less than 3.56 volts. The range of a Fermi distribution assuming one electron per atom is 5.6 volts in silver.[8]

Since the continuum of permitted electron levels up to 3.56 volts above the lower level are occupied, the minimum potential required to ionize the lower level and excite any of the radiation is 3.56 volts. The intensity voltage curve for silver (fig. 5) measures the excitation of the selective band and the intercept 1.7 volts gives $V+W=3.8$ volts in fair agreement with the predicted value. Further, the form of the curve is like that of a curve of ionization versus voltage.[9]

Corresponding to electron excitation one would expect to find photo-electric absorption extending from the threshold of the emission band toward shorter wave lengths. The absorption curve of Figure 7 gives evidence of such an absorption band though the short-wave-length edge of the emission and the long-wave-length edge of the absorption are not exactly coincident. However, other features of the absorption curve are not explained and the distinctive feature of silver absorption is the low value near 3,200 A rather than the high value at shorter wave lengths.[10]

3. THE VARIATION OF INTENSITY WITH VOLTAGE

There have been many studies of the photo-electric effect of the total radiation from an anticathode bombarded by electrons with energies ranging from 3 or 4 to over 1,000 electron volts.[11] The current voltage curves, in general, rise with increasing voltage, but with many sharp bends where the slope either increases or decreases. It was originally considered that these bends measured excitation potentials of characteristic X-rays, but it has become evident that known atomic energy levels can not account for all the observed discontinuities. The continuous spectrum observed in our experiments must account for at least part of this effect and it is seen from the voltage intensity curves of Figures 5 and 6 that the integrated photo-electric effect of this continuous spectrum will give sharp inflections in the current-voltage curve.

It has been shown in the preceding section that characteristic X-radiation of long wave length will give wide continuous bands and not lines and it is evident that, if there were a selective emission like that of silver with its high-frequency limit in the Schumann region and its excitation potential 7 or 8 volts the whole observed spectrum might increase at this potential. This is qualitatively what was observed for aluminum radiation. A sudden increase in intensity began near $V=7$ volts $V+W=9$ volts. The increase extended to beyond 5,000 A, which would require an electron distribution of over 6.5 volts, much greater than silver. But Be, Kα from metallic beryllium

[8] Darrow, Phys. Rev. Supplement, vol. 1, p. 122; 1929.
[9] Franck and Jordan, Anregung von Quanten Sprüngen durch Stösse, p. 183. Julius Springer.
[10] Kronig (Proc. Roy. Soc., vol. A 124, p. 409, 1929) accounts for the observed optical properties of silver by transitions of the free electrons to a continuum of levels. A sharp selection principle, however, permits transitions of a given electron to but one of the many possible levels.
[11] Holweck, De la Lumiere aux Rayons X; Univ. of France Press.

is a band over 12 volts wide, so the lower limit of 6.5 volts is not unreasonable. Sommerfeld's theory gives the range of the Fermi distribution with 1 electron per atom as about 5.6 volts for aluminum as well as silver. However, the above considerations do not explain why the aluminum intensity curve should have a sharp maximum at 11 volts and the evidence for ascribing the peak in the voltage curve to characteristic radiation is not conclusive.

There are other factors which will modify the intensity voltage variation of the continuous spectrum and the integrated photoelectric effect, notably internal scattering of the electrons. If the incident electron penetrates the metal to a depth such that emergent radiation is strongly absorbed, then the occurrence of scattering at some potential may increase the emergent radiation simply by keeping the electrons nearer the metal surface.[12] Since scattering is probably a difraction process, any potential variation of intensity from this cause will depend on crystal structure and orientation rather than on atomic energy levels. Experiments are in progress to investigate the part played by crystal structure, but at present we can add little to existing evidence for and against a correlation between electron scattering and radiation potentials.[13] [14]

In conclusion we wish to acknowledge our indebtedness to Mr. Wahler, of this laboratory, who made all the discharge tubes used in this work. The making and mounting of suitable probes of various materials involved many technical problems which he ingeniously solved.

WASHINGTON, August 5, 1931.

---

[12] Rudberg, Proc. Roy. Soc., vol. 120, p. 386; 1928, has proposed this explanation, but in recent correspondence he expresses doubt as to whether it is an important factor.
[13] Rupp, Natur. Wiss., vol. 18, p. 880; 1930.
[14] Richardson, Proc. Roy. Soc., vol. 123, p. 63; 1930.